ktu
kaunas university of technology
1922

# MEDICAL PHYSICS in the BALTIC STATES 2019

PROCEEDINGS OF THE 14th INTERNATIONAL CONFERENCE ON *MEDICAL PHYSICS*

7-9 November, 2019
Kaunas, Lithuania

ISSN 1822-5721

**KAUNAS UNIVERSITY OF TECHNOLOGY**

# MEDICAL PHYSICS IN THE BALTIC STATES

## Proceedings of the 14th International Conference on Medical Physics

**Kaunas, Lithuania**
**7– 9 November, 2019**

Executive editor **Diana Adlienė**

## *CONFERENCE IS ORGANIZED BY*:

Kaunas University of Technology
Skåne University Hospital, Lund University
Medical Physicists Society
University Hospital of Lithuanian University of Health Sciences „Kauno klinikos“

## *PROGRAM COMMITTEE*

Diana ADLIENĖ - Kaunas University of Technology
Sören MATTSSON - Lund University, Skåne University Hospital (Sweden)
Todorka DIMITROVA - Paisii Hilendarski University, Plovdiv, Bulgaria
Birutė GRICIENĖ– Vilnius University Hospital „Santaros klinikos“
Evelina JASELSKĖ - Hospital of Lithuanian University of Health Sciences „Kauno klinikos”
Elona JUOZAITYTĖ – Lithuanian University of Health Sciences
Jurgita LAURIKAITIENĖ – Kaunas Medical University Hospital, Oncology Hospital
Marius LAURIKAITIS - Medical Physicists Society
Saulius MICKEVIČIUS - Vytautas Magnus University
Judita PUIŠO - Kaunas University of Technology
Benas Gabrielis URBONAVIČIUS - Kaunas University of Technology

## *ORGANISING COMMITTEE*

Lena CIBULSKYTĖ - Kaunas University of Technology
Dalia BAREIŠIENĖ - Kaunas University of Technology
Inga ANDRIULEVIČIŪTĖ - Kaunas University of Technology
Kamilė DAMBRAUSKAITĖ - Kaunas University of Technology
Antonio JREIJE - Kaunas University of Technology
Lali KESHELAVA - Kaunas University of Technology
Mantvydas MERKIS - Kaunas University of Technology
Sahar SHIRZADI DEH KOHNEH - Kaunas University of Technology
Lamiaa Salah Zaki ABDELRAZIK- Kaunas University of Technology

## *CONFERENCE IS SUPPORTED BY:*

Kaunas University of Technology
Lund University
Skåne University Hospital
Lithuanian Radiation Protection Centre
Medical Physicists Society
Lithuanian Radiation Protection Society
Lithuanian Association of Medical Physics and Biomedical Engineering

Papers included in the Proceedings were reviewed by independent peer reviewers

*MEDICAL PHYSICS IN THE BALTIC STATES 14 (2019)*

Proceedings of International Conference "Medical Physics 2019"
7 – 9 November 2019, Kaunas, Lithuania

# RADIATION SAFETY IN HIGH -DOSE RADIOPHARMACEUTICAL THERAPY

Sören MATTSSON[1,2], Martin ANDERSSON[1]
[1]Medical Radiation Physics Malmö, Lund University, Skåne University Hospital, SE-205 02 MALMÖ, Sweden
[2]Department of Physics, Kaunas University of Technology, Studentų 50, LT - 51368 Kaunas, Lithuania
soren.mattsson@med.lu.se; martin.andersson@med.lu.se

***Abstract*:** $^{131}$I - iodide has long been used for the treatment of thyrotoxicosis and thyroid cancer. New types of radiopharmaceuticals and new techniques are now increasingly being used for treating various tumours. Personalised dosimetry is based on an individual radionuclide biokinetics and the anatomy is essential to plan and verify the therapeutic procedures. The new ICRP Publication 140 provides recommendations on the radiological protection of patients, hospital staff, patient's family, carers, neighbours, and the general public.

***Keywords*:** radiopharmaceutical therapy (RPT), radionuclide therapy (RNT), molecular radiotherapy (MRT), theranostics, radiation protection.

## 1. Introduction

Radiopharmaceutical therapy using $^{131}$I-iodide for the treatment of thyrotoxicosis and thyroid cancer, and $^{32}$P-phosphate for polycythaemia and for palliation of bone pain, has been practised for more than 70 years [1-4]. Radiopharmaceutical therapy (also named as radionuclide therapy or molecular radiotherapy) is now increasingly being used for treating various tumours using new radionuclides, tracer molecules, and application techniques [5]. The increasing use of radiopharmaceuticals for cancer therapy opens a new treatment options for patients [6]. Examples of recently developed methods used in clinical practice are $^{177}$Lu-labelled peptides for treating neuroendocrine tumours [7] and $^{223}$Ra-dichloride for the treating bone metastases from castration-resistant prostate cancer [8, 9]. The goal of all radiation therapy is to optimize the relation between the probability for the tumour control (or the necessary suppression of hyperactive thyroid function by $^{131}$I-iodide) and normal tissue complications. Therapeutic radiopharmaceuticals exhibit large variation in biokinetics from patient to patient. Therefore, personalized dosimetry - based on the individual radiopharmaceutical biokinetics and the individual anatomy - is necessary to ensure that the subsequent treatment administration does not exceed organ or tissue tolerance levels and that the treatment is effective [10, 11]. The practice and optimisation of radiopharmaceutical therapy requires different competencies, including medical physicists, nuclear medicine physicians, nuclear medicine technologists, endocrinologists and oncologists.

## 2. New ICRP Publication 140

Exposure situation in the nuclear medicine diagnostics and therapy is more complex than in X-ray imaging, external beam radiation therapy and brachytherapy. The radiation source exposes individuals before as well as after the diagnostic or therapeutic procedure. Reported occupational exposure levels suggests great variability between work tasks and facilities. The group of individuals influencing the exposure and being exposed is wide. The current ICRP recommendations related to therapy with radiopharmaceuticals are found in ICRP Publications 94 [12], 103 [13] and 105 [14]. A new report, ICRP Publication 140 [11] provides recommendations on the radiological protection related to the radiopharmaceutical therapy of patients, staff, and members of the public. It details a framework to perform individualised dosimetry, to plan therapeutic procedures and to verify the absorbed dose delivered. It contains detailed recommendations for justification and optimization of a number of radiopharmaceutical therapy methods, methods for biokinetic data collection and absorbed dose calculations. Specific radiation protection issues for patients, hospital staff, the patient's family, carers, neighbours, and the general public are also discussed.

Target audience of this report includes nuclear medicine physicians and oncologists, medical physicists, clinicians, practitioners and prescribers, referrers, radiopharmacists, nuclear medicine technologists, radiographers, radiation protection officers, regulatory authorities, medical and scientific societies, industry, patients, patient advocacy groups and public protection officials.

Report will be available during 2019. There is a plan to continue the work focusing on a number of new $^{177}$Lu-

labelled agents as well as on some alpha-emitters, not covered by ICRP Publication 140.

## 3. Absorbed dose to organs and tissues in the patient

Challenge for all radiation therapy is to optimize the ability to treat cancer successfully (tumour control probability) against potential adverse effects and normal tissue complications. Radiopharmaceutical therapy provides opportunities to improve both treatment efficacy and safety.

In radiopharmaceutical therapy, the absorbed dose to an organ or tissue is governed by the individual patient biokinetics (uptake, retention, and clearance), which may vary widely from one patient to another. Measurements of radiopharmaceutical biokinetics provide essential information needed for internal dose assessment.

### 3.1. Patient dosimetry is a key issue

The effects of radiation on tissue are primarily dependent on the absorbed dose to that tissue. This is a fact accepted in external beam radiotherapy and brachytherapy. Still, today, however prescriptions in radionuclide therapy are most commonly based on a fixed amount of activity for all patients, sometimes adapted to patient weight or body surface area. This continues in spite of an increasing evidence that treatment outcome correlates with the absorbed doses delivered to tumours and to healthy organs [15]. Radiopharmaceutical therapy has much to learn from external beam radiotherapy and brachytherapy and has a need for a systematic approach for treatment planning, monitoring the effect, and archiving the data. Today we see more cures and less toxicity in external beam radiotherapy than 30 years ago thanks to more precise localization, better dosimetry and more precise delivery system. Also for radiopharmaceutical therapies, a development of personalized prescription alternatives based on dosimetry is likely to improve the outcome and cost-benefit of the therapy.Due to biokinetic differences, personalized dosimetry must be performed for the each patient. The dosimetry includes both the radiation absorbed dose to target (tumour) and normal healthy tissues. The estimations should be done prior to therapy using a trace-labelled diagnostic administration or post-therapy on the basis of a retrospective assessment of the administration.

In principle, a fully personalized approach based on patient-specific measurements can ensure treatment with an appropriate activity level without exceeding normal organ and tissue toxicity thresholds [16-20]. A current clinical practise combines diagnosis and therapy to enhance the efficacy and safety of procedures to an individual patient. This could be done by combining diagnosis and therapy to enhance the efficacy and safetyof procedures to the individual patient [21]. Such combinations of therapeutic and diagnostic procedures are called theranostic. See Table 1 for examples.

### 3.2. When absorbed dose estimates to the tumour cannot be performed

In radiopharmaceutical therapy there are patients or situations where the absorbed dose to the target volume cannot be calculated or reliably predicted for technical or practical reasons. It may be because metastatic lesions are not measurable or there may be too many lesions with different uptake. Another reason could be that the molecule used in the tumour pre-treatment dosimetry may have limited power to predict the absorbed dose of the therapeutic agent during treatment.

**Table 1.** Examples of combinations of **thera**peutic and diag**nostic** procedures (= **theranostic** procedures) for various nuclear medicine treatments.

| Treatment procedure | Imaging with γ- or $\beta^+$-emitters | Treatment with $\beta^-$- or α- emitters |
|---|---|---|
| Thyrotoxicosis and thyroid cancer | $^{123}$I-, ($^{124}$I-), $^{131}$I-iodide | $^{131}$I-iodide |
| Non-Hodgkin's lymphoma | $^{111}$In-ibritumomab tiuxetan (Zevalin) | $^{90}$Y-ibritumomab tiuxetan |
| Neuroendocrine tumours | $^{68}$Ga-DOTATATE $^{68}$Ga-($^{64}$Cu-, $^{18}$F-) peptides | $^{177}$Lu-DOTATATE $^{90}$Y- or $^{177}$Lu-peptides $^{213}$Bi-peptides |
| Metastatic or treatment-resistant prostate cancer | $^{68}$Ga-PSMA | $^{177}$Lu-, $^{225}$Ac- or $^{213}$Bi-PSMA |

In such situations, **the next best alternative** is to base therapy planning on the maximum tolerable absorbed dose to non-target organs or tissues. Examples of organs at risk in radiopharmaceutical therapy is red bone marrow (for most therapies), kidneys (for peptide therapy), liver (for mIBG) and lungs (for metastatic thyroid cancer therapy).

### 3.3. Pregnancy and breast-feeding

Special consideration should be given to pregnant women and children exposed to ionizing radiation. Radiopharmaceutical therapy is contraindicated in pregnancy, unless the therapy is life-saving **[**22].

If radio iodide is administered to a woman after 8-10 weeks post-conception, the foetal thyroid concentrates iodide which crosses the placenta. Treatment with $^{131}$I-iodide during pregnancy can, without treatment, lead to foetal permanent hypothyroidism and even a totally destroyed thyroid, severe mental retardation, dwarfism and increased malignancy risk in the infant.

For the similar reasons, breast feeding should be discontinued in patients receiving radiopharmaceutical therapy.

### 3.4. Good dosimetry also gives a possibility to estimate long term risks for patients

The goal is to cure patients and to get the population of cancer survivors to grow. Therefore, there is a need to understand the long-term health of this population (cancer, non-cancer effects, hereditary effects). "Second primary malignancies" are a leading cause of morbidity and mortality among cancer survivors. The risk for secondary cancer development from external radiotherapy is investigated extensively. Less is known about the radiation-induced cancer risk from

radiopharmaceutical therapy. Absorbed dose, dose distribution and dose rate differs between external and molecular radiotherapy.
An example, of a risk estimation, based on Table 2, using lifetime attributable risk (LAR) for treatment of a thyroid cancer with 3.7 GBq $^{131}$I-iodide [23] is given in Fig, 1 below.

**Table 2.** Examples of estimated organ/tissue absorbed doses at treatment of thyroid cancer with 3.7 GBq 131I-iodide [23].

| Organ/tissue (adult male) | Absorbed dose for 3.7 GBq, mGy |
|---|---|
| Brain | 70 |
| Kidneys | 740 |
| Liver | 190 |
| Lung | 180 |
| Redbone marrow | 170 |
| Salivary glands | 990 |
| Stomach wall | 2 400 |
| Urinary bladder wall | 540 |

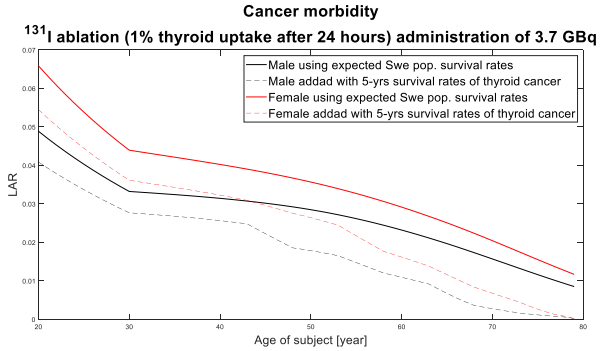


Fig. 1. Cancer risk after a thyroid treatment with 3.7 GBq $^{131}$I iodide.

The figure shows the radiation-induced cancer risk for both sexes. The broken line takes into account that patients do not have the same life expectancy as the normal Swedish population [23].

## 4. Exposure of individuals caring for and comforting patients and of members of the public

While medical exposures are predominantly delivered to individuals (patients), other individuals caring for and comforting patients are also exposed to the radiation. Young children and infants, as well as visitors not engaged in direct care or comforting, should be treated as members of the public and should be subject to the public dose limit of 1 mSv per year. The exposure of parents and others, normally family or close friends, who may come close to patients after administration of radiopharmaceuticals is considered as medical exposure [13]. ICRP Publication 94 [11] recommends that for individuals directly involved in comforting and caring (other than young children and infants), a dose constraint of 5 mSv per episode (for the duration of a given release from hospital after therapy) is reasonable. Radiological protection in radiopharmaceutical therapy has unique aspects, because unsealed radionuclides are used with much greater activities than commonly employed in diagnostic nuclear medicine. These greater activities may require the hospitalization of patients in wards specifically designed and equipped with special shielding and contamination control. The criteria for the release of patients or treatment as outpatients must be determined based on the potential dose to the family and friends. Patientsm who receive radiopharmaceuticals for therapeutic purposes become radiation sources with larger doses and for longer periods compared with those who receive radiopharmaceuticals for diagnostic purposes. Special protective measures must be taken with regards to contact with other people, especially children and pregnant women. If these patients travel or pass by radiation monitors, alerts may be activated. Therefore, patients should carry relevant documents issued by the hospitals.
Breast feeding must be stopped and conception should be avoided for certain periods of time. A special considerations for radiological protection are also necessary if radioactive patients are on dialysis.
Hospital staff, who deal with radiopharmaceutical therapy, need special training and experience in safety measures, in addition to those for regular radiation workers, to avoid contamination from unsealed radiation sources. They also need to know how
to decontaminate in case of contamination. Special care is required to contain contamination within controlled areas.

## 5. Conclusions

In radiopharmaceutical therapy, the absorbed dose to an organ or tissue is governed by the individual patient biokinetics (uptake, retention, and clearance), which may vary widely from one patient to another.
Due to biokinetic differences, personalized dosimetry must be performed for each patient. The dosimetry includes both the radiation absorbed dose to target (tumour) and normal healthy tissues. The estimations should be done prior to therapy using a trace-labelled diagnostic administration or post-therapy on the basis of a retrospective assessment of the administration.
Risk estimates for patients undergoing radionuclide therapy, have to take into account both the age of the patient at exposure, and his/her life-expectancy post therapy. These may be used to inform practitioners so that they can be considered as part of the justification and consenting processes.

## 6. References

1. Lawrence J.H. Nuclear physics and therapy: Preliminary report of a new method for the treatment of leukaemia and polycythaemia. Radiology 35, 51-60, 1940.
2. Hertz S. and Roberts A. Radioactive iodine in study of thyroid physiology VII. The use of radioactive iodine therapy in hyperthyroidism. JAMA 131, 81-86, 1946.
3. Chapman E.M. and Evans R.D. The treatment of hyperthyroidism with radioactive iodine. JAMA 131, 86-91, 1946.
4. Reinhard E.H., Moore C.V., Bierbaum O. and Moore S. Radioactive phosphorus as a therapeutic agent. A review of the literature and analysis of the results of treatment of 155 patients with various blood diseases, lymphomas and other

malignant neoplasstic diseases. J. Lab. Clin. Med. 31(2), 107-215, 1946.

5. Divgi C. The current state of radiopharmaceutical therapy. J. Nucl. Med. 59, 1706-1707, 2018.
6. Sgouros G. and Goldenberg D.M. Radiopharmaceutical therapy in the rea of precision medicine. Eur. J. Cancer 50(13), 2360-2363, 2014.
7. Bodei L., Pepe G., Paganelli G. Peptide receptor radionuclide therapy (PRRT) of neuroendocrine tumors with somatostatin analogues. Eur. Rev. Med. Pharmacol. Sci. 14, 347–351, 2010.
8. Parker C., Nilsson S., Heinrich D., Helle S.I., O'Sullivan J.M., Fossa S.D., Chodacki A., Wiechno P., Logue J., Seke M., et al. Alpha emitter radium-223 and survival in metastatic prostate cancer. N. Engl. J. Med. 369, 213–223, 2013.
9. Parker C., Heidenreich A., Nilsson S., Shore N. Current approaches to incorporation of radium-223 in clinical practice. Prostate Cancer Prostatic Dis. 21, 37–47, 2018.
10. Flux G. Individualised treatment planning for radionuclide therapy (Molecular radiotherapy). *http://www.icrp.org/docs/2017fuk/5%20Flux%20Presentation.pdf*
11. ICRP. Radiological protection in therapy with radiopharmaceuticals. ICRP Publication 140. Ann. ICRP, 2019 (in press).
12. ICRP. Release of patients after therapy with unsealed radionuclides. ICRP Publication 94. Ann. ICRP 34 (2), 2004.
13. ICRP. The 2007 recommendations of the International Commission on Radiological Protection. ICRP Publication 103. Ann. ICRP 37 (2-4), 2007.
14. ICRP. Radiological protection in medicine. ICRP Publication 105. Ann. ICRP 37 (6), 2007.
15. Strigari L., Konijnenberg M., Chiesa C., Bardies M., Du Y., Gleisner K.S., et al. The evidence base for the use of internal dosimetry in the clinical practice of molecular radiotherapy. Eur. J. Nucl. Med. Mol. Imaging 41, 1976–1988, 2014.
16. Pauwels S., Barone R., Walrand S., Borson-Chazot F., Valkema R., Kvols L.K., Krenning E.P. and Jamar F. Practical dosimetry of peptide receptor radionuclide therapy with $^{90}$Y-labeled somatostatin analogs. J. Nucl. Med. 46, 92S–98S, 2005.
17. Barone R., Borson-Chazot F., Valkema R., Walrand S., Chauvin F., Gogou L., Kvols L.K., Krenning E.P., Jamar F., and Pauwels S. Patient-specific dosimetry in predicting renal toxicity with 90Y-DOTATOC: relevance of kidney volume and dose rate in finding a dose-effect relationship. J. Nucl. Med. 46(1 suppl), 99S, 2005.
18. Maxon H.R., Englaro E.E., Thomas S.R.., Hertzberg V.S., Hinnefeld J.D., Chen L.S., Smith H., Cummings D., Aden M.D. Radioiodine-131 therapy for well-differentiated thyroid cancer—a quantitative radiation dosimetric approach: outcome and validation in 85 patients. J. Nucl. Med. 33, 1132–1136, 1992.
19. Flux G.D. Imaging and dosimetry for radium-223: the potential for personalized treatment. Br. J. Radiol. 90 (1077), 20160748, 2017.
20. Flux G.D., Sjogreen Gleisner K., Chiesa C., Lassmann M., Chouin N., Gear J., Bardiès M., Walrand S., Bacher K., Eberlein U., Ljungberg M., Strigari L., Visser E. and Konijnenberg M.W. From fixed activities to personalized treatments in radionuclide therapy: lost in translation? Eur. J. Nucl. Med. Mol. Imaging 45, 152–154, 2018.
21. Hosono M. Radiation protection in therapy with radiopharmaceuticals. Int. J. Rad. Biol.

https://doi.org/10.1080/09553002.2018.1516910

22. ICRP. Pregnancy and medical radiation. ICRP Publication 84. Ann. ICRP 30 (1), 2000.
23. Andersson M., Eckerman K., Mattsson S. Lifetime attributable risk as an alternative to effective dose to describe the risk of cancer for patients in diagnostic and therapeutic nuclear medicine. Phys. Med. Biol. 62, 9177-9188, 2017.

*MEDICAL PHYSICS IN THE BALTIC STATES 14 (2019)*

Proceedings of International Conference "Medical Physics 2019"
7 - 9 November 2019, Kaunas, Lithuania

# PROPOSAL OF QUALITY ASSURANCE SYSTEM FOR POSITRON EMISSION TOMOGRAPHY IN THE RUSSIAN FEDERATION

Larisa CHIPIGA[1], Aleksandr VODOVATOV[2], Galina KATAEVA[3], Daria RYZHKOVA[4], Mikhail DOLGUSHIN[5], Mikhail MEN'KOV[6], Nikolay KOSTENIKOV[7], Kristina SERGUNOVA[8], Alexey SMIRNOV[9], Christian BERNHARDSSON[10]

[1]Research Institute of Radiation Hygiene, Mira str. 8, 197101 St. Petersburg, Russian Federation; [1,7]A.M Granov Russian Scientific Centre of Radiology and Surgical Technologies, Leningradskaya str. 70, 197758 Saint-Petersburg; [3]nstitute of Human Brain named after N. Bekhtereva of the Russian Academy of Sciences, Saint-Petersburg, [4]National Medical Research Centre named after V. Almazov of the Ministry of Health of the Russian Federation, Saint-Petersburg, [5,6]National Medical Center for Oncology named after N. Blokhin, Moscow, [7,8]Scientific-Practical Clinical Centre for Diagnostics and Telemedicine Technologies of the Moscow Healthcare Department, [10]Medical Radiation Physics Malmö, Department of Translational Medicine, Lund University, Skåne University Hospital Malmö, Inga Marie Nilssons gata 49, 205 02 Malmö, Sweden

larisa.chipiga@gmail.com, vodovatoff@gmail.com, kataevagalina@mail.ru, d_ryjkova@mail.ru, mdolgushin@mail.ru, mnkv870327@yandex.ru, nkostenikov@yandex.ru, ska@rpcmr.org.ru, 6707470@gmail.com, christian.bernhardsson@med.lu.se

***Abstract*:** High diagnostic efficiency as well as the optimization of patient and staff doses in positron emission tomography (PET) can be achieved by implementing quality assurance program. This study was focused on the requirements and basic aspects of quality assurance (QA) in PET combined with computed tomography (CT), that include equipment quality control (QC). QA systems include methods of image QC, examination protocols, radiation monitoring and optimization of radiation protection of the staff and patients. This paper contains the proposals for the QC of equipment and diagnostic images, as well as values of diagnostic reference levels (DRLs) for identification of abnormally high patient doses and optimization of radiation protection. Authors propose the system of quality assurance in PET considering the features of Russian healthcare and radiation protection.

***Keywords*:** positron emission tomography, computed tomography, quality assurance, quality control, diagnostic reference levels, radiation protection

## 1. Introduction

Positron emission tomography (PET) is a diagnostic method, which is based on gamma-rays emitted from radiopharmaceuticals injected into the patient. The distribution of radiopharmaceuticals in organs and tissues modulates pathological and biochemical processes. The PET modality is used for diagnostics of endocrinological, neurological, cardiological and other diseases. However, PET is mainly used for diagnostics and staging of oncological diseases as well as the assessment of treatment effectiveness of oncological patients. Modern PET systems are commonly combined with computer tomography (CT), which provides additional information of the structure that can be combined with PET images of functions of the investigated organs.

The amount and quality of diagnostic information obtained by PET depends on the different medical and technical factors. The medical factors include methods of patient preparation and examination protocols, which should be standardized and executed by the medical staff. Technical factors include detector's characteristics, settings and calibration of diagnostic and measuring equipment, acquisition and processing protocols. Different methods of patient preparation, examination protocols and different PET equipment can provide incomparable quantative results if the examinations are performed in different medical facilities [1,2]. This is especially important for oncological patients, who have to repeat the examination after the treatment, which should be done at the same hospital using the same equipment as prior to the treatment. The inaccessibility of specific equipment can postpone necessary examinations and lead to negative consequences for the patient.

The PET method is rapidly developing in the Russian Federation [3,4]. In the past decade the number of PET departments in the country has increased by a factor of 5. Currently, there are about 37 departments and their number continues to increase. An availability of the PET method makes it possible to perform PET/CT

examinations for the same patient at different stages of treatment in various medical facilities. This expansion requires that national quality assurance (QA) system in PET diagnostics is developed. Such system should include harmonization of examination protocols, consider the features of national clinical and regulatory aspects of PET diagnostics, and should be harmonized with international standards and guidelines [5,6].

The European Association of Nuclear Medicine (EANM) developed a program for the accreditation of PET departments (EARL) [7–9] based on the control of quantitative parameters of a PET image using a standard phantom. Departments that fulfil the requirements of that program receive a certificate of complians to the EANM standard. That program allows harmonizing examination protocols of PET equipment from different vendors and obtaining comparable results. Accreditation in that program additionally allows participating in the different international clinical trials without an additional equipment testing.

Unfortunately, only some vendor specific quality control (QC) procedures has been published in Russia, as a draft of QA programs in PET and CT separately. The standardized QA system for combined PET/CT examinations is not available in Russia. Hence, the aim of this study was to analyse the existing requirements for QA in PET/CT and to present proposals for developing a unified QA system to harmonize clinical practice and protocols in various Russian PET departments.

## 2. General requirements for QA in PET

The QA system should include QC of diagnostic and measuring equipment, image QC, standardization and optimization of examination protocols, as well as radiation protection of patients and staff by applying the principles of justification, optimization and dose limits [10,11]. Existing Russian national requirements are aimed only at ensuring the integrity of diagnostic equipment [12–14]. It is implemented mainly as a part of an acceptance tests and periodic monitoring of parameters.

### 2.1. QC of the equipment

QC of equipment is one of the main parts of the QA in diagnostics. QC procedures allow to identify equipment malfunction and its source. Constant QC allows monitoring the stability of the PET/CT system and its components as well as providing the possibility to plan and adjust the calibration and maintenance schedule and order of spare parts.

*QC of the measuring equipment*

The PET departments should be equipped with a radiometer or other equipment for measuring the administered activity of the radiopharmaceutical [11]. The activity administered to the patient is considered during the reconstruction of the PET image and affects the examination result. In addition, the correct measurement of activity during packaging of radiopharmaceuticals is important for proper accounting of the radionuclides in the department. Hence, it is necessary to have reliable equipment for such measurements.

According to the national requirements, a radiometer or other measuring equipment have to pass an annual calibration according to an approved methodology [11]. In addition, it is necessary to perform periodic QC procedures of that equipment according to the user manual. According to the international recommendations, the radiometer have to pass a mandatory QC to verify the accuracy and stability of measurements with the following frequency [15]:

- constant monitoring of the zero value;
- daily stability control with the same radioactive source (for example, $^{137}$Cs);
- annual accuracy control with calibration sources preferably in the range of low, medium and high energies (for example, $^{57}$Co - 122 keV, $^{133}$Ba - 356 keV and $^{137}$Cs - 662 keV);
- annual linearity control covering the entire range of work activities (usually from a few GBq for daily package to the lowest diagnostic activities - tens of MBq).

The radiometer has to be calibrated for all radionuclides intended for use in the department.

One of the problems in national clinical practical is the lack of knowledge and non-fulfilment by the staff of appropriate QC measuring equipment. To ensure a continuous diagnostic process in a department, it is recommended to have additional measuring equipment for replacement in case of malfunction of the main one.

*QC of diagnostic equipment*

The local concentration of the radiopharmaceutical administered to the patient is measured during a PET examination. The detection system counts the number of annihilation photons in the coincidence mode and single events that have occurred in the field of view. After that, the image reconstruction starts, including normalization, correction for scattering and attenuation, based on calibration files and transmission (CT) scanning [16]. Climate changes in the room can affect the characteristics of the detection system, received signal and the resulting image. Hence, constant QC of the diagnostic equipment is required to identify deviations of the system and its timely recalibration.

The vendor specific acceptance tests and tests in accordance with the standards of the of National Association of Electrical Equipment Manufacturers [17] as well as national required tests have to be performed during commissioning. Due to the lack of the clear requirements in Russia, control of the PET/CT characteristics is currently limited to the QC procedures declared by the vendor. That complicates the standardization and harmonization of PET diagnostic in the country [6].

All commissioning procedures of the equipment are performed by the vendor engineers. The results of acceptance tests of the equipment are used as the basic values for comparison with the periodic QC results [16,18]. For the new equipment, after replacing parts of the detecting system or after the relocation of the equipment, the assessment of scatter contribution,

random and lost events, checks of the sensitivity, spatial resolution of the system and PET image quality are performed. For PET/CT units, monitoring of CT parameters and check of the coincidence of PET and CT images are added. A constant QC is necessary to maintain the stability of the system, which is performed periodically (daily/weekly/quarterly/annually), in the case of suspected malfunction and after replacement or repair of the major components. CT QC includes assessing the quantitative characteristics of a CT image: CT units, image noise, uniformity, spatial resolution, slice thickness, table position accuracy and verification of dosimetric characteristics (CTDI – CT dose index and DLP - dose length product) [13–14]. Daily PET QC is the basis on assessing the capacity of the system. It can be performed automatically and includes scanning a standard phantom or an embedded source. The results of daily QC are compared with the reference values obtained after calibration, and can be used as indicators for a calibration or normalization.

The activity or standardized uptake value (SUV) which reflects the radiopharmaceutical accumulation in the area of interest (in a pathological tissue) is used for interpreting PET examinations in clinical practice [19–21]. That requires the comparable activity administered to the patient and the one measured in the PET image. Hence, one of the important QC procedures is the cross-calibration of the radiometer and the PET: time synchronization and verification/calibration of the activity value [2,6,17].

### 2.2. Image QC

*PET image*

In practice, physicians have to determine the patient treatment tactics based on the results of the PET examinations and the amount of radiopharmaceutical accumulated in the lesion. The accuracy of the estimating accumulated activity in a PET image depends on the following parameters: the design and characteristics of the detection system, the acquisition and reconstruction protocols, the characteristics of the investigated object, the level of activity accumulated in the lesion [22]. The partial volume effect (PVE) is manifested in the PET image due to the non-ideal detection system and reconstruction algorithms [19–23]. The reconstructed PET image needs to correspond to the radionuclide distribution with an uniform accuracy over the field of view. However, due to the PVE, the activity in the reconstructed PET image depends on the size of the lesion and the ratio of activity in lesion to the surrounding structures. The maximum PVE manifested with small lesions leads to an underestimation of the accumulated activity in the lesion.

To assess PVE the influence on PET image and to compare and harmonize the PET protocols, the image QC is performed. Image QC involves monitoring and comparing the parameters of the PET image of standard phantom with the defined criteria and is based on the estimation of the recovery coefficient (RC). The RC is a quantitative parameter of the PET image, which is defined by the following equation 1:

$$RC = \frac{A_{image}}{A_{injected}}, \quad (1)$$

where: $A_{image}$ is the activity in lesion imitator on the image (kBq/ml); $A_{injected}$ is injected activity calculated to the scan time (kBq/ml) [19,22,24]. The RC varies with the size of the lesion and is specific for each acquisition, reconstruction and processing protocols. Hence, an important part of the QA of PET is the estimation and monitoring of RC for analysis and comparison of protocols. The NEMA IEC [7,17] or the MADEIRA [19,23] phantoms with spherical or conical imitators of lesions of different sizes are commonly used for the evaluation of PET images quality.

Figure 1 presents the examples of the dependences of RC values on the size of the lesions obtained with the NEMA IEC phantom. In case of comparable results, obtained on different model/protocols, the values of activities in the lesion determined on the models/protocols will coincide with each other. That provides the possibility to monitor the treatment process of patients undergoing PET examinations on different PET systems.

Table 1 presents the RC for the mean and maximum values of activity in the spheres of the NEMA IEC phantom. That criteria for RC was proposed based

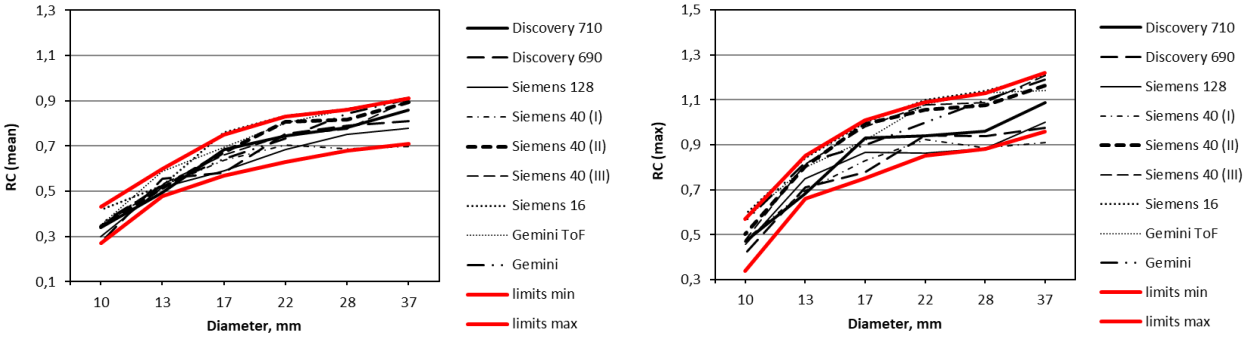


**Fig. 1.** Examples of the relationship between the recovery coefficient (RC) and the lesion size. Data is presented for different PET models with the NEMA IEC phantom [21]: to the left - mean values of activity; to the right - maximum values of activity.

on the results obtained in Russian PET departments and the EARL accreditation program [7–9]. If the RC value does not fall within the intervals, an investigation should be performed. The most common causes are procedural errors during the QC, an un-calibrated equipment or non-standard reconstruction algorithms.

**Table 1.** Ranges of recovery coefficients (RC): mean ($RC_{mean}$) and maximum ($RC_{max}$) obtained with the NEMA IEC phantom.

| Lesion size, mm | $RC_{mean}$ | $RC_{max}$ |
|---|---|---|
| 10 | 0.27 - 0.43 | 0.34 - 0.57 |
| 13 | 0.48 - 0.60 | 0.66 - 0.85 |
| 17 | 0.57 - 0.75 | 0.75 - 1.01 |
| 22 | 0.63 - 0.83 | 0.85 - 1.09 |
| 28 | 0.68 - 0.86 | 0.88 - 1.13 |
| 37 | 0.71 - 0.91 | 0.96 - 1.22 |

*CT image*

The CT method is based on the attenuation of X-rays by an object and the resulting image depends on the protocol parameters [25]. Based on CT (transmission) scanning, the attenuation coefficients matrix is created. It is used in the reconstruction of the PET image. Hence, the results of the CT scans affect the PET image.

For a visual and quantitative assessment of the structure density by the CT method an X-ray attenuation scale is used (the Hounsfield unit, HU). There are two ways to evaluate CT images: objective and subjective methods. The objective method involves evaluating the quantitative parameters of the CT image, such as image uniformity, image noise, and spatial resolution with test objects and phantoms [13,14]. Subjective methods such as ROC or FROC involve evaluating image quality by experts (radiologists) [26]. Objective methods are suitable for assessing the calibration and comparing CT protocols with each other. However, when introducing a new protocol an expert is needed for assessing the image quality.

## 3. Harmonization of the standard operating procedures

Diagnostic examination is performed according to standard operating procedure (SOP) that is developed according to national standards and approved by hospitals. The SOP include:

- perquisites for the examination;
- requirements for preparation of the patient for the examination;
- methods for calculating the administered activity of radiopharmaceutical;
- requirements for radiopharmaceutical injection;
- time from the injection to the scanning;
- acquisition and reconstruction protocols, as well as image processing;
- staff involved at each stage of the examination.

Different SOPs of the PET/CT examinations and different diagnostic equipment can lead to incomparable results of the examination of the same patient, when obtained in different medical facilities. Currently, two different guidelines on whole body PET/CT examinations with $^{18}$F-FDG have been published in Russia [27,28]. Hence, it is necessary to harmonize SOPs and standards of examinations between different regions. In order to confirm the absence of contraindications the patients should be notified of the analyses, instructed in preparation for the examination and sign an voluntary information consent [11,29].

It is recommended to create different CT protocols for the different groups of patients (age, weight) and for different research purposes (for example, low-dose, diagnostic and multiphase) as a part of PET/CT examination. The choice of one or another CT protocol is justified by the physician prior to the examination.

## 4. Radiation monitoring and optimization of radiation protection

Constant radiation monitoring of the department and the surrounding environment should be performed [11,30] to record and control the doses of personnel, patients of other departments and public. Based on the results of radiation monitoring of the department and individual dose monitoring, the level of radiation protection in the department is assessed. The results of radiation and dose monitoring must not exceed the norms [10,11]. Based on the achieved dose rate levels, staff individual dose reference levels are developed in order to track changes in staff doses, identify the causes of overexposure and correct the staff behaviour to optimize radiation protection of staff and public.

To optimize the radiation protection of patients the diagnostic reference levels (DRLs) are used. DRLs are the criteria for comparing the typical doses or typical activities of patients with a common practice and are used to detect abnormally high and low doses. The assessment of DRLs in PET/CT considers the activity of radiopharmaceutical injected to the patients and external exposure from CT [31]. In Russian PET/CT diagnostic, up to 90% of the patient dose is generated by the CT scan, while typical activities are lower compared to the mean administered activity in other countries [1]. Hence, it is necessary to consider abnormally low activity values and high dose values from CT. Optimization of radiation protection of patients should involve the following next steps:

- typical dose/activity estimation and comparison with the DRLs;
- optimization protocols in case of abnormally low or high dose/activity values;
- evaluation of image quality by objective and subjective parameters.

Currently, DRLs for CT examinations are not implemented in Russia. However, based on the available data (60% of the operating departments), the DRL values for CT scans for PET/CT examinations of the brain and the whole body were proposed (Table 2) [1,32]. DRLs were established in two dose quantities: DLP and effective dose. That allows the staff and inspection bodies to identify systematic excesses of the DRLs and the causes of high doses.

**Table 2.** Proposed diagnostic reference levels (DRLs) of whole body and head computed tomography (CT) scans as a part of PET/CT examinations.

| Anatomical region | DLP, mGy·cm | Effective dose, mSv |
|---|---|---|
| Head | 1200 | 2 |
| Whole body* (low-dose protocol) | 600 | 9 |
| Whole body* (diagnostic protocol) | 1000 | 15 |

**From vertex of skull to high third of hip.*

## 5. Staff requirements

The staff members have to comply with the professional requirements, attend professional training courses and pass through periodical tests. Staff of the department has to know and apply in daily practice basic principles of radiation protection (justification, optimization and dose limits). Physicians, medical physicists, engineers, technicians and nurses are responsible for the radiation safety of staff and patients and have to keep their radiation doses as low as possible (and not above 20 mSv/year).

It is important to have a medical physicist in PET department [33]. Medical physicists are responsible for the implementation of the QA system including acceptance tests and calibration of equipment, training of technicians in QC procedures and verification of the obtained results, monitoring of the diagnostic examinations, training of medical staff in the field of radiation protection, estimation of standard activities and doses and examination protocol optimization. Unfortunately, the number of medical physicists in Russian PET departments is limited; they are employed only in major national medical centres. Their responsibilities are mainly focused on the radiation control issues. The PET departments lack dedicated equipment for quality control. Hence, the implementation of QA system in PET in Russia should be accompanied by the promotion and employment of medical physicist in PET departments.

## 6. Conclusion

Development of nuclear medicine in Russia requires to improve radiation protection of patients and staff, as well as to add the equipment needed for proper QC and to develop standard SOP with acquisition, reconstruction and processing protocols.

This paper proposes the development and implementation of QA system in PET diagnostics in Russia, which includes:

- QC of diagnostic and measuring equipment;
- a systematic evaluation of PET and CT image quality, based on objective parameters and subjective methods with involvement of experts;
- SOP maintenance;
- systematic analysis of staff performance to identify procedural errors;
- estimation of staff doses, determination of typical patient doses and their comparison with the DRLs;
- optimization of PET and CT protocols in order to reduce the typical dose or improve image quality.

Implementation of the QA system in practice will improve the efficiency of PET diagnostic in Russia. It is necessary to have medical physicists in PET department in order to implement that system into the practice. Proposed QA system in PET/CT is compatible with the EARL accreditation program; its implementation in medical practice will provide harmonization of national and international PET diagnostics. The QA system in PET presented in this paper was published in 2019 in Russia and is currently been reviewed by the ministry of healthcare and the radiation protection authorities.

## 7. References


1. Chipiga L.A., Zvonova I.A., Ryzhkova D.V., et al. Levels of patient's exposure and a potential for optimization of the PET diagnostics in the Russian Federation. Radiation Hygiene, 10(4). 31-43, 2017.. (In Russ.) https://doi.org/10.21514/1998-426X-2017-10-4-31-43.
2. Chipiga L., Vodovatov A., Kataeva G., et al. Proposals of quality assurance in positron emission tomography in Russia. Medical physics, 82(2). 78-92, 2019. (In Russ.).
3. Onischenko G.G., Popova A.Y., Romanovich I.K., et al. Modern principles of the radiation protection from sources of ionizing radiation in medicine. Part 1: Trends, structure of X-ray diagnostics and doses from medical exposure. Radiation Hygiene, 12(1). 6-24, 2019.. (In Russ.) https://doi.org/10.21514/1998-426X-2019-12-1-6-24.
4. Onischenko G.G., Popova A.Y., Romanovich I.K., et al. Modern principles of the radiation protection from sources of ionizing radiation in medicine. Part 2: radiation risks and development of the system of radiation protection. Radiation Hygiene, 12(2). 6-24, 2019.. (In Russ.) https://doi.org/10.21514/1998-426X-2019-12-2-6-24.
5. Chipiga L. Workshop of IAEA member states in Europe and Africa regions on Quality Management Audits in Nuclear Medicine Practices (QUANUM). Medical physics, 2019. 81(1). 122-125 (In Russ.).
6. Inozemtsev K.O., Narkevich B.Ya., Menkov M.A., et al. The development of quality assurance program for combined PET/CT scanner in the conditions of Russian PET centre. Medical physics, 57(1). 65-77, 2013. (In Russ.).
7. http://earl.eanm.org/cms/website.php. Accessed: 24.09.2019.
8. Boellaard R., Hristova I., Ettinger S. et. al. EARL FDG-PET/CT accreditation program: Feasibility, overview and results of first 55 successfully accredited sites. J. Nucl. Med., 54(2) Suppl. 20-52, 2013.
9. Kaalep A., Sera T., Oyen W., et al. EANM/EARL FDG-PET/CT accreditation - summary results from the first 200 accredited imaging systems. Eur. J. Nucl. Med. Mol. Imaging, 45(3). 412–422, 2018.
10. Sanitary rules and norms. SanPiN 2.6.1.2523-09. Norms of the radiation safety (NRB 99/2009). Moscow: Rospotrebnadzor, 14.08.2009. P. 100. Available on: http://www.consultant.ru/document/cons_doc_LAW_90936/ (Accessed: 24.09.2019).
11. Sanitary norms and rules. SanPiN 2.6.1.3288-15. Hygienic requirements for the provision of the radiation safety in positron emission tomography. Moscow: Rospotrebnadzor, 20.07.2015. P.59. (in Russ). Available on: http://docs.cntd.ru/document/420296595 (Accessed: 24.09.2019)

12. National standard of Russian Federation: (61675-1-2013) Radionuclide imaging devices. Characteristics and test conditions. Part 1. Positron emission tomograph. / GOST R MEK 61675-1-2013 – Moscow: Standartinform, 2014. (in Russ)
13. National standard of Russian Federation: (61223-3-5 – 2008) Evaluation and routine testing in medical imaging departments – Part 3-5: Acceptance tests – Imaging performance of computed tomography X-ray equipment. / GOST R MEK – Moscow: Standartinform, 2008. (in Russ)
14. National standard of Russian Federation: (61223-2-6 – 2001) Evaluation and routine testing in medical imaging departments – Part 2-6: Constancy tests. X-ray equipment for computed tomography. / GOST R MEK – Moscow: Gosstandart of Russia, 2002. (in Russ)
15. European Association of Nuclear Medicine. Best practice in nuclear medicine. EANM. Part 2. A technologist's guide. 2016. Vienna, Austria.
16. Bailey D.L., Townsend D.W., Valk P.E. et. al. Positron emission tomography: basic sciences. Springer, 688, 2005.
17. NEMA Standards Publication NU 2-2018: Performance Measurements of Positron Emission Tomographs (PETs). National Electrical Manufacturers Association (NEMA). 2018. Washington.
18. European Association of Nuclear Medicine. Technologists guide. Quality control of nuclear medicine instrumentation and protocol standardization. EANM, 2017. Vienna, Austria.
19. Chipiga L., Sydoff M., Zvonova I. et. al. Investigation of partial volume effect in different PET/CT systems: a comparison of results using the MADEIRA phantom and the NEMA NU-2 2001 phantom. Rad. Prot. Dosim, 169(1-4). 365-370, 2016.
20. Hoffman E.J., Huanq S.C., Phelps M.E. Quantitation in positron emission computed tomography: 1. Effect of object size. J. Comput. Assist. Tomogr, 3(3). 299–308, 1979.
21. Rousset O.G., Ma Y., Evans A.C. Correction for Partial Volume Effects in PET: Principle and Validation. J. Nucl. Med, 39 904–911, 1998.
22. Geworski L., Knoop B.O., Cabrejas M.L., et. al. Recovery correction for quantitation in emission tomography: a feasibility study. Eur. J. Nucl. Med, 27(2). 161-169, 2000.
23. Soderberg M., Engeland U., Mattsson S. et. al. Initial tests of a new phantom for investigation of spatial resolution, partial volume effect and detectability in nuclear medicine tomography. J. Phys. Conf. Ser, 317,012017, 2011.
24. Srinivas S. M., Dhurairaj T., Basu S., et al. A recovery coefficient method for partial volume correction of PET images. Ann. Nucl. Med, 23. 341–348, 2009.
25. Kalender W.A. Computed tomography: fundamentals, system technology, image quality, applications. 3rd Rev. Edition. Wiley-VCH. Weinheim, 220, 2011.
26. Verdun R.F., Racine D., Ott J.G., et al. Image quality in CT: From physical measurements to model observers. Phys. Med, 31(8). 823–843, 2015.
27. Smolyarchuk M.Ya., Agafonova O.A., Morozov S.P. Guidelines on the conductions of PET/CT examinations with $^{18}$F-FDG in Moscow covered by the state assurance. // Series «Guedelines on the best practices of the medical imaging and instrumental diagnostics». Vol. 5. – Moscow, . 26, 2017
28. Dolgushin M.B. Turin I.E. Standards of the US, MRI, CT and PET/CT examinations in oncology. Ed. by Dolgushin M.B. Turin I.E. 2016.
29. International Atomic Energy Agency. Applying radiation safety standards in nuclear medicine. Safety reports series № 40. – Vienna: IAEA, 2006. P. 137.
30. International Atomic Energy Agency. Radiation protection and safety of radiation sources: international basic safety standards. IAEA safety standards series, ISSN 1020-525X; No. GSR Part 3 (Vienna: IAEA) (2014), P. 518.
31. International Commission on Radiological Protection. Diagnostic Reference Levels in Medical Imaging Ann. // ICRP Publication 135. ICRP, 46(1). P. 144, 2017.
32. Chipiga L.A., Vodovatov A.V., Golikov V.Yu. et. al. Potential for the establishment of national CT diagnostic reference levels in the Russian Federation. Proceedings of International Conference on Radiation Protection in Medicine: Achieving Change in Practice. – Vienna, 2017. IAEA, book of contributions. P. 52–55. https://www.iaea.org/sites/default/files/18/02/rpop-session2.pdf
33. International Atomic Energy Agency. Clinical Training of Medical Physicists Specializing in Nuclear Medicine. – Vienna: IAEA,. 278, 2011.

*MEDICAL PHYSICS IN THE BALTIC STATES 14 (2019)*

Proceedings of International Conference "Medical Physics 2019"
7 – 9 November 2019, Kaunas, Lithuania

# PET-CT IN ONCOLOGICAL PATIENTS WITH OCCUPATIONAL EXPOSURE TO IONIZING RADIATION

Mikhail V. OSIPOV[1], Andrey V. VAZHENIN[2], Anna I. KUZNETSOVA[2], Irina A. AKSENOVA[2], Daria A. VAZHENINA[2], Mikhail E. SOKOLNIKOV[1]
[1]Southern Urals Biophysics Institute, Ozyorsk, Russia; [2]Chelyabinsk Regional Clinical Center of Oncology and Nuclear Medicine, Chelyabinsk, Russia; [2]Southern Urals State Medical University, Chelyabinsk, Russia
ferrum76@mail.ru; 2443632@mail.ru

***Abstract*:** The paper describes the results of follow-up study of oncological patients who underwent PET-CT in Chelyabinsk Regional Clinical Center of Oncology and Nuclear Medicine from 2010 to 2019. Cancer mortality was analyzed in relation to age, sex, PET-CT component, and occupational exposure to ionizing radiation for those patients who were nuclear production workers. Logistic regression has been applied to assess the significance of factors influencing cancer mortality.

***Keywords*:** PET CT, atomic workers, cancer, medical exposure, radiation risk

## 1. Introduction

Positron emission tomography (PET) is a modern imaging technique in nuclear medicine that is helpful in oncology to vizualize metabolic processes in malignant tissue. Combined with X-ray computed tomography (CT) it substantially enhances diagnostic results [1]. Radiation doses delivered to patients subject to PET-CT are relatively low, but repeated procedures may lead to higher exposure levels [2]. This is especially important in the cases when the patient had had previous ocupational exposure. The objective of the work was to estimate exposure levels of patients subject to PET-CT and determine possible risk factors.

## 2. Material and Methods

Data were retrospectively collected in Chelyabinsk Regional Center of Oncology and Nuclear Medicine for 347 Ozyorsk residents examined using hybrid PET-computed tomography (PET-CT) systems Biograph-40 and Biograph-64. The follow-up period started since the start of PET-CT operation in 2010 and ended in the middle of 2019. Whole-body examinations with radiopharmaceutical $^{18}$F-2-fluoro-2-deoxy-d-glucose (FDG) were performed for all patients except those examined in early 2010 without FDG administration (CT-mode). The following parameters such as age of the patient, gender, clinical diagnosis, number of repeated examinations and administered activity of FDG were recorded. Vital status has been updated up to 1.06.2019 for all patients. Patient effective doses from CT component were calculated taking into account National Radiation Safety Standards recommendations using conversion coefficients [3]. Effective doses from PET component were calculated using conversion coefficients recommended by ICRP 80 [4]. Logistic regression was used for the analysis. Parameter fitting was performed using Chi-square test at 95% level of significance.

## 3. Results

651 PET-CT protocols for 347 patients were collected. 42.9% males and 57.1% females were examined between 2010 and 2019. Follow-up period varied from 0 to 9 years; 8.8% of patients died in the first year of follow-up. Age of patients at 1$^{st}$ PET-CT varied from 19 to 91 (average 57 years). Distribution of patients by age categories and gender is shown in Table 1:

**Table 1.** Distribution of patients by age at exposure and gender

| Age category | Male,% | Female,% | Both gender,% |
|---|---|---|---|
| 19-29 | 6.0% | 0.5% | 2.9% |
| 30-39 | 8.7% | 7.6% | 8.1% |
| 40-49 | 9.4% | 17.7% | 14.1% |
| 50-59 | 30.9% | 23.7% | 26.8% |
| 60-69 | 30.2% | 37.9% | 34.6% |
| 70-79 | 12.1% | 9.6% | 10.7% |
| 80+ | 2.7% | 3.0% | 2.9% |
| Total | 100.0% | 100.0% | 100.0% |

* age at 1$^{st}$ PET-CT

During the follow-up period 64.6% of the patients had been examined once, the rest of the patients were subject to up to 11 repeated PET-CT examinations. Average administered FDG activity of 397.5 (200.0-834.0) mBq resulted in average effective dose of 7.5 (3.0-12.8) mSv per one PET-CT. Total effective dose estimate for 1 whole body PET-CT with FDG was 23.8 (2.3-71.7) mSv,

whereas for patients with repeated examinations the mean estimate of cumulative effective dose reached 41.2 mSv.

Distribution of patients by number of PET-CT, and cumulative effective doses from PET and CT components is shown in Table 2:

**Table 2.** Proportion (%) of PET-CT, effective dose from PET-component ($ED_{FDG}$), effective dose from CT-component ($ED_{CT}$) and total effective dose at the end of follow-up ($ED_{SUM}$) by number of examinations (Ex)

| Ex | % | $ED_{FDG}$* | $ED_{CT}$* | $ED_{SUM}$* |
|---|---|---|---|---|
| 1 | 64.6 | 7.3 (0.1) | 15.7(0.5) | 22.2 (0.5) |
| 2 | 19.0 | 14.6 (0.3) | 30.8 (1.3) | 46.9 (1.4) |
| 3-5 | 12.1 | 25.8 (1.4) | 61.3 (6.3) | 92.3 (6.5) |
| 6-12 | 4.3 | 56.6 (7.0) | 131.0 (25.8) | 180.7 (34.6) |
| Total | 100% | 12.6 (0.6) | 27.8(1.8) | 41.2 (2.3) |

* mean estimate in mSv with standard deviation (in brackets)

21.7% of the patients were nuclear workers hired to reactor, radiochemical, plutonium production and auxiliary plants from 1948 to 2000.

87.3% patients had information on diagnosis and stage of malignant tumor before PET-CT examination. 35.1% of malignant tumors were diagnosed using PET-CT. 51.4% of examined patients had died by the end of follow-up at the average age of 60 (proportion of malignant neoplasms as a cause of death was 94%).

Distribution of patients by vital status as of 01.06.2019 (alive, dead and lost to follow-up), gender and occupational exposure is shown in Table 3:

**Table 3.** Distribution of patients by vital status, gender and occurrence of occupational exposure

| Vital status | Male | Female | Both gender | Worker* |
|---|---|---|---|---|
| Alive | 39.6% | 48.5% | 44.7% | 8.1% |
| Dead | 57.1% | 46.9% | 51.4% | 13.3% |
| Lost | 3.4% | 4.6% | 3.9% | 0.2% |
| Total | 100.0% | 100.0% | 100.0% | 100.0% |

*percent of those with given vital status

Cancer death was used as the event to be analyzed. Odds ratio (OR) was considered as the ratio of probability of an event occurred to the probability of its non-occurrence (1):

$$OR = P/(1 - P) \quad (1)$$

To identify possible risk factors, a multifactorial analysis was applied using logistic regression model (2):

$$P(y_i \neq 0|x_i) = exp(x_i \beta) / 1 + exp(x_i \beta) \quad (2)$$

Model was fitted using following parameters: gender ($X_1$), age at 1st PET-CT ($X_2$), malignant tumor stage ($X_3$), professional exposure to ionizing radiation ($X_4$), and repeated PET-CT ($X_5$). Comparison of models with different sets of parameters was performed using likelihood ratio test (Table 4):

Testing of the model showed that inclusion of parameters $X_4$ and $X_5$ did not improve significantly the quality of fit, while statistical significance of the coefficients obtained for those parameters were insufficient.

**Table 4.** Predictive risk factors affecting the event

| Risk factor | z | P(z) | $\beta_i$ | z | P(z) | $\beta_i$ |
|---|---|---|---|---|---|---|
| | Model A | | | Model B | | |
| $\beta_0$ (const.) | -2.54 | 0.011 | -2.08 | -1.86 | 0.06 | -1.74 |
| $X_1$ | -2.36 | 0.018 | -0.78 | -1.95 | 0.05 | -0.68 |
| $X_2$ | 3.29 | 0.001 | 0.04 | 2.79 | 0.005 | 0.04 |
| $X_3$ | 2.61 | 0.009 | 0.31 | 2.72 | 0.007 | 0.33 |
| $X_4$ | - | - | - | 0.99 | 0.324 | 0.42 |
| $X_5$ | - | - | - | -0.88 | 0.378 | -0.24 |
| LRT | $\chi 2(3)=21.7$; p=0.0001 | | | $\chi 2(5)=23.6$; p=0.0003 | | |

### 3.2. Discussion

We analyzed the information on all Ozyorsk residents who were exposed to low doses of diagnostic radiation during PET-CT procedures. Although radiation exposure is a proven carcinogenic factor, there was no statistically significant effect of repeated PET-CT on cancer mortality in the study group. However, while administered FDG activity was relatively constant, dose of occupational exposure could vary greatly, that could lead to heterogeneity in the group of professionals. Also, radiotherapy and chemotherapy are possible risk factors that could lead to changes in mortality rate. Contribution of previous CT scans performed outside the Chelyabinsk Regional Clinical Center of Oncology and Nuclear Medicine as an additional radiation factor, should also be assessed using data of CT register [5].

### 4. Conclusions

The effect of gender, age and stage of a malignant neoplasm on cancer mortality among patients exposed to PET-CT has been defined. Among the study group, repeated PET-CT and occupational exposure were not associated with changes in cancer mortality rates.

### 5. References

1. Beyer T., Townsend D.W., Brun T. et al. A combined PET/CT scanner for clinical oncology. J Nucl Med 2000, 41: 1369–1379.
2. Brix G., Nekolla E.A., Borowski M. et al. Radiation risk and protection of patients in clinical SPECT/CT. Eur J Nucl Med Mol Imaging. 2014; 41 Suppl 1: S125-136.ICRP, 1998.
3 .Radiation Dose to Patients from Radiopharmaceuticals (Addendum to ICRP Publication 53). ICRP Publication 80. Ann. ICRP 28 (3).
4. Basic Sanitary Rules for Radiation Safety OSPORB-99/2010. SP 2.6.1.25 - 10. (in Russian).
5. Osipov M.V., Sokolnikov M.E. Fomin E.P. Prospects for using the medical dosimetric register of computed tomography to assess the contribution of medical diagnostic radiation to radiogenic risk. Issues of Radiation Safety. 2018; 89 (1): 67-73 (in Russian).

*MEDICAL PHYSICS IN THE BALTIC STATES 14 (2019)*

Proceedings of International Conference "Medical Physics 2019"
7 – 9 November 2019, Kaunas, Lithuania

# IMPLEMENTATION OF NUCLEAR MEDICINE QUALITY ASSURANCE PROGRAMME IN LITHUANIAN HOSPITALS

Vaida GRIGONIENĖ[1]; Kirill SKOVORODKO[2,3]; Mažena MACIUSOVIČ[4]; Rūta URBANAVIČIŪTĖ[3]; Laurynas GILYS[5]; Birutė GRICIENĖ[3,6]

[1]Radiation Protection Centre, Vilnius, Lithuania. [2]State research institute Center for Physical Sciences and Technology, Vilnius, Lithuania. [3]Vilnius University Hospital Santaros Klinikos, Vilnius, Lithuania. [4]National Cancer Institute, Vilnius, Lithuania. [5]The Hospital of Lithuanian University of Health Sciences, Kauno klinikos, Kaunas, Lithuania. [6]Department of Radiology, Nuclear medicine and Medical physics, Faculty of Medicine, Vilnius University, Vilnius, Lithuania.

vaida.grigoniene@rsc.lt; kirill.skov@gmail.com; m.maciusovic@gmail.com; laurynas.gilys@kaunoklinikos.lt; birute.griciene@gmail.com.

***Abstract*:** In accordance with national legislation, international guidelines and recommendations, the quality assurance (QA) programme must be established in nuclear medicine departments and it must meet high quality standards. QA programme should cover many aspects such us radiation protection of patient and staff, waste management, records keeping and report writing, training and continuing education of personnel, audits, quality control (QC) of imaging modalities, radionuclide dose calibrators, radiopharmaceuticals, etc. In this paper aIn order to develop national guidelines for improvement of QA system including QC in nuclear medicine, there were comprehensively analysed recommendations of different national and international organizations (IAEA, EANM, ACR, AAPM, NPL) and manufacturer supplied information. In addition, problems and needs in nuclear medicine in Lithuania are discussed. The appropriate QA and QC programme, traceability of measurements, written procedures, the acceptance and commissioning procedures and routine tests are the fundamental part of proper quality management programme. The analysis of the current status of national QA and QC content revealed that there are requirements in Lithuania legislation for QA management system, but there is lack of criteria for their implementation and QA management systems are implemented inconsistently in nuclear medicine departments in Lithuania.

The purpose of this work is to compare the recommendations of different international organisations for equipment used in nuclear medicine department and in near future develop the national guidelines for QA system in nuclear medicine to ensure the quality of QA programmes and consistency of these programmes implementation in Lithuanian hospitals to assure the safety of patients.

***Keywords:*** Quality control, quality assurance, acceptance tests, nuclear medicine, calibration.

## 1. Introduction

Quality assurance system is mandatory to guarantee smooth nuclear medicine department activity, patients and workers radiation safety each day. QA is a set of procedures that focuses on providing assurance that quality requested in each aspect of clinical practise (submission of requests for procedures, the preparation and dispensing of radiopharmaceuticals, the protection of patients, staff and the general public against radiation hazards and accidents, the setting-up, use and maintenance of equipment and etc.) by giving treatment to patient will be achieved. QA is an important part of all aspects of nuclear medicine practice [1, 8].

QA covers a series of QC tests carried out through the whole life cycle of instruments and its goal is to ensure, that all equipment satisfy certain criteria as well as to identify equipment's deviations of parameters and defects. The purpose of QC programme (QC tests according to the schedule) is to guarantee a high performance of the equipment depending on its age or other factors.

The QC usually starts with initials acceptance tests. Acceptance and commissioning tests are performed in order to verify equipment prior to the clinical use in patients [1, 2]. Routine QC starts after acceptance and commissioning testing and continues on a regular basis [3] and after changes or repairs of equipment components, system updates made by manufacturer. The acceptance testing is highly important, because that for future periodic and routine QC tests the results of all

acceptance tests will be used as the reference values for data analysis [1, 4].

It is very important that all QC measurements will be carefully described in QC programme, carried out in the same way each time, results recorded and analysed [5]. QC programme in the nuclear medicine department should be designed by following international guidelines such as those from International Atomic Energy Agency (IAEA), European Association of Nuclear Medicine (EANM), American Association of Physicists in Medicine (AAPM), International Electrotechnical Commission (IEC) and National Electrical Manufacturers Association (NEMA) in case of radiopharmaceuticals usage – recommendations of the European Pharmacopoeia [6]. These recommendations must be considered by following any national guidelines and legislations as well. In case of acceptance and commissioning tests it is very important to consider manufacturer requirements [1, 2]. The problem is that in different international guidelines there are different recommendations for the same QC tests.

The paper presents comparison of different requirements of international guidelines for QC tests for SPECT, gamma cameras, PET, radionuclide calibrators. As well QC procedures for radiopharmaceuticals based on the European Pharmacopoeia [6] and QC procedures for other equipment. The task of this article is to formulate a brief overview and prepare most effective and consistent QC programme for nuclear medicine departments in Lithuania to ensure that patient treatment meets high standards and to cover all aspect of nuclear medicine.

## 2. Quality assurance and quality control programme (acceptance, reference and routine tests) in nuclear medicine department

Every nuclear medicine department, should have an implemented QA system that all staff (physician, medical physicists and engineers, radiology technologists, nurses and other staff) is aware of. Very important part of any QA system is QC. It verifies that specific measures are taken to ensure that each particular aspect of the procedure is satisfactory. QC measurements helps ensure that the equipment functions properly. When the imaging equipment is not well controlled, it is difficult to determine whether the errors are due to personnel or equipment. A cycle of QA and QC processes for medical imaging equipment is shown in Fig. 1. This cycle is based on the IEC 61223-1 [7].

In further sections routine quality control measurements for equipment related to nuclear medicine procedures and suggested periodicity of the tests are presented. Additional reading is recommended for technical information on the instrumentation covered in this article.

### 2.1. QC procedures for SPECT and gamma camera

Tests recommended by different international recommendations and their periodicity for SPECT and gamma camera are shown in Table 1.

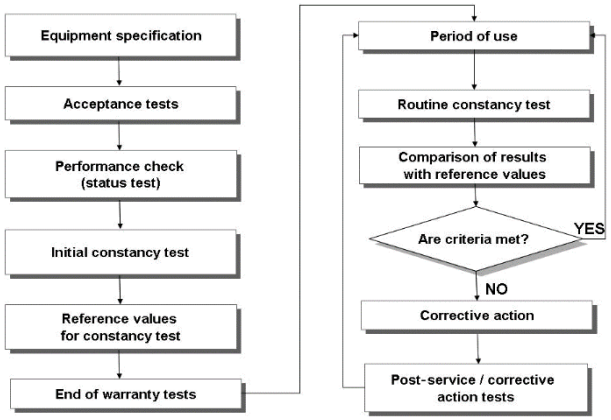


**Fig. 1.** QA and QC sequence of processes of medical imaging device (based on [7]).

**Table 1.** Recommended tests and periodicity for QC of SPECT and gamma camera.

| Procedure | IAEA [8] | EANM [3] | NEMA [9] | AAPM TG177 [10] |
|---|---|---|---|---|
| Intrinsic flood field uniformity for $^{99}$Tc | Ac, A, W | Ac, W/M | Ac, A | Ac, M |
| Intrinsic resolution and linearity | Ac, A, ½Y | Ac, ½Y | Ac, A | Ac, A |
| System spatial resolution and linearity | Ac, A, W | Ac, ½Y | Ac, A | Ac, W |
| System flood flied uniformity | A, ½Y | - | - | - |
| System planar sensitivity | Ac, A, ½Y | - | Ac, A | Ac, A |
| Energy resolution | - | Ac | Ac, A | Ac, A |
| Energy peaking (energy spectrum) | W | - | - | - |
| Whole body (WB) spatial resolution | - | Ac, A | Ac, A | Ac, A |
| Centre of rotation (COR) alignment | Ac, W/M | W/M | Ac, A | M |
| Pixel size | Ac, ½Y | Ac, ½Y | - | - |
| Tomographic uniformity | Ac, ½Y | - | - | Ac, A |
| Tomographic spatial resolution | - | Ac, ½Y | Ac, A | - |
| Total system performance | Ac, ½Y | ½Y | - | - |
| Slice thickness | Ac, ½Y | - | | - |

Ac – acceptance, A – annual, ½Y – half yearly, M – monthly, W – weekly, D – daily.

### 2.2. QC procedures for PET

Tests recommended by different international recommendations and their periodicity for PET scanners are shown in Table 2.

### 2.3. QC procedures for radionuclide calibrator

Tests recommended by different international recommendations and their periodicity for radionuclide calibrator are shown in Table 3.

**Table 2.** Recommended tests and periodicity for PET scanner.

| Procedure | IAEA [11] | EANM [12] | NEMA [13] | ACR-AAPM [14] |
|---|---|---|---|---|
| Spatial resolution | Ac, | Ac | Ac, A | A |
| Sensitivity | Ac, | Ac | Ac, A | A |
| Scatter fraction, count losses and random measurements | Ac | Ac | Ac, A | A |
| Energy resolution | Ac | Ac, D | - | Q |
| Image quality and accuracy of attenuation and scatter correction | Ac, A | Ac | Ac, A | A, Q |
| Coincidence timing resolution for TOF PET | Ac | Ac | - | - |
| Accuracy of PET/CT image registration | Ac | - | - | Q |
| PET detector stability test | D | D | - | - |
| Coincidence timing resolution tests | D | D | - | - |
| Test of PET/CT scan in clinical mode | D | - | - | - |
| Uniformity | Ac, Q | Ac | - | A, Q |
| PET normalization | Ac, M | Ac | - | - |
| 2-D–3-D Radioactivity concentration calibration | Ac, M | Ac | - | - |
| PET/CT offset calibration | Ac, Q | - | - | - |
| Routine image quality PET/CT test | Q | - | - | Q |

Ac – acceptance, A – annual, Q – quarterly, M – monthly, D – daily.

**Table 4.** Recommended tests and values for QC of radiopharmaceuticals.

| Radiopharmaceutical | Method | Limits (%) [6]* |
|---|---|---|
| $^{99m}$Tc- nanocoll | TLC | >95 |
| $^{99m}$Tc- mercaptoacetyltriglycine | TLC | >95 |
| $^{99m}$Tc-sestamibi | TLC | >94 |
| $^{99m}$Tc-macro albumin aggregated | TLC | >95 |
| $^{99m}$Tc- methylene diphosphonate | TLC | >95 |
| $^{99m}$Tc-tetrafosmin | TLC | >90 |
| $^{99m}$Tc-diethylenetriamine pentaacetic acid | TLC | >95 |
| $^{99m}$Tc-mebrofenin | TLC | >94 |
| $^{99m}$Tc-pyrophosphate | TLC | >90 |
| $^{99m}$Tc-exametazime | TLC | >80 |
| $^{99m}$Tc-octreotide | TLC | >90 |
| $^{99m}$Tc-dimercaptosuccinic acid | TLC | >95 |

***** according European Pharmacopoeia limits.

**Table 3.** Recommended tests and frequencies for QC of radionuclide calibrator.

| Procedure | IAEA [2, 15] | EANM [1, 3, 4] | AAPM [16] | NPL [17] |
|---|---|---|---|---|
| High voltage | Ac, A, M, D | Ac, A, D | Ac, A, D | Ac, A, M, D |
| Display | C, Ac, A, M, D | - | - | Ac, A, M, D |
| Zero adjustment | C, Ac, A, M, D | D | Ac, A, D | Ac, A, M, D |
| System Electronic | - | - | Ac, A, D | - |
| Physical inspection | - | D | Ac, A, D | - |
| Clock accuracy | C, Ac, A, M, D | D | Ac, A, D | - |
| Background | C, Ac, A, M, D | D | Ac, A, D | Ac, A, M, D |
| Check source response | C, Ac, A, M, D | D | Ac, A, D | - |
| Accuracy | C, Ac, A | Ac, A | Ac, A | Ac, A |
| Precision | Ac, A, M | Ac, A, M | Ac, A | Ac, A |
| Subsidiary calibrations | Ac, A | - | - | Ac, A |
| Linearity | Ac, A | A | Ac, A | Ac, A |
| Geometry | Ac | Ac | Ac | - |

Ac – acceptance, A – annual, M – monthly, D – daily

### 2.4. QC procedures radiopharmaceuticals

Recommended values for commonly used radiopharmaceuticals QC according to international recommendations are shown in Table 4. In Lithuania, most procedures are performed with $^{99m}$Tc: $^{99m}$Tc-MIBI (methoxy isobutyl isonitril sestamibi); $^{99m}$Tc-MAA (macro aggregated albumin); $^{99m}$Tc-MDP (methylene diphosphonate); $^{99m}$Tc-MAG3 (mercaptoacetyltriglycine); $^{99m}$Tc-DTPA (diethylene triamine pentaacetic acid); $^{99m}$Tc-DMSA (dimercaptosuccinic acid); $^{99m}$Tc-nanocoll; $^{99m}$Tc-tetrafosmin, $^{99m}$Tc-mebrofenin, $^{99m}$Tc-pyrophosphate, $^{99m}$Tc-HMPAO (exametazime), $^{99m}$Tc-octreotide labelled radiopharmaceuticals.

### 2.5. QC procedures for other equipment

Recommended QC procedures by different international recommendations and their periodicity for other equipment (radiation monitoring instruments: exposure meter, contamination monitor, personnel monitor; intraoperative probe; thyroid uptake probe; automatic gamma counting system) are shown in Table 5.

## 3. Results and discussion

Guidelines from different organizations (IAEA, EANM, ACR, AAMP, NPL) have different opinions about the periodicity of the routine test and what they should contain. In some recommendations (such as EANM) only the purpose and periodicity are specified, but no suggestions on how to carry out the measurements nor any limits of acceptability are given [5].

**Table 5.** Recommended tests and frequencies for QC of other equipment.

| Equipment | Procedure | EANM [1, 3, 4] |
|---|---|---|
| Radiation monitoring instruments | Physical inspection, battery voltage, background, sensitivity, accuracy, precision and linearity of response. | Ac, A |
| Automatic gamma counting system or well counters | Physical inspection, constancy, energy window calibration, energy resolution, background count rate. | Ac, A, D |
| | Linearity of energy response, counting precision, sensitivity | Ac, A, Q |
| | Efficiency | Ac, A |
| Intraoperative probe | Physical inspection, power source, energy window, energy resolution, background count, sensitivity, counting precision, linearity of count rate. | Ac, A, before use |
| | Stability, energy spectrum | Ac, A, |
| Thyroid uptake probe | Physical inspection, energy calibration and energy window setting, energy resolution, background count rate, sensitivity. | Ac, A, before use |
| | Linearity of energy response, counting precision, linearity. | Ac, A |

Ac – acceptance, A – annual, Q – quarterly, D – daily.

Meanwhile IAEA provides suggestions on how the measurements should be carried out. ACR-AAPM provides minimal recommendations for tests (PET/CT) that should be done and references other recommendations (IAEA, NEMA) where all remaining tests and their details are provided.

Discussed recommendations were published at different time, thus there is a shortage of information for modern equipment, for example in the case of equipment based on CZT detectors. In the case of radionuclide calibrator international and national recommendations for QC procedures are in general agreement in terms of procedures and periodicity of tests, such as: high voltage, zero adjustment, background, accuracy, linearity, however, for physical inspection, geometry, clock accuracy there is are no standardised requirements.

Comparison of recommended tests and periodicity for different equipment presented in Tables 1-5 showed that some QC tests should be carried out daily, weekly, before use, monthly, quarterly, half year, yearly, during acceptance and commissioning tests. Due to a plethora of different technical solutions in the equipment, standardisation of QC periodicity is complicated. Other manufacturers use different hardware and software which mandates special maintenance. Quality control procedures should follow manufacturer's defined schedule. Although it would useful to harmonize the routine procedures.

After analysing the recommendations for radionuclide calibrators, gamma cameras, PET and other equipment, it can be noted that acceptance, reference and commissioning tests may reveal a problem with a system performance before the system is accepted. Some reference and commissioning tests are simplified versions of the acceptance tests.

According to European Pharmacopoeia and IAEA recommendations, radionuclidic and radiochemical purity tests should be performed [6, 15, 18]. For $^{99m}$Tc which is eluted from $^{99}$Mo/$^{99m}$Tc generators, $^{99}$Mo breakthrough test results should be within 0.1%. For radiochemical purity thin layer chromatography (TLC) is the most commonly used method to test $^{99m}$Tc labelled radiopharmaceuticals. Aluminium breakthrough test and pH of the prepared radiopharmaceutical, should be within the acceptable range. To improve the QA of radiopharmaceuticals automated TLC systems should be used in daily practice.

To comply with all the recommendations, hospitals should have the appropriate means (phantoms, chromatography equipment, solvents etc.) and trained medical physicists, radiologists and other staff.

## 4. Conclusion

Periodicity of the QC tests should be in accordance with the manufacturer's and national/international recommendations. Comparison of recommended tests and their periodicities for different equipment and modalities demonstrated that there is a need to harmonise QC procedures. Minimum daily, weekly, quarterly, annual quality control tests should be included, in accordance with the manufacturer's schedule of quality control procedures and should be performed collectively.

In nuclear medicine, administration of correct radiopharmaceuticals' activity to the patient is strongly dependent on the accuracy of the QC measurements. First, it is very important that dose calibrators show correct activity of radiopharmaceuticals. Second, the quality of radiopharmaceuticals should be checked and meet the recommendations. Finally, patient scanning systems: gamma cameras, SPECT/CT, PET/CT should be checked and meet the manufacturers' parameters. In order to implement all recommendations, hospitals should have appropriate means. Recommendations of the IAEA and EANM describes in greater detail the QA and QC programme, thus hospitals QA should be based on these recommendations. All these steps are important to make the study of nuclear medicine effective and to protect the patient and the personnel from unnecessary radiation exposure.

## 5. References


1. Busemann Skole, E., Plachcinska A., Britte A. Acceptance testing for nuclear medicine instrumentation. Eur J Nucl Med Mol Imaging, 2010. 37:672–681.
2. Bailey D.L., Humm J.L., Todd-Pokropek A. Nuclear Medicine Physics. A Handbook for Teachers and Students. IAEA, Vienna, 2014. ISBN 978–92–0–143810–2.
3. Busemann Skole E., Plachcinska A., Britte A, Georgosopoulou M. L., Indale W., Klett R.. Routine quality control recommendations for nuclear medicine instrumentation. Eur J Nucl Med Mol Imaging, 2010. 37:662–671.
4. Rep S. Quality control of nuclear medicine instrumentation and protocol standardisation. EANM, 2017. ISBN: 978-3-902785-13-8.
5. Oddstig J., Minarik D., Gunnarsson M. Quality Control of Gamma Cameras, SPECT/CT and PET/CT Units. In: Mattsson S., Hoeschen C. (eds) Radiation Protection in Nuclear Medicine. Springer, Berlin, Heidelberg, 2013.
6. Maioli C., Lucignani G., Strinchini A., Tagliabue L., Del Sole A. Quality control on radiochemical purity in Technetium-99m radiopharmaceuticals labelling: three

years of experience on 2280 procedures. Acta Biomed, Vol. 88, 2017. N. 1: 49-56.
7. INTERNATIONAL ECTROTECHNICAL COMMISSION. Evaluation and Routine Testing in Medical Imaging Departments — Part 1: General Aspects, IEC 61223-1, IEC, Geneva, 2017.
8. IAEA Human health series No. 6. Quality assurance for SPECT systems. Vienna: International Atomic Energy Agency, 2009. STI/PUB/1394.
9. National Electrical Manufacturers Association (NEMA), Standards Publication NU 1-2012, Performance Measurements of Gamma Cameras, NEMA, Rosslyn, VA, 2012.
10. THE REPORT OF AAPM TASK GROUP 177: Acceptance Testing and Annual Physics Survey Recommendations for Gamma Camera, SPECT, and SPECT/CT Systems, 2019. ISSN: 0271-7344.
11. INTERNATIONAL ATOMIC ENERGY AGENCY, Quality Assurance for PET and PET/CT Systems, Human Health Series No. 1, IAEA, Vienna, 2009.
12. Camoni L., Rep, S., Santos A., Attard M. C.. Quality Control of Nuclear Medicine Instrumentation and Protocol Standardisation. EANM TECHNOLOGIST'S GUIDE. European Association of Nuclear Medicine, Vienna, 2017. ISBN: 978-3-902785-13-8.
13. Electrical Manufacturers Association (NEMA), Standards Publication NU 2-2012, Performance Measurements of Positron Emission Tomographs, NEMA, Rosslyn, VA, 2012.
14. National American College of Radiology. ACR–AAPM technical standard for medical physics performance monitoring of pet/ct imaging equipment. 2018. Available at: https://www.acr.org/-/media/ACR/Files/Practice-Parameters/pet-ct-equip.pdf?la=en
15. INTERNATIONAL ATOMIC ENERGY AGENCY. Quality Assurance for Radioactivity Measurement in Nuclear Medicine. No.454, Vienna, 2006.
16. Carey J., E., Byrne P., DeWerd L., Lieto R., Petry N. The Selection, Use, Calibration, and Quality Assurance of Radionuclide Calibrators Used in Nuclear Medicine. American Association of Physicists in Medicine, Report No. 181, College Park, MD., 2012. ISSN: 0271-7344.
17. Gadd R., Baker M., Nijran K.S., and ect. Protocol for establishing and maintaining the calibration of medical radionuclide calibrators and their quality control. National Physical Laboratory. Measurement Good Practice Guide No. 93, Teddington, Middlesex, UK, 2006.
18. European Pharmacopoeia Commision. European Pharmacopoeia (8th edition.). Strasbourg: Directorate for the Quality of Medicines & HealthCare of the Council of Europe (EDQM), 2013.

*MEDICAL PHYSICS IN THE BALTIC STATES 14 (2019)*

Proceedings of International Conference "Medical Physics 2019"
7 – 9 November 2019, Kaunas, Lithuania

# MEASUREMENTS TRACEABILITY THROUGH COMPARISONS: RESULTS OF FIVE RADIONUCLIDE DOSE CALIBRATORS

Kirill SKOVORODKO[1]; Arūnas GUDELIS[2]
[1]Vilnius University Hospital Santaros Klinikos, Vilnius, Lithuania.
[2]State research institute Center for Physical Sciences and Technology, Vilnius, Lithuania.
kirill.skov@gmail.com; arunas.gudelis@ftmc.lt

***Abstract*:** Number of nuclear medicine procedures is constantly growing in the world and in Lithuania as well. Correct activity of the radiopharmaceuticals, which are administered for diagnostic and therapeutic purposes, strongly depends on the accuracy of the measuring equipment used in nuclear medicine. In 2016 and 2019, Ionizing Radiation Metrology Laboratory of the Center for Physical Sciences and Technology (FTMC) performed a comparison of radionuclide calibrators in Vilnius University Hospital Santaros Klinikos Nuclear medicine department. Responses of five radionuclide calibrators that are used in daily hospital practice were compared with the reference standard - the secondary standard ionization chamber Capintec CRC-15R. Activity measurements in P6 vial and syringe geometries were fulfilled for $^{99m}$Tc, $^{18}$F, $^{123}$I and $^{137}$Cs radionuclides. In this paper, the results of intercomparison between the secondary standard radionuclide calibrator and five hospital radionuclide calibrators are presented and discussed.

***Keywords:*** Radionuclide calibrators; radionuclide; radiopharmaceutical; secondary standard chamber; nuclear medicine; traceability.

## 1. Introduction

Field of nuclear medicine continues to grow around the world, thus the safe, efficient and efficacious practice of diagnostic and therapeutic procedures involves the integration of a number of processes [1].
Correct prescribed activity of radiopharmaceuticals prior to administration to the patient is one of the most important parts of these processes. Equipment used to measure the activity is radionuclide dose calibrator (also called activity calibrator, activity meter, radionuclide calibrator and etc.) – a gas-filled ionization chamber coupled to a high voltage supply, an electrometer and a display. Such a setup is widely used due to good stability, simple service and relatively low price. In accordance with national and international recommendations and legislations, appropriate quality assurance programme should cover all clinical aspects of smooth nuclear medicine work including quality control of radionuclide calibrators. According to international recommendations, dosimetry instrumentation (including dose calibrators) should be traceable to a standards dosimetry laboratory [2].
Whereas radionuclide calibrators are not absolute assay systems, this equipment should be calibrated directly or indirectly, using standard reference sources traceable to absolute assay systems [3, 4]. Measurements with a radionuclide calibrator are susceptible to geometrical influences and container type, especially for radionuclides that are emitting beta radiation or low-energy photons (a substantial amount of self-absorption can occur) [6].
In a recent study, Vargas et al. and Bauwens et al. [5, 6] performed intercomparisons among radionuclide calibrators in hospitals and they found numerous deviations in measurements of activity value of up to 72% for certain radionuclides in syringe geometry, while the response for the syringe sample was typically 15% to 35% higher than that of the vial sample.
Radionuclide calibrators need on-site calibration and validation, because, usually this equipment is stationary fixed in hot laboratories' laminar box or other shielded mobile injectors [6].
The aim of this paper was to evaluate the deviation of measured activities by five radionuclide dose calibrators with the help of the secondary standard radionuclide calibrator.

## 2. Materials and methods

Responses of five radionuclide calibrators that are used in Vilnius University Hospital Santaros Klinikos (VUHSK) Nuclear medicine department daily practice were compared with the readings of the secondary standard radionuclide calibrator Capintec CRC-15R (4π

γ ionization chamber) brought to hospitals by the Ionizing Radiation Metrology Laboratory of the Center for Physical Sciences and Technology that is the National Metrology Institute (NMI) in Lithuania (Fig. 1).

**Fig. 1.** Secondary standard radionuclide calibrator Capintec CRC-15R.

**Fig. 2.** Standard 3 ml syringe and a vial that were used for the measurements.

Radionuclides $^{18}$F, $^{99m}$Tc, $^{131}$I, $^{137}$Cs and $^{57}$Co were selectively measured in standard geometries: in standard 3 ml syringes, P6 vials (54 mm x 21.75 mm, wall thickness 1.2 mm) and $^{57}$Co stick geometry. Ten readings of experimental values were taken with each instrument, corrections for the decay and background were applied. Then, differences between experimental mean values and reference values were determined, the deviations were calculated.

For all radionuclide calibrators the standard sample holders were used, routine quality control procedures were applied for each radionuclide calibrator before measurements. All radionuclide calibrators were synchronized to the same time.

### 2.1. Radionuclide calibrators used in comparison

For prescribed dose measurement the following instruments were used: Veenstra VDC-404, Veenstra VDC-405, COMECER ALTHEA-PC A and B PITAGORA dose calibrators, COMECER IRIDE with dose calibrator PITAGORA.

ALTHEA is an automatic fractionator with ion chamber for syringes in conjunction with wireless injection system. This system is s fully shielded hot cell with two dose calibrators. Automatic Infusion System IRIDE is a fully shielded, motorized cart with the internal dose calibrator. PITAGORA dose calibrators are used for procedures with $^{18}$F-FDG. Veenstra VDC-404 and VDC-405 are used for conventional nuclear medicine procedures with $^{99m}$Tc and $^{123}$I.

Calibration settings of the radionuclide calibrators are presented in Table 1.

### 2.2. Syringe and vial preparation

Syringes and vials with radionuclide solutions were prepared by radiology technologist in the hot laboratory (Fig. 2). $^{99m}$Tc was extracted from $^{99}$Mo/$^{99}$Tc generator and was used as $^{99m}$TcO4$^{-}$, $^{18}$F ($^{18}$F-FDG) and $^{123}$I ($^{123}$I-MIBG) were used as bought-in radiopharmaceuticals.

**Table 1.** Calibration settings of the radionuclide calibrators.

| Radionuclide calibrators model | Radionuclide | Calibration settings number and geometry |
|---|---|---|
| Veenstra VDC-404 | $^{57}$Co | 380 (stick) |
| | $^{137}$Cs | 587 (P6) |
| | $^{123}$I | 618 (P6) |
| | $^{99m}$Tc | 236 (Syringe) |
| Veenstra VDC-405 | $^{57}$Co | 380 (stick) |
| | $^{137}$Cs | 573 (P6) |
| | $^{99m}$Tc | 236 (Syringe) |
| PITAGORA A | $^{18}$F | 854.313 (P6) |
| | $^{137}$Cs | 1533.776 (P6) |
| PITAGORA B | $^{18}$F | 893.258 (P6)<br>851.163 (Syringe) |
| | $^{137}$Cs | 1603.694 (P6)<br>1528.12 (Syringe) |
| PITAGORA IRIDE | $^{18}$F | 870.471 (P6)<br>915.222 (Syringe) |
| | $^{137}$Cs | 1562.784 (P6)<br>2522.2 (Syringe) |

## 3. Results

Results of the intercomparison showed that the deviation for check sources was up to 9% for $^{137}$Cs and 1.4% for $^{57}$Co. Results of the measurements in a syringe, stick and P6 geometry are shown in Table 2.

Deviations for $^{99m}$Tc in a syringe and P6 geometries were lower than 4%; for $^{18}$F in the syringe geometry were lower than 2%, for P6 geometry a maximum deviation of 8.9% was observed only in a single measurement. Other measurements showed lower than 5% (n=5); for $^{123}$I it was lower than 2%.

Deviations for $^{57}$Co and $^{137}$Cs calibrations sources in stick and syringe geometry were within 4%; for P6 geometry - 5 out of 11 measurements were within 5-9%, other results were lower than 4%.

In the majority of measurements for all radionuclide calibrators and radionuclides - maximum deviation was lower than 10% (Fig. 3, 4).

**Table 2.** Activity measurements and deviations for different radionuclide calibrators in a syringe, stick and P6 geometry.

| **Radionuclide calibrators model** | **Radionuclide** | **Highest deviation from reference value (%)** |
|---|---|---|
| Veenstra VDC-404 | $^{57}$Co | 1.4 (stick) |
| | $^{137}$Cs | 8.0 (P6) |
| | $^{99m}$Tc | 3.6 (Syringe) |
| | $^{123}$I | 1.7 (P6) |
| Veenstra VDC-405 | $^{57}$Co | 1.3 (stick) |
| | $^{137}$Cs | 3.5 (P6) |
| | $^{99m}$Tc | 2.3 (Syringe) |
| PITAGORA A | $^{18}$F | 8.9 (P6) |
| | $^{137}$Cs | 3.3 (P6) |
| PITAGORA B | $^{18}$F | 4.8 (P6)<br>1.8 (Syringe) |
| | $^{137}$Cs | 8.9 (P6)<br>2.3 (Syringe) |
| PITAGORA IRIDE | $^{18}$F | 4.6 (P6)<br>1.1 (Syringe) |
| | $^{137}$Cs | 5.9 (P6)<br>4.0 (Syringe) |

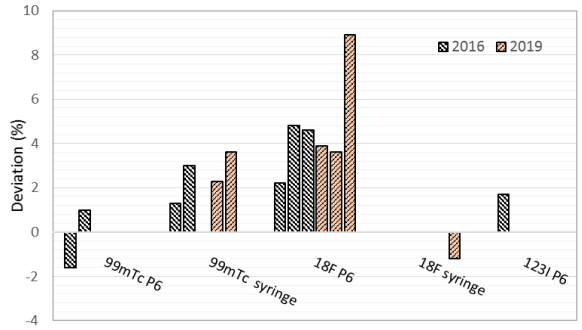


**Fig. 3.** Results of deviations for diagnostic radionuclides.

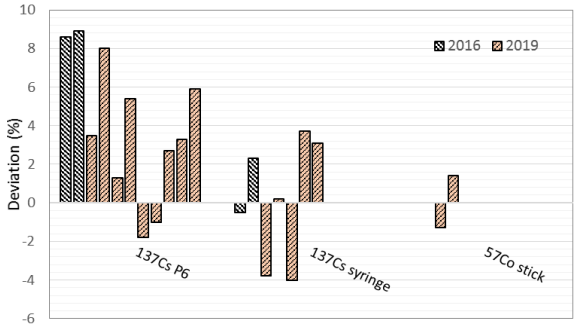


**Fig. 4.** Results of deviations for calibration isotopes.

## 4. Discussion

Measurement deviations for diagnostic radionuclides were generally lower than 5% for radionuclide calibrators. Only a single radiopharmaceutical had a deviation as high as 9% for P6 geometry.

Nevertheless, a few measurements showed that some dose calibrators underestimated the activity by less than 2% for diagnostic radionuclide and up to 4% for calibration source.

The intercomparison of measurements with secondary standard reference chamber and traceable radioactive sources could identify problems in the accuracy of measurements done by the radionuclide calibrators in the hospitals, especially for different source geometries at low energy and/or low activities. Our results revealed that regular tests of radionuclide calibrators is necessary in order to meet the recommendations to be within 5% (at $k$ = 2 level) of the reference values for the therapeutic radionuclides and within 10% of the prescribed dosage for diagnostic procedures [2, 4].

## 5. Conclusion

An appropriate quality management programme, traceability of measurements (reference instrument calibrated against standardised reference sources traceable to the National Metrological Institute) are necessary to ensure the accuracy of the administered patient dose. The quality of nuclear medicine procedures is dependent on the accuracy of dose calibrators besides other factors such as quality control procedures of hybrid imaging equipment, radiation protection of both patients and staff, radiopharmaceutical preparations and total quality management. Correct measurement of administered activity in different geometries is important for imaging, patient dose optimisation, setting the local diagnostic reference levels, administration of beta emitters and for measurement of activity for quantitative imaging in molecular radiotherapy (activity-time integral within the defined volume) [5, 6].

Measurement accuracy of five radionuclide calibrators from two different manufacturers (PITAGORA, Veenstra) in two geometries showed that the deviations are not exceeding the limits recommended in national and international guidelines.

A comprehensive quality assurance programme with calibration sources could help minimize potential deviations in administered dosages.

## 6. References

1. International Atomic Energy Agency. Quality Assurance For Radioactivit Measurement in Nuclear Medicine No. 454, Vienna, 2007.
2. International Atomic Energy Agency. Radiation Protection and Safety in Medical Uses of Ionizing Radiation No. SSG-46, Vienna, 2019.
3. Gadd R., Baker M., Nijran K.S., and ect. Protocol for establishing and maintaining the calibration of medical radionuclide calibrators and their quality control. National Physical Laboratory. Measurement Good Practice Guide No. 93, Teddington, Middlesex, UK, 2006.
4. Carey J., E., Byrne P., DeWerd L., Lieto R., Petry N. The Selection, Use, Calibration, and Quality Assurance of Radionuclide Calibrators Used in Nuclear Medicine. American Association of Physicists in Medicine, Report No. 181, College Park, MD., 2012. ISSN: 0271-7344.
5. Vargas C., S., Pérez S., R., Baete K., Pommé S., Paepen, J., Van Ammel R., Struelens L. Intercomparison of 99mTc, 18F and 111In activity measurements with radionuclide calibrators in Belgian hospitals. Physica Medica. 45, 2018. p. 134-142.
6. Bauwens M., Pooters I., Cobbe R., Visser M., Schnerr R., Mottaghy F., Wildberger J., Wierts R. A comparison of four radionuclide dose calibrators using various radionuclides and measurement geometries clinically used in nuclear medicine. Physica Medica 60, 2019. p. 14-21.

*MEDICAL PHYSICS IN THE BALTIC STATES 14 (2019)*

Proceedings of International Conference "Medical Physics 2019"
7 – 9 November 2019, Kaunas, Lithuania

# A ROAD-MAP FOR THE DEVELOPMENT OF THE REFERRAL GUIDELINES FOR DIAGNOSTIC IMAGING IN THE RUSSIAN FEDERATION

Aleksandr VODOVATOV[1], Sergey RYZHOV[2], Zoya LANTUKH2, Kirill TOLKACHEV[2], Sergey MOROZOV[2]
[1]Research Institute of Radiation Hygiene, Mira str. 8, 197101 St. Petersburg, Russian Federation; [2]Research and Practice Centre of Diagnostics and Telemedicine Technologies, Raskovoy st., 16/26-1, 125124, Moscow, Russian Federation.
vodovatoff@gmail.com; s.ryzhov@npcmr.ru

***Abstract*:** A practical implementation of the justification of medical exposure is based on the use of referral guidelines for medical imaging. The current study is focused on the evaluation of the existing status of the justification of the medical exposure in the Russian Federation as well as the process of development of the regional referral guidelines. Presented road-map allows predicting first feedback from practical implementation of referral guidelines in 2021.

***Keywords*:** medical exposure, justification, referral guidelines, medical imaging

## 1. Introduction

Justification is one of the main and fundamental principles of radiation protection in medicine. According to ICRP Publications 103 [1], IAEA BSS GSR part 3 [2] and Specific Safety Guide SG-46 [3], the diagnostic or therapeutic benefits of exposure should be weighed against the radiation detriment they might cause, with account taken of the benefits and risks of available alternative techniques that do not involve medical exposure. Application of the justification principle to medical exposure requires a special approach, using three levels (the three-level approach). As an overarching justification of medical exposure, it is accepted that the proper use of radiation in medicine does more good than harm (level 1). At the next level (level 2), generic justification of a given radiological procedure should be carried out by the health authority in conjunction with appropriate professional bodies. For the final level of justification (level 3), the application of the radiological procedure to a given individual patient including the specific objectives of the exposure, the clinical circumstances and the characteristics of the individual involved should be considered.

It should be emphasized that the responsibility for the implementation of the principle of justification belongs to the health authorities, operating jointly with the relevant professional bodies. In practice, justification is implemented through sets of guiding documents, that related various ionizing (IR) and non-ionizing (non-IR) imaging modalities with the clinical indications/pathologic syndromes. In that case the considerations of the health authority (Ministry of Healthcare) may differ from the considerations of the radiation protection authorities. The list of imaging modalities, recommended by the health authority would be sorted based on 1) availability of the equipment and technologies; 2) expenses per examination (especially for the countries with wide coverage with governmental health insurance); and 3) diagnostic efficiency. On the other hand, radiation protection authorities would prioritize the imaging modalities that are not associated with ionizing radiation (US, MRI, etc.) or the modalities with the least radiation doses (detriment). Additionally, performing a proper risk-benefit analysis [4] is complicated, as the data on the complications and side-effects for the different diagnostic protocols is limited or unavailable. Hence, the development of the guiding documents (referral guidelines, clinical decision support, etc.) is complicated.

In the Russian Federation the principle of the justification is integrated into the main legislative documents: Federal state law FZ-3 [5], Norms of the Radiation Safety [6], Basic sanitary rules for the provision of the radiation safety, guidelines on radiation protection for different imaging modalities. According to these documents, medical exposure should be justified considering the clinical indications, the use of the imaging modalities with the lowest doses and the use of alternative (non-radiation) diagnostic methods. Justification of the imaging is considered to be a responsibility of the medical staff, but it assessed by the radiation protection authorities.

The approach of the Russian radiation protection authority (Rospotrebnadzor agency) towards the justification was based on the assessment of the radiation risks from medical imaging. That approach was backed up with prevalent use of effective dose as a main dose

quantity in radiation protection in medicine. In 2015 Methodical guidelines "Assessment of radiation risks for the patients undergoing diagnostic examinations with the use of ionizing radiation" [7] were developed and published by the Institute of Radiation Hygiene. These guidelines included the lists of different imaging modalities and examinations, divided according to the categories of radiation risk for three age groups (children under 18 years, adults 18-64 years and older persons older than 65 years). However, this document was seldom used in clinical practice since it was not harmonized with the existing clinical standards and assessments of the radiation risk (even in the simplest form) were complicated for the medical staff.

In 2017 the activities related to the justification of medical imaging were supplemented within the project "Practical arrangements between Rospotrebnadzor and IAEA", task 2 "Justification of medical imaging".

Responsibilities of Rospotrebnadzor and Institute of Radiation Hygiene included the evaluation of the existing structure of Russian justification-related documents of the Ministry of Healthcare and the development of the proposals for their improvement from the point of the radiation protection.

Hence, the current study was aimed at the analysis of the existing situation in the Russian Federation with the justification of medical imaging and evaluation of the possible strategies for the development and implementation of the referral guidelines for medical imaging.

## 2. Materials and methods

During 2017-2018 an analysis of the existing regulative documents of the Ministry of Healthcare was performed by the Institute of Radiation Hygiene in collaboration with the St-Petersburg Radiological Society. The summary is presented in Table 1.

**Table 1.** Comparison of the existing regulative documents related to the justification of medical exposure.

| Category of document | Developer | Objective | Actuality | Evidence-based medicine | Radiation protection data | Status |
|---|---|---|---|---|---|---|
| Clinical standards | Ministry of healthcare | Basic standards of diagnostics and treatment | Outdated | - | - | Mandatory |
| Medical-economical standards | Regional healthcare authorities | Regional standards of diagnostics and treatment | Outdated | - | - | Mandatory |
| Recommendations of the professional bodies | Professional clinical associations | Decision-making support | Actual | + | - | Voluntary |
| Clinical recommendations of the Ministry of Healthcare | Ministry of healthcare + Professional clinical associations | Standards + decision-making support | Actual | + | - | Mandatory |

Each category contains several (up to 100) stand-alone documents specific for the given disease/syndrome/pathology. The base of the justification-related documents is formed by the orders of the Ministry of Healthcare, that contain the list of basic diagnostic procedures, including X-ray diagnostics. These diagnostic procedures are fully covered by the Federal Mandatory Medical Insurance (FMMI). It should be noted, that orders contain two indicators: frequency of admission (how many patients may receive that procedure) and mean number of procedures per hospital stay. Medical-economical standards are developed based on the existing orders, on the regional level, considering the actual capabilities of the local healthcare system (availability of imaging modalities and coverage by the FMMI). These two categories do not contain evidence-based medicine principles and are outdated (contain no modern diagnostic imaging modalities). However, they are being gradually replaced with the clinical recommendations of the Ministry of Healthcare, which are mandatory as well, but are based on the evidence-based medicine. Clinical recommendations of the professional bodies (for example, Russian society of oncologists, pulmonologists, etc.) exist as additional stand-alone documents, based on the evidence-based medicine as well. However, they are not fully covered by FMMI.

These categories of documents inherit several significant drawbacks, judging from the point of radiation protection in medical imaging.

First, the selection of the proper procedure (imaging modality in particular) is based mainly on the economic factors (availability of the equipment, price of examination, coverage by state insurance, etc.). Hence, they contain no information on the radiation detriment

(risk) for the available imaging modalities. This factor is seldom considered.

Second, the majority of documents is outdated and the modern diagnostic methods (MRI, SPECT/CT, PET/CT, etc.) are not included.

Third, all the documents were developed by clinicians, without considering the radiologists professional bodies. Additionally, all these documents cover all diagnostic methods (functional and laboratory diagnostics, medical imaging). Hence, it is not practicable to update them considering the requirements of the system of the radiation protection in medicine.

## 3. Results

A possible solution was to use the international referral guidelines/clinical decision support system (ACR Appropriateness Critera [8], iRefer [9], iGuide [10], etc.), translate them and to implement into the existing radiological practice. However, the availability of the equipment and clinical standards differ in different countries. Hence, the referral guidelines from the USA or UK had to be significantly adopted considering the features of the Russian medical imaging.

The translation of iRefer guidelines was performed by the specialists of Diagnostics and Telemedicine Centre, Moscow, in collaboration with the Russian Society of Radiology for use in Moscow and Moscow region in form of methodical recommendations (guidelines) "The Best practices of X-ray and instrumental diagnostics". These guidelines were developed by the radiologists for referral physicians and available in printed form since 2018 [11]. The guidelines cover the diagnostics of the pathologies of urinary tract, gastro-intestinal tract, chest, muscular-skeletal system and central nervous system for adult patients. The structure of guidelines includes the list of symptoms/syndromes with their ICD-10 code; list of possible imaging modalities; their priority (primary, additional or not recommended) and brief description of the indications.

To consider the radiation protection requirements and to keep the structure of the document as simple as possible, the existing structure was supplemented with the data on the categories of the radiation risk and range of typical patient doses for adult (18-65 years) and elderly (older than 65 years) patients. Example of an updated structure of the guidelines is presented in table 2.

**Table 2.** Example of the referral guidelines for the diagnostics of acute abdominal pain.

| Syndrome/symptom | ICD-10 code | Imaging modality | Priority | Description | Category of radiation risk [7] | | Typical dose range, mSv [7] |
|---|---|---|---|---|---|---|---|
| | | | | | Adults | Elderly persons | |
| Acute abdominal pain | R10 R19-3 | Ultrasound | Primary method | * | - | - | - |
| | | Computed tomography | Additional method | * | Low ☢☢☢☢ | Very low ☢☢☢ | 2-20 |
| | | Radiography of the abdomen | Additional method | * | Very low ☢☢☢ | Negligible ☢☢ | 0,2-2 |
| | | MRI | Additional method | * | - | - | - |
| ***Existing part*** | | | | | ***Additional part*** | | |

* Not included in this manuscript

The update of the first guidelines for the diagnostics of the pathological conditions and diseases of the chest was completed in 2019. Currently they are under a review of the Moscow radiological society. The following roadmap for the final process of implementation of the referral guidelines was developed in 2019, including the following steps.

- An update of other guidelines from the set "Best practices of X-ray and instrumental diagnostics" – to be finished before the end of 2019;
- A review of the full set of the proposed referral guidelines by the members of Russian Radiological Society – to be completed in 2020;
- An implementation of the referral guidelines into clinical and radiological practice in Moscow – starting from the end of 2020;
- A Feedback from practitioners and finalization of the referral guidelines – to be finished in 2021;

At the same time, it was proposed to present the referral guidelines to the professional radiological societies in other cities and regions of the Russian Federation for consideration of implementing them in local clinical and radiological practice as well. The whole process of development is scheduled for 3 years.

## 4. Discussion

The proposed solution for the development of the referral guidelines was selected as relatively a fast and efficient way to introduce the consideration of radiation risks from medical imaging to clinicians and radiologists. The referral guidelines are developed on the base of the existing document that is used in medical facilities in Moscow. The data on the radiation risks is presented in the clear and simple way which is harmonized with the existing referral guidelines and/or clinical decision support systems. Hence, the existing documents can be updated in a short time.

However, the proposed approach has several significant drawbacks from both the clinical and radiation protection points of view. First, it is impracticable to use the data on radiation risk (detriment) as a stand-alone factor for the justification of the medical imaging. As it was mentioned before, justification should be based on a calculated risk-benefit ratio, prioritizing imaging modalities with the high diagnostic effectiveness and corresponding low probability of false-positive or false-negative outcomes. The radiation risks should be weighed against the risk of development of complications and/or side-effects when selecting different strategies for X-ray diagnostics. Additional factors are the availability of the imaging modalities in a region/city/hospital, the price of the examination and the coverage of the selected imaging modality by the insurance. All this data is hard to obtain. Data on sensitivity and specificity of the imaging modalities is available at the ACR web-portal, but the possibility to use it for the regional clinical practice in the other country is questionable.

Second, the referral guidelines should be used in clinical practice. It means, that the presented information should be harmonized with the existing clinical standards, including coverage by the state insurance and, what is more important, should be included into the education and training programs of the healthcare professionals. Otherwise the guidelines would be seldom used. It should be noted, that referral guidelines present the typical (average) diagnostic strategies, leaving the possibility to use other methods if needed and justified.

Third, the existing set of guidelines "The best practices of X-ray and instrumental diagnostics" [11] and the updated referral guidelines were developed for Moscow – the city with the best imaging equipment in Russia. For example, in 2017 more than 10% of all CT and 15% of all interventional examinations in Russia were performed in Moscow. Other regions, especially rural, have significantly lower availability of modern equipment (CT, nuclear medicine, etc.). Hence, the possibilities of directly implementing the developed guidelines in other regions/cities are under discussion.

## 5. Conclusions

The development of referral guidelines is a complicated process. The guidelines should consider the specifics of national or regional healthcare and radiological practice, include updated list of imaging modalities, comply to the principles of evidence-based medicine and at the same time be simple and user-friendly. The presented approach to the development of the regional referral guidelines was selected as relatively fast and efficient way to introduce the consideration of the radiation risks from medical imaging to clinicians and radiologists. The developed roadmap allows receiving a feedback and the testing the proposed concept within a short time, presenting a basis for future updates. Successful integration of the concept of justification into existing clinical environment would allow harmonizing Russian and international radiological practices.

However, there are several important issues to consider for the successful implementation of referral guidelines: complexity of estimation of the proper risk-benefit ratios; motivation for the physicians and radiologists to use the guidelines; and differences in practices and equipment between different regions in a big country. These issues should be discussed during the process of development and post-feedback update of the referral guidelines.

## 6. References


1. International Commission of Radiological Protection. The 2007 Recommendations of the International Commission on Radiological Protection. ICRP publication 103. Ann. ICRP 37, 1-332 (2007).
2. International Atomic Energy Agency. Radiation Protection and Safety of Radiation Sources: International Basic Safety Standards. GSR Part 3. Vienna: IAEA, 518 p. (2015).
3. International Atomic Energy Agency. Radiation Protection and Safety in Medical Uses of Ionizing Radiation. Specific Safety Guide №SSG-46. – Vienna: IAEA, 340 p. (2018).
4. M.Moores. Cost–risk–benefit analysis in diagnostic radiology: A theoretical and economic basis for radiation protection of the patient. Rad. Prot.Dos. (2015). doi:10.1093/rpd/ncv506
5. Russian Federal State law №3-FZ "On Radiation Safety of the Public". 09.01.1996, (1996). Available from (in Russian): http://kremlin.ru/acts/bank/8724
6. Sanitary rules and norms. SanPiN 2.6.1.2523-09. Norms of the radiation safety (NRB 99/2009). Registered in the Ministry of Justice of the Russian Federation 14.08.2009 N 14534. Available from: http://www.consultant.ru/document/cons_doc_LAW_90936/ Last accessed 11.09.2018.
7. Methodical guidelines "Assessment of the radiation risk of the patients from diagnostic X-ray examinations" MR 2.6.1.0098-15. Available from: http://niirg.ru/PDF/MR-2.6.1.0098-15.pdf
8. ACR Appropriateness Critera. Available from: https://acsearch.acr.org/list
9. iRefer. Making the best use of clinical radiology. Available from: https://www.irefer.org.uk/
10. ESR iGuide. Available from: https://www.myesr.org/esriguide
11. Guidelines "Best practices of X-ray and instrumental diagnostics". Available from: http://medradiology.moscow/mr

*MEDICAL PHYSICS IN THE BALTIC STATES 14 (2019)*

Proceedings of International Conference "Medical Physics 2019"
7 – 9 November 2019, Kaunas, Lithuania

# FEATURES OF THE PERCEPTION OF RADIATION RISKS BY RUSSIAN RADIATION SAFETY SPECIALISTS

Artem DAVYDOV, Artem BIBLIN, Leonid REPIN, Nadezhda VISHNYAKOVA, Alexandr VODOVATOV
Research Institute of Radiation Hygiene after P.V. Ramzaev, Saint-Petersburg, Russia
a.davidov@niirg.ru, a.biblin@niirg.ru, n.vishnyakova@niirg.ru, a.vodovatov@niirg.ru

***Abstract:***
An assessment of the subjective perception of radiation risks by experts working in the field of radiation protection is important as they play a major role in the risk-communication with public. 138 experts were interviewed using a dedicated questionnaire on their attitude to the radiation risk. A significant differences were estimated between groups of experts divided by the work experience, gender and education in their perception of radiations risks and preferable radiation safety theories.

***Keywords:*** risk perception, radiation risk, risk communication, low doses of ionizing radiation.

## 1. Introduction

Radiation safety experts play a major role in the process of the risk communication on radiation accidents and biological effects of the ionizing radiation. A risk communication can be defined as "an interactive process of sharing information and opinions about risks between risk assessors, decision - makers, the media, interest groups and the general public [5]. Specialists in the field of radiation safety are one of the parties involved in the process of risk communication, so their attitudes may have a direct impact on changing attitudes on the risk perception of other people and their behaviour. Their opinions are considered by journalists, public figures and the general public. Additionally, among the experts themselves, there is no consensus on a number of issues.
Aim of the study was to assess the possible impact of specialists' attitude on the risk communication process.
The objectives of the study were to determine the commonality of attitudes of experts on radiation risk and comparison the obtained results with the results of surveys among the public.
The experience of recent radiation accidents showed that experts in post-soviet countries would be required to have risk communication skills to ensure radiation protection of the population and at the same time to reduce radioanxiety.
In other studies, on radiological risk perception by experts, Perko et. al. [1] indicated the discrepancy between experts and the public in the perception of risks associated with nuclear waste, medical X-ray exposure, accidents at nuclear facilities, natural radiation. Ki Moong Seong et. al. [8] argued that risk perception of low dose radiation exposure (several microsieverts) inversely correlated with the amount of working experience. These authors as well as Sjoberg [10], Slovic [11] mentioned that opinions of experts on radiation are very important to public.
It should be noted that the linear no-threshold theory of the effect of low doses of ionizing radiation on human health forms the basis of the modern system of radiation protection [2]. Following this theory, the likelihood of negative health effects associated with the effects of low doses of ionizing radiation for an individual or his offspring is directly proportional to the dose of radiation. However, there are not only no-threshold theory in radiation safety. There are others: hormesis, threshold theory and superlinear theory. Different scientists are supporters of different theories. We have an assumption that experts who adhere to the threshold theory or hormesis will underestimate the effect of the radiation on the body and do not warn journalists and the public about the possible danger in case of a slight excess of the radiation background.

## 2. Materials and methods

A questionnaire survey of the conference participants was held within the framework of the international scientific-practical conference "Current Issues of Radiation Hygiene" held in St. Petersburg October 22–24, 2018. The survey involved 138 specialists (67 men, 69 women; 2 n/a) in the field of radiation safety. A detailed description of the sample is presented in table 1. Rospotrebnadzor is the federal service responsible for the supervision of consumer rights protection and human wellbeing in Russia. Regulators of this organization are responsible for administrative work, inspectors – for laboratory measurements and radiation control.

**Table 1.** Data on sample, %

| **Place of work** | | | |
|---|---|---|---|
| Regional offices of Rospotrebnadzor (Regulators) | Hygienic and Epidemiological Centers of Rospotrebnadzor in regions (Inspectors) | Research Institutes (Scientists) | Other/ Missing |
| 26.1 | 31.2 | 32.6 | 10.1 |
| **Education** | | | |
| Medical and Biological | Physical and Technical | Liberal arts | Missing |
| 65.2 | 26.8 | 5.8 | 1.4 |
| **Experience in the field of radiation protection** | | | |
| < or =5 years | >5 years | Missing | |
| 22.5 | 71.7 | 5.8 | |
| **Sex** | | | |
| Male | Female | Missing | |
| 48.6 | 50.0 | 1.4 | |

To study the attitudes of radiation safety specialists, three hypotheses were formulated:

1. A positive attitude to the development of nuclear energy is predominant among specialists in the field of radiation safety.
2. A significant proportion of specialists adhere to the threshold theory of the effect of radiation on a person or the theory of radiation hormesis.
3. Different categories of specialists perceive small doses of radiation differently. Specialists perceive non-radiation risks as "existing" i.e. as inalienable living conditions, so the experts will base their recommendations regarding radiation risks on ignoring risk competition.

To test the stated hypotheses, we used direct questions on the first (closed question) and second (semi-closed question) hypotheses.

1. In your opinion, what types of energy should be developed in the Russian Federation, and what ones should be banned/prohibited, if possible?
2. In the modern radiation protection system, a linear no-threshold hypothesis is used to assess the effects of low doses of ionizing radiation on human health. This hypothesis is not confirmed, but not refuted. What the existing hypotheses do you personally prefer? Please choose one answer.

To test the third hypothesis, we suggested that respondents advise their friends the best vacation spot for their child. The question was:

3. The average annual individual effective dose of anthropogenic radiation for residents of a village located in the territory subjected to radioactive contamination due to the accident at the Chernobyl nuclear power plant is three mSv. Your good friends living in the city said that they want to send their primary school child to the grandmother living in this village for the summer and ask you for advice. Please choose which one of the proposed options most accurately reflects your point of view.

To answer the third question, we developed two types of questionnaires, differing in the list of answer options.

In the first version contained the following answer options:

1. It is safe;
2. A fairly safe with certain security measures;
3. Radiation doses are small, but it is a better to find another place;
4. I do not want to take a responsibility for health;
5. I do not understand much about this issue;
6. Other;

The second version of the questionnaire included additional answers: "it is safer than staying in the city for the summer". Hence, the second version of the questionnaire contained a hint about a possible competition of risks.

Additionally, we asked respondents about their fears of radiation and other types of risks (we used a list of risks from Sjoberg et. al. [9]) and rights of the authorities to restrict access to the information in case of a radiation emergency.

## 3. Results and its discussion

The analysis of sociological data on the issue of the prevalence of a positive attitude towards the development of nuclear energy indicated that among all categories of specialists, the prevailing view is the need to develop nuclear energy. 68.8% of respondents expressed support for the development of nuclear energy. More women experts believe that nuclear energy should be reduced (27% versus 7.8% among men, significance of chi-square is 0.04).

For the second question 63% of respondents chose the linear-threshold hypothesis, 17.4% chose radiation hormesis, 10.1% noted the threshold hypothesis and 2.2% - superlinear, 5.8% of respondents did not answer this question. The distribution of answers by groups of respondents is presented in table 2. There were no statistically significant differences between groups. Significant number of experts do not adhere to the conventional theory (27%).

**Table. 2.** Preferences in radiation safety theories, %

| **Group/theory** | **Linear no-threshold** | **Hormesis or Threshold** |
|---|---|---|
| **Sex** | | |
| Male | 63.3 | 36.7 |
| Female | 77.8 | 22.2 |
| **Place of work** | | |
| Regulators | 64.5 | 35.5 |
| Inspectors | 70.7 | 29.3 |
| Scientists | 67.5 | 32.5 |
| **Education** | | |
| Medical and Biological | 70.0 | 30.0 |
| Physical and Technical | 62.9 | 37.1 |
| Liberal arts | 85.7 | 14.3 |
| **Experience in the field of radiation protection** | | |
| < or =5 years | 65.5 | 34.5 |
| >5 years | 70.5 | 29.5 |

For the third question 44.2% of survey participants would recommend finding another place to rest, 23.2% described the place of rest as safe, subject to protection

measures, 16, 7% chose not to take responsibility for the health of another child and 9.4% summing over two options of the questionnaire consider such a vacation quite safe (i.e. they chose the answer “it's safe” and “it's safer than staying for the summer in the town"). However, only four people out of 61 who filled out the second version of questionnaire chose an additional answer. For analysis, we combined first three answers options in one category “safe”. We estimated statistically significant difference in answers between women and men (Fisher exact test = 0.42), experts with different education background (significance of chi-square is 0.013), experience in the radiation safety (significance of chi-square is 0.05), from the various place of work (significance of chi-square is 0.00). (Table 3.) On the other jand, experts with more experience (>5 years) selected “safe” options more frequently (42.5% versus 12.5% for less experienced experts) (significance of chi-square is 0.005).

**Table 3.** Recommendation for sending a child to the village, %

| **Group** | **Safe** | **It’s better to find another place** | **Don’t want to take responsibility** |
|---|---|---|---|
| **Sex** | | | |
| Male | 42.2 | 46.9 | 10.9 |
| Female | 25.4 | 49.2 | 25.4 |
| **Place of work** | | | |
| Regulators | 23.5 | 73.5 | 2.9 |
| Inspectors | 18.9 | 59.5 | 21.6 |
| Scientists | 52.3 | 20.5 | 27.3 |
| **Education** | | | |
| Medical and Biological | 31.8 | 56.5 | 11.8 |
| Physical and Technical | 44.1 | 23.5 | 32.4 |
| Liberal arts | 42.9 | 42.9 | 14.3 |
| **Experience in the field of radiation protection** | | | |
| < or =5 years | 12.5 | 68.8 | 18.8 |
| >5 years | 42.7 | 39.3 | 18.0 |

Women were less likely to take responsibility for the health of someone else's child compared to men. Medical experts more worry about the health of the child and advise you to avoid traveling to the village compared to physical experts. Experts with more solid experience are more likely to say that staying in the village is more or less safe.

Only one-third of the experts denied the authorities the right to restrict information in the event of a radiation accident. This share less by the factor of two compared to the public or young professionals [7]. (Table 4). Hence, we can expect that some experts would not inform the public on accidents in some situations, for example, to avoid panic if they think it would be more dangerous than a lack of information. In addition, experts are less afraid of the risk of exposure to ionizing radiation than medical students (average score for experts is 3.4 versus 3.8 for medical students, Likert-scale: 1 – not afraid at all, 5 – very afraid).

At the present stage, this is the first survey of Russian expert’s attitudes towards radiation risks. Moreover, we have a different focus in our study.

**Table 4.** Answers to a question: **“**Do the authorities have the right to restrict access to the information on radiation and nuclear accidents”, %

| **Answer option/groups** | **Public (Arkhangelsk region) (n=802)** | **Young medical professionals (n=121)** | **Experts in radiation safety (n=138)** |
|---|---|---|---|
| Certainly yes | 4.2 | 4.1 | 13.8 |
| Rather yes | 4.2 | 0.8 | 4.3 |
| It make sense in some situations | 5.6 | 22.3 | 35.5 |
| Rather not | 9.8 | 8.3 | 15.2 |
| Absolutely not | 72.2 | 63.6 | 29.0 |
| It’s hard to say, I don’t know | 3.9 | 0.8 | 2.2 |

We asked experts about their preferred theories about the effect of small doses on health, asked for advice on sending a child to a village on the radiation-contaminated territory, and asked about the authorities' right to restrict public access to information in case of a radiation accident. As you can see, the questions have a strong post-soviet specificity.

The limitation of the study is the inability to assess the real reasons for selecting different answers by the experts. A qualitative sociological study is required to answer this question. Additional expert interviews and roundtables are planned to further investigate the presented questions.

The results of the study indicated that 20-30 percent of experts chose sub-optimal (biased or contradictive to the basic principles of radiation safety) answers. That indicates the need for additional training of experts in risk communication.

The impact of experts' attitudes on effects of low doses of ionizing radiation on human health to decision-making process requires further research.

Most of the professionals were civil servants. For further research is important to assess the attitudes on radiation risk among nuclear industry, military and paramilitary specialists.

The results obtained during the research would be used in the planning of measures to improve the knowledge of specialists in the field of risk communication.

## 4. Conclusions

In the study, Russian radiation safety experts were interviewed about their attitudes towards radiation exposure and nuclear energy. The following results were obtained:

1. The results of the study confirmed the predominance of support for the development of nuclear energy by specialists in the field of radiation safety for all groups of professionals.
2. Although the majority of respondents are inclined to the linear no-threshold theory of low-dose exposure, a significant number of specialists (27.5% of respondents, i.e. 29.2% of those who answered this question) share the opinion that the threshold theory or the theory of radiation hormesis.
3. There were significant differences in attitudes on the low doses of radiation exposure between scientists

and practitioners in the matter of practical recommendations in a simulated situation of the impact of ultralow (up to 10 mSv) doses of ionizing radiation on children. These differences were reflected as well in the theories about the effects of low doses of radiation on health.

4. The study confirmed the relevance of analysis of the perception of radiation risks by different categories of specialists. Hence, it is necessary to develop practical recommendations on risk communication between specialists and identifying possible risk-communication scenarios of specialists with representatives of other stakeholders depending on the nature of the facilities of the participating specialists.
5. Despite the expert status of the respondents, gender had an impact on respondents' perception of radiation risks. This is confirmed by previous studies among general public in different countries [5, 6, 7], which suggest that females are more anxious on radiation risks. Females are more likely to avoid responsibility in the matter of sending a child to the village. Among them, there are less individuals who believe that it is safe and more who believe that nuclear energy should be prohibited.
6. Significant differences were estimated between the public and experts regarding the assessment of the risk of exposure to radiation exposure and the authorities' right to restrict information.

## 5. References


1. Pero, T. (2014). Radiation risk perception: a discrepancy between the experts and the general population. Journal of Environmental Radioactivity, 133, 86–91. doi:10.1016/j.jenvrad.2013.04.005
2. ICRP, 2007. The 2007 Recommendations of the International Commission on Radiological Protection. ICRP Publication 103. Ann. ICRP 37 (2-4).
3. Sandman P.M. Responding to community outrage: Strategies for effective risk communication AIHA, 1993.
1. Regulations on the Unified state system of control and accounting of individual doses of radiation of citizens – M., 2000. (In Russian).
4. Arikawa, H., Cao, Y., & Matsumoto, S. (2014). Attitudes toward nuclear power and energy-saving behaviour among Japanese households. Energy Research & Social Science, 2, 12–20. doi:10.1016/j.erss.2014.04.002
5. Siegrist, M., Sutterlin, B., & Keller, C. (2014). Why have some people changed their attitudes toward nuclear power after the accident in Fukushima? Energy Policy, 69, 356–363. doi:10.1016/j.enpol.2014.02.026
6. Roh, S.; Jin, W.L. Differentiated influences of risk perceptions on nuclear power acceptance according to acceptance targets: Evidence from Korea. Nucl. Eng. Technol. 2017, 49, 1090–1094.
7. Davydov. A.A. Informing the public in the event of an accident at a nuclear facility as an ethical problem: public opinion against the opinion of experts // Actual problems of humanitarian and social research, Novosibirsk. 2019. (In Russian) Manuscript submitted for publication.
8. Seong, K. M., Kwon, T., Seo, S., Lee, D., Park, S., Jin, Y. W., & Lee, S.-S. (2017). Perception of low dose radiation risks among radiation researchers in Korea. PLOS ONE, 12(2), e0171777. doi:10.1371/journal.pone.0171777
9. Sjoberg, L., & Sjoberg, B. M. D. (2009). Public risk perception of nuclear waste. International Journal of Risk Assessment and Management, 11(3/4), 264. doi:10.1504/ijram.2009.023156
10. Sjöberg, L. (1998). Risk Perception: Experts and the Public. European Psychologist, 3(1), 1–12. doi:10.1027/1016-9040.3.1.1
11. Slovic, P. (2012). The perception gap: Radiation and risk. Bulletin of the Atomic Scientists, 68(3), 67–75. doi:10.1177/0096340212444870

*MEDICAL PHYSICS IN THE BALTIC STATES 14 (2019)*

Proceedings of International Conference "Medical Physics 2019"
7 – 9 November 2019, Kaunas, Lithuania

# DIAGNOSTIC REFERNCE LEVELS AND PATIENT DOSES FOR ADULT PATIENTS IN CONVENTIONAL X-RAY EXAMINATIONS IN LATVIA

Agnese KATLAPA, Emils ZALCMANIS
Radiation Safety Centre of State Environmental Service of Latvia
agnese.katlapa@gmail.com; emils.zalcmanis@gmail.com

***Abstract*:** The purpose of this paper is to present a national survey that was performed in Latvia for the establishment of national Diagnostic Reference Levels (DRLs) for the most common adult x-ray examinations. Dose-area product (DAP) values were collected from 53 x-ray machines from different medical institutions in Latvia. Also, the effective dose to the patient was estimated. The preliminary national DRLs were generally comparable with values from similar studies. A Large variation of the DAP values among medical institutions was observed.

***Keywords*:** Conventional x-ray, diagnostic reference levels, dose, radiation safety, DAP-meter, effective dose

## 1. Introduction

Quite a large and increasing number of conventional x-ray examinations are performed every year. The contribution to the effective dose to the European population of conventional x-ray examinations in comparison with other common diagnostic radiology techniques (computed tomography, fluoroscopy and interventional radiology) is estimated at 23% [1]. Therefore, optimization of patient radiation protection is very important. One of the tools for the optimization is diagnostic reference levels (DRLs) which were defined in European Council Directive 97/43/EURATOM as dose levels in medical radiodiagnostic practices for typical examinations for groups of standard-sized patients or standard phantom for broadly defined types of equipment [2].

Currently, there are established DRLs for conventional radiography in the legislation of Latvia. They are published in Cabinet Regulations No 482 "Regulations Regarding Protection Against Ionizing Radiation in Medical Exposure" (entry into force 01.10.2014.) [3]. However, they are not based on a national dose survey as they are derived from a respective European study [4] and they are expressed as entrance surface dose to the patient. The need of setting DRLs based on national data was identified by Radiation Safety Centre of State Environmental Service (RSC SES) of Latvia which is the regulatory body in the field of radiation safety in the country.

The purpose of this paper is to present the results of a national survey that was performed in Latvia in 2018-2019 for the establishment of national DRLs for nine most common conventional x-ray examinations for adult patients. This study was the first attempt to evaluate patient doses in health care institutions of Latvia as well as to establish national DRLs for conventional x-ray examinations.

## 2. Materials and methods

All data used in this study was collected after specific requests by RSC SES. Data was collected in the specially designed *MS Excel* spreadsheets which were sent to all medical institutions in Latvia performing conventional x-ray examinations. 6 months were given to the medical institutions for data collection (October 2018-March 2019). Medical institutions were asked to provide doses expressed in DAP values as this dose indicator is commonly used in conventional x-ray examinations in Latvia (the use of DAP-meters on x-ray systems is mandatory according to the national legislation). Also, together with the DAP values the exposure factors (tube potential, tube current, filtration, focus-detector distance, field size, use of grid) and data about the patient (weight and age) was collected. Before the distribution of the survey sheets, RSC SES organized several meetings with the representatives of the biggest medical institutions and professional societies in Latvia where the necessity of national DRLs and proposed data collection sheets got approved.

Data was received regarding 54 x-ray units (out of 151 totally available in Latvia at the end of the survey), used for different examinations. One of the reasons why data covered just a part of the total number of units, was that some x-ray examinations are performed rarely in the medical institution or an x-ray unit is used only for some specific examinations. Also, not every x-ray machine is used daily in the medical institution. Nevertheless, in this study, data was considered to represent the x-ray unit and the practice if there was data of at least 10 patient.

Number of x-ray machines where there was data of at least 10 patients for each of examination is seen in Table 1. Data was received from different size medical institutions – large, medium and small – and from all regions of Latvia therefore representing all population.

**Table 1.** Amount of data received from medical institutions

| | Number of systems | Number of patients |
|---|---|---|
| Lumbar spine AP | 27 | 555 |
| Lumbar spine LL | 27 | 507 |
| Pelvis AP | 16 | 305 |
| Hip AP | 20 | 396 |
| Chest PA | 48 | 914 |
| Chest LL | 27 | 539 |
| Thoracic spine AP | 17 | 379 |
| Thoracic spine LL | 17 | 373 |
| Sinuses | 20 | 404 |

Data covered different x-ray unit manufacturers (see Table 2). The oldest x-ray machine was manufactured in 1985 and the newest in 2017. 29 x-ray machines were digital radiography (DR) systems and 24 were computed radiography (CR) systems.

**Table 2.** Manufacturers of x-ray machines in the study

| **Manufacturer** | **Number of systems** |
|---|---|
| Philips | 22 |
| Siemens | 12 |
| GE | 3 |
| Villa Systems Medical | 3 |
| Carestream | 3 |
| Bochum | 2 |
| Raymed | 2 |
| Sedecal | 1 |
| Samsung | 1 |
| DMS Imaging | 1 |
| Xcan Swiss Digital Xray | 1 |
| Sevkavrentgen | 1 |

For each type of examination, the median DAP value from each x-ray machine were calculated. This value was considered as representative of the x-ray machine for delivering of dose to typical adult patient. Although request from RSC SES was to send in data only about patients with weight of 60 to 80 kg, patients with weight 50 to 90 kg were accepted at the end of the survey. None of the medical institutions are logging patient weight during an x-ray examination therefore it was an additional step for the radiation technologists' to find out patients' weight for the study.

All DAP-meters used in medical institutions were calibrated and the calibration factors were factored in.

The rounded third quartile of median DAP-values from all received x-ray machines were proposed as the DRLs for each examination. Also, the mean effective dose to the typical patient from each of mentioned examination was estimated, using the conversion factors (effective dose per DAP) published in the literature [5]. Formula used for this conversion was:

*Effective dose= (conversion factor) x (mean DAP value)*

## 3. Results and discussion

Results of the median DAP-values among all medical institutions and x-ray machines are summarized in Table 3. Big variations are seen between minimum and maximum median values among different x-ray machines in different medical institutions (up to 23.5 times for lumbar spine AP examinations) which leads to the conclusion that an additional analysis of examination protocols and optimization of doses is necessary.

**Table 3.** Median DAP-values for adults among different x-ray machines

| **Median DAP values (µGym$^2$)** | | | | | |
|---|---|---|---|---|---|
| | Min | Max | Max/ min | 1st Quartile | 3rd Quartile |
| Lumbar spine AP | 24.7 | 580.3 | 23.5 | 89.5 | 169.2 |
| Lumbar spine LL | 81.8 | 1139.3 | 13.9 | 113.9 | 281.8 |
| Pelvis AP | 62.5 | 330.1 | 5.3 | 72.7 | 175.5 |
| Hip AP | 25.3 | 175.7 | 7.0 | 36.7 | 70.7 |
| Chest PA | 3.4 | 51.9 | 15.3 | 5.7 | 12.6 |
| Chest LL | 10.0 | 143.2 | 14.3 | 15.8 | 143.2 |
| Thoracic spine AP | 18.2 | 221.2 | 12.2 | 29.6 | 68.6 |
| Thoracic spine LL | 24.0 | 255.2 | 10.6 | 43.0 | 103.1 |
| Sinuses | 8.6 | 117.7 | 13.7 | 18.9 | 47.8 |

When comparing median DAP values from medical institutions with and without medical physicists available, there was no clear difference. This could indicate that medical physicists are not involved in dose optimization processes in medical institutions.

Preliminary adult DRLs for Latvia and in comparison, with published values of two other countries – United Kingdom [6] and Germany [7] – as well as the most common DRLs values from European countries [4] are summarized in Table 4.

Preliminary DRL values of this study are generally comparable to values of United Kingdom and Germany. For some examinations even lower values are observed, which could lead to the conclusion that the general practice of conventional x-ray examinations is quite good in Latvia. Also, it is noticeable that all preliminary DRLs are lower than those published by European Commission as the most common DRL values in European countries.

**Table 4.** Comparison of preliminary adult DRLs of this study with other studies

| | **DRLs as DAP values (µGym$^2$)** | | | |
|---|---|---|---|---|
| | **This study** | **UK** | **Germany** | **European countries** |
| Lumbar spine AP | 170 | 150 | 200 | 230 |
| Lumbar spine LL | 280 | 250 | 350 | 420 |
| Pelvis AP | 175 | 220 | - | 300 |
| Hip AP | 70 | - | 110 | - |
| Chest PA | 13 | 15 | 15 | 16 |
| Chest LL | 35 | - | 40 | 60 |
| Thoracic spine AP | 70 | 100 | 110 | 130 |
| Thoracic spine LL | 100 | 150 | 140 | 170 |
| Sinuses | 50 | - | - | - |

Only a few medical institutions exceeded DRLs published by European Commission (in some examinations) – this is important because current guidelines of Latvia (published by RSC SES) suggested to use exactly these values as national DRLs until now. Based on the data of this study, these values are too high for Latvia and therefore the need of DRLs based on national survey is clearly seen.

Estimated mean effective doses from single exposure examinations are summarized in Table 5.

**Table 5.** Estimated effective doses

| | **Conversion coefficient (mSv/Gycm$^2$) [5]** | **Mean effective dose (mSv)** |
|---|---|---|
| Lumbar spine AP | 0.22 | 0.346 |
| Lumbar spine LL | 0.092 | 0.219 |
| Pelvis AP | 0.14 | 0.199 |
| Hip AP | 0.13 | 0.098 |
| Chest PA | 0.16 | 0.018 |
| Chest LL | 0.13 | 0.045 |
| Thoracic spine AP | 0.24 | 0.174 |
| Thoracic spine LL | 0.091 | 0.088 |

## 4. Conclusions

This paper presents the preliminary national DRLs as the DAP values for the most common conventional x-ray examinations for adults in Latvia. DAP values are commonly used, as a method for evaluating dose of the patient in Latvia, therefore these national DRLs will be of practical use for medical institutions to optimize their examinations and to establish local DRLs. However, establishing DRLs as entrance surface dose (ESD) values is also suggested for the future.

Preliminary DRLs from this study were presented to the work group of medical exposure, established by RSC SES which represents the biggest medical institutions in Latvia as well as professional societies. No objections were received about proposed preliminary DRLs therefore they will be published in the homepage of RSC SES as guidelines for DRLs in Latvia.

There were big differences in median dose values among different x-ray machines in different medical institutions. Partly it can be explained by differences in radiology equipment and techniques but also different exposure parameters were used among medical institutions for the same examinations. This indicates the need for optimization in medical institutions. Evaluation of clinical protocols used and clinical practice performed was/or will be suggested for medical institutions with biggest median DAP values (inspections of RSC SES were or will be performed in medical institutions with biggest median DAP values).

## 5. References

1. European Commission, 2014. Radiation Protection No.180: Medical Radiation Exposure of the European Population, Part 1/2, Luxembourg: Directorate-General for Energy and Transport Directorate D — Nuclear Safety&Fuel Cycle Unit D3 — Radiation Protection.
2. European Union. Laying down basic safety standards for protection against the dangers arising from exposure to ionising radiation, and repealing Directives 89/618/Euratom, 90/641/Euratom, 96/29/Euratom, 97/43/Euratom and 2003/122/Euratom. Council Directive 2013/59/Euratom. Official. J. Eur. Union. 13, 1–73 (2014).
3. Cabinet Regulations No 482 "Regulations Regarding Protection Against Ionizing Radiation in Medical Exposure" (entry into force 01.10.2014.). Latvijas Vestnesis, 165 (5225).
4. European Commission, 2014. Radiation Protection No.180: Diagnostic Reference Levels in Thirty-six European Countries, Part 2/2, Luxembourg: Directorate-General for Energy and Transport Directorate D — Nuclear Safety&Fuel Cycle Unit D3 — Radiation Protection.
5. Wall, B. F. et al., 2011. Radiation Risks from Medical X-ray Examinations as a Function of the Age and Sex of the Patient, Oxfordshire: Health Protection Agency.
6. Hart, D. et al., 2012. Doses to Patients from Radiographic and Fluoroscopic X-ray Imaging Procedures in the UK – 2010 Review, Oxfordshire: Health Protection Agency.
7. Bundesamt für Strahlenschutz, 2016. Bekanntmachung der aktualisierten diagnostischen Referenzwerte für diagnostische und interventionelle Röntgenanwendungen, Bundesamt für Strahlenschutz.

*MEDICAL PHYSICS IN THE BALTIC STATES 14 (2019)*

Proceedings of International Conference "Medical Physics 2019"
7 - 9 November 2019, Kaunas, Lithuania

# PATIENT DOSES FROM TYPICAL RADIOGRAPHY EXAMINATIONS IN THE LENINGRAD REGION

Polina DRUZHININA[1], Ludmila EREMINA[2], Alexander VODOVATOV[1], Ilya SHATSKY[1]
[1]St-Petersburg Research Institute of Radiation Hygiene after professor P.V. Ramzaev, Mira st.8, 197101, St-Petersburg, Russia; [2]Federal Service for Surveillance on Human Well-being and Consumer Rights Protection in the Leningrad region;
druzhininapauline@gmail.com; vodovatoff@gmail.com;

***Abstract*:** The aim of the current study was to present the preliminary results of the patient dose survey from typical radiography examinations in the Leningrad region, which was performed in 2018-2019. The survey included collecting parameters of the typical X-ray examinations and estimating effective doses based on both existing and collected imaging protocols. Based on the results of the survey preliminary diagnostic reference levels for the Leningrad region were established. The results of the study indicate significant regional differences compared to the previously published results of regional and national dose surveys in the Russian Federation.

***Keywords*:** conventional X-ray examinations, radiography, effective dose, diagnostic reference level

## 1. Introduction

Over the past years, the collective dose from medical exposure in the Russian Federation is increasing by 3-5% per year [1,2]. In 2018 it contributed 14.9% to annual collective dose of the Russian population [1,2] – 82 thousand-man Sv. Radiographic examinations have second largest contribution to the collective dose from medical exposure – 21,2%, corresponding to 94,5% of the total number of X-ray examinations. The contribution to the collective dose has been constant over last five years, along with the decrease in the number of radiographic examinations per year. That means that the average patient doses are increasing, indicating the need for optimization.

An international common approach to optimization is to use diagnostic reference levels (DRLs) [3-6], allowing reducing (or keeping constant) patient doses from medical exposure without the decrease of the obtained diagnostic information. In the Russian Federation DRLs concept was the first introduced in "Basic sanitary rules of the provision of the radiation safety (OSPORB 99/2010)" [7] and detailed in MR 2.6.1.0066-12 "The use of diagnostic reference levels to optimize the radiation protection of the patient in general X-ray examinations" [8]. National DRLs for radiographic examinations were proposed in 2016 [6, 9] based on the collecting data in 6 regions of the Russian Federation, but they are still at the approval stage.

However, there is a need to verify the proposed approach for national DRLs establishment [6, 9], by performing additional regional dose surveys and establishing regional DRLs considering the regional specifics of equipment and radiological practice.

It should be noted that apart from dedicated dose surveys performed by the Institute of Radiation Hygiene, patient dose assessments are performed in hospitals as a part of mandatory framework of informing the patients on the possible radiation risk (detriment) from medical imaging. It is fulfilled through the calculation of the effective dose, based on radiation output of the X-ray unit or a dose-area product (DAP) and conversion coefficients [10]. These 'mean' effective doses are later used for the reporting to the Federal Joint Dose Data Collection System (ESKID). However, the calculations are performed by medical staff and/or representatives of the radiation control laboratories with the corresponding a low confidence level. Hence, it is additionally necessary to verify the existing patient dose data and to assess the possibility to use it for the establishment of the DRLs.

The Leningrad region was selected for the establishment of the regional DRLs in 2018. The Leningrad region is located in the northwest of the European part of the country, bordering St-Petersburg, and corresponds to a representative rural region. Its area is 83908km$^2$ and population − 1813816 people (on the 1$^{st}$ of January 2018). According to the federal dose data collection form 3-DOZ [11], effective doses from medical imaging in this region are the lowest in the Russian Federation.

Hence, the aim of this study was to perform a preliminary patient dose assessment in Leningrad region with the subsequent analysis of the results.

Objectives of this study were:

1. To perform a survey on patient doses from most common radiography X-ray examinations;
2. To perform the assessment of the typical effective doses.
3. To validate the existing patient dose data.
4. To analyse the patient doses from different sources and to propose preliminary DRLs for radiography examinations.

## 2. Materials and methods

Based on the statistical form №30 "Information on medical organizations" 227 X-ray units were operational in the Leningrad region in 2018. Fourteen governmental general practice hospitals were selected for the survey. This study presents the data from eight hospitals and fifty X-ray units (23%).

Nineteen standard radiographic examinations were selected for the dose survey (see table 1).

**Table 1.** Standard radiographic examinations and projections

| Examination | Projections* |
|---|---|
| Skull | AP, LAT |
| Chest | AP, PA, LAT |
| Ribs | AP |
| Cervical spine | AP, PA, LAT |
| Thoracic spine | AP, LAT |
| Lumbar spine | AP, LAT |
| Abdomen | AP, LAT |
| Pelvis | AP, LAT |
| Hip | AP, LAT |

**AP – anterior-posterior; PA-posterior-anterior, LAT-lateral*

Data collection was performed manually by distributing dedicated spreadsheets for radiologists/technicians for each X-ray room/unit. These spreadsheets included the following parameters of the radiographic protocols: type of examination, projection, age, weight, height of patients, tube voltage (kV), tube current (mA), exposure time (s), focal-image distance (cm), image field size ($cm^2$). Dose – Area Product, DAP ($mGy \cdot cm^2$) was also collected, if the X-ray unit had an operational calibrated clinical dosimeter. Typical patient doses for selected examinations were estimated using and effective dose (E).

For the X-ray units, operating without an automated exposure control (AEC), parameters of the examinations and DAP-values (if available) were collected for 15-30 adult patients with body mass of 70±5 kg, 170±5 cm height and normosthenic constitution (standard patients).

For the X-ray units operating with an AEC, parameters of the examinations were collected either for 15-30 standard adult patients, or for 50 adult patients regardless of their anthropometric characteristics.

That method of patient data collection assured that patient anatomy corresponded to a standard patient and that the data could be used for estimation of E [9].

It should be noted that all the surveyed X-ray units were operating either without a clinical dosimeter, or the dosimeter was out of service. Hence, the calculation of the effective dose was based on entrance-surface dose (ESD).

ESD was calculated based on the radiation output, exposure current-time product and focal-image distance according the following equation.

$$ESD\ (mGy) = \frac{Q \times R \times d^2}{f^2}$$

where:

*R – the radiation output, $(mGy \cdot m^2)/(mA \cdot s)$;*
*Q – exposure current-time product, mAs*
*d – focal-image distance, cm*
*f - focal-skin distance, cm*

Input doses were calculated without a backscatter.

Radiation output was measured by the authors using a "Piranha Black" dosimeter (RTI Electronics AB, Sweden) for each X-ray unit prior to the data collection.

Effective doses were assessed using the "PCXMC 2.0" software (STUK, Finland) based on previously calculated ESD using tissue weighting coefficients from ICRP Publication 60 [12].

Effective doses and imaging parameters from the existing protocols of the patient dose estimation were collected for the comparison as well. Comparison of the data processing for the assessment of typical effective doses is presented in table 2.

**Table 2.** Comparison of the methods of the effective dose estimation.

| **Parameters** | **Protocols** | **Surveys** |
|---|---|---|
| Imaging parameters | Existing protocols with estimated patient doses | Data from manually filled spreadsheets |
| Radiation output | Existing protocols of X-ray unit quality control | Measurement by IRH staff |
| Estimation of E | Existing guidelines [10] | PCXMC 2.0 software |

Effective doses using existing protocols were recalculated using PCXMC 2.0 [13] with the same imaging parameters and updated radiation output.

Descriptive statistic was generated from the collected data using "Statistica12.0". Differences between samples were estimated using Kruskall-Wallis test with the subsequent pair comparison with Mann-Whitney non-parametric test. Differences were considered significant with $p<0.05$.

## 3. Results

The results of the effective dose estimations are presented in Table 3.

Comparison of distributions of the effective doses between analogue and digital X-ray units based on the data of protocols and surveys is presented on Figures 1 and 2 for the radiography of the chest and lumbar spine respectively.

A comparison of the estimated 75%-percentiles of effective dose distributions based on the survey data with the preliminary DRLs proposed in previous studies is presented in Table 4.

**Table 3.** Effective doses (mSv) for each selected X-ray examination for different data sources. Results are presented as mean±SD (min-max).

| Examination | Protocols | | Surveys | |
|---|---|---|---|---|
| | Analogue | Digital | Analogue | Digital |
| Skull AP | 0.02±0.01 (0.001-0.04) | 0.03±0.02 (0.001-0.06) | 0.01±0.01 (0.01-0.02) | 0.03±0.02 (0.01-0.06) |
| Skull LAT | 0.02±0.01 (0.001-0.03) | 0.02±0.01 (0.002-0.04) | 0.05±0.02 (0.03-0.07) | 0.05±0.03 (0.01-0.09) |
| Chest AP | 0.08±0.08 (0.005-0.31) | 0.09±0.06 (0.008-0.22) | 0.11±0.05 (0.04-0.21) | 0.07±0.09 (0.01-0.44) |
| Chest LAT | 0.04±0.04 (0.002-0.15) | 0.08±0.07 (0.003-0.29) | 0.20±0.14 (0.05-0.40) | 0.06±0.06 (0.01-0.21) |
| Chest PA | 0.04±0.05 (0.001-0.18) | 0.10±0.06 (0.006-0.25) | - | 0.09±0.13 (0.01-0.35) |
| TS AP | 0.15±0.11 (0.009-0.33) | 0.42±0.25 (0.006-0.72) | 0.08±0.07 (0.01-0.14) | 0.30±0.20 (0.03-0.50) |
| TS LAT | 0.07±0.04 (0.009-0.15) | 0.14±0.11 (0.006-0.28) | 0.12±0.09 (0.06-0.18) | 0.16±0.12 (0.01-0.31) |
| CS AP | 0.05±0.04 (0.006-0.14) | 0.08±0.11 (0.007-0.28) | 0.07±0.01 (0.07-0.08) | 0.08±0.08 (0.01-0.24) |
| CS LAT | 0.07±0.06 (0.006-0.20) | 0.08±0.10 (0.004-0.28) | 0.11±0.14 (0.01-0.20) | 0.06±0.05 (0.01-0.14) |
| Abdomen AP | 0.26±0.27 (0.01-0.84) | 0.41±0.30 (0.02-0.65) | 0.08±0.06 (0.04-0.13) | 0.54±0.12 (0.45-0.62) |
| Pelvis AP | 0.62±1.25 (0.02-4.31) | 0.51±0.39 (0.03-1.10) | 0.20±0.22 (0.01-0.44) | 0.84±0.30 (0.48-1.22) |
| Hip AP | 0.13±0.16 (0.003-0.52) | 0.40±0.24 (0.005-0.70) | 0.15±0.14 (0.01-0.35) | 0.25±0.12 (0.03-0.42) |
| LS AP | 0.21±0.21 (0.004-0.66) | 0.64±0.51 (0.02-1.22) | 0.46±0.21 (0.22-0.76) | 0.62±0.33 (0.02-1.01) |
| LS LAT | 0.30±0.41 (0.02-1.37) | 0.49±0.40 (0.007-1.01) | 0.61±0.31 (0.11-0.88) | 0.46±0.22 (0.10-0.77) |
| Ribs AP | 0.11±0.07 (0.02-0.21) | 0.22±0.28 (0.006-0.69) | - | 0.05±0.04 (0.01-0.10) |

**Table 4.** Comparison of the 75% - percentiles of effective dose distributions (mSv).

| Examination | 75%-percentiles of effective dose distributions | | | | | |
|---|---|---|---|---|---|---|
| | Current studies | | Russian Federation [6,9] | | St-Petersburg [6,9] | |
| | A* | D* | A* | D* | A* | D* |
| Skull AP | 0,02 | 0,05 | 0,10 | | 0.08 | |
| Skull LAT | 0,07 | 0,07 | 0,05 | | 0.03 | |
| Chest AP | 0,13 | 0,08 | - | | - | |
| Chest LAT | 0,29 | 0,05 | 0,22 | | 0.17 | |
| Chest PA | - | 0,05 | 0,10 | | 0.09 | |
| TS AP | 0,14 | 0,49 | 0,41 | | 0.39 | |
| TS LAT | 0,18 | 0,26 | 0,33 | | 0.34 | |
| CS AP | 0,08 | 0,11 | 0,11 | | 0.08 | |
| CS LAT | 0,2 | 0,09 | 0,09 | | 0.06 | |
| Abdomen AP | 0,13 | 0,62 | 1,03 | | 0.88 | |
| Pelvis AP | 0,44 | 1,03 | 0,93 | | 0.81 | |
| Hip AP | 0,26 | 0,31 | 0,93 | | 0.81 | |
| LS AP | 0,57 | 0,86 | 0,82 | | 0.92 | |
| LS LAT | 0,84 | 0,66 | 0,93 | | 0.87 | |
| Ribs AP | - | 0,1 | 0,25 | | 0.48 | |

## 4. Discussion

The results of the study indicate significant differences between the existing (protocols) and collected (surveys) typical patient doses for all selected radiography X-ray examinations (Kruskall-Wallis test, with the subsequent Mann-Whitney test, $p<0,05$), see Table 3.

These differences can be explained by the following factors:

- Biased data collection by the hospital staff and representatives of the external radiation control laboratories;
- Incorrect measurement of the radiation output by the representatives of the external radiation control laboratories;
- Procedural errors in typical dose estimation (failure to fulfil the requirements on the patient samples [8]);
- For the X-ray units operating with automated exposure control (AEC) – the use pre-examination tube current-time product (mAs) instead of the post-examination mAs for the calculation of ESD.

Performed local investigations allowed determining that typical procedural errors included the use of a limited (less than 5) number of patients and the use of old imaging protocols (parameter from the X-ray unit user manuals or even from the old X-ray units) for the calculation of the effective dose. As it is visible from Table 3 as well as Figures 1 and 2, statistically significant differences between the analogue and digital X-ray units were determined both for the existing (protocols) and collected (surveys) typical dose samples.

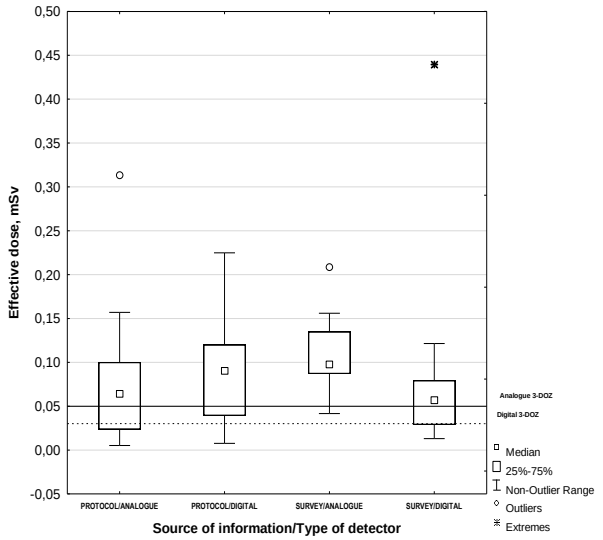


**Fig. 1.** Dose distributions (mSv) for the radiography of the chest in anterior-posterior projection. Solid and dotted lines correspond to the mean effective dose of the Federal Joint Dose Data Collection System for digital and analogue X-ray units respectively

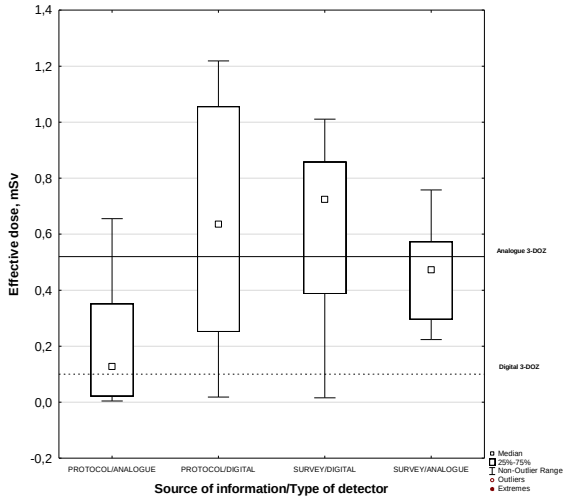


**Fig. 2.** Dose distributions (mSv) for the radiography of the lumbar spine in anterior-posterior projection. Solid and dotted lines correspond to the mean effective dose from the Federal Joint Dose Data Collection System for digital and analogue X-ray units respectively.

Moreover, the typical patient doses for the digital X-ray units were significantly higher compared to the analogue X-ray units for the examinations of skull, thoracic and lumbar spine, abdomen, pelvis and hip. It is different in comparison to the previous studies performed in Russia [5-6, 9]. These differences can be explained by the following factors:

- in all surveyed X-ray departments digital X-ray units were used for film-based imaging as well. The default vendor imaging protocols were developed for the film, with the corresponding impact of the patient dose;
- all surveyed digital X-ray units were equipped with the CCD-matrix or CR types of detectors. Most of them were installed in 2008 or earlier; detectors have been seldom calibrated. Low sensitivity of these detectors requires performing imaging with high tube-current exposure time product.

These factors could be confirmed by the comparison of the typical values of tube current-time product and tube voltage between analogue and digital X-ray units (see Figure 3 and 4 respectively).

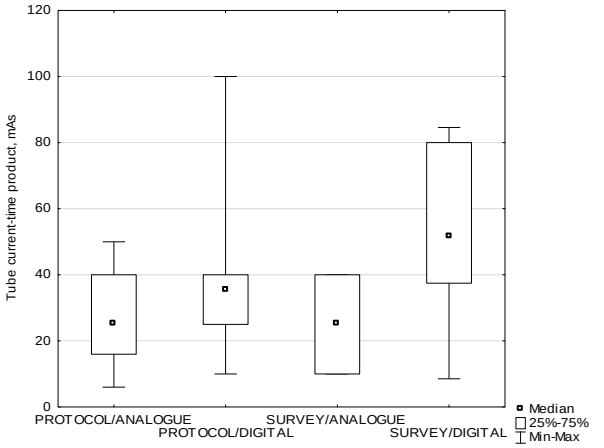


**Fig. 3**. Comparison of the tube current – time product of analogue and digital X-ray units for the examination of skull in anterior-posterior projection.

It is obtaineed in that both tube current-time product and tube voltage are significantly higher for digital X-ray units compared to the analogue X-ray units ( Fig. 3 and Fig. 4). It is still unclear what is the reason: the existing protocols are a result of "dose creep" [14] or poor technical condition of digital detectors. A further investigation on the capabilities of optimization of imaging protocols for digital X-ray units is required.

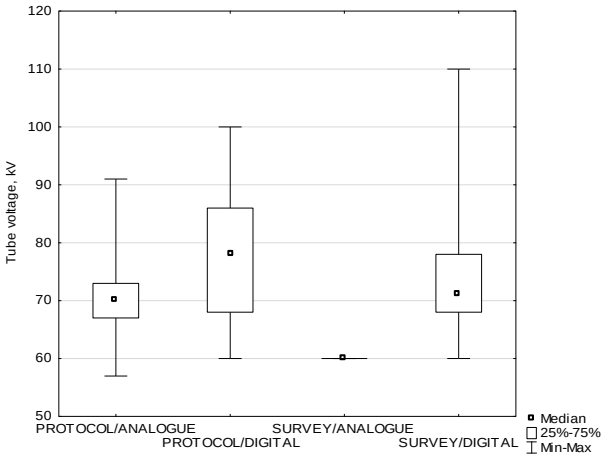


**Fig. 4.** Comparison of the tube voltage for analogue and digital X-ray units for the examination of skull in anterior-posterior projection.

Collected data allowed establishing preliminary DRLs, which were compared with previously proposed national DRLs and DRLs for St-Petersburg [6, 9] (see Table 4). The preliminary DRLs for the Leningrad region are a significantly lower (up to a factor of 3) for all X-ray examinations except for the examinations of skull and cervical spine in lateral projection. It could be explained mainly by differences in the local radiological practice and/or relatively small X-ray unit sample. In additionally, the differences in the distributions of the typical patient doses require establishing separate DRLs for analogue and digital X-ray units. The patient dose surveys would

continue in 2020-2021 with the final goal of collecting the data from at least 80% of the regional X-ray equipment.

## 5. Conclusions

The presented results of the typical patient dose assessment from typical radiography X-ray examinations in the Leningrad region indicate significant differences compared to the previous regional and national dose surveys. Significant differences between the existing (protocols) and collected (surveys) typical dose samples were determined. These differences can be mainly explained by the biased data collection performed by the hospital staff and representatives of the external radiation control laboratories. In contrary to the previous studies, significant differences between the typical effective doses for analogue and digital X-ray units were determined as well. Typical patient doses of the digital X-ray units were significantly higher compared to the analogue X-ray units for the examinations of skull, thoracic and lumbar spine, abdomen, pelvis and hip. It can be explained by the use of a low-sensitive digital detectors and/or default vendor examination protocols developed for film-based imaging. 75%-percentiles of patient effective dose distributions were selected as a preliminary regional DRLs. They were significantly lower compared to the previously published DRLs for St-Petersburg and the Russian Federation for all examinations except for the examinations of skull and cervical spine in lateral projection. Additionally, it was necessary to establish separate DRLs for digital and analogue X-ray examinations.

## 6. Acknowledgements

The authors would like to thank the representatives of Directorate of Federal Service for Surveillance on Human Well-being and Consumer Rights Protection in the Leningrad region and staff of the X-ray departments from all collaborating hospitals for the support in the data collection.

## 7. References

1. Onischenko G.G., Popova A.Y., Romanovich I.K., Vodovatov A.V., Bashketova N.S., Istorik O.A., Chipiga L.A., Shatsky I.G., Repin L.V., Biblin A.M. Modern principles of the radiation protection from sources of ionizing radiation in medicine. Part 1: Trends, structure of x-ray diagnostics and doses from medical exposure. // Radiatsionnaya Gygiena = Radiation Hygiene. V.12(1), p.6-24 (2019). (In Russ.) – [Electronic resource]. – Available at: https://doi.org/10.21514/1998-426X-2019-12-1-6-24 Accessed: 1.04.2019
2. Onischenko G.G., Popova A.Y., Romanovich I.K., Vodovatov A.V., Bashketova N.S., Istorik O.A., Chipiga L.A., Shatsky I.G., Sarycheva S.S., Biblin A.M., Repin L.V. Modern principles of the radiation protection from sources of ionizing radiation in medicine. Part 2: radiation risks and development of the system of radiation protection. Radiatsionnaya Gygiena = Radiation Hygiene. 2019;12(2):6-24. (In Russ.) https://doi.org/10.21514/1998-426X-2019-12-2-6-24
3. International Atomic Energy Agency. Radiation Protection and Safety in Medical Uses of Ionizing Radiation. Specific Safety Guide №SSG-46. – Vienna: IAEA, 318 p. (2018).
4. International Commission on Radiological Protection. Diagnostic reference levels in medical imaging. ICRP Publication 135. Ann. ICRP 46(1) (2017)
5. Vodovatov A.V., Kalnitsky S.A., Balonov M.I., Kamyshanskaja I.G. Development of diagnostic reference levels (drl) of patients x-ray exposure in diagnostic radiology. Radiatsionnaya Gygiena = Radiation Hygiene. 2013;6(3):29-36. (In Russ.)
6. Vodovatov A.V. Practical implementation of the diagnostic reference levels concept for the common radiographic examinations. // Radiatsionnaya Gygiena = Radiation Hygiene. V.10(1), p.47-55 (2017). (In Russ.) – [Electronic resource]. – Available at: https://doi.org/10.21514/1998-426X-2017-10-1-47-55 Accessed: 1.04.2019
7. Basic sanitary rules of the provision of the radiation safety (OSPORB 99/2010): Sanitary rules and norms SP2.6.1.2612-10. Moscow, Federal center of hygiene and epidemiology of Rospotrebnadzor, 2010, 83p.
8. Methodical recommendation MP 2.6.1.0066-12 “Implementation of diagnostic reference levels to optimize the radiation protection of the patient in conventional radiology”.- M.: Rospotrebnadzor, 2012.- 28 p.
9. Vodovatov A.V., Balonov M.I., Golikov V.Yu., Shatsky I.G., Chipiga L.A., Bernhardsson C. Proposals for the establishment of national diagnostic reference levels for radiography for adult patients based on regional dose surveys in Russian Federation. // Rad. Prot. Dos. V.173(1-3), p.223-232 (2017)
10. Rospotrebnadzor. Assessment of effective dose to the patients undergoing X-ray examinations. Methodical guidance 2.6.1.2944-11.
11. Results of radiation and hygienic certification in the subjects of the Russian Federation for 2017: Radiation-hygienic passport of the Russian Federation. 2018 (Moscow: Rospotrebnadzor) 128 p. (in Russian)
12. International Commission on Radiological Protection. The 2007 Recommendations of the International Commission on Radiological Protection. ICRP Publication 103: translation from English / edited by M. F. Kiselev, N. K. Shandala. - M.: «Alana», 312 p. (2009). (In Russ.)
13. M. Tapiovaara, T. Siiskonen. PCXMC: A Monte Carlo program for calculating patient doses in medical x-ray examinations. 2nd Ed. STUK (2008).
14. ECRI. Dose Creep: Unnoticed Variations in Diagnostic Radiation Exposures. HealthManagement, Volumen15-Issue 2, 2015.

*MEDICAL PHYSICS IN THE BALTIC STATES 14 (2019)*

Proceedings of International Conference "Medical Physics 2019"
7 – 9 November 2019, Kaunas, Lithuania

# PRACTICAL COMPARISON OF DIFFERENT PATIENT'S DOSE ESTIMATION METHODS DURING MEDICAL X-RAY PROCEDURES

Timūr JARIOMENKO[1,2], Nikolajus MEDVEDEVAS[2]
[1]Kaunas University of Technology, Kaunas, Lithuania
[2]Republical Hospital of Kaunas, Kaunas, Lithuania

***Abstract*:** In this paper usage of different methods for evaluating patient exposure in X-ray medical procedures is discussed. Usually medical staff uses dose-area product (DAP) readings on the X-ray console for this task. In this paper, measured DAP values will be compared with the DAP values calculated from entrance surface dose (ESD). For ESD measurements thermoluminescence dosimeters were used.

***Keywords*:** patient's dose, entrance surface dose (ESD), dose-area product (DAP), TLD dosemeter, medical x-ray diagnostic, diagnostic reference level (DRL).

## 1. Introduction

Establishing the national Diagnostic Reference Levels (DRLs) for the most common medical x-ray procedures is one of the major and most important step to optimise patient's doses. These levels are expected to not be exceeded for standard medical x-ray procedures when established procedures regarding diagnostic and technical performance are followed [1]. Main goal of the DRLs is to control/ensure optimal patient exposure during medical x-ray procedures [1].

Diagnostic reference levels are not to be considered as dose limits [2]. Dose limit is a dose value that is not to be exceeded, a diagnostic reference level can be exceeded if the clinical needs demands it [3]. Diagnostic reference levels are used as a threshold to identify medical facilities that uses unusually high doses in a specific radiological procedures, in which case optimization actions are needed [3].

According to an overview, by competent authorities, presented in [4], 23 out of 31 European countries involved in the study have national DRLs in medical radiography [4]. According to the presented results, Lithuania is one of the countries which have established DRLs, which in turn are based on the results of a national survey. Until 2016 national surveys were based on patient-based dosimetry which was performed by measuring entrance surface dose of patient during real medical x-ray procedures by putting TLD dosemeter on the patient surface in the exposure field. But this data collection method, for the establishment of national DRLs, was very inconvenient due to considerable time and financial resources required, since all countries' hospitals involved in the survey had to measure ESD for all procedures performed and to evaluate each piece of x-ray equipment separately [5].

Due to these reasons Radiation Protection Center of Lithuania in 2016 prepared and announced the „*Methodical recommendations of patient's dose estimation during medical x-ray procedures*". The aim of this document was to explain the basis of patient's dose estimation possibilities and to make data collection more practical for DRL establishment surveys. It was also important, because accordingly to latest hygiene standard in radiation protection, dose received during medical x-ray procedures must be evaluated for each patient and for every medical x-ray procedure individually. These recommendations became a tool which enabled hospitals' radiological departments' staff to estimate patient's doses received from medical x-ray procedures independently. *N.B. it is more important for hospitals in which there are no established staff positions for medical physicist.*

Patient's dose estimation methods for medical x-ray radiography discussed in these mentioned recommendations are based on two practical dose quantities. Depending on the x-ray machines' specifications, namely the presence of a DAP meter, calculation of entrance surface dose (ESD) or a record of DAP values accumulated, are used.

The aim of this article is to evaluate the reliability of data, collected using different patients' dose estimation methods, for further use in the establishment of the national DRLs.

## 2. Methodology

Study was performed on a stationary digital X-ray device for medical purposes Shimadzu RadSpeed Pro EDGE No. LM5249F5C006, 2015, X-ray tube 0.6/1.2P324DK-85 No. RM6D8585C008. First phase of the work was to determine the radiation output dependence on the tube voltage. Second phase of the

study involved measurement of ESD and DAP and checking the reliability of readings.

### 2.1. Measuring patient exposure through ESD

Unfors Multi-O-Meter 517 L, No. 128100 multimeter was used to assess the dependence of radiation output on tube voltage. 30 cm x 30 cm radiation field was used for these measurements. Distance between focal spot of the field and the detector was set at 100 cm. Anode voltage range was set between 40 and 125 kV. Measurements performed at 5 kV steps. Anode current was 5.0 mA.
Obtained results are shown in Fig 1.

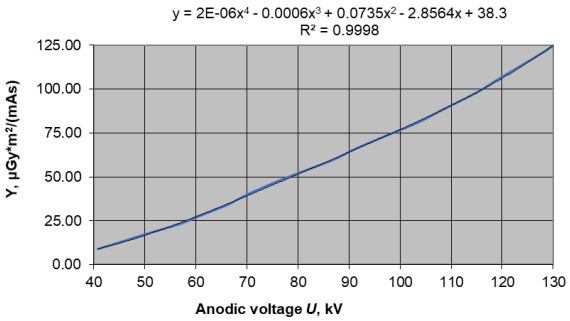


**Fig 1.** Shimadzu RadSpeed Pro EDGE No. LM5249F5C006 dependence of radiation output on tube voltage.

Entrance surface dose study setup is shown in Fig 2. In this experiment anode voltage (kVp), anode current and exposure time product (mA•s) values were measured. Using these values entrance surface dose was calculated with reference to radiation output dependence on tube voltage.

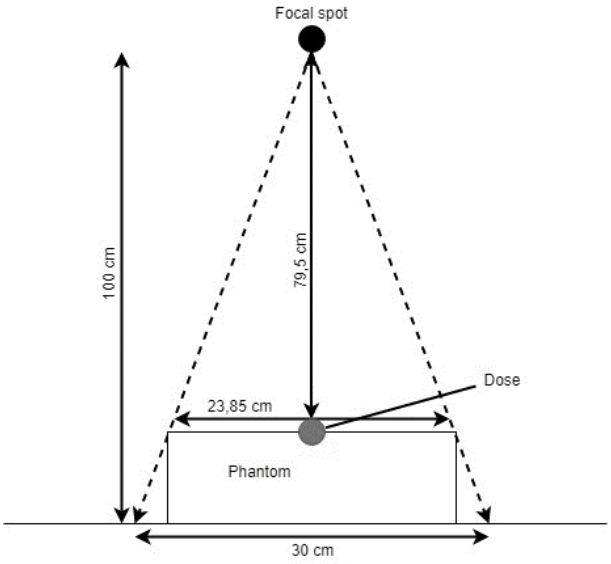


**Fig 2.** Entrance surface dose study setup

Additionally, a set of TLD 100 dosimeters which was calibrated using an upgraded RIALTO TLD reader was placed on a PMMA phantom to experimentally evaluate the ESD on a simulated patient. Field was still set at 30 x 30 cm, but since the phantom had a thickness of 20.5 cm the irradiation field shrunk to 23.85 x 23.85 cm. 20 exposures were performed with the X-ray machine set at 100 kV, 160 mA and exposure time of 17-18 ms. Results of this study are presented in table 4a,b in greater detail.

### 2.2. Evaluation of patient exposure using DAP values

Experimental DAP values were obtained using two methods.
In the first case, the experimental dose and area product values were calculated by multiplying the X-ray field area on patient‘s body surface and kerma values, which were calculated from the radiation output curve, taking into account the exposure parameters of the X-ray machine (anode voltage (kVp), anode current (mA), exposure duration (ms)) and distance from the focal point to the patient‘s surface (d=79.5 cm) (DAPcalc). Table 2 shows the calculated kerma values when the distance from the focal spot to the patients’ body surface is 79.5 cm.

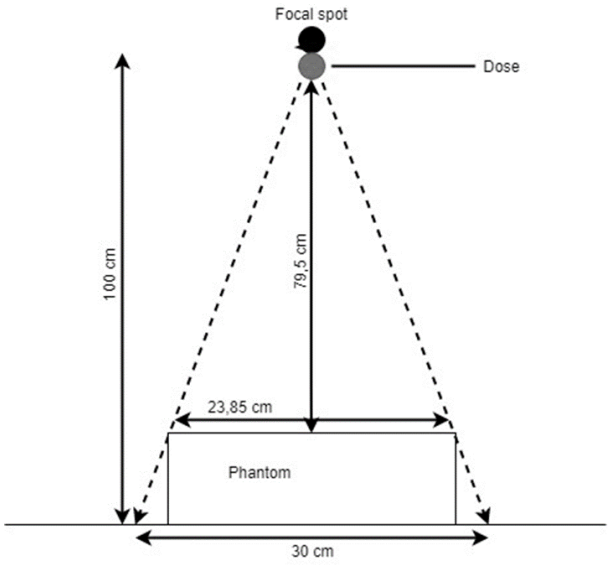


**Fig 3.** Dose and area product study setup.

## 3. Results and discussion

Estimated DAP values were calculated by Shimadzu RadSpeed Pro EDGE X-ray machine’s software, based on radiation output curve and exposure parameters (anode voltage (kVp), anode current (mA), exposure duration (ms), X-ray field area on detector surface) and are presented in table 3a and 3b.
Calculated entrance surface dose values are considerably higher than calculated $D_{79.5cm}$ values or TLD measured values, though TLD values have a considerably wider confidence interval, which might mean that the dosimeters are not that accurate.
Study has also shown that when evaluating ESD values, calculated values are always higher because the result is inflated by evaluation coefficients and with the help of TLD dosimeters ESD values are closer to calculated kerma at the distance of 79.5 cm ESD.

**Table 1.** A comparison of the results of the experimental and theoretical evaluation of DAP values.

| Evaluation method | Mean ESD value, µGy | *95 % confidence interval (ESD)* |
|---|---|---|
| **$D_{79.5cm}$ calculation** | 396,1 | ±3,6 |
| **ESD calculation** | 566,4 | ±5,1 |
| **TLD measurement** | 323,5 | ±19,1 |

**Table 2.** A comparison of the results of the experimental and estimated evaluation of DAP values.

| Evaluation method | Mean DAP value, µGy•m$^2$ | *95 % confidence interval (DAP)* |
|---|---|---|
| **$DAP_{estimated}$ (X-ray machine console readings)** | 20,68 | ±0,04 |
| **$DAP_{experimental}$ (based on the calculated kerma values from the radiation output curve)** | 22,52 | ±0,21 |
| **$DAP_{experimental}$ (based on the dose values obtained from measurements from the TLD)** | 18,40 | ±1,09 |

Based on results presented in table 2 it can be seen that X-ray machine console readings ($DAP_{estimated}$) show very small variation based on confidence interval calculations. X-ray machine evaluated is quite new and was not very intensively used, older and less maintained X-ray machines might have considerably higher variation of the readings.

Experimental DAP values based on calculated kerma values from radiation output curve show somewhat higher mean DAP value from which we can get calculated correction coefficient by dividing the experimental value from estimated value. In this case the correction coefficient is equal to 1.089.

## 4. Conclusions

Calculated entrance surface dose values were considerably higher than $D_{79.5cm}$ calculated values or TLD measured values, though TLD measured values have considerably wider confidence interval. Study has shown that evaluating ESD values, calculated values are always higher because the result is inflated by evaluation coefficients and with the help of TLD dosimeters ESD values come closer to the calculated kerma at the distance of 79.5 cm ESD. X-ray machine readings can be trusted because given result is higher than obtained and calculated by measuring with TLD dosimeters.

**Acknowledgement**

Authors are grateful to the Kaunas University of Technology for the TLD readout and to the Republican Hospital of Kaunas for the possibility to use medical x-ray machine and perform measurement in a real clinical environment.

## 5. References

1. J. Damilakis, G. Frija, M. Hierath, W. Jaschke, U. Mayerhofer-Sebera, G. Paulo, J. Repussard, A. Schegerer, V. Tsapaki, M. Verius. European Study on Clinical Diagnostic Reference Levels for X-ray Medical Imaging. Deliverable 2.1: Report and review on existing clinical DRLs. European Commission, 2018: p. 28-33.
2. Gholami M., Maziar A., Khosvari H. R. , Ebrahimzadeh F., Mayahi S. Diagnostic reference levels (DRLs) for routine X-ray examinations in Lorestan province, Iran. International Journal of Radiation Research, January 2015; 13(1): p. 85-90. doi: 10.7508/ijrr.2015.01.012.
3. Vassileva J., Rehani M. Diagnostic Reference Levels. American Journal of Roentgenology. 2015; 204: W1-W3. doi: 10.2214/AJR.14.12794.
4. International Commission on Radiological Protection (ICRP). Radiological protection and safety in medicine: ICRP publication 73. Ann ICRP 1996; 26:23–24.
5. Tonkopi E., Daniels C., Gale M. J., Schofield S. C., Sorhaindo V. A., VanLarkin J. L. Diagnostic reference levels (DRLs) for routine X-ray examinations in Lorestan province, Iran. Canadian Association of Radiologists Journal 63, 2012: p. 237-241. doi: 10.1016/j.carj.2011.02.004.

**Table 3a**

| **Measurement number** | **1** | **2** | **3** | **4** | **5** | **6** | **7** | **8** | **9** | **10** |
|---|---|---|---|---|---|---|---|---|---|---|
| **Anode voltage, kVp** | 100 | 100 | 100 | 100 | 100 | 100 | 100 | 100 | 100 | 100 |
| **Anode current, mA** | 160 | 160 | 160 | 160 | 160 | 160 | 160 | 160 | 160 | 160 |
| **Exposition time, ms** | 18 | 18 | 18 | 18 | 18 | 18 | 18 | 18 | 17 | 18 |
| **mA•s** | 2,88 | 2,88 | 2,88 | 2,88 | 2,88 | 2,88 | 2,88 | 2,88 | 2,72 | 2,88 |
| **$DAP_{estimated}$[4], µGy•m$^2$** | 20,67 | 20,57 | 20,57 | 20,68 | 20,78 | 20,68 | 20,69 | 20,78 | 20,74 | 20,78 |

**Table 3b.**

| **Measurement number** | **11** | **12** | **13** | **14** | **15** | **16** | **17** | **18** | **19** |
|---|---|---|---|---|---|---|---|---|---|
| **Anode voltage, kVp** | 100 | 100 | 100 | 100 | 100 | 100 | 100 | 100 | 100 |
| **Anode current, mA** | 160 | 160 | 160 | 160 | 160 | 160 | 160 | 160 | 160 |
| **Exposition time, ms** | 17 | 18 | 18 | 18 | 18 | 18 | 18 | 18 | 17 |
| **mA•s** | 2,72 | 2,88 | 2,88 | 2,88 | 2,88 | 2,88 | 2,88 | 2,88 | 2,72 |
| **$DAP_{estimated}$[4], µGy•m$^2$** | 20,57 | 20,78 | 20,68 | 20,78 | 20,78 | 20,68 | 20,57 | 20,68 | 20,47 |

**Table 4a.**

| **Measurement number** | **1** | **2** | **3** | **4** | **5** | **6** | **7** | **8** | **9** | **10** |
|---|---|---|---|---|---|---|---|---|---|---|
| **Anode voltage, kVp** | 100 | 100 | 100 | 100 | 100 | 100 | 100 | 100 | 100 | 100 |
| **Anode current, mA** | 160 | 160 | 160 | 160 | 160 | 160 | 160 | 160 | 160 | 160 |
| **Exposition time, ms** | 18 | 18 | 18 | 18 | 18 | 18 | 18 | 18 | 17 | 18 |
| **mA•s** | 2,88 | 2,88 | 2,88 | 2,88 | 2,88 | 2,88 | 2,88 | 2,88 | 2,72 | 2,88 |
| **$ESD_{TLD}$[3], µGy** | 316,3 | 323,5 | 376,1 | 307,7 | 333,3 | 310,1 | 314,8 | 339,6 | 386,2 | 337,3 |

**Table 4b.**

| **Measurement number** | **11** | **12** | **13** | **14** | **15** |
|---|---|---|---|---|---|
| **Anode voltage, kVp** | 100 | 100 | 100 | 100 | 100 |
| **Anode current, mA** | 160 | 160 | 160 | 160 | 160 |
| **Exposition time, ms** | 17 | 18 | 18 | 18 | 18 |
| **mA•s** | 2,72 | 2,88 | 2,88 | 2,88 | 2,88 |
| **$ESD_{TLD}$[3], µGy** | 314,8 | 285,5 | 333,0 | 223,9 | 350,0 |

*MEDICAL PHYSICS IN THE BALTIC STATES 14 (2019)*

Proceedings of International Conference "Medical Physics 2019"
7 – 9 November 2019, Kaunas, Lithuania

# DOSE ASSESSMENT OF MEDICAL EXPOSURE OF RADIOGRAPHIC DENTAL STUDIES

Ilya SHATSKIY
St.-Petersburg Research Institute of Radiation Hygiene, Russian Federation

***Abstract*:** Doses of patients for the most common radiographic dental studies were evaluated and compared with the published data.
44 X-ray units were examined at 37 dental medical facilities in St. Petersburg and the Leningrad Region in 2016-2018. Seven radiographic studies were included: radiographs of three groups of teeth (incisors, premolars, and molars) for the upper and lower jaw and bite radiography.
Physical-technical and geometrical parameters were collected for selected types of the standard patient studies: X-ray tube voltages, total filtration, radiation output, combination of the time and the current of exposure or the exposure, area of the study, size of the irradiation field; the focal length. Further, the input (surface) dose was calculated from the radiation output of the device. Then, based on the initial information about the parameters of the procedures and the input dose, the absorbed doses and the effective dose were calculated using the PCXMC program.
For most devices, the dose values are in the range of 0.5 to 10.7 μSv. Results of evaluating the effective dose for these devices are fairly homogeneous, but on one device, there were doses exceeding the values of doses on other devices.
Median value of the effective dose for the units with films detectors was 3.2 μSv for the maxillary incisors, 3.8 μSv for the maxillary premolars, 6.8 μSv for the maxillary molars, and for the mandibular incisors, premolars and molars – 3.2, 3.4 and 5.8 μSv, and for bitewing – 6.7 μSv.
For the unit with digital detectors, effective doses were 1 μSv, 1,2 μSv, 2,2 μSv for maxilla, 1 μSv, 1,3 μSv, 2 μSv for mandibula and 2,8 μSv for bitewing. Attention is drawn to the substantial width of the ranges without emissions for the examination of premolars of the upper jaw, molars of both jaws and occlusion, which is the reason for the possible enhancement of optimization measures in these studies.
When comparing with published data, it was found that the effective doses in St. Petersburg and the regional institutions are lower than the values obtained using standard round collimator and medium and high sensitivity films (class D and F, respectively), as well as lower dose levels in the European Commission Guidelines. However, the effective doses in St. Petersburg and the Leningrad Region are higher than those obtained using a square collimator and high-sensitivity films.
These results suggest that it is necessary and possible to carry out optimization in X-ray dental studies in St. Petersburg and the Leningrad Region. Analysis of similar studies on other X-ray diagnostic techniques allows to extrapolate this statement to other regions of Russia.

***Keywords*:** radiation protection, medical exposure, radiographic examinations, dental examinations, patients, effective dose.

## 1. Introduction

X-ray dental studies are one of the most common types of X-ray studies of the population [1, 2], and their number tends to constant growth over time. In recent decades, more than 30 million radiographs of teeth, jaws, and other bones of the facial skull are performed annually in Russia, which makes up more than 20% of all images and about 40% of radiographs of the osteoarticular system.
Traditional task of x-ray dentistry - the identification and clarification of the nature of diseases of the dentition - is supplemented by the use of radiological techniques in assessing the dynamics of the pathological processes, determining the results of conservative and surgical treatment and completeness of convalescence.
For this reason, a dose assessment is necessary in order to be able to optimize the implementation of X-ray dental examinations and develop a system for substantiating the appointment of procedures [3]
The purpose of this study is to evaluate the effective patient doses for dental examinations (intraoral aiming images), comparing the obtained data with the published data.

## 2. Materials and methods

As part of this work 44 X-ray dental units were examined in 37 dental medical organizations in St. Petersburg and the Leningrad Region in 2016-2018. Seven radiographic

examinations were included: radiographs of three groups of teeth (incisors, premolars and molars) for the upper and lower jaw and x-ray of the bite.

Data collection has been standardized. In all the organizations, for each apparatus, information on the average parameters of the procedures was recorded in the questionnaire.

As initial information for determining the effective dose were used:

- physico-technical measured parameters that determine the x-ray field
  - X-ray tube voltage (kV);
  - material and total filtration of the x-ray tube (mm Al);
  - radiation output of the x-ray tube ($mGy \cdot m^2$)/(mA·s)
  - combination of exposure time (s) and current (mA) or exposure (mA·s);
- X-ray geometric parameters
  - field of study;
  - dimensions of the radiation field (height and width of the beam on the skin);
  - focal distance (distance from the focus of the x-ray tube to the image receiver).

Total filtration was at least 2.5 mm Al; the source-receiver distance was 20 cm for all studies.

In this case, the radiation output of the X-ray unit was determined on the basis of measurements within the framework of monitoring the operational parameters of the X-ray unit in accordance with the requirements national guideline. The incident air kerma was calculated according to the Equation 1:

$$K_{a,i} = R \cdot Q/(r)^2 = R \cdot i \cdot t/(r)^2, \text{ мГр} \quad (1)$$

where: R – radiation output, $mGy \cdot m^2/mA \cdot s$;

r – distance from the focus of the tube to the surface of the patient's body, m;

Q – exposure, mA·s;

i – anode current, mA;

t – exposure time, s.

Then, based on the initial information of the parameters of the procedures and the incident air kerma, the absorbed doses in organs and tissues necessary for evaluating the effective dose were calculated [3, 4, 5]. Both absorbed and effective doses were calculated using the PCXMC program [5] for the phantom of a standard adult 174 cm tall and 71.1 kg in weight. Axis of the beam was in the sagittal plane of the phantom for modeling the radiography of the incisors and bite, and at an angle of 30° and 60° for the radiography of premolars and molars, respectively. The coordinates of the center of the beam were selected based on the projections of the periapical regions of the corresponding groups of teeth on the surface of the phantom. A craniocaudal angle of 60° was also used to model the study of the bite. In all cases, the focus-skin distance was 20 cm, and the field size was 5.3×5.3 cm (equivalent in area to a circular collimator with a diameter of 6 cm).

## 3. Results and discussion

Typical parameters of the procedures for intraoral radiography and the calculated values of the effective doses are presented in Table 1. Calculated values of the effective doses for all devices and all studies included in this work are presented in Fig. 1.a and 1.b. For most devices the values of effective doses are in the range from 0.5 to 10.7 μSv.

**Table 1**. Typical parameters of the procedure and effective doses for intraoral radiography

| Examination | | X-ray tube voltage (kV) | Exposure time (s) | EAK (mGy) | Effective Dose ICRP103 (μSv) |
|---|---|---|---|---|---|
| film | maxilla incisor | 50 | 1,43 | 8,75 | 12,4 |
| | | 60 | 0,22 | 1,39 | 2,5 |
| | | 70 | 0,20 | 1,39 | 3,4 |
| | maxilla premolar | 50 | 2,14 | 13,13 | 17,4 |
| | | 60 | 0,28 | 1,67 | 2,9 |
| | | 70 | 0,25 | 1,73 | 4,0 |
| | maxilla molar | 50 | 2,14 | 13,13 | 31,0 |
| | | 60 | 0,34 | 2,11 | 5,7 |
| | | 70 | 0,31 | 2,18 | 7,1 |
| | mandibula incisor | 50 | 1,43 | 8,75 | 14,6 |
| | | 60 | 0,20 | 1,25 | 2,7 |
| | | 70 | 0,16 | 1,11 | 3,2 |
| | mandibula premolar | 50 | 2,14 | 13,13 | 20,4 |
| | | 60 | 0,21 | 1,37 | 2,8 |
| | | 70 | 0,20 | 1,39 | 3,8 |
| | mandibula molar | 50 | 2,14 | 13,13 | 33,2 |
| | | 60 | 0,25 | 1,67 | 4,9 |
| | | 70 | 0,25 | 1,67 | 6,0 |
| | bitewing | 50 | 2,14 | 13,13 | 18,9 |
| | | 70 | 0,25 | 2,15 | 5,9 |
| digital detector | maxilla incisor | 60 | 0,06 | 0,54 | 1,1 |
| | | 65 | 0,06 | 0,46 | 1,0 |
| | | 70 | 0,06 | 0,66 | 1,6 |
| | maxilla premolar | 60 | 0,08 | 0,52 | 1,0 |
| | | 63 | 0,06 | 0,73 | 1,5 |
| | | 65 | 0,08 | 0,57 | 1,1 |
| | | 70 | 0,08 | 0,81 | 1,8 |
| | maxilla molar | 60 | 0,10 | 0,65 | 1,9 |
| | | 63 | 0,08 | 0,97 | 2,9 |
| | | 65 | 0,10 | 0,72 | 2,1 |
| | | 70 | 0,09 | 0,98 | 3,1 |
| | mandibula incisor | 60 | 0,05 | 0,44 | 1,0 |
| | | 65 | 0,05 | 0,37 | 0,9 |
| | | 70 | 0,05 | 0,47 | 1,2 |
| | mandibula premolar | 60 | 0,06 | 0,41 | 0,9 |
| | | 63 | 0,05 | 0,61 | 1,5 |
| | | 65 | 0,06 | 0,47 | 1,1 |
| | | 70 | 0,07 | 0,63 | 1,6 |
| | mandibula molar | 60 | 0,06 | 0,41 | 1,3 |
| | | 63 | 0,06 | 0,73 | 2,4 |
| | | 65 | 0,08 | 0,60 | 1,9 |
| | | 70 | 0,08 | 0,74 | 2,7 |
| | bitewing | 60 | 0,05 | 0,32 | 0,7 |
| | | 70 | 0,08 | 1,16 | 2,9 |

Results of the effective doses evaluation for these devices are quite homogeneous, which indicates the similarity of the conditions for conducting procedures on them. But on one device, doses are significantly higher than the doses on the other devices.

Typical values of effective doses and organs with the highest absorbed doses and the values of absorbed doses in them for each type of examination considered in the work, are presented in table 2.

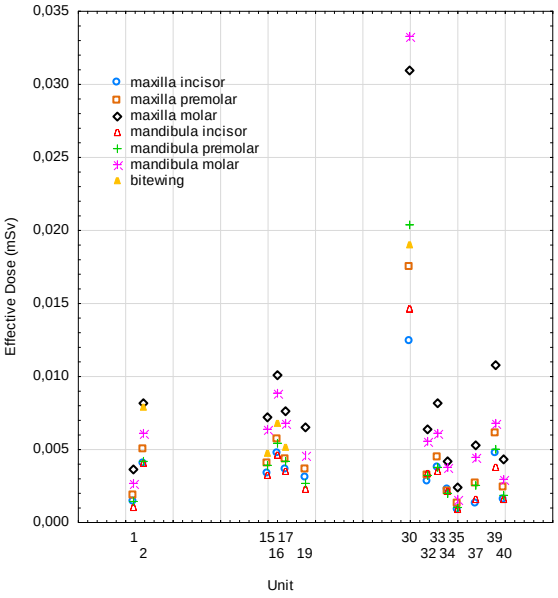


**Fig 1a.** Values of the effective dose of patients for radiographic dental studies on x-ray units with films in St. Petersburg and Leningrad region.

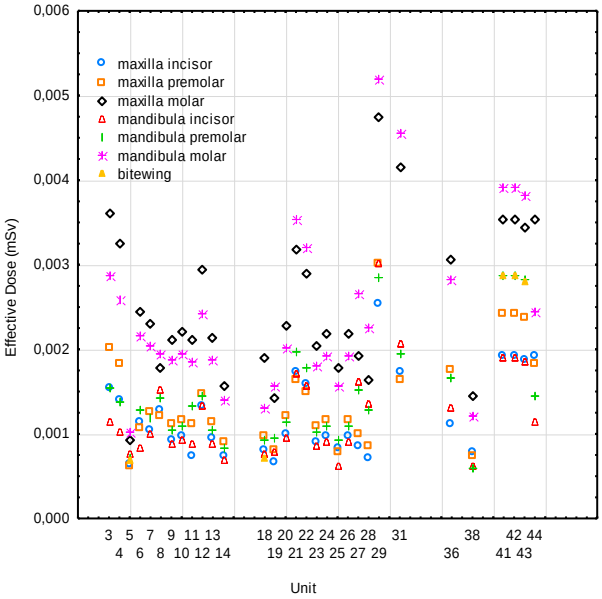


**Fig 1b.** Values of the effective dose of patients for radiographic dental studies on x-ray units with digital detector in St. Petersburg and Leningrad region.

**Table 2.** Effective dose (μSv) for the examination and organs with the highest absorbed doses (μGy)

| Examination | Organ, organ dose (μGy) | | | | | | | | Effective Dose (μSv) |
|---|---|---|---|---|---|---|---|---|---|
| film | | | | | | | | | |
| maxilla incisor | Oral mucosa, 147,4 | Extrathoracic airways, 67,2 | Skeleton, 23,1 | Brain, 11,2 | Lymph nodes, 9,8 | Salivary glands, 9 | RBM[1)], 4,6 | Skin, 4 | 3,2 |
| maxilla premolar | Oral mucosa, 170,3 | Extrathoracic airways, 71,2 | Skeleton, 26,5 | Brain, 16,6 | Salivary glands, 14,6 | Lymph nodes, 10,9 | RBM, 5,3 | Skin, 5 | 3,8 |
| maxilla molar | Salivary glands, 370,9 | Oral mucosa, 132,9 | Lymph nodes, 33 | Skeleton, 26,2 | Brain, 24,3 | Extrathoracic airways, 23,8 | Skin, 6,8 | RBM, 5,3 | 6,8 |
| mandibula incisor | Oral mucosa, 138,4 | Extrathoracic airways, 44 | Salivary glands, 39,8 | Skeleton, 17,4 | Lymph nodes, 9,5 | Thyroid, 8 | Skin, 4,5 | RBM, 3,5 | 3,2 |
| mandibula premolar | Oral mucosa, 147,1 | Extrathoracic airways, 46,6 | Salivary glands, 45,7 | Skeleton, 18,1 | Lymph nodes, 10,3 | Thyroid, 7 | Skin, 5,5 | RBM, 3,5 | 3,4 |
| mandibula molar | Salivary glands, 320,7 | Oral mucosa, 110,6 | Lymph nodes, 30,3 | Extrathoracic airways, 28,4 | Skeleton, 16,1 | Skin, 7,3 | Thyroid, 4,5 | RBM, 3,2 | 5,8 |
| bitewing | Oral mucosa, 189,6 | Thyroid, 58,4 | Extrathoracic airways, 39,2 | Skeleton, 26,6 | Salivary glands, 21,4 | Skin, 14,1 | Lymph nodes, 10,6 | RBM, 5,6 | 6,7 |
| digital detector | | | | | | | | | |
| maxilla incisor | Oral mucosa, 48,4 | Extrathoracic airways, 20,6 | Skeleton, 7,5 | Brain, 3,4 | Lymph nodes, 3 | Salivary glands, 2,8 | RBM, 1,4 | Skin, 1,3 | 1 |
| maxilla premolar | Oral mucosa, 54,8 | Extrathoracic airways, 21,5 | Skeleton, 8,4 | Brain, 5 | Salivary glands, 4,4 | Lymph nodes, 3,3 | Skin, 1,7 | RBM, 1,6 | 1,2 |
| maxilla molar | Salivary glands, 123,2 | Oral mucosa, 42,4 | Lymph nodes, 10,9 | Skeleton, 8,2 | Brain, 7,5 | Extrathoracic airways, 7,3 | Skin, 2,3 | RBM, 1,6 | 2,2 |
| mandibula incisor | Oral mucosa, 42,4 | Extrathoracic airways, 13,8 | Salivary glands, 12,5 | Skeleton, 5,3 | Lymph nodes, 3 | Thyroid, 2,5 | Skin, 1,4 | RBM, 1,1 | 1 |
| mandibula premolar | Oral mucosa, 55,3 | Extrathoracic airways, 18,5 | Salivary glands, 18,2 | Skeleton, 6,8 | Lymph nodes, 4,1 | Thyroid, 2,8 | Skin, 2 | RBM, 1,3 | 1,3 |
| mandibula molar | Salivary glands, 112,3 | Oral mucosa, 39,9 | Extrathoracic airways, 11,7 | Lymph nodes, 10,6 | Skeleton, 6,1 | Skin, 2,6 | Thyroid, 1,9 | RBM, 1,3 | 2 |
| bitewing | Oral mucosa, 81,6 | Thyroid, 24 | Extrathoracic airways, 16 | Skeleton, 11,2 | Salivary glands, 8,7 | Skin, 6,4 | Lymph nodes, 4,3 | RBM, 2,3 | 2,8 |

1) RBM – red bone marrow

Maximum absorbed doses are observed in the oral mucosa, only for examination of molars it is inferior to the salivary glands. In general, red bone marrow and thyroid gland, which are tissues with large weighting factors $w_T$, receive only a small fraction of the dose, with the exception of bite studies, where the thyroid gland is the organ with the second largest absorbed dose.

For other organs, the values of absorbed doses are significantly lower than those given in the table, and it can be recognized that they do not significantly contribute to the calculation of the effective dose.

The medians of the effective dose for X-ray units with film receivers were 3.2 μSv for the maxillary incisors, 3.8 μSv for the maxillary premolar, 6.8 μSv for the maxillary molars, and respectively, 3.2 μSv; 3.4 μSv and 5.8 μSv for the mandibulary incisors, premolars and molars, and for radiography of the bite - 6.7 μSv. For units with digital receivers: 1 μSv, 1.2 μSv, 2.2 μSv for the upper jaw, 1 μSv, 1.3 μSv, 2 μSv for the lower jaw and 2.8 μSv for the bite, respectively.

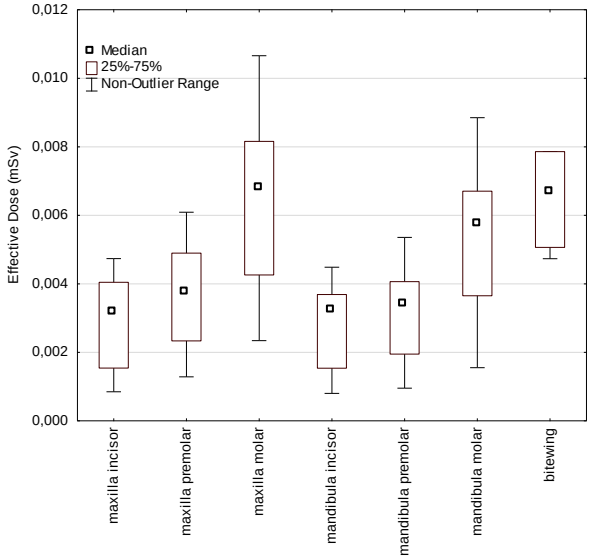


**Fig. 2a.** Medians, quantiles and ranges without emission of effective dose values for various examinations on x-ray units with films

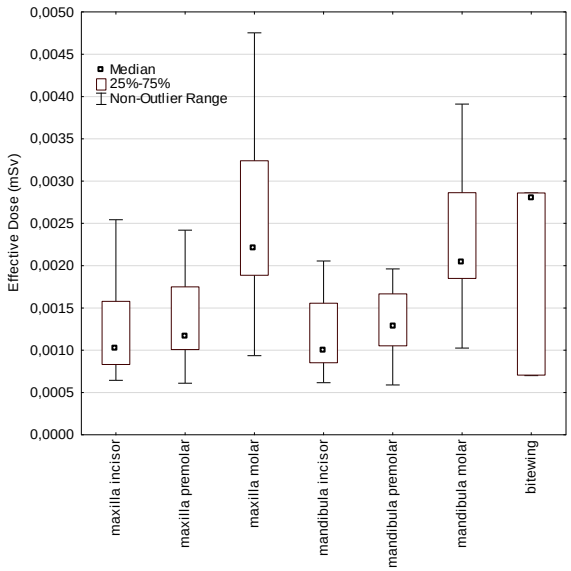


**Fig. 2b.** Medians, quantiles and ranges without emission of effective dose values for various examinations on x-ray units with digital detectors

Quantiles and non-outlier ranges of effective dose values for various studies are presented at Figures 2.a and 2.b. The significant width of the non-outlier ranges for examinations of molars of both jaws is noteworthy, which is the reason for the possible strengthening of optimization measures in carrying out these studies. The medians of the values in the distribution of effective doses for units with a film receiver are biased towards high doses, which suggests insufficient optimization for this examination mode. For units with digital receivers, on the contrary, the medians are biased towards lower values, which indicates a rather high level of optimization of the X-ray dental examinations.

Since effective doses for medical exposure in dentistry are rarely published, and measurable dosimetric values are used and published (input dose, product of dose by area, etc), the possibilities of comparing the results of this work were limited. Comparison of typical effective doses per study in medical institutions of St. Petersburg and the Leningrad Region with similar published data is presented in Fig. 3.

Effective doses for units with a film in St. Petersburg and the Leningrad Region are lower than the values obtained using a standard round collimator and films with medium and high sensitivity (class D and F, respectively) [6], and lower than the dose levels in the recommendations of the European Commission [7].

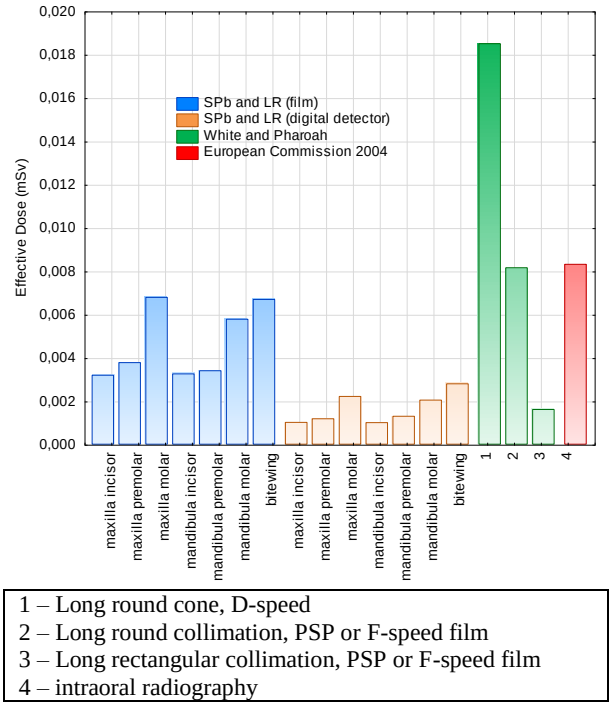


1 – Long round cone, D-speed
2 – Long round collimation, PSP or F-speed film
3 – Long rectangular collimation, PSP or F-speed film
4 – intraoral radiography

**Fig. 3.** Comparison of typical (median) doses in medical organizations in St. Petersburg and the Leningrad Region with published data and values used to fill in the 3-DOS form.

However, effective doses in St. Petersburg and the Leningrad Region are higher than those obtained using a square collimator and high-sensitivity films.

Assuming direct comparison of effective doses for X-ray units with digital receivers and high-sensitivity films, the values obtained in this study for units with digital receivers are close to the published values using a square collimator and high-sensitivity films.

As possible options for optimization measures, the use of the fastest available films corresponding to satisfactory diagnostic results [7], such as films of class E or F ISO, can be recommended for intraoral radiography. They reduce the patient's dose by more than 50% compared to class D films [7, 8, 9, 10]. Currently, the most suitable digital image detectors are sensors based on a charge-coupled device (CCD), built on solid-state technology. With their use, the dose is reduced by almost 50% compared with a class E film [10, 11].

Also, reducing the irradiation field to the minimum size necessary to obtain an image of an object of interest is an obvious means of limiting the dose of patients [7] and improves image quality [6] by reducing the scattered radiation. Traditionally, circular collimation has been used for intraoral radiography. The area of circular collimation with a diameter of 6 cm is approximately 135% larger than the area of a conventional dental film of size No. 2, ($S = 12.71\ cm^2$), which indicates significant opportunities for further collimation [12]. Since a rectangular collimator significantly reduces the dose compared to a round one [13, 14, 15], radiographic equipment should have a rectangular collimation for radiographs of teeth and occlusion [11].

## 4. Conclusion

Levels of patient exposure for dental intraoral examinations on X-ray units with film receivers in St. Petersburg and the Leningrad Region are lower than most of the published data. Moreover, the effective dose values obtained in this work are higher than those obtained using high-level optimization methods (square collimator and high-sensitivity films). This confirms the real possibility of further lowering patient exposure levels during x-ray dental examinations.

Patient exposure levels for devices with digital receivers are significantly lower compared to devices with film receivers.

## 5. References


1. United Nations Scientific Committee on the Effects of Atomic Radiation. Effects of Ionizing Radiation, UNSCEAR 2006 Report, Volume I, Annex A, NY, United Nations, 2008.
2. Tomohiro Okano Jaideep Sur. Radiation dose and protection in dentistry. Japanese Dental Science Review, Volume 46, Issue 2, August 2010, Pages 112-121
3. International Commission on Radiological Protection "Radiological Protection in Medicine", ICRP Publication 105, Ann ICRP 37 (6). Elsevier; 2007.
4. Cristy M. Mathematical phantoms representing children of various ages for use in estimates of internal dose. Oak Ridge National Laboratory, ORNL/NUREG/TM-367 (1980).
5. Tapiovaara M., Lakkisto M., Servomaa A. PCXMC: A PC-based Monte Carlo program for calculating patient doses in medical x-ray examinations. Report STUK-A139, 2nd Edition. Helsinki, Finnish Centre for Radiation and Nuclear Safety, 2008.
6. S.C. White, M.J. Pharoah. Oral radiology: principles and interpretation. (6th ed.), Mosby Elsevier, St. Louis (2009)
7. European Commission. Radiation Protection 136. European Guidelines on Radiation Protection in Dental Radiology. Luxembourg: Office for Official Publications of the European Communities, 2004
8. American Dental Association Council on Scientific Affairs: The use of dental radiographs. Update and recommendations. J Am Dent Assoc 2006;137:1304–12.
9. K. Syriopoulos, X.L. Velders, G.C.H. Sanderink, P.F. van der Stelt Sensitometric and clinical evaluation of a new F-speed dental X-ray film Dentomaxillofac Radiol, 30 (2001), pp. 40-44
10. M. Alcaraz, C. Parra, Y. Martinez Beneyto, E. Velasco, M. Canteras Is it true that the radiation dose to which patients are exposed has decreased with modern radiographic films? Dentomaxillofac Radiol, 38 (2009), pp. 92-97
11. S.C. White, E.W. Heslop, L.G. Hollender, K.M. Mosier, A. Ruprecht, M.K. Shrout Parameters of radiologic care: an official report of the American Academy of oral and maxillofacial radiology Oral Surg Oral Med Oral Pathol Oral Radiol Endod, 91 (2001), pp. 498-511
12. K. Horner, P.N. Hirschmann Dose reduction in dental radiography J Dent, 18 (1990), pp. 171-184
13. L.T. Kircos, L.L. Angin, L. Lortan Order of magnitude dose reduction in intraoral radiography J Am Dent Assoc, 114 (1987), pp. 344-347
14. J.P. Freeman, J.W. Brand Radiation doses of commonly used dental radiographic surveys Oral Surg Oral Med Oral Pathol, 77 (1994), pp. 285-289
15. K. Horner Radiation protection in dental radiology Br J Radiol, 67 (1994), pp. 1041-1049

*MEDICAL PHYSICS IN THE BALTIC STATES 14 (2019)*

Proceedings of the International Conference "Medical Physics 2019"
7 - 9 November 2019, Kaunas, Lithuania

# FIRST APPROACH TO 3D DOSIMETRY VERIFICATION USING LEKSELL GAMMA KNIFE® ICON™

Evelina JASELSKĖ[1,2], Linas KUDREVIČIUS[1], Viktoras RUDŽIANSKAS[1,2], Tadas DIDVALIS[1], Diana ADLIENĖ[2],
[1]The Hospital of Lithuanian University of Health Sciences Kaunas Clinics, Oncology Institute
[2]Kaunas University of Technology, Physics Department
evelina.jaselske@ktu.edu, diana.adliene@ktu.lt, viktoras.rudzianskas@kaunoklinikos.lt, kudreviciuslinas@gmail.com, tadas.didvalis@kaunoklinikos.lt

***Abstract:*** Gamma knife radiosurgery is a very precise method to treat the brain diseases. Since high energy gamma rays are very focused to the target accurate dosimetry solutions are mandatory [1]. Due to the steep dose gradients in the irradiation field close to the target, dosimetry method is required which provides information on 3D dose distribution and might be followed visually. Polymer gel dosimetry is the only method which fulfils these requirements [2]. Polymerized gels are sensitive enough to register absorbed doses in the wide range from starting from 0.1 Gy [3] to tens of Gy. According to the type of ionising radiation and target volume different formulations of dose gels are possible, however the quality of the final measurement result depends on the individual physical properties of dose gels, on accuracy and precision of gel dosimeters and their read out methods.
The aim of this work was to initiate application of gel dosimetry for dose verification in gamma knife treatment.

***Keywords:*** 3D dosimetry, polymerized gels, Gamma knife, dose verification, MRI read-out.

## 1. Introduction

Polymer gel dosimetry is still only one known method which provides visualization possibility for three - dimensional dose distribution in irradiated volume. Gel dosimeters are recognized as being very useful for the treatment dose verification in radiotherapy [4]; however their application requires specific knowledge regarding selection of suitable materials, proper gel manufacturing procedure, selection of irradiation geometry and parameters and also selection of most sensitive dose read out method and read out technique. Due to the high gamma photon energies and precise beam positioning using Gamma knife unit, application of individual dosimetry method for the visualization of spatial dose distribution is beneficial in terms of avoiding of possible errors and uncertainties during the treatment procedure. It is also to note, that the density of polymer gels is almost the same as of human soft tissues (ex. $\rho_e^w$ muscle/nPAG=0.94/1.035 etc) [5].
Polymer gel based dose measurements are mainly adjusted for large volumes. However dose measurements in microscale targets that are smaller than 1 $cm^3$ are challenging since high uncertainties may occur due to a small volumes or small doses [6].
The visualization of the 3D dose distribution in irradiated microscale targets and evaluation of the absorbed dose values in these targets followed by the comparison of experimental data with Gammaplan ATR 10 algorithm simulated data was the main purpose of this study.

## 2. Materials, instruments and methods

### 2.1. Manufacturing of gels

Normoxic polyacrylamide (nPAG) and N-vinylpyrrolidone based VIPAR polymer gels were selected for performing of experiments, taking into account gels sensitivity and simplicity of their manufacturing.
nPAG gel was made of 5% gelatin (porcin skin, 300 bloom), 3% Acrylamide (AAm), 3% N,N'- methylene-Bis-acrylamide (BIS), 10mM/l (Hydroksimetil) phosphonium chloride (tetrakis, THPC) and ultrapure distiled water.
Modified formula of VIPAR gels was used for production of VIPARnd (VIPAR-normoxic-double) dose gel containing of 8% N-vinylpyrrolidone, 7.5% gelatine (from porcin skin, 300 bloom), 4% N,N′-methylenebisacrylamide (BIS), 0.0008% copper sulphate ($CuSO_4$ x$5H_2O$), 0.007% ascorbic acid and ultrapure distiled water [7]. Modification of the VIPAR gel was performed in order to achieve higher sensitivity in low dose region.
Gels were prepared strictly following manufacturing procedure discribed in our previous publication [8]. Ready gels were poured into 100 ml experimental vials,

tightly closed and left in a dark cool room for 24 hours to set. Dose gel filled vials are shown in Fig.1.

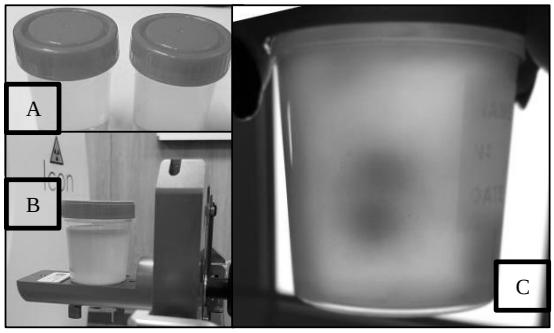


**Fig. 1.** Manufactured (A), prepared for irradiation (B) and irradiated (C) dose gels vials.

### 2.2. Gels irradiation and read-out

Dose gels samples were irradiated in Gamma knife Icon TM unit (192 $^{60}$Co sources) combining 4 and 8mm collimator sizes according to the „Gammaplan" simulated clinical dose treatment plan for real patient. Irradiation was performed in two shots for both types of gels: first shot was performed at location 100x130x100 mm and the second one - at location 90x120x110mm. The first target is marked in Fig.1C as I and the second – as II respectively. Treatment time for the first shot was 12.12min, for second – 8.14 min; 12.0Gy@50% prescribed dose was used for irradiation. The dose rate at the focus was 1.91 Gy/min and 2.85 Gy/min respectively. Irradiated vials were left for 24 hours in the dark place to complete polymerisation reactions.

Irradiated dose gel samples were scanned in Siemens Magnetom 1.5T MRI unit. There are several methods to evaluate scanned images, but we have have chosen a method based on comparison of two MRI image parameters selecting different echo times from T2 sequence [9], having in mind that better dose resolution can be achieved in irradiated dose gels using T2 sequence.

Following parameters were used for MRI dose read out from irradiated gel samples: T2 TSE transversal sequence; HE 1-4 head coil element; 0,4x0,4x5,0 mm voxel size; field of view (FoV) 230 mm, repetition time (TR) 4080ms; and few variations of echo times TE (11, 89, 145ms). Selected echo times were close to those recommended by other authors [10] for reading-out of polymer gel dosimeters. Scanning was performed at room temperature.

Transfer relaxation time (T2) weighted images of each 5mm thick slice were obtained and relaxation time T2 ($R_2^{-1}$) calculations were performed using appropriate equations (Eq1 and Eq2) [11, 12]:

$$\boldsymbol{R_2 = \frac{1}{T_2} = \frac{1}{TE_2 - TE_1} ln\left(\frac{S_1}{S_2}\right)} \quad (1)$$

$$\boldsymbol{T_2 = \frac{TE_2 - TE_1}{ln\left(\frac{S_1}{S_2}\right)}} \quad (2)$$

where $TE_i$ are echo times, $S_1$ and $S_2$ – signal intensities at selected data points, T2 – relaxation time.

Images were obtained and analyzed using ImageJFX, Weasis medical viewer 2.5.0 open source softwares and visualized with SigmaPlot 14.0 software.

Series of MRI scanns of each vial were obtained for the selected echo times: 10 ms, 89 ms and 145 ms. Relative pixel intensity values were evaluated in five points following simulated dose profile line. Each point was in the same image slice and has the same x, y and z coordinates. The first point was selected at isocenter position where the dose is the highest, another points were distributed in 4 mm steps along X axis at both sides of isocenter.

Output factors were also calculated [13].

## 3. Results

### 3.1. Pixel intensities measurements

Polymerized nPAG and VIPARnd samples were scanned in MRI unit keeping the same set of parameters varying T2 echo times (10 ms, 89 ms and 145 ms) and the sequences of MRI images for each dose gel were obtained. Pixel intensity values were evaluated by selecting five different points as data points in the same image slice along dose profile line as it was described in previous section of this article. Evaluation of pixel intensities was performed for each target (at shot I and shot II location) separately.

The results for the first shot I are provided in Fig.1. and for the shot II - in Fig.2.

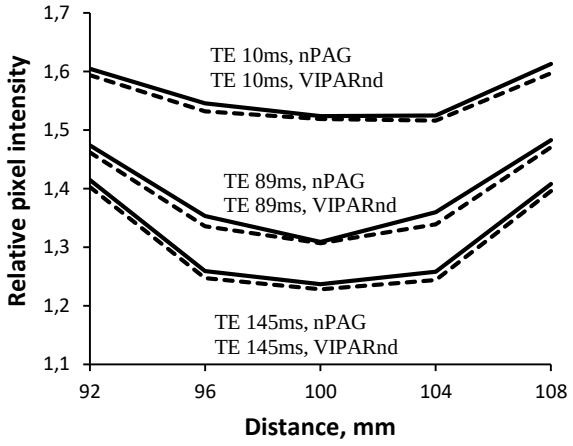


**Fig.1.** Distance dependent pixel intensity variations for the first target (shot I).

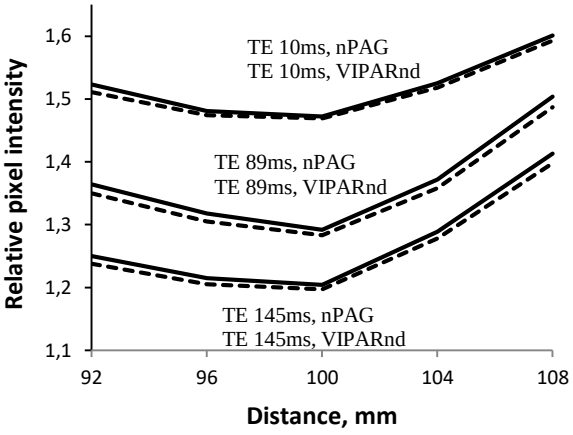


**Fig.2.** Distance dependent pixel intensity variations for the first target (shot II).

It was shown that MR images were dependent on the selected T2 echo time, indicating higher image resolution with lower T2 echo time. The same tendency was demonstrated for both, nPAG and VIPARnd gels after their irradiation in Gamma knife facility.

### 3.2. Evaluation of T2 relaxation time

T2 relaxation time has been calculated for nPAG and VIPARnd dose gels and comparison between TE10/TE89ms and TE89/TE145ms sequences in the same image slice were performed selecting pixels from region of interest at isocenter area. It should be noted that relaxation time varies with a temperature. Our irradiated gels were stored in MRI room for 24 hours before the reading-out procedure. Calculation results for the first target (shot I) and for the second target (shot II) are provided in Fig.3 and Fig.4 respectively.

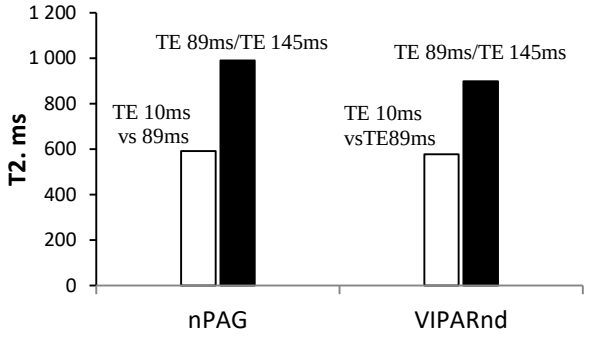


**Fig. 3.** Comparison of calculated T2 times for nPAG and VIPARnd gels for the first target (shot I).

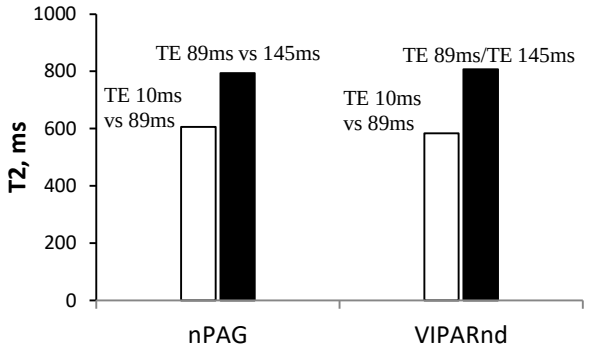


**Fig. 4.** Comparison of calculated T2 times for nPAG and VIPARnd gels for the first target (shot II).

Calculation results indicate applicability of the explored methodology to perform measurements with selective T2 echo times for the estimation of specific gel's response to irradiation dose. It was found that the calculated VIPARnd gel relaxation time was longer and corresponding relative pixel intensities were lower as compared to nPAg gel in all investigated cases. This led to suggestion that VIPARnd gels might be more sensitive to high irradiation doses (24 Gy in total, as per this investigation) than nPAG gel.

### 3.3. Output factor calculation

Output factors (OF) calculations are needed for the adjustment of the dose to the target values when isocenter coordinates are different from 100x100x100 mm. Output factor of 0.9645 for the first target with 100x130x100mm coordinates was calculated when applying 8mm Leksell Gamma knife Icon™ unit collimator and of 0.9666 for the second target with 90x120x110mm coordinates respectively.

## 4. Discussions and conclusions

nPAG and VIPAR dose gels were sensitive enough to record 3D absorbed dose distribution demonstrating closely similar shape as compared to simulated with Gammaplan software. MRI scanning of nPAG and VIPARnd gel samples was performed using the same parameter set but selectively applying different T2 echo times. Relative pixel intensities in MR images scans of two different polymer gels have been evaluated at the selected points along dose profile line. It was found that higher MR image resolution could be achieved with lower T2 echo time. Relative pixel intensities measurements demonstrated good agreement between nPAG and VIPARnd after irradiation under the same conditions. Differences did not exceed 0.5% at the selected point from ROI with isocenter for the target I with TE 10ms, 89ms and 0.75% with TE 145ms respectively. Estimated values for the second target were 0.5%, 0.7% and 0.6% for TE 10ms, TE 89ms and TE 145ms respectively.

Comparison of the obtained T2 relaxation time related results allowed for estimation of gels response to the irradiation dose. It was found that the calculated VIPARnd gel relaxation time was longer and corresponding relative pixel intensities were lower as compared to nPAg gel in all investigated cases. This led to suggestion that VIPARnd gels might be more sensitive to higher irradiation doses (24 Gy in total, as per this investigation) than nPAG gel. However more detailed investigations are needed for the approval of the specific dose gel suitability for clinical dosimetry in Gamma Knife therapy.

## 5. Acknowledgment

This work was partly supported by the research grant No. S-MIP-17-104 of Lithuanian Reserach Council

## 6. References

1. Theodorou K, Stathakis S, Lind B, Kappas C (2009) Dosimetric and radiobiological evaluation of dose distribution perturbation due to head heterogeneities for Linac and Gamma Knife stereotactic radiotherapy. Act. Onc. Vol. 47(5): 917-927;
2. Baldock, C., De Deene, Y., Doran, S. Polymer gel dosimetry, Phys. Med. Biol. 55 (2010) R1–R63;
3. Urbonavicius B.G, Adliene D (2018) In situ assessment of X-ray induced changes in polymerized gels using surface plasmon resonance detector. Nucl. Instr. Meth. In Phys. Res. Sec. B. 435: 236-241;
4. Pak F, Vaezzadeh V, Eqlimi E, Mirheydari M (2019) Analysis of induced error by susceptibility effect in low-density gel dosimeters. J. of Can. Res. and Ther. Vol 15(3): 498-503;

5. Farajollahi A, Pak F, Horsfield M, Myabi Z (2014) The basic radiation properties of the Nisopropylacrylamide based polymer gel dosimeter. Int. Jour. Rad. Res. Vol. 12 (4): 347-354;
6. Keshtkar M, Takavar A, Zahmatkesh M.H, Montazerabadi A.R (2017) Uncertainty analysis in MRI-based Polymer Geld Dosimetry. Biomed. Phys. Eng. 7(3): 299-304;
7. Kozicki M, Maras P, Rybka K, Bieganski T (2007) On the Development of VIPAR Polymer Gel Dosimeter for Three-Dimentional Dose Measurements. Macr. Symp. 254(1): 345-352;
8. Adliene D, Jakstas K, Vaiciunaite N (2014) Application of optical methods for dose evaluation in normoxic polyacrylamide gels irradiated at two different geometries. Nucl. Instr. Meth. In Phys. Res. A. 741: 88–94;
9. Fanea L, Sfrangeu S A (2011) Relaxation Times Mapping Using Magnetic Resonance Imaging. Rom. Rep. Phys. Vol 63(2): 456-464;
10. Lepage M (2006) Magnetic resonance in polymer gel dosimetry: techniques and optimization. J. of Phys. 56: 86-94;
11. Watanabe Y, Mizukami Sh, Eguchi K, Maeyama T, Hayashi Sh et al (2019) Dose distribution verification in high-dose-rate brachytherapy using a highly sensitive normoxic N-vinylpyrrolidone polymer gel dosimeter. Phys. Med. 57: 72-79;
12. Chang Y, Lin J, Hsieh B, Yao Ch (2014) Dose evaluation of an NIPAM polymer gel dosimeter using gamma index. Rad. Phys. and Chem. 104: 180-187;
13. Pantelis E, Antypas C, Petrokokkinos L, Karaiskos P, Papagiannis P et al (2008) Dosimetric characterization of CyberKnife radiosurgical photon beams using polymer gels. Med. Phys. Res and Prac. Vol 35(6): 2312-2320.

*MEDICAL PHYSICS IN THE BALTIC STATES 14 (2019)*

Proceedings of International Conference "Medical Physics 2019"
7 – 9 November 2019, Kaunas, Lithuania

# BENEFITS OF USING AUTOMATED ARTIFICIAL INTELLIGENCE OPTIMIZATION ALGORITHM IN RADIATION THERAPY

Romualdas GRIŠKEVIČIUS[1], Marijus ASTRAUSKAS[1], Kęstutis. AKELAITIS[1], Ieva MARKEVIČIENĖ[1], Jonas VENIUS[1,2]
[1]National Cancer Institute, Department of Medical Physics
[2]National Cancer Institute, Biomedical Physics Laboratory
romualdas.griskevicius@nvi.lt; jonas.venius@nvi.lt;

***Abstract*:** National Cancer Institute has introduced the possibility to use AI solutions to perform dosimetric treatment planning tasks.
Our aim was to evaluate the quality and the plan preparation time of the automated optimization module.
In conclusion – AI models significantly accelerates the optimization process, increase consistency and could improve the quality of created RT plans alone or in combination with manual adjustments.

***Keywords*:** Radiotherapy, knowledge-based treatment planning,

## 1. Introduction

Radiation therapy is a complex process which involves certain steps: the definition of the treatment target and the healthy tissues to be protected, the creation of a dosimetric plan, its realization and the follow-up of the patient. The latest Radiation Therapy (RT) equipment allows you to plan and realize intensity modulated radiation therapy. Modulation can take place in fixed gantry angles (IMRT - Intensity Modulated Radiation Therapy) and during gantry rotation (VMAT - volumetric modulated Arc Therapy). All this is a complex individualized process that depends on the specific clinical situation, patient's anatomy and experience of the clinicians. Processes could be optimized and accelerated using intelligent computer solutions. In clinical work, the contours of the target and surrounding organs are defined in each slice of computed tomography (CT), which takes a long time and depends on the experience of the person performing the contouring. Artificial Intelligence (AI) systems that are currently commercially available can be used to facilitate and improve this process. Such systems help to automatically define treatment targets and organs to be protected, and to prepare a radiation therapy treatment plan. However, at present, such assistance is rarely used in routine clinical practice. One reason is the limited ability of the software to take into account the individual patient's anatomy. Another time-consuming task is to prepare a dosimetric treatment plan. The National Cancer Institute has introduced the possibility to use AI solutions to perform dosimetric RT treatment planning tasks. An automated knowledge-based treatment planning algorithm RapidPlan (RP) is trained with the best dosimetric plans created by the experts. Consequently, taking into account all the data from the sample plans accelerates the optimization process. During the optimization, the treatment planning system looks for the most appropriate solution based on the formulated tasks. Based on the data used to train the model, the system is able to recognize the localization of the structures, its overlap and is able to replicate the parameters of optimal treatment plans. During the optimization process algorithm adapts data from the sample plans to the new patient. For the successful functioning of the RP algorithm the treatment preparation process should be standardized – planning data must include the same number of the structures as it was in the sample plans, the same contouring pattern and arrangement of treatment fields. However, it is common that the model for the RP is used from the leading RT centers and the rules for the contouring and treatment planning could be different in the local hospital. On the other hand, when creating a model in your own hospital it could be rather difficult to preserve an identical contouring and treatment planning conditions.
The aim of this work was to evaluate the quality of the dosimetric treatment plans created by different RP models for different localizations. The secondary objective was to compare the plan preparation time and complexity of the plans.

## 2. Methods

For the comparison of the plan's quality two different scenarios were chosen: simple one – low risk prostate; and complicated – head&neck (H&N). The prostate case includes the prostate as the target (prescribed dose - 78Gy

in 39 fractions) and the typical critical structures (bladder and rectum). H&N cases includes three targets irradiated with simultaneous integrated boost technique with three different dose levels (high dose – 66.9Gy; middle dose – 60Gy; low dose – 54Gy in 30 fractions) and large amount of critical organs at risk (OAR): (spinal cord, parotid glands, oral cavity, mandibular, larynx, esophagus, pharyngeal constrictor muscles). In total 16 patients who has been treated for prostate cancer and 29 for the H&N cancer has been extracted from NCI database. Mainly it was VMAT plans: (prostate 12 plans, H&N – 26 plans;) IMRT (prostate 4 plans, H&N – 3). Target coverage and dosimetric criteria for critical organs were consistent with the RT methodological descriptions approved in NCI. The contouring and the planning has been performed on Varian treatment planning system (TPS) Eclipse v.15.5 (Palo Alto, California, USA). Dose volume histograms (DVH) were extracted from TPS and analyzed with RStudio package DVHmetrics.

### 2.1. Automated optimization methodology

For prostate patients, RP plans were created using Washington University Prostate Model, St. Louis MO, USA (WUSTL). For H&N patients two different models were evaluated: WUSTL (Washington University H&N Model, St. Louis MO, USA.) and CCMB (CancerCare Manitoba, Winipeg MB, Canada). Plan creation with RP methodology has been performed with one optimization, i.e. the generated plan was not re-optimized and adjusted. Plans have been normalized so that the average dose in the target volume is equal to the prescribed dose in order to compare the initial plans with the RP generated plans.

### 2.2. Comparison of treatment plans

For the comparison of dosimetric treatment plans, the dosimetric indicators for target and critical organs were used:

- The target coverage (%): 5% dose of target volume (D5) and 95% dose of target volume (D95);
- Dose homogeneity index (DHI) according to ICRU 83: (DHI = (D2%-D98%)/D50%);
- Conformity index: ratio of volume of target prescribed isodose to volume of target).
- Mean dose in Gy to organs at risk
- Maximum dose in Gy to organs at risk (spinal cord, mandibular)
- The assessment of the plan complexity. Number of monitor units (MU) used to realize the dose.
- Plan generation time. Time in minutes to create treatment plan.

## 3. Results

The goal during RT treatment planning is to distribute the prescribed dose homogeneously and conformally within the target. The prescribed dose (100%) should cover the entire volume of the target (100%), but the complicated form of the tumor, localization and surrounding healthy tissues always leads to a compromised coverage of the target. As a result, it is recommended that at least 95% of the dose should cover 95% of the target. On the other hand, doses strongly exceeding prescribed dose should be avoided, because it becomes ineffective based on radiobiological background. For that, D5% should be kept as close to the prescribed dose as possible.

In prostate cases, 95% of the target volume should be covered by 74.1 Gy. Both planning methods – NCI and RP generates better dose coverage. In plans generated by RP, D95% is increased by an average of 0,7% (0.5 Gy) till 76.7Gy compared to the conventionally (NCI) created plan 76.2Gy (fig.1). The difference was statistically significant (p = 0.018). D5% for the RP is decreased by an average of 0,3% (0.2 Gy) till 79.2Gy compared to the conventionally created plan 79.4Gy (fig.1). The difference was statistically significant (p = 0.036).

DHI with the RP technique improved in 12 out of 16 cases – 0.06 for NCI and 0.05 for WUSTL model. The difference was statistically significant (p = 0.047).

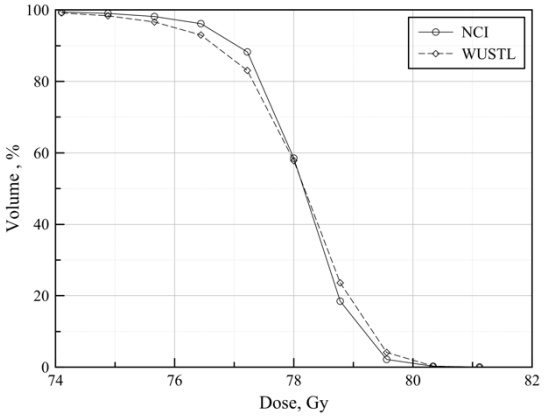


**Fig. 1.** DVH fragment for prostate PTV.

There was also a slight increase in the CI: 0.59 for NCI and 0.60 for WUSTL. The difference was not statistically significant (p = 0.519). Thus, the auto-optimization algorithm did little to improve the quality of the plan.

For the H&N patients SIB technique was used, where three targets should be covered homogeneously and conformally with different prescribed doses. Target coverage statistics are presented in table 1. In the low dose target D95% should be at least 51.3Gy. For the WUSTL model D95% was statistically significantly lower than in NCI plans 52.08Gy vs 52.58Gy (Fig. 2)(Table 1), while CCMB had insignificantly better coverage 52.61Gy vs 52.58Gy.

D5% for the low dose target should be kept as close as possible to 54Gy. In this case WUSTL model had significantly better D5% value in comparison to NCI plans – 55.6Gy vs 56.34Gy. While CCMB had significantly worse D5% value – 56.74Gy vs 56.34Gy.

DHI for WUSLT algorithm was insignificantly better in comparison to NCI – 0.09 vs 0.1, while CCMB algorithm had significantly worse DHI – 0.11 vs 0.1.

CI for WUSTL model was significantly worse than for NCI plans – 1.3 vs 1.25; CCMB model performed significantly better – 1.19 vs 1.25.

In the middle dose target, D95% should be at least 57 Gy. Both WUSTL and CCMB models D95% was statistically significantly lower than in NCI plans WUSTL – 58.85Gy CCMB – 58.95Gy vs NCI – 59.03Gy (Fig. 3).

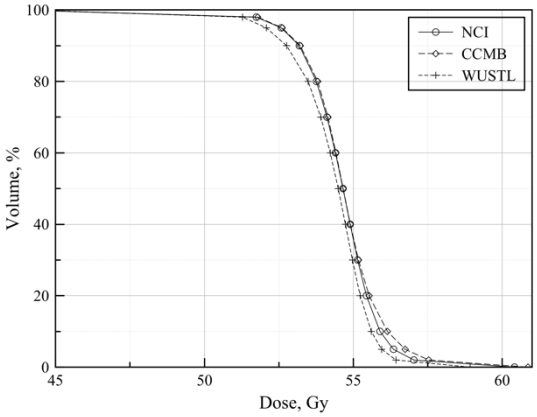


**Fig. 2.** Fragment of DVH for PTV_54 structure.

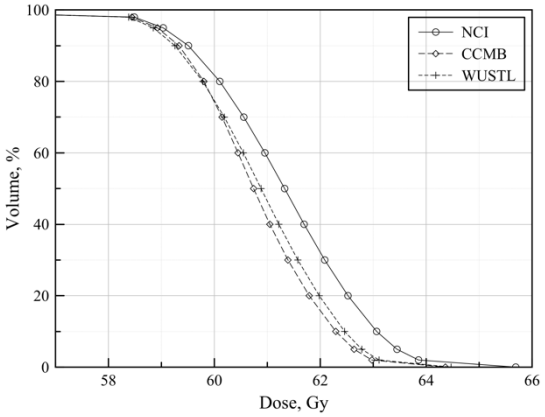


**Fig. 3** Fragment of DVH for PTV_60 structure.

D5% for the middle dose target should be kept as close as possible to 60Gy. WUSTL and CCMB models had significantly better D5% values in comparison to NCI plans: WUSTL – 62.79Gy CCMB – 62.64Gy vs NCI – 63.45Gy.

DHI for both WUSLT and CCMB algorithms was significantly better in comparison to NCI – 0.09 vs WUSTL – 0.08; CCMB – 0.07;

CI for WUSTL model was significantly better than for NCI plans – 0.89 vs 0.94; CCMB model performed similar – 0.89 vs 0.88.

**Table 1.** Comparison of dosimetric plans

| **Metric** | **NCI_54** | **CCMB_54** | **WUSTL_54** |
|---|---|---|---|
| DHI | 0.10 | 0,11<br>p=0,045 | 0,09<br>p=0,54 |
| CI | 1.25 | 1.19<br>p=0.007 | 1.3<br>p=0.02 |
| D95% | 52.58Gy | 52.61<br>p=0,73 | 52.08<br>p=0,00001 |
| D5% | 56.34Gy | 56.74<br>p=0,007 | 55.60<br>p= 0,005 |
| | **NCI_60** | **CCMB_60** | **WUSTL_60** |
| DHI | 0,09 | 0.07<br>p=0,0015 | 0,08<br>p= 0,006 |
| CI | 0.89 | 0.88<br>p=0.6 | 0.94<br>p=0.0004 |
| D95% | 59.03 | 58.92<br>p=0,2208 | 58.85<br>p=0,0465 |
| D5% | 63.45 | 62.64<br>p=0,0002 | 62.79<br>p=0,0014 |
| | **NCI_66.9** | **CCMB_66.9** | **WUSTL_66.9** |
| DHI | 0,08 | 0,08<br>p=0,22 | 0,08<br>p=0,47 |
| CI | 1.04 | 0.87<br>p=0,02 | 1,22<br>p=0.000005 |
| D95% | 64,33 | 64.16<br>p=0,2 | 64.15<br>p=0,14 |
| D5% | 68.50 | 68.57<br>p= 0,39 | 68.58<br>p=0,3 |

For the high dose target, D95% should be at least 63.6 Gy. Neither WUSTL nor CCMB models had no significant difference in D95% comparing with NCI plans - 64.33Gy vs WUSTL – 64.15Gy and CCMB – 64.16Gy (Fig. 4).

D5% for the high dose target should be kept as close as possible to 66.9Gy. WUSTL and CCMB models had performed similarly without statistically significant difference in D5% value in comparison to NCI plans – 68.5Gy vs WUSTL – 68.58Gy; CCMB – 68.57.

DHI for NCI, WUSLT and CCMB algorithms was the same 0.08.

CI for WUSTL model was significantly worse than for NCI plans – 1.22 vs 1.04; the same was for CCMB model – 0.87 vs 1.04.

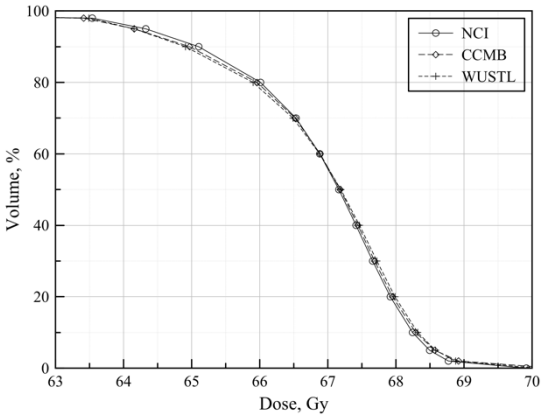


**Fig. 4.** DVH fragment for PTV_66.9 structure.

### 3.1. Evaluation of healthy organ / tissue sparring for prostate cases

Significant differences were observed in rectal and bladder DVHs for different planning approaches. WUSTL model developed a 17% more rectal protective plan (Fig. 5.): mean dose for NCI 38.84Gy vs 33.12Gy for WUSTL. The difference is significant ($p<0.001$).

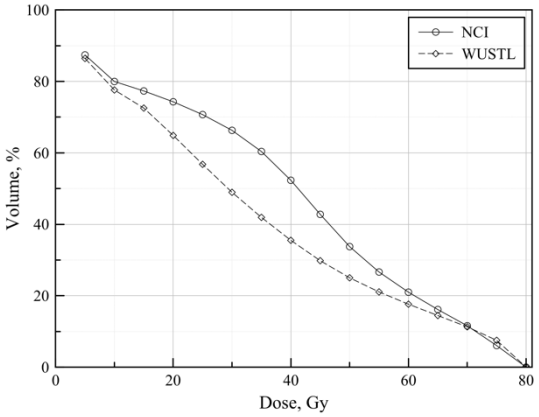


**Fig. 5.** DVH for rectum structure

Comparison of bladder DVHs revealed similar trends Fig. 6. The mean dose to bladder structure was 2.55 Gy lower in WUSTL model (30.5 Gy in WUSTL vs 33.05 Gy in NCI). The difference was significant ($p<0.001$).

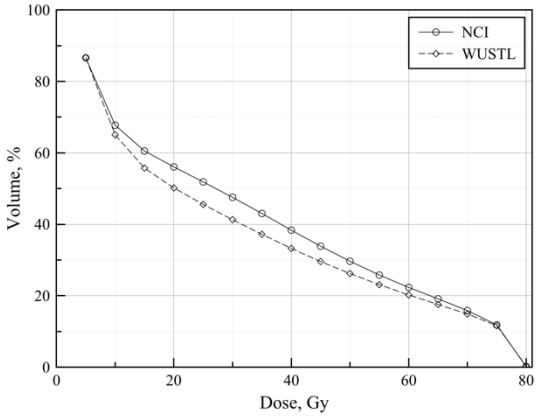


**Fig. 6** DVH for the bladder structure.

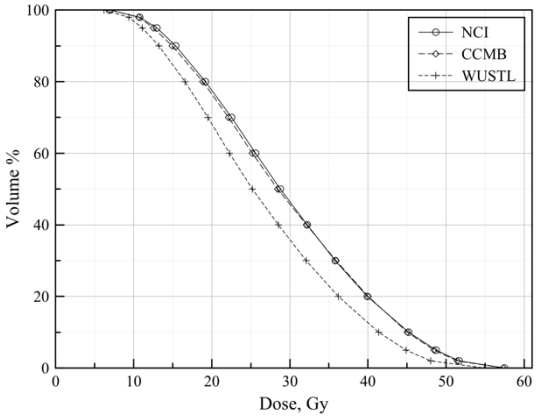


**Fig. 7** DVH for Oral cavity structure

### 3.2. Evaluation of healthy organ / tissue sparring for H&N cases

Creating good quality treatment plans for the H&N cases is challenging, because of big target volumes, different prescribed dose levels to targets, and a lot of critical healthy organs, which are located close to the target. Sparing those organs can increase quality of life for H&N patients. It is always a difficult and time consuming task to find the right balance between target coverage and OAR sparing. According to ALARA principle we should seek for the minimum doses to OAR not compromising target coverage. OAR statistics are presented in table 2.

**Table 2.** OAR statistics for NCI, CCMB, WUSTL treatment plans.

| Metric | NCI | CCMB | WUSTL |
|---|---|---|---|
| *Oral cavity* | | | |
| DMEAN | 29,60 | 29,38 p=0,67 | 26,38 p=0.0000002 |
| *Esophagus* | | | |
| DMEAN | 29.47 | 32.25 p=0,0008 | 22.66 p=1.83121E-07 |
| *Larynx* | | | |
| DMEAN | 37,37 | 37,87 p=0,68 | 34,56 p=0,08 |
| *Spinal cord* | | | |
| DMAX (Gy) | 36,4 | 40.29 p=1.3434E-08 | 38.82 p=0.0001 |
| *Mandibulla* | | | |
| DMAX | 61,35 | 62,16 p=0,008 | 61,53 p=0,66 |
| *Parotis sin* | | | |
| DMEAN | 27,06 | 26,22 p=0,17 | 29,69 p=0,0004 |
| *Parotis dex* | | | |
| DMEAN | 25,02 | 25,38 p=0,25 | 28,60 p=0,000006 |
| *Inferior pharyngeal constrictor muscle* | | | |
| DMEAN | 43,98 | 43,80 p=0,86 | 43,11 p=0,49 |
| *Superior pharyngeal constrictor muscle* | | | |
| DMEAN | 45,61 | 46,13 p=0,34 | 45,38 p=0.71 |
| *Middle pharyngeal constrictor muscle* | | | |
| DMEAN | 45,67 | 46,07 p=0,71 | 47,37 p=0,21 |

On oral cavity structure WUSLT algorithm did better than NCI, lowering mean dose by 3Gy (Fig. 7).
Difference is statistically significant ($p<0.001$). The difference between CCMB and NCI was insignificant.
Esophagus (Fig.8) mean dose was smaller in WUSTL created plans (WUSTL 22.66Gy vs. NCI 29.47Gy), difference is statistically significant ($p<0.001$).

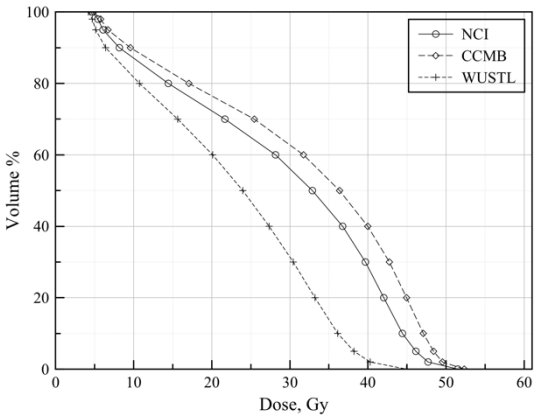


**Figure 8** DVH for esophagus structure

Larynx (Fig.9) mean dose was smaller in WUSTL model plans (WUSTL 34.56Gy vs. NCI 37.37Gy), difference is statistically insignificant ($p<0.001$).

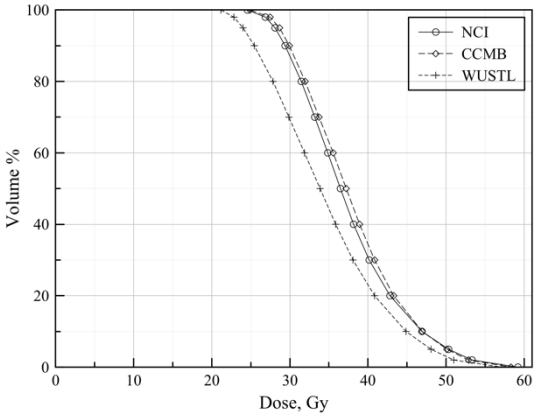


**Figure 9** DVH for larynx structure

Maximum dose for spinal cord and mandibula structures was smaller in NCI created plans. (WUSTL 38.82Gy vs. NCI 36.4Gy), difference is statistically significant (p=0.001); (CCMB 40.29Gy vs. NCI 36.4Gy), difference is statistically significant (p<0.001).

Mean dose of both parotid glands with CCMB model was similar to NCI, whereas WUSTL model created significantly poorer plans compared to NCI. Mean dose for both parotid glands was significantly higher (p<0,001).

Doses to constrictor muscle (inferior, superior and middle) were similar for all three models NCI, CCMB and WUSTL (no significant difference).

### 3.3. Assessing the complexity of a treatment plan

The complexity of a treatment plan at some extent can be evaluated as a number of monitor units (MU). This relative number represents the amount of radiation coming from the target to the patient through the beam collimation devices. Given that the patient is receiving the same dose, a higher number of MUs reflects the complexity of the prepared plan. More complex plan is characterized by a larger number of small fields and a more intense movement of the multileafs. This allows for a more consistent dose distribution and greater protection of critical organs. However, it is worth noting, that over-modulation can lead to plan implementation errors due to the limited ability of apparatus and movements of internal organs and the target. However, before realizing the plan to the patient, a dosimetric verification of the plan is performed and an assessment is made whether the equipment is able to deliver the planned dose distribution. This determines the capabilities of the machine, but does not count the movement of the internal organs and the target.

Due to the additional multileaf diaphragm modulation for greater protection of critical organs, RP model generated prostate plans have a higher number of monitor units (MUs). On average, prostate RP plans had 111.2 MU more than conventional plans (NCI plan 570.3, RP plan 681.5). On average, RP plans for H&N cases had 57 MU less than NCI plans (NCI plan 584,8, CCMB plan 523,8, WUSTL plans 532,3).

### 3.4. RP Plan Generation Duration

One of the potential benefits of RP methodology is the reduction of time needed to create an acceptable plan. For the prostate cases, on average it took 2.7 minutes for the RP methodology to optimize the plan compared to 40-90 minutes for the NCI (manual) method. For the H&N cases it took on average 4,3 minutes for the RP methodology to optimize plans and 60-100 minutes for the NCI (manual) method. This time may be longer depending on the experience of the medical physicist.

## 4. Conclusions

For the prostate cases an automated plan optimization algorithm (WUSTL model) created plans with slightly better target coverage. Model also spared healthy tissues more in low-middle dose region, whereas in the high-dose region, no such sparing has been observed. We could say that the WUSTL prostate model generated plans could provide better tumor control because of increased target coverage and could reduce toxicity and complications for the patients, resulting increase in quality of life. However, if such benefits are statistically important only a study with a greater quantity of patients could answer. Nevertheless, WUSTL prostate model could be used as an option during treatment planning of standard prostate cases.

Analyzing coverage of H&N targets we can conclude, that RP models performed better on medium dose target (PTV_60), slight improvements were observed in D5%, D95%, also on DHI, and CI metrics. For the low dose target (PTV_54) CCMB coverage was the same as NCI, but WUSTL coverage was poorer. No difference was observed in high dose target. For the healthy organs WUSTL model did better on oral cavity, larynx and esophagus structures, while CCMB model achieved similar results to NCI DVH's. For the other OARS, such as spinal cord and mandibular, both RP models created plans with higher doses than NCI. In general – in most parameters NCI plans were slightly better, however some critical organs were spared more by models. The possible recommendation could be to start creating a plan with a model, that already results in an acceptable plan and then the rest of the time manually adjust it to receive even better results.

On the other hand, RP-generated plans in prostate cases are much more complex (has 20% more MU), which increases the failure possibility and raises load on the hardware. Nevertheless, this could explain the better target coverage and better OAR sparing. For the H&N cases the plans created in NCI were slightly more complex, what could explain a better target coverage and the observed higher doses for some OAR in RP generated plans.

In conclusion – in the simple prostate cases the automated plan optimization algorithm performed slightly better, whereas in the complex H&N cases, manual optimization method had slightly better performance. Nevertheless, all the plans, generated by either algorithm is acceptable for the treatment, and for the standard situations and relatively simple plans, RP methodology can be a useful

tool that can generate a clinically acceptable RT dosimetric plan in a significantly shorter time.

## 5. References


1. Chanyavanich V, Das SK, Lee WR, Lo JY. Knowledge-based IMRT treatment planning for prostate cancer. Med Phys. 2011;38:2515–22.
2. Moore KL, Brame RS, Low DA, Mutic S. Experience-based quality control of clinical intensity-modulated radiotherapy planning. Int J Radiat Oncol Biol Phys. 2011;81:545–51.
3. Zamburlini, M. et al. EP-1441: Evaluation of Eclipse Rapidplan for semi-automatic treatment planning of prostate radiation treatment, Radiotherapy and Oncology , Volume 115 , S779
4. Krayenbuehl J, Norton I, Studer G, Guckenberger M. Evaluation of an automated knowledge based treatment planning system for head and neck. Radiat Oncol. 2015;10:226.
5. Boon IS, Au Yong TPT, Boon CS. Assessing the Role of Artificial Intelligence (AI) in Clinical Oncology: Utility of Machine Learning in Radiotherapy Target Volume Delineation. Medicines (Basel). 2018;5(4):131. Published 2018 Dec 11. doi:10.3390/medicines5040131
6. RStudio Inc. (2019). RStudio: Integrated development environment for R [Computer software]. URL http://www.rstudio.org/ (Version 1.2.1335).
7. Daniel Wollschlaeger and Heiko Karle (2019). DVHmetrics: Analyze Dose-Volume Histograms and Check Constraints. R package version 0.3.9. https://CRAN.R-project.org/package=DVHmetrics

*MEDICAL PHYSICS IN THE BALTIC STATES 14 (2019)*

Proceedings of International Conference "Medical Physics 2019"
7 – 9 November 2019, Kaunas, Lithuania

# VARIAN REAL-TIME POSITION MANAGEMENT SYSTEM OVERVIEW – VERIFICATION OF MARKER BLOCK POSITION AFTER TREATMENT COUCH SHIFTS

Marijus ASTRAUSKAS[1], Romualdas GRIŠKEVIČIUS[1], Kęstutis AKELAITIS[1], Jonas VENIUS[1,2]
[1]National Cancer Institute, Department of Medical Physics
[2]National Cancer Institute, Biomedical Physics Laboratory
marijus.astrauskas@nvi.lt;

***Abstract*:** Correct patient breathing baseline selection, using Varian Real-time Position Management (RPM) system, is the first important step for correct patient positioning and gating during a radiation therapy session. In this work, possible blind spots in the acquisition of the respiratory baseline are discussed. Using an optical surface monitoring system AlignRT to verify actual RPM position, highlights the potential for an unseen shift in patient position and breathing pattern, and prompts a discussion and recommendations on how to minimize it.

***Keywords*:** Motion management (MM), Optical surface monitoring system (OSMS), Radiation therapy (RT), Gated Radiotherapy (GR).

## 1. Introduction

Patient motion and breathing management is an essential part of quality control in radiation therapy. There are a number of systems which enable user to observe and control the breathing motions of the patient. One commonly used system is Varian Real-time Position Management and Respiratory Gating for Scanners (RPM and RGSC) – used in a variety of Varians' product line LINACs, for gated radiotherapy. Used during free breathing or breath hold, it allows for better control of both patient and tumour motion in real time during the CT scan and treatment.
Using this system, it is possible to accurately observe the breathing characteristics of a patient using a special marker block (Fig.1), positioned on the patient, usually on the thorax, where breathing motion is more pronounced. However, there seem to be some potential shortcomings with the system. First - using a fixed breathing amplitude values from a relative breathing baseline. Second – after any treatment couch motion is made, the system automatically relearns the breathing pattern of the patient. Both of these parts of the RPM system, if left unchecked, can lead to changes in patient position, of which the user is left unaware.

The goal of this work was to highlight such possible "blind spots" existing in the RPM system, using optical surface monitoring system AlignRT to track the changes in marker block spatial position, and provide recommendations on how to avoid potential risks associated with having incorrect baseline during treatment.

## 2. RPM baseline

RPM uses an infrared camera system to record the spatial position of a specialised marker block. When placed on the thorax of a patient it provides real time vertical, longitudinal and lateral axis data to the system, from which we can characterize breathing motion.

**Fig. 1.** RPM marker block.

To analyse the breathing pattern of the patient, the system registers the movement of the marker block at the start of the session, using four free breathing cycles (expiration-inspiration). It then averages the amplitude of these cycles and sets a baseline – the lowest point of the expiration. This baseline is therefore a relative value in space, as it depends on the current breathing pattern of the patient and the placement of the marker block [1].
While preparing the patient for a breath hold treatment, a gated computed tomography (CT) is done. There are two

stages of the gated CT: free breathing and breath hold. To get an accurate treatment session, the patient has to be able to reproduce the same deep breathing during the treatment as during the CT.

First - the free breathing stage. System learns the free breathing pattern of the patient and sets a baseline. Next - a deep inspiration is made and held to determine the gating thresholds. There are two thresholds – upper and lower, making an interval of vertical motion that the marker block has to be in order to perform the CT or treatment. These thresholds are noting a fixed distance value (cm) from the baseline. Therefore, during treatment, patient has to breathe in and hold the breath exactly at the same inspiration amplitude, as in the CT. Thresholds are set individually for each patient, looking at the reproducibility and stability of the deep inspiration hold.

At the start of a new treatment session, the same workflow is used. However, the gating thresholds are now fixed, according to the treatment plan. Every time the treatment couch moves, for example after position verification using on board imaging (OBI), system automatically restarts, relearns the breathing pattern and sets a new baseline for respiratory control. During treatment couch travel, system does not account for the changes in patient position or breathing pattern. Therefore, if patient moves during this travel time, the system and the user are unable to identify this additional patient motion. If a patient induced shift was in a vertical direction, the newly acquired baseline will be incorrect, resulting in reduced patient treatment accuracy. This is very important, when talking about peripheral tumour sites, where centring the treatment couch is necessary in order to do the patient imaging, or if the patients breathing or block position changes, due to couch motion, coughing or other irregular movements. This would cause the marker block to be in a different initial vertical expiration position (baseline) during the breathing pattern relearning phase, therefore the new baseline will cause the patient to miss the absolute vertical motion that was determined in the planning CT and matched with OBI.

Another problem occurs if patients' breathing changes over the course of cone beam CT (CBCT). The scan takes time, so usually a couple of breath holds are needed to complete it. In some cases, after the patient has made a few deep inspirations, breathing pattern changes in reference to the baseline (Fig. 2A). This usually happens due to an increase of residual air in the lungs from repeated deep inhaling and holding the breath. In this case, the breathing curve never fully comes back to the baseline. This becomes a problem, since RPM restarts after couch moves to the isocentre and the current patient expiration position becomes the new baseline. However, the system still expects the patient to inhale with the height of the primary amplitude, which becomes difficult for the patient and will be different from the treatment plan (Fig.2B). In figure 2B, we see the original patients' breathing pattern (grey), that should be repeated during treatment, and the one that is shown and expected by RPM (blue). Since the vertical threshold amplitude remains fixed, in reality patient has to breathe in more during treatment to reach the required vertical position.

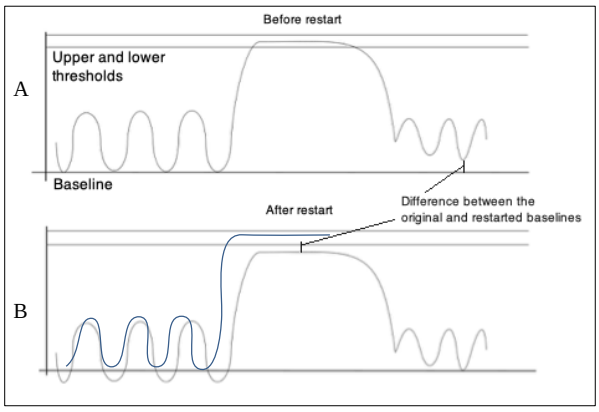


**Fig. 2.** Actual breathing curve before and after restart

In both previously described cases treatment accuracy is reduced by the differences between the old and new baselines, however the system is not able to recognise it.

## 3. Methods

An experiment was set up using a homemade breathing simulation phantom and two patient monitoring systems – RPM and AlignRT. Both systems were monitoring the marker block position.

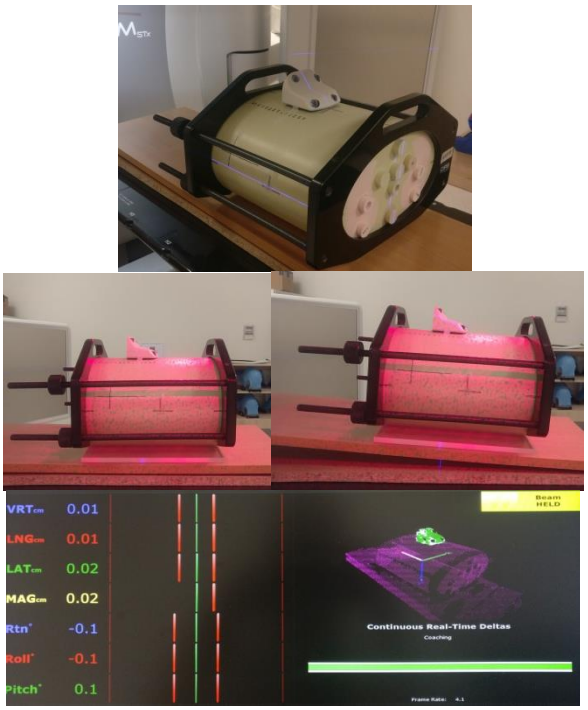


**Fig. 3.** Phantom position with marker block and monitored in AlignRT (bottom)

AlignRT is a surface guided radiation therapy (SGRT) system. By using cameras from three directions and projecting a pseudorandom pattern on a surface, it can track a selected surface zone in real time. Tracking the surface with the system gives surface delta values – shifts in 6 axes from a set initial position [2]. Similarly, to RPM baseline, there must be an initial reference position set. However, it does not automatically reset every time the couch moves, and is spatially fixed to the isocentre, therefore it allows the user to react to patient position

change during couch travel. If patient moved during that time, it is possible to calculate the difference, by comparing the OBI shifts to the deltas shown by AlignRT. If they do not match, the difference shows the positional shift of the tracked surface – the unwanted patient induced motion.

Experiment protocol:

1. Set up of the phantom with the marker block in the isocentre.
2. Move the couch laterally 3cm and take a reference capture with AlignRT. This is our initial (treatment) position.
3. Start the gated phantom and let the RPM system learn the breathing pattern.
4. Check that the amplitude of vertical movement of the marker block is the same on both RPM and AlignRT.
5. Use the "center couch" function to move the phantom to imaging position. Once it is centered, check if both systems are still showing the same vertical position.
6. Raise the phantom by 1cm (simulation of patient induced motion) to increase the baseline. Check to see if both systems register this shift correctly.
7. Return the couch to initial position.
8. Check the readings from both systems.

## 4. Results

Since the main tracking and gating data in RPM is vertical marker block position, by tracking with both systems at the initial resting position, we get that the marker block is moving vertically 2.27cm.

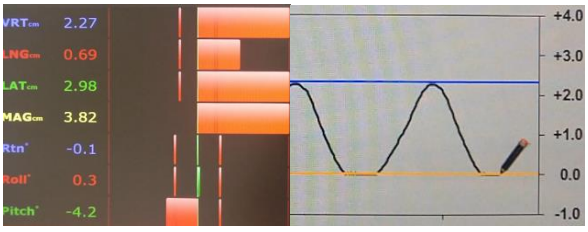


**Fig. 4.** Breathing pattern in AlignRT and RPM

After moving the phantom to imaging position, both systems still showed that the vertical amplitude is the same – 2.27cm, but with AlignRT we could see the lateral shift of 3cm as well.


**Fig. 5.** Lateral shift registered with AlignRT

Simulating the patient induced motion (adding 1cm of elevation under the phantom), both systems correctly register the change in vertical position.

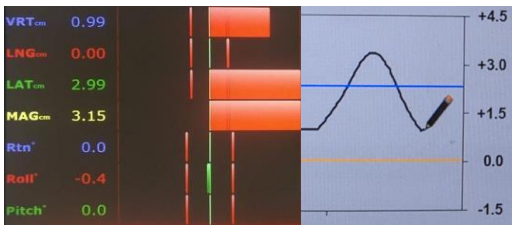


**Fig. 6.** Breathing pattern in AlignRT and RPM with 1cm elevation

However, after couch is moved back to the initial position the RPM system stops and automatically restarts, resetting the baseline, while AlignRT still shows that the marker block is elevated 1cm at expiration.

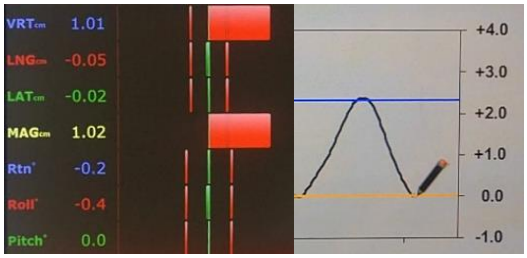


**Fig. 7.** Difference between AlignRT and RPM

This simple experiment shows the potential danger of the automated RPM restart –after the restart the information about the true baseline (which should be considered as the one during the CT/CBCT) is lost. We are left with a new, 1 cm shifted baseline, which is accepted as correct by RPM system and tells the user that everything is ready for treatment. This shows, that if the patient is breathing regularly (same amplitude), any shift, that happens before or during restart, is not accounted for.

It is unfortunate, that Varian RPM does not provide absolute marker block coordinates, which would help monitor the change of at least the vertical position of the maker. If the initial position is known, as well as the shift of the couch, it would be possible to calculate the new marker vertical position after the couch moves and compare it to the initial one.

## 5. Discussion and Recommendations

The main question that comes to mind is what can and should be done to reduce the possibility of getting a bad baseline in the first place.

Firstly – a good patient selection and instruction process. This is an important step in order to ensure that the patient can reproduce a good and stable baseline before and after the breath hold. Patient has to be well instructed on how to prepare for gated procedures. E.g. before the CT/CBCT, a "warm up" period of deep breaths could be implemented. Additionally, patient stability and potential for movement during treatment should be taken into account.

Secondly – a well-executed workflow and qualified staff that understands the ins and outs of this system is required. Recognizing the potential blind spots, such as the conditions for baseline uncertainties, and instructing the patient to avoid them, is key to a successful treatment session. Furthermore, there should be written procedures

already in place, so that as soon as a baseline drift, due to a change in patients' breathing pattern, is detected, actions could be taken immediately to ensure that the baseline of the treatment is the same as it was during imaging. These could include adapting the treatment thresholds, confirming patient position with a different imaging modality – for example MV or kV 2D imaging, or redoing the CBCT. Unfortunately, there is no way of tracking patient position changes during the couch travel time and relearning process, therefore the only option is to carefully observe the patient or use third party systems. Thirdly – an additional patient tracking system, that can provide absolute marker or patient surface data, could be implemented. In our case we were using AlignRT system which tracks patients' surface data. This allows the user to confirm that the marker block position did not change during the couch movement, by comparing the delta shifts before and after the CBCT. If they do not match, that means the patient position changed at some point. This could prompt for further action depending on the treatment protocols.

Using AlignRT, it is possible to track both the free breathing and breath hold surface of the patient, thus eliminating the need for a baseline. Also, using AlignRT to track the marker block on the patient, that is being treated with RPM, it is possible to determine how often such patient baseline shift can occur. Furthermore, this could help evaluate gaps in workflow, patient instructions and management during treatment. That in turn will help to prepare standard operating procedures for safe respiratory controlled radiotherapy.

## 6. References

1. "Respiratory Gating for Scanners Instructions for Use", Varian Medical Systems, Palo Alto, United States of America, 2018, p.41.
2. "AlignRT 5.0 User Guide", London N3 2JU, 0002-0003, 17 May 2017, p.14.

*MEDICAL PHYSICS IN THE BALTIC STATES 14 (2019)*

Proceedings of International Conference "Medical Physics 2019"
7 – 9 November 2019, Kaunas, Lithuania

# SUPERDIFFUSION AND AUGER THERAPY PRODUCED WITH X-RAYS

Arvydas Juozapas JANAVIČIUS
Višinskio str. 25, Šiauliai University, LT-77156 ,Lithuania
AYanavy@gmail.com

***Abstract:*** X-rays causes very fast crystallization of NaCl, KCl in a saturated water solution and allows for the introduction of phosphorus, boron and carbon in crystal silicon at room temperature. These new techniques or superdiffusion, based on the introduction of impurities to the Si lattice without damaging it can be used for production of a new kind of electronics devices including solar cells of high quality. Similarly, superdiffusion based on Auger effect, generates electrons of low kinetic energy, which can be used for DNA cell damage, over a very short range, for cancer therapy. It is a more progressive method than radiation therapy by ions or protons with energies of about 100 MeV. Low energy (10 – 20 eV) Auger electrons or initial X-ray photons (10-20 keV) damages the DNA or its components, but leaves the remainder of the cell intact.

***Keywords:*** superdiffusion, auger's effect, x-rays, cancer therapy. PACS 78.70.Ck – X-ray scattering, PACS 32.80.Hd – Auger effect, PACS 61.72.-y – Defects and impurities in crystals; microstructure

## 1. Introduction

We applied soft X-rays for the generation of metastable vacancies in a Si crystal [1-2]. This is sufficient for practical realization of new kind of superdiffusion [1], for introduction of boron and phosphorus in a crystal silicon [3-4] at room temperature. The proposed technology does not damage the Si lattice. This is due to fact that Auger electrons, with energies of 10-20 eV, are used for the displacement of a single atom in a crystal silicon, where an impurity can be introduced. This allows for the production of new materials and electronic devices with fewer defects.

It is important that the energies of the Augers electrons does not depend on the energies of the particles or photons producing vacancies in $KL_1L_2$ shells, which have the highest binding energies of electrons in atoms. Energy of the emitted electron depends on the energy of the initial vacancy and the energy of the vacancies created by spontaneous transitions of external electrons

$$E_A = E(a^{-1}) - E(b^{-1}c^{-1}) \qquad (1)$$

By changing the energy of the monochromatic X-rays we can induce the inner-shell ionization and change the energies of the produced Auger electrons. Photoelectric effect in the body cells can cause dissociation reactions of water molecules [5-6]

$$H_2O \rightarrow H + OH\,,\ H_2O \rightarrow H^+ + OH^- \qquad (2)$$

A photon can also produce hydrated electrons $e_a$ and unstable radicals $H_2O^+$ [6]

$$\begin{aligned} &H_2O + h\nu \rightarrow H_2O^+ + e_a + h\nu_f\,, \\ &\nu_f < \nu\,, \\ &H_2O^+ + H_2O \rightarrow H_3O^+ + OH \end{aligned} \qquad (3)$$

where weakly bound metastable radicals $H_3O^+$ are produced. It's interactions acting like the collectors of negative ions eliminate water ionization in cells

$$H_3O^+ + OH^- \rightarrow 2H_2O \qquad (4)$$

It was also found that irradiation of NaCl[5] and KCl[6] water solution had a big influence on two-step processes of crystallization. Irradiation of the solution produced metastable radicals of water and excited seeds which stimulated, a very fast process (about 100 faster than usual) of supercrystallization [5-6] and repair of the damaged molecules/ions with irradiated vacancies [1-2].

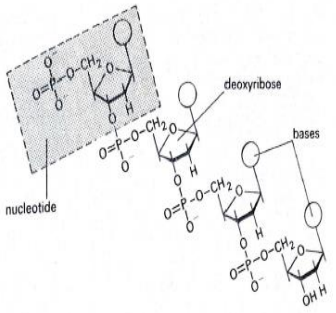


**Fig. 1.** Structure of sugar-phosphate backbone

### 2. Cancer therapy method using soft X-rays

It is possible that Auger effect can be used for modification of genetic material defined by DNA taking part in the protein synthesis structure. perspective to use low energy (>2148 eV) X-ray photons [4], for the irradiation of electrons in K shell of phosphorus, in group phosphate nucleotides (Fig. 1) [7]. This causes the removal of the phosphorus atoms and the production of free oxygen, which in turn causes the disintegration of the double helical structure of the DNA [7].

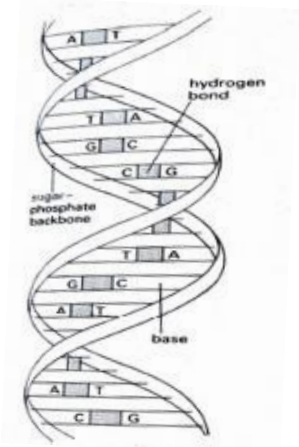


**Fig. 2.** Structure of DNA

This also allows to induce damage in the fast dividing chains of the DNA with the electrons produced by Auger effect in the phosphorus atoms, which were excited by the initial photons with the energies of as low as 11keV [4]. This allows to avoid expensive irradiation with protons and ions using particle accelerators.

DNA is a nucleic acid composed from two chains of nucleotides rounded by two chains linked by hydrogen bonds between four bases ACGT of nucleotides (Fig. 2).

### 3. Conclusions

This proposed method for inducing damage in the phosphate nucleotide is connected with production of three oxygen atoms which also take part in killing of the cancer's cell. It has the potential to be more progressive than the standard radiotherapy [8], but further research is needed regarding the methodologies of producing the necessary monochromatic X-rays with photon energies depending on position of tumors in human's body.

### 4. References

1. Janavičius A. J, Banys J., Purlys R., and Balakauskas S. "Lithuanian Journal of Physics", 42, No. 5, 2002, p. 337.
2. Janavičius A. J., Norgėla Ž., and Purlys R. "Eur. Phys. J. Appl. Phys", 29, 2005, p. 127.
3. Janavičius A. J., et all. PCT publication number WO/ 2014/062045, PCT declaration number PCT/ LT2013/ 000017, Declaration in USA No. 14/436,934
4. Janavičius A. J., S. Balakauskas, V. Kazlauskienė, A. Mekys, R. Purlys and Torasta J. "Acta Phys. Pol. A.", 114, 008, p. 779.
5. Janavičius A. J., Purlys R. and Rinkūnas R. "Acta Phys. Pol. A." 123, 2013, 777.
6. Janavičius A. J., Rinkūnas R. and Purlys R., epl, A Letters journal exploring the frontiers of physics, 116, 2016, p. 27001-p1. Science Dictionary, Oxford University Press, Oxford, New York, 1991, p. 758.
7. Wang CG, US Patent 8, 278, 315, Radio therapy Method using X-rays, 2012.

*MEDICAL PHYSICS IN THE BALTIC STATES 14 (2019)*

Proceedings of International Conference "Medical Physics 2019"
7 – 9 November 2019, Kaunas, Lithuania

# ACUTE RADIODERMATITIS CLINICAL MANIFESTATION IN COMPARISON WITH REFLECTANCE CONFOCAL MICROSCOPY

Juras KIŠONAS[1], Jonas VENIUS[2], Olga SEVRIUKOVA[3],
Mindaugas GRYBAUSKAS[4], Arvydas BURNECKIS[5], Ričardas ROTOMSKIS[6]
[1,4,5] National Cancer Institute, Department of Radiation oncology, Vilnius Lithuania
[1]Vilnius University Department of Neurobiology and Biophysics, Vilnius, Lithuania
[2]National Cancer Institute, Medical physics department, Vilnius Lithuania
[2,6]National Cancer Institute, Biomedical physics laboratory, Vilnius Lithuania
[3]Radiation Protection Centre, Vilnius, Lithuania
juras.kisonas@gmail.com; jonas.venius@nvi.lt; olga.sevriukova@rsc.lt ; mindaugas7415@gmail.com;
arvydas.burneckis@nvi.lt; ricardas.rotomskis@nvi.lt

***Abstract*:** During radiotherapy (RT) ionizing radiation (IR) affects not only malignant, but also healthy organs and tissues. Skin is altered for the most part of patients treated with external beam RT. Evaluation of radiation dermatitis (RD) is performed by physician and is based on visual assessment of the clinical symptoms. Optical biopsy by reflectance confocal microscopy (RCM) can reveal skin changes in cellular resolution. In this work we present a comparison of RCM imaging and clinical manifestation of RD.

***Keywords*:** acute radiation dermatitis, reflectance confocal microscopy, radiotherapy.

## 1. Introduction

According to the cancer treatment guidelines, up to 52% of newly diagnosed cancer patients should undergo external beam RT [1]. During RT ionizing radiation affects not only malignant, but also healthy organs and tissues. Up to 95% of patients receiving external beam RT suffer from skin injury (radiation dermatitis). Skin damage begins in a few hours after IR exposure and can last up to 90 days from the beginning of the RT. A basal layer keratinocytes in epidermis, hair follicle stem cells and melanocytes are radiosensitive cells of the skin. The death of these cells determines inflammatory reaction of the skin - acute radiation dermatitis (ARD). The clinical manifestation of ARD ranges from mild erythema to ulceration depending on various risk factors. Total IR dose to the skin is the most important factor for the development of skin lesions. Erythema appears at the first and can be noticed after a couple radiation treatment fractions (from 2 to 12 Gy). After 12-20 Gy dose (2-3 weeks of treatment) epilation and hyperpigmentation occur. Dry desquamation emerges in 4$^{th}$ week of the treatment, when after the exposure dose reaches 20-25 Gy, Moist desquamation appears after 30-40 Gy dose and ulceration – after 40 Gy [2]. Common Toxicity Criteria-Adverse Event (CTCAE) toxicity scoring scale (table 1) is the most commonly used for evaluation of radiotherapy adverse effects. Unfortunately, there is no gold standard method for objective evaluation of skin lesions. In some clinical researches other scales with more than 4 degrees are used. Moreover, assessment of symptoms based on scoring scales can be subjective and dependent on evaluators clinical experience. Optical skin biopsy could reveal ongoing changes in the skin during radiation treatment with no damage to the tissues. RCM is a relatively new, but already widely used visualization method for the diagnosis of various skin conditions.
In this work we present first results of 10 patients from biomedical research during which patients underwent conventional radiotherapy and radiation dermatitis was dynamically evaluated by a standard method (CTCAE scale) and RCM.

## 2. Materials and methods

### 2.1. Radiotherapy

All ten patients were diagnosed with early stage breast cancer and underwent surgical treatment (lumpectomy). RT to the whole breast was prescribed to all patients according to the breast cancer treatment guidelines [3]. Patients were immobilized in a supine position with hands above the head and chest computed tomography (CT) scans were performed. Treatment planning system Eclipse® version 15.5 was used for RT planning. Clinical target volume (CTV) and organs at risk (OAR) were delineated according to RTOG recommendations [4].

The prescribed dose to the breast planning target volume (PTV) was 50 Gy delivered in 2 Gy per fraction (fx), 5 fx/week.

### 2.2 Assessment of skin lesions

Before the treatment and after every 5 fx clinical skin evaluation was performed together with RCM.
Three radiation oncologists visually evaluated skin's conditions according to the CTCAE scale. The evaluations were combined and the final manifestation and the degree of ARD was determined when at least two out of thee evaluators agreed. This resulted in SUM evaluation. Only the supportive care was used for the prevention of ARD until the second degree of ARD then treatment with calendula ointment was prescribed.
RCM images were taken with a commercially available device VivaScope® 1500 (MAVIG GmbH, Munich, Germany), which provides a lateral resolution of 1.0 μm and an axial resolution of 3.0 μm. Firstly, a mosaic images of 4 mm × 4 mm were taken in spinose-granular skin layer, then 500 μm × 500 μm images were taken in three selected points every 5 μm up to 100 μm in depth. Two observers evaluated all images. Lesion was graded as 1 if it was present in less than 50% of the image and 2 if it was in more than 50%.

## 3. Results

### 3.1.Clinical evaluation of ARD

Clinical assessment of ARD with accordance to CTCAE scale (table1) was performed before treatment and once a week (every 5 fractions).

**Table 1.** Common Toxicity Criteria-Adverse Event scale*

| Score | Symptoms |
|---|---|
| 1 | Faint erythema or dry desquamation |
| 2 | Moderate to brisk erythema; patchy moist desquamation, mostly confined to skin folds and creases; moderate edema |
| 3 | Moist desquamation in areas other than skin folds and creases; bleeding induced by minor trauma or abrasion |
| 4 | Life-threatening consequences; skin necrosis or ulceration of full thickness dermis; spontaneous bleeding from involved site; skin graft indicated |
| 5 | Death |

**From National Cancer Institute Common Terminology Criteria for Adverse Events (CTCAE) version 4*

Radiation induced skin reactions were independently evaluated by three physicians (Table 2). The degree of ARD is accepted if at least two of three physicians come into agreement.
In the beginning of the treatment skin condition of all patients was determined as healthy (0 degree according to CTCAE scale). After 5 RT fractions first degree of ARD was diagnosed for 3 patients, for two patients – after 10 treatment fractions, for 3 – after 15 fr., and for 2 patients only in the end of treatment (after 25 fx).
For 6 of patients ARD did not reach the second degree untill the end of RT. For 2 of patients second degree of ARD was diagnosed after 20 fr., and after 25 fr. for the remaining two patients.

**Table 2.** Clinical evaluation of ARD

| Pat. No | Fx No | Ev. 1 | Ev. 2 | Ev. 3 | SUM |
|---|---|---|---|---|---|
| **1** | 0 | 0 | 0 | 0 | 0 |
| | 5 | 1 | 1 | 1 | 1 |
| | 10 | 1 | 1 | 1 | 1 |
| | 15 | 1 | 1 | 1 | 1 |
| | 20 | 1 | 1 | 1 | 1 |
| | 25 | 2 | 1 | 1 | 1 |
| **2** | 0 | 0 | 0 | 0 | 0 |
| | 5 | 0 | 0 | 0 | 0 |
| | 10 | 1 | 1 | 1 | 1 |
| | 15 | 1 | 1 | 1 | 1 |
| | 20 | 1 | 1 | 1 | 1 |
| | 25 | 1 | 1 | 1 | 1 |
| **3** | 0 | 0 | 0 | 0 | 0 |
| | 5 | 0 | 0 | 0 | 0 |
| | 10 | 0 | 0 | 0 | 0 |
| | 15 | 1 | 1 | 1 | 1 |
| | 20 | 1 | 2 | 2 | 2 |
| | 25 | 2 | 2 | 2 | 2 |
| **4** | 0 | 0 | 0 | 0 | 0 |
| | 5 | 1 | 1 | 1 | 1 |
| | 10 | 1 | 1 | 1 | 1 |
| | 15 | 1 | 1 | 1 | 1 |
| | 20 | 2 | 1 | 1 | 1 |
| | 25 | 2 | 2 | 2 | 2 |
| **5** | 0 | 0 | 0 | 0 | 0 |
| | 5 | 0 | 0 | 0 | 0 |
| | 10 | 1 | 0 | 0 | 0 |
| | 15 | 1 | 1 | 1 | 1 |
| | 20 | 1 | 1 | 1 | 1 |
| | 25 | 1 | 1 | 1 | 1 |
| **6** | 0 | 0 | 0 | 0 | 0 |
| | 5 | 0 | 0 | 0 | 0 |
| | 10 | 0 | 0 | 1 | 0 |
| | 15 | 1 | 1 | 1 | 1 |
| | 20 | 1 | 2 | 1 | 1 |
| | 25 | 2 | 2 | 2 | 2 |
| **7** | 0 | 0 | 0 | 0 | 0 |
| | 5 | 0 | 0 | 0 | 0 |
| | 10 | 0 | 0 | 0 | 0 |
| | 15 | 0 | 0 | 0 | 0 |
| | 20 | 0 | 0 | 1 | 0 |
| | 25 | 1 | 0 | 1 | 1 |
| **8** | 0 | 0 | 0 | 0 | 0 |
| | 5 | 0 | 0 | 0 | 0 |
| | 10 | 0 | 1 | 1 | 1 |
| | 15 | 1 | 1 | 0 | 1 |
| | 20 | 1 | 1 | 1 | 1 |
| | 25 | 1 | 2 | 1 | 1 |
| **9** | 0 | 0 | 0 | 0 | 0 |
| | 5 | 0 | 1 | 1 | 1 |
| | 10 | 1 | 1 | 2 | 1 |
| | 15 | 1 | 1 | 1 | 1 |
| | 20 | 2 | 1 | 2 | 2 |
| | 25 | 2 | 2 | 2 | 2 |
| **10** | 0 | 0 | 0 | 0 | 0 |
| | 5 | 0 | 0 | 0 | 0 |
| | 10 | 0 | 0 | 0 | 0 |
| | 15 | 0 | 0 | 0 | 0 |
| | 20 | 0 | 0 | 0 | 0 |
| | 25 | 1 | 1 | 1 | 1 |

Pat. No – patient number, Fx No – number of fractions, Ev. – evaluator; SUM – combined evaluation of radiodermatitis when at least two evaluators agree.

### 3.1. RCM imaging of the skin

During RCM imaging signs of skin damage like spongiosis, exocytosis, mild contrast cells (MCC), disarrayed epidermis (DE) and abnormal dermalpapillae (ADP) were evaluated: fig 1.

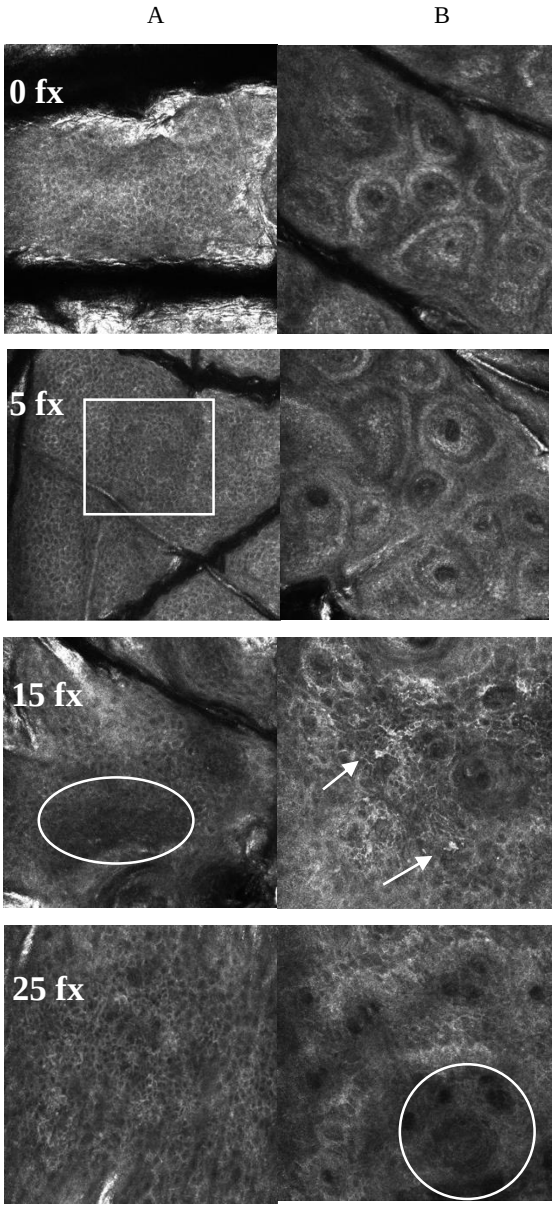


**Fig. 1. RCM imaging of the skin.** A –images at the spinous-granular layer: (0 fx) normal honeycomb pattern before treatment; (5fx) aggregates of round-to-polygonal cells (white rectangle) corresponding to exocytosis after 1 treatment week; (15fx) darker area the stratum spinosum with intercellular spaces between keratinocytes larger than normal (white oval), corresponding to spongiosis after 3 treatment weeks; (25fx) loss of the normal honeycomb pattern in more than 50% of the image of the epidermis in the end of treatment. B – images at the dermo-epidermal junction: (0 fx) normal view of dermo-epidermal junction before treatment and after 1 week (5 fx); (15fx) diffuse polygonal mildly refractive cells (white arrows) corresponding inflammatory cells after 3 treatment weeks; (25fx) abnormal dermal papillae (white circle) in the end of treatment.

**Table 3.**RCM features of radiation dermatitis

| No | Fx No | S | E | MCC | ADP | DE |
|---|---|---|---|---|---|---|
| **1** | 0 | 0 | 0 | 0 | 0 | 0 |
| | 5 | 0 | 1 | 0 | 0 | 0 |
| | 10 | 1 | 1 | 0 | 0 | 0 |
| | 15 | 1 | 2 | 1 | 0 | 0 |
| | 20 | 2 | 2 | 1 | 1 | 1 |
| | 25 | 1 | 2 | 1 | 1 | 1 |
| **2** | 0 | 0 | 0 | 0 | 0 | 0 |
| | 5 | 0 | 1 | 0 | 0 | 0 |
| | 10 | 0 | 1 | 0 | 0 | 0 |
| | 15 | 1 | 1 | 1 | 0 | 0 |
| | 20 | 1 | 1 | 1 | 1 | 0 |
| | 25 | 2 | 2 | 2 | 2 | 2 |
| **3** | 0 | 0 | 0 | 0 | 0 | 0 |
| | 5 | 0 | 1 | 1 | 0 | 0 |
| | 10 | 0 | 1 | 0 | 0 | 0 |
| | 15 | 1 | 1 | 0 | 0 | 0 |
| | 20 | 1 | 1 | 1 | 0 | 1 |
| | 25 | 1 | 2 | 1 | 1 | 2 |
| **4** | 0 | 0 | 0 | 0 | 0 | 0 |
| | 5 | 0 | 1 | 1 | 0 | 0 |
| | 10 | 0 | 1 | 1 | 0 | 0 |
| | 15 | 1 | 1 | 1 | 0 | 0 |
| | 20 | 1 | 2 | 2 | 1 | 1 |
| | 25 | 2 | 2 | 2 | 1 | 2 |
| **5** | 0 | 0 | 0 | 0 | 0 | 0 |
| | 5 | 1 | 0 | 1 | 0 | 0 |
| | 10 | 1 | 1 | 1 | 0 | 0 |
| | 15 | 2 | 2 | 2 | 1 | 0 |
| | 20 | 2 | 2 | 2 | 2 | 1 |
| | 25 | 2 | 2 | 2 | 1 | 2 |
| **6** | 0 | 0 | 0 | 0 | 0 | 0 |
| | 5 | 1 | 1 | 1 | 0 | 0 |
| | 10 | 1 | 1 | 1 | 0 | 0 |
| | 15 | 1 | 2 | 2 | 1 | 1 |
| | 20 | 2 | 2 | 2 | 1 | 2 |
| | 25 | 2 | 2 | 2 | 1 | 2 |
| **7** | 0 | 0 | 0 | 0 | 0 | 0 |
| | 5 | 0 | 1 | 1 | 0 | 0 |
| | 10 | 1 | 1 | 0 | 0 | 0 |
| | 15 | 2 | 2 | 1 | 0 | 0 |
| | 20 | 2 | 2 | 2 | 0 | 1 |
| | 25 | 2 | 2 | 2 | 0 | 2 |
| **8** | 0 | 0 | 0 | 0 | 0 | 0 |
| | 5 | 1 | 1 | 0 | 0 | 0 |
| | 10 | 1 | 1 | 0 | 0 | 0 |
| | 15 | 1 | 2 | 0 | 0 | 0 |
| | 20 | 1 | 2 | 0 | 0 | 0 |
| | 25 | 2 | 2 | 1 | 1 | 1 |
| **9** | 0 | 0 | 0 | 0 | 0 | 0 |
| | 5 | 0 | 1 | 0 | 0 | 0 |
| | 10 | 0 | 1 | 0 | 0 | 0 |
| | 15 | 0 | 2 | 1 | 2 | 2 |
| | 20 | 1 | 2 | 1 | 0 | 1 |
| | 25 | 1 | 2 | 2 | 1 | 1 |
| **10** | 0 | 0 | 0 | 0 | 0 | 0 |
| | 5 | 0 | 1 | 0 | 0 | 0 |
| | 10 | 0 | 1 | 0 | 0 | 0 |
| | 15 | 1 | 2 | 1 | 0 | 0 |
| | 20 | 1 | 1 | 1 | 0 | 1 |
| | 25 | 1 | 2 | 1 | 0 | 1 |

Pat. No – patient number, Fx No – number of fractions, S – spongiosis, E – exocytosis, MCC – mild contrast cells (lymphocytes, neutrophils or melanophages), ADP - abnormal dermal papillae, DE disarrayed epidermis.

The first signs of IR induced skin injury for all patients were detected after 1 treatment week (5 fx). At the level of the stratum spinosum single or aggregates of round-to-polygonal cells (corresponding to exocytosis) were determined for 9 patients after 5 fx. Spongiosis along with exocytosis after 5 fx was detected for 3 patients. For 5 patients MCC were also visible in the superficial skin layer after one week of RT (table 3).
DE or BGP after 15 RT fx were present in 3 patients in RCM images, after 20 fx - in 6 patients, and in 1 at the end of treatment (table 3).

## 4. Discussion

Spongiosis, exocytosis and MCC are the early signs of radiation induced skin injury which do not result in structural damage. While DE and ADP are IR induced symptoms of damaged skin structure.
As it was mentioned above, early signs of IR induced skin injury determined by RCM was present in all patients after one treatment week (table 3). In that moment total doze of 10 Gy was given to the whole breast. At the same time, I degree of ARD was diagnosed clinically only in 30% of the patients (table 2). This fact is not surprising because microscopic features should be seen earlier than clinical symptoms. However, this is the first research to show that IR induced skin changes could be detected so early. Vano-Galvan S et al. demonstrated that first histopathological changes may be detected after 15 days of RT [5]. Case study of RCM application for early diagnosis or ARD [6] showed the same results as in this paper but such results were associated with high individual radiosensitivity. Our results are the first to indicate that during RCM imagining skin changes could be detected very early when patients are treated with RT.
In order to compare microscopic changes with clinical evaluation we classified RCM features as the first degree if there were no damage of the skin structure and as the second degree, if skin architecture was altered (table 4).
This comparison once again proved that radiation induced skin changes microscopically could be detected earlier than clinical symptoms appear. For all patient's lesions of skin architecture were present at the end of RT but only for 3 of them second degree of ARD was diagnosed according to CTCAE scale. It is very likely that same of these patients will suffer form worsening of clinical symptoms after RT. DE or ADP appearance in RCM imaging could be a signal for the clinician to expect a worsening of patient skin condition.
We think that DE could be related with dry desquamation – a clinical symptom which is assigned to the first degree ARD in CTCAE scale. While ADP could be associated with moist desquamation which is assigned to the second degree ARD. Unfortunately, dry and moist desquamation are not individually evaluated then CTCAE scale is used. This could suggest to use other scales (i.e. Oncology Nursing Society scale) for ARD assessment in the future. To strongly support this recommendation research with bigger sample size should be done.

**Table 4.** Degree of radiation dermatitis (CTCAE) compared to RCM features

| No | Fx No | CTCAE | RCM |
|---|---|---|---|
| **1** | 0 | 0 | 0 |
| | 5 | 1 | 1 |
| | 10 | 1 | 1 |
| | 15 | 1 | 1 |
| | 20 | 1 | 2 |
| | 25 | 1 | 2 |
| **2** | 0 | 0 | 0 |
| | 5 | 0 | 1 |
| | 10 | 1 | 1 |
| | 15 | 1 | 1 |
| | 20 | 1 | 2 |
| | 25 | 1 | 2 |
| **3** | 0 | 0 | 0 |
| | 5 | 0 | 1 |
| | 10 | 0 | 1 |
| | 15 | 1 | 1 |
| | 20 | 2 | 2 |
| | 25 | 2 | 2 |
| **4** | 0 | 0 | 0 |
| | 5 | 1 | 1 |
| | 10 | 1 | 1 |
| | 15 | 1 | 1 |
| | 20 | 1 | 2 |
| | 25 | 2 | 2 |
| **5** | 0 | 0 | 0 |
| | 5 | 0 | 1 |
| | 10 | 0 | 1 |
| | 15 | 1 | 2 |
| | 20 | 1 | 2 |
| | 25 | 1 | 2 |
| **6** | 0 | 0 | 0 |
| | 5 | 0 | 1 |
| | 10 | 0 | 1 |
| | 15 | 1 | 2 |
| | 20 | 1 | 2 |
| | 25 | 2 | 2 |
| **7** | 0 | 0 | 0 |
| | 5 | 0 | 1 |
| | 10 | 0 | 1 |
| | 15 | 0 | 1 |
| | 20 | 0 | 2 |
| | 25 | 1 | 2 |
| **8** | 0 | 0 | 0 |
| | 5 | 0 | 1 |
| | 10 | 1 | 1 |
| | 15 | 1 | 1 |
| | 20 | 1 | 1 |
| | 25 | 1 | 2 |
| **9** | 0 | 0 | 0 |
| | 5 | 1 | 1 |
| | 10 | 1 | 1 |
| | 15 | 1 | 2 |
| | 20 | 2 | 2 |
| | 25 | 2 | 2 |
| **10** | 0 | 0 | 0 |
| | 5 | 0 | 1 |
| | 10 | 0 | 1 |
| | 15 | 0 | 1 |
| | 20 | 0 | 2 |
| | 25 | 1 | 2 |

Pat. No – number of patient, Fx No – number of fractions. RCM: 0 – no skin changes, 1 – if S, E or MCC is present; 2 – if DE or ADP is present

## 4. Conclusions

The results of this study showed that RCM is capable to detect radiation induced skin changes earlier, before clinical manifestation. After 5 fx of RT skin lesions was detected for 100% of patients during RCM imaging, while clinical symptoms were diagnosed only for 30% of them. After 5 fx in RCM images exocytosis was present in 90%, MCC in 50% and spongiosis in 30% of patients. At the end of RT lesions (DE, ADP) which are associated with damage of the skin structure were visible in all patients RCM images, but second degree of ARD was diagnosed only for 30% of them. DE or ADP appearance in RCM imaging could be a signal for the clinician to expect a worsening of patient skin condition after treatment. RCM possibly could help to reduce misdiagnosis of severe IR induced skin injury.

## 5. References

1. Delaney G, Jacob J, Featherstone C, Barton M. The role of radiotherapy in cancer treatment: estimating optimal utilization from a review of evidence-based clinical guidelines. Cancer. 104, 1129–1137 (2005)..
2. Julie L. Ryan. Ionizing Radiation: The Good, the Bad, and the Ugly. Journal of Investigative Dermatology. 132, 985–993 (2012).
3. Gradishar W.J, Anderson B.O, Balassanian R, Blair S.L, Burstein H.J, Cyr A, et al. NCCN Guidelines Insights: Breast Cancer, Version 1.2017. Journal of the National Comprehensive Cancer Network: JNCCN. 15(4), 433–51 (2017).
4. White J, Tai1 A, Douglas A, Buchholz T, MacDonald S, Marks L, Pierce L, Recht A, Rabinovitch R, Taghian A et al. Breast Cancer Atlas for Radiation Therapy Planning: Consensus Definitions.
5. Vano-Galvan S, Fernandez-Lizarbe E, Truchuelo M, Diaz-Ley B, Grillo E, Sanchez V, Rıos-Buceta L, Paoli J, Sancho S, Montero A. et al. Dynamic skin changes of acute radiation dermatitis revealed by in vivo RCM. J. Eur. Acad. Dermatol. 27, 1143–1150 (2013).
6. J Kišonas, J Venius, O Sevriukova, M Grybauskas, K Guogytė, A Burneckis, R Rotomskis, Application of reflectance confocal microscopy for early diagnosis of radiation-induced acute dermatitis in radiosensitive patient: case study, *Radiation Protection Dosimetry*, Volume 182, Issue 1, December 2018, Pages 93–97, https://doi.org/10.1093/rpd/ncy135.

*MEDICAL PHYSICS IN THE BALTIC STATES 14 (2019)*

Proceedings of International Conference "Medical Physics 2019"
7 – 9 November 2019, Kaunas, Lithuania

# MEASUREMENT OF THE CONCENTRATION OF FUNCTIONALIZED POLYMER NANOPARTICLES IN LIQUID SUSPENSIONS USING LIGHT REFRACTION

Vladimirs KOZLOVS[1], Margit HEINLAAN[2], Dmitrijs MERKULOVS[3]
[1]Institute of Microbiology and Virology, Riga Stradin University, [2]National Institute of Chemical physics and Biophysics, Tallinn, Estonia, [3]ELMI Ltd., Riga, Latvia
Vladimirs.Kozlovs@rsu.lv, margit.heinlaan@kbfi.ee, dmitrijs_merkulovs@yahoo.co.uk

***Abstract***: Refractivity of aqueous suspensions of polystyrene nanoparticles were measured in the size range of 26-100 nm and in the concentration range of 1-100 mg/l. It was shown that the choice of the temperature at which measurements are made and the developed data processing algorithm allow determining the concentration of nanoparticles with an accuracy ~ 1 μg/l.

***Keywords*:** nanoparticles, ecotoxisity, refractive index, suspension, concentration measurement.

## 1. Introduction

Microplastic (MP) is a common denominator for contaminant group of ≤ 5 mm plastic particles [1] that have the potential to negatively affect the well-being of both, human as well as of environmental organisms. MP occurrence has been confirmed in all the sampled environmental media including different levels of the food chain [2]. MP includes nanosized fraction termed nanoplastic (1-100 nm; NPL) which, unlike the bigger size fractions, may have nano-specific properties and is thus potentially biologically more hazardous [3]. According to the current MP ecotoxicity research, particle ingesting fresh water organisms are among the most vulnerable to MP-related stress [4] however on the whole, the knowledge on biological impacts of MP is in its infancy [5]. Progress of MP toxicity research is significantly hindered by challenging detection and quantification of MP, but furthermore of its nanosized fraction [6]. The organic nature and small size render it very difficult to discriminate NPL from naturally occurring particles. Customized methods are urgently needed to fill this gap. Viability and limitations of critical angle refratometry of turbid colloids are discussed in paper [7]. We previously [8-10] proposed an alternative method for measuring the refractive index, and using silicon dioxide nanoparticles as an example, we showed the possibility of measuring their concentration in aqueous suspensions. The aim of the current study was to optimize a refractometric method for quantification of nanosized polymer particles in different ecotoxicological aqueous test media (OECD201 mineral freshwater and natural freshwater) using 26, 40 and 100 nm commercial carboxylated polystyrene spheres as model NPL. Quantification of NPL would enable understand the fate of NPL in the course of toxicity experiments and increase the applicability of MP ecotoxicity data for both regulative and scientific purposes.

## 2. Materials and methods

Model particles, used in this study, were carboxylated polystyrene (PS-COOH) spheres with primary particle diameters of 26, 40 and 102 nm. Particles will be hereafter referred to as 26, 40 and 100 nm PS-COOH. 26 nm PS-COOH were purchased from Bangs Laboratories Inc. and the other two from Magsphere Inc. All the PS-COOH were provided as aqueous suspensions of 9.97 (26 nm) and 10 (40 and 100 nm) wt%. Suspensions contained undisclosed anionic surfactants (≤0.5% for 26 nm) and antimicrobial additive sodium azide $NaN_3$ (0.05% for 26 nm and ≤0.09% for 40 and 100 nm). Polystyrene density was 1.06 (26 nm) and 1.05 (40 and 100 nm) g/mL and parking areas were 68.4 (26 nm), 80.6 (40 nm) and 66 (100 nm) $Å^2$/COOH. Refractive index (RI) of polysterene equals 1.587 for light with wavelength 633 nm. For refractometric analysis, the original PS-COOH stock suspensions were diluted into i) ultrapure water (MQ –water) (MilliQ>18.2 MΩ, Merck Millipore, Germany), ii) OECD202 artificial freshwater (OE-water) (mg/L of deionized water: 294 $CaCl_2 \cdot 2H_2O$, 123.25 $MgSO_4 \cdot 7H_2O$, 64.75 $NaHCO_3$, 5.75 KCl; pH 7.8 ± 0.2) [2] and iii) natural fresh water from Lake Ülemiste (UL-water), Tallinn Estonia. OECD202 medium and natural fresh water are both ecotoxicological test media. Prior to

usage, natural freshwater was filtered using 0.45 μm sterile Sartorius cellulose nitrate filters and stored in the dark at +4°C. PS-COOH working stock suspensions were prepared in sterile conditions, stored in the dark at +4°C and rigorously vortexed before use. Basic elements of the device by means of which measurements were made are given in Fig.1.

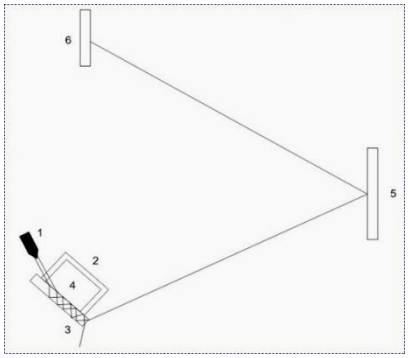


**Fig.1.** Scheme of device for RI measurement.

1- laser diode (λ= 650 nm, power 4mW), 2- measuring cuvette, 3- detector of refractive index (RI), 4- liquid under study, 5- mirror, 6-photodetector (CCD). All elements are fixed on the surface of the thermostat which temperature can be changed within 20-50$^0$ C (at stabilization of temperature about ~ 0.1$^0$ C). The operation principle of the device is described in detail in [8,10] where it was shown that position of the beam on the CCD-sensor is uniquely determined by RI of liquid. RI, in turn, is uniquely determined by the concentration of nanoparticles in suspension.

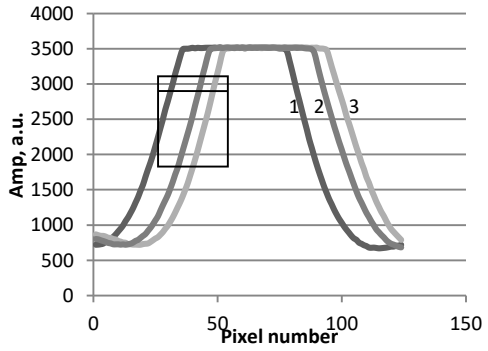


**Fig.2.** Dependence of CCD-sensors signals Amp (arb. units) on pixel number for MQ-water (1), UL-water (2) and OE-water (3).

Fig.2. shows the signals of CCD sensors for pure (without nanoparticles) aqueous media that was used to prepare suspensions. Position of the signal is uniquely determined by the number of the pixel at which the signal amplitude AMP takes a predetermined value (AMP=2500 in this case) [8]. The areas of linear decrease in amplitude are identified in Fig.2. by straight lines. A signal movement of 1 pixel corresponds to a change in the RI of the sample by $4 \cdot 10^{-6}$ [8]. From the data in Fig. 2 it follows that RI of MQ-water ($n_m$), UL-water ($n_u$) and OE-water ($n_o$) differ considerably: $n_m$-$n_u$= 4.4$\cdot 10^{-5}$ ,$n_m$-$n_o$= 6.8$\cdot 10^{-5}$. This must be taken into account when interpreting the measurement results. Measurements were carried out at elevated temperature of 40 $^0$C. This choice is dictated by the following experimental observation: the shift of the sensor signal for the suspension relative to the signal of pure water (without nanoparticles) increases with increasing temperature, as shown in Fig.3.

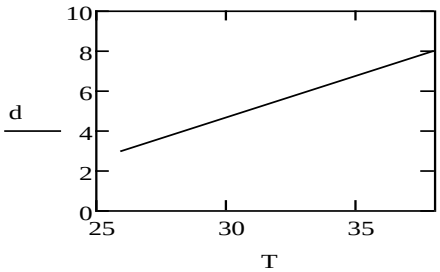


**Fig.3.** The dependence of the displacement d (in pixels) of the sensor signal on the temperature T($^0$C) of the sample.

Due to this, we are able to significantly increase the accuracy of measurements. Initially, suspensions of nanoparticles with a concentration of 100 mg/l were prepared; lower concentrations were obtained by diluting the suspensions.

### 3. Results and discussion

In our case as well as in the case of transparent binary liquid mixtures there is the unique dependence between the value of RI and concentration of components [11]. Therefore for the determination of concentration of components it is enough to measure RI. It means that we have to find relation between RI of the sample (suspension of nanoparticles in water) at different concentrations of nanoparticles and signals of CCD-sensors. Figures 4-6 show such relationships for suspensions of nanoparticle s in ultrapure water.

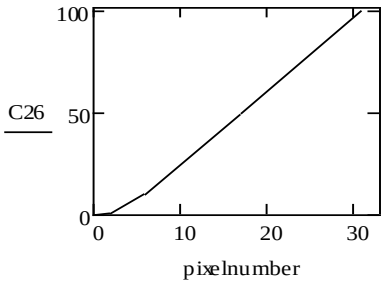


**Fig.4.** Dependence of the concentration C26 (mg/l) of nanoparticles with a size of 26 nm on the position of the CCD-sensor signal, pixelnumber.

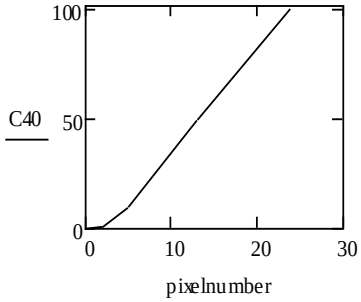


**Fig.5.** Dependence of the concentration C40(mg / l) of nanoparticles with a size of 40 nm on the position of the sensor signal, pixelnumber.

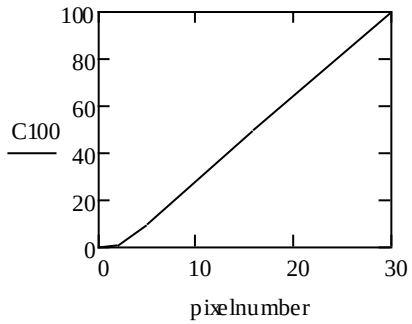


**Fig.6.** Dependence of the concentration C100 (mg / l) of nanoparticles with a size of 100 nm on the position of the sensor signal pixelnumber.

In the case of suspensions of nanoparticles in natural water (UL- or OE-), such dependences cannot be obtained, since the signal displacements were only 2–4 pixels, which is not enough to build the scale of the device.

Detailed description of propagation of light in the liquids containing nanoparticles has to be described within Mie's theory [13]. By means of this theory the phase shifts (and the change of a refractivity connected with it) arising at light scattering by nanoparticles can be calculated. But in case of suspensions with the small maintenance of nanoparticles, it is possible to describe light propagation by means of some efficient dielectric constant [14]:

$$\varepsilon_s = \varepsilon_l + c \cdot 3 \cdot (\varepsilon_p - \varepsilon_l) \cdot \varepsilon_l / (\varepsilon_p + 2 \cdot \varepsilon_l), \quad (1)$$

where $\varepsilon_s$, $\varepsilon_l$, $\varepsilon_p$ - dielectric constants of suspension, liquid and nanoparticle; c – concentration of nanoparticles in liquid. Since $RI^2 = \varepsilon_s$, at small values of c, it must be proportional to RI (see Fig.4.-Fig.6.). Another approach is considered in [12], where it is shown that the refractive index can be represented as

$$RI = n_l + const \cdot f \cdot Re\{i \cdot S(0)\}, \quad (2)$$

where $n_l$ is the refractive index of the aqueous medium, f - the volume fraction of nanoparticles, S(0) is the amplitude of forward scattering of light by nanoparticles. Since the mass density of polystyrene practically coincides with the density of water, the volume fraction of nanoparticles coincides with the mass concentration. This also explains the linear relationship between the concentration of NPL and the RI of suspensions.

## 4. Conclusions

In this work we experimentally showed that for suspensions of polymer nanoparticles (with sizes of 26-100 nm) in ultrapure water, using our refractive index measuring device, it is possible to measure nanoparticle concentrations in a wide range of 1-100 mg/l. For suspensions of nanoparticles in natural fresh water and artificial fresh water, measurements are possible only for sufficiently large concentrations of ~ 100 mg/l.

## Acknowledgements

This research was funded by Estonian Research Council grant PUT1512. We thank AS TallinnaVesi for providing access to Lake Ülemiste for water collection and physico-chemical analysis results for Lake Ülemiste water.

## 5. References

1. GESAMP. 2015. Sources, fate and effects of microplastics in the marine environment: a global assessment (Kershaw, P. J., ed.). IMO/ FAO/UNESCO-IOC/UNIDO/WMO/IAEA/ UN/UNEP/UNDP Joint group of experts on the scientific aspects of marine environmental protection. Reports and studies GESAMP 93:96.
2. Toussaint, B., Raffael, B., Angers-Loustau, A., Gilliland, D., Kestens, V., Petrillo, M., Rio-Echevarria, I.M., Van den Eede, G. 2019. Review of micro- and nanoplastic contamination in the food chain, Food Additives & Contaminants: Part A, 36:5, 639-673
3. SAPEA, Science Advice for Policy by European Academies. 2019. A Scientific Perspective on Microplastics in Nature and Society. Berlin: SAPEA. https://doi.org/10.26356/microplastics
4. Besseling, E., Redondo-Hasselerharm, P., Foekema, E.M., Koelmans, A.A. 2019. Quantifying ecological
1. risks of aquatic micro- and nanoplastic, Critical Reviews in Environmental Science and Technology 49:1, 32-80.DOI:10.1080/10643389.2018.1531688
5. de Sá, L.C., Oliveira, M., Ribeiro, F., Rocha, T.L., Futter, M.N. 2018. Studies of the effects of microplastics on aquatic organisms: What do we know and where should we focus our efforts in the future? Science of the Total Environment 645, 1029–1039.
6. Silva, A.B., Bastos, A.S., Justino, C.I.L., da Costa, J.P., Duarte, A.C., Rocha-Santos, T.A.P. 2018. Microplastics in the environment: Challenges in analytical chemistry -A review. Analytica Chimica Acta 1017, 1-19.
7. Morales-Luna G.,Garcia-Valenzuela A. Viability and fundamental limits of critical-angle refractometry of turbid colloids. Meas. Sci.Technol. 2017, 28:125203(7pp.)
8. Vilitis O., Merkulovs D., Kozlovs V. Measurement of low concentration of nanosized objects in biofluids by means of refractomttric methods.Proceedings of 13th Intern.Conf. "Medical physics in the Baltic States",Kaunas,2017,pp.134-136
9. Merkulovs D., Vilitis O., Kozlovs V. Measurement of low concentration of nanosized objects suspended in liquid medium. Latv.J. of Phys. Tech. Sci. 2018,52(2): p.77-82.
10. Kozlov V., Merkulov D., Vilitis O. New method for measuring refractive index of liquids. Proceedings of SPIE 2001, V. 4318 , p.89-92.
11. IoffeB.V. Refractometric methods in chemistry. Second edition, Khimya, 1974, 402p. (in Russian).
12. van de Hulst H.C. Light scattering by small particles. New York – Dover,1981,801p.
13. Bohren G.F., Huffman D.R. Absorption and scattering of light by small particles. J.Wiley@ Sons,1983, 521 p.
14. Landau L., Lifsitz E. Electrdynamics of continuous media. Nauka, 1982, 620 p. (in Russian)

*MEDICAL PHYSICS IN THE BALTIC STATES 14 (2019)*

Proceedings of International Conference "Medical Physics 2019"
7 – 9 November 2019, Kaunas, Lithuania

# EVALUATION OF IRRADIATED DOSE GELS USING PHOTO-SCANNING METHOD

Neringa ŠEPERIENĖ[1,2], Rimas ŠEPERYS[2], Diana ADLIENĖ[1]
[1]Kaunas University of Technology; [2]MB Šeši partneriai
neringa.vaiciunaite@ktu.lt; r.seperys@gmail.com

***Abstract*:** Optical density of polymer dose gels, which are hydrogels, increases after photon, proton, neutron, electron irradiation. This feature of dose gels is used for radiation dose assessment. The advanced chemical composition nMAG dose gel has been investigated in this study. The aim of this study was to estimate the expansion of polymerized gel to not irradiated gel volume in order to manufacture high accuracy and high spatial resolution dose gel which is able to indicate doses in the range of 0.5 – 5 Gy.

***Keywords*:** dose gel, photo-scanning, polymerization

## 1. Introduction

Dose gels are known as highly radiation-sensitive materials, which are able to change physical, chemical, and mechanical properties after interaction with high-energy photons, electrons, neutrons and protons [1]. Dose gels are hydrogels made of water, gelatine and monomers, which proceed to polymers after irradiation, Dose gels have a high potential to visualize radiation dose with high accuracy [2]. When ionizing radiation is applied, the polymerization process triggers, and the amount of polymerized material becomes a function of absorbed radiation dose [3]. It is known that radiation induces water radiolysis, and cross-linked structure of gel starts to form. The type of formed radiolytic products depends on the primary particle energy and irradiation type. When doses are increasing, the net structure becomes denser. The density of the cross-linked network is a potential property that enables evaluation of polymerized structures. It was shown [4] that high ionizing radiation doses, >50 Gy, initiate nano and macro sized clusters, i.e., "spurs", which may migrate within gel's volume. However, the polymerization proliferation when low-dose <10 Gy photon irradiation is applied are not well defined. The evaluation of expansion of polymerized gel to not irradiated gel volume is essential in order to manufacture high accuracy and high spatial resolution dose gel which is able to indicate doses in the range of 0.5 – 5 Gy.

## 2. Materials and methods

In this study we have investigated the spatial distribution of polymerized derivatives in photon irradiated advanced nMAG dose gels and analyzed polymerization expansion to the neighboring space around the irradiated volume. The research steps carried out to evaluate the polymerization proliferation to not irradiated gel volume were as follows:

1. Preparation and irradiation of advanced nMAG gels to low doses (0-5 Gy) using 15 MeV X-rays;
2. Analysis of irradiated advanced nMAG gels using newly developed photo scanning-method;
3. Defining limits for proliferation by calculating penumbra of irradiation profiles.

Advanced nMAG dose gel samples containing 8% w/w of methacrylic acid, 15 mM of (hydroxymetyl) phosphonium choloride, 6% w/w of gelatine and 86 % w/w of purified water were manufactured at Kaunas University of Technology, Physics Department. The manufacturing procedure was performed in normal atmospheric conditions in a fume hood. In order to minimize the possible oxidation, the prepared gel was poured up to the top into the standard PMMA cuvettes, which were immediately sealed. The cuvettes were kept at room temperature at least for 8 hours and then stored in cool and dark place until irradiation [5].

The irradiation of gel samples was performed in medical linear accelerator Clinac DMX (Varian) at the Hospital of Oncology of Lithuanian University of Health Sciences. The following irradiation parameters were used: max dose dep th was 1.5 cm; SSD, was set to 100 cm; field size was10×10 $cm^2$; dose rate was 3 Gy/min. Advanced nMAG gel samples were irradiated up to 5 Gy doses using 15 MeV X-ray beam.

Newly constructed photo-scanner (Fig. 1) was used for polymerization proliferation assessment in dose gel samples. The prototype of the photo-scanning system allowed the dose evaluation along the longitudinal axis of the irradiated sample with a spatial resolution of 0.20mm. The measurements were performed as follows:

cuvette with the irradiated dose gel inside was inserted and fixed in the sample holder of the scanner, which was designed to accommodate the standard cuvette. The diode laser (Thornlabs) was installed on the top of the scanning chamber. The photovoltaic elements (Thornlabs) were mounted on the opposite side of the scanner in front of the laser aiming to detect the intensity of the through sample transmitted light, which changes with the irradiation dose of the sample. The scanning chamber was mounted on the 10 cm long motorized axial stage 8MT175 (Standa) with the space resolution of 0.31 μm (1/8 step); the resolution in full step was equal to 2.5 μm; the scanning speed was set to 1 mm/s. I/O board was connected to a computer and scanning chamber. The system was driven by using a self-developed computer algorithm (Arduino and MatLab based) and was able to measure through the experimental sample transmitted laser light intensity and evaluate the intensity profile that was corresponding to the absorbed dose [5].

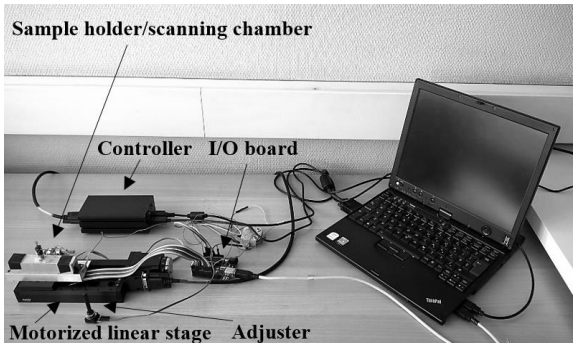


**Fig. 1.** Photo-scanning system for the evaluation of the transmitted light intensity in cuvette based samples [5]

### 3. Results and discussion

In order to evaluate the polymerization proliferation in advanced dose gel nMAG samples 3 irradiation scenarios were applied: 1) irradiation of a well-defined, 1 cm long part of gel volume to doses up to 5 Gy leaving the rest of the volume irradiation free; 2) dividing gel volume in two well-defined parts and irradiating one part of the gel to one selected dose and another part of the gel - to different doses up to 5 Gy; 3) irradiation of well-defined (0.5 cm long) part in the middle of gel sample to 4 Gy and 5 Gy doses. The first scenario was applied to find out whether polymerization proliferates to not irradiated gel volume and how this expansion depends on radiation dose. The second scenario was applied to identify the boundary shift between two irradiated parts of the sample and to find out interception of different doses. The third scenario was used to find out polymerization propagation to not irradiated volume when there is no container wall limitation. The polymerization propagation to not irradiated site and possible shift of polymerization boundary to gel volume irradiated by lower dose are essential characteristics in the case when polymerized gel is used as radiation detector.

**Scenario No.1: Partially irradiated dose gel sample:** Implementing this scenario 1 cm thick part of dose gel volume inside the cuvette was irradiated to doses from 0.5 Gy to 5 Gy and another part of the gel was left not irradiated. The sharp boundary between irradiated and not irradiated area was achieved adjusting parameters of medical linear accelerator as it is shown in Fig. 2.

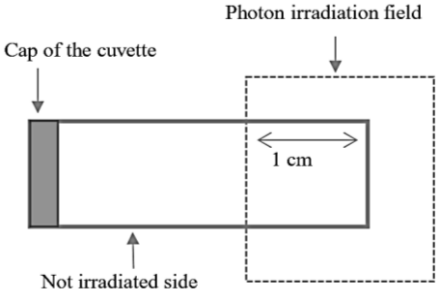


**Fig. 2.** Irradiation geometry of advanced nMAG dose gel samples [5]

Photograph of some advanced nMAG dose gel samples after irradiation to doses up to 5 Gy are provided in Fig.3. Radiation induced polymerization causes changes in optical density of the irradiated gels [6]. Provided picture indicates that the main radiation induced changes are present in the region up to 1 cm from the bottom of cuvette, however some expansion of the polymerized area with less intensity is clearly seen.

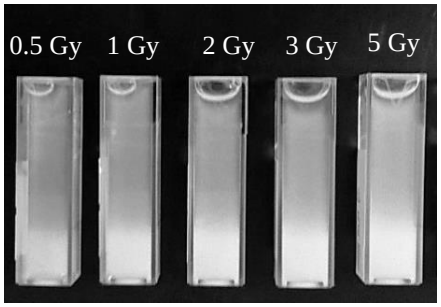


**Fig. 3.** Some advanced nMAG dose gel samples after irradiation to different doses

Samples were scanned along longitudinal axis and dose response profiles of the irradiated cuvettes filled with advanced nMAG dose gels are shown in Fig.4. The irradiated zone is marked by dashed lines. Scanning was performed in 0.20 mm steps.

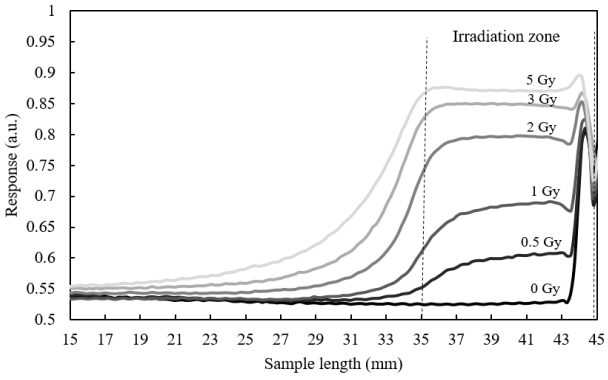


**Fig. 4.** Scanned dose response profiles of advanced nMAG dose gels irradiated according to Scenario No.1 with indicated 1 cm thick irradiation zone [5]

Scanned dose response profiles indicated clearly the absence of the sharp edge between irradiated and not

irradiated zone. This confirms non-uniform distribution of polymerized derivatives close to the boundary in irradiated area due to the diffusion of the created reactive radicals from irradiated zone towards zone without irradiation. The profile near the boundary between two zones becomes steeper with the increased absorbed dose and the distribution of polymerized derivatives becomes more uniform in the whole irradiated area, because higher doses are responsible for the formation of well-developed polymer network structure [7]. The penumbra appearing due to curves slopes of the different doses were calculated. A quantitative measure of the penumbra, *ΔP*, can be defined as the distance over which the dose increases from 10% to 90% of its maximum value [8]. The penumbra in our experiments was observed due to polymerization propagation towards not irradiate gel volume. The evaluated *ΔP* values were as follows: 5 Gy – 6 mm, 3 Gy – 5 mm, 2 Gy – 4 mm, 1 Gy – 3 mm, 0.5 Gy – 2 mm. The non-linear, however monotonic tendency of increasing penumbra due to increased irradiation dose is presented in Fig. 5. It could be assumed that for a higher doses (>5 Gy) the penumbra may reach the saturation level which means that penetration of polymerized derivatives into not irradiated area is finite.

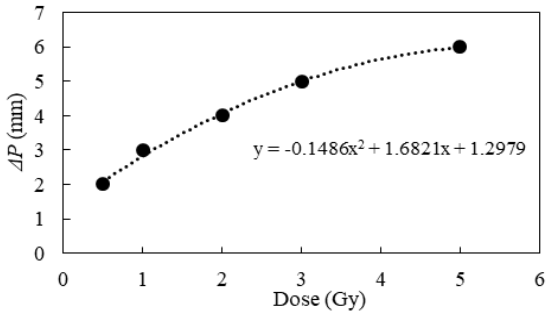


**Fig. 5.** The increase of penumbra due to irradiation dose

**Scenario No.2**: In order to evaluate "overlapping" of polymerized areas in the boundary region between two zones irradiated to different doses, another batch of advanced nMAG gel dose samples was fabricated. Fabricated samples were irradiated in linear accelerator adjusting its parameters to the geometry shown in Fig.6. Gel filled cuvette was divided in two parts: the A part of the cuvette was dedicated for irradiation to doses from 0.5 Gy to 5 Gy; the B part of the cuvette was dedicated for the irradiation of all samples to the constant 2 Gy dose.

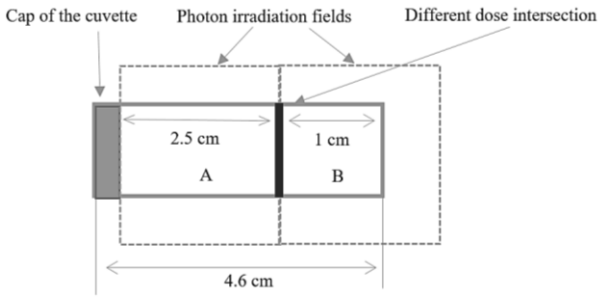


**Fig. 6.** Irradiation geometry of advanced nMAG dose gel samples (Scenario No.2) [5]

First, corresponding zone of each sample was irradiated to 2 Gy and then immediately after the first irradiation - to doses from 0.5 Gy to 5 Gy. A photograph of irradiated advanced nMAG doses is shown in Fig. 7. It is visually seen that the bottom part of the cuvette was irradiated to various doses; the upper part to the same dose in all samples.

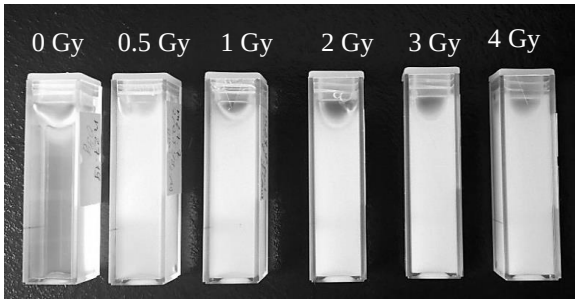


**Fig. 7.** Photograph of some advanced nMAG dose gel samples after irradiation according to Scenario No.2 [5]

The response profiles of advanced nMAG samples scanned along the longitudinal axes are provided in Fig.8.

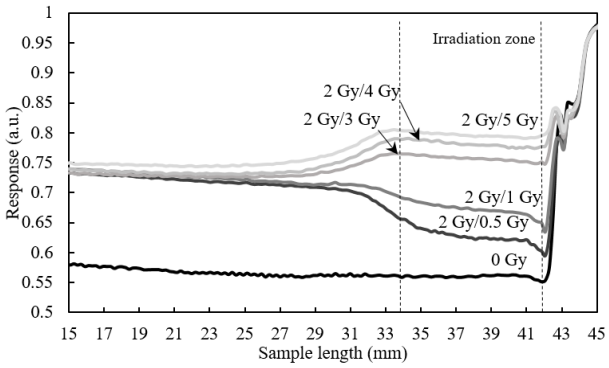


**Fig. 8.** Scanned dose response profiles of advanced nMAG dose gels irradiated according to Scenario No.2 with indicated 1 cm thick irradiation zone

Scanned dose response profiles indicated the presence of transition zone close to the boundary between differently irradiated parts of the cuvette. The width of this zone was dependent on irradiation doses: polymerization expansion up to 3.2 mm was estimated for samples part of which was irradiated to 0.5 Gy and 1 Gy doses. Also, the increase of the spread was observed up to 4.1 mm close to the boundary between two zones for samples part of which was irradiated to higher (3 Gy, 4 Gy, 5 Gy) doses as compared to a standard 2 Gy dose. This might be explained by two way diffusion of free radicals in gel from one cuvette part to another depending on irradiation doses. Taking into account that irradiation of gel in both cuvette parts was not performed simultaneously, radiation induced diffusion of free radicals to not irradiated part started immediately (in a time period of $10^{-15}$ s to $10^{-14}$ s) after the first irradiation [9]. After $10^{-11}$ s a local thermal equilibrium in the recombination of reactive particles may be reached. Taking into account that average diffusion coefficient of the reactive particles in water is $4\times10^{-9}m^2s^{-1}$, it is probable that after $10^{-11}$s the root mean square displacement of the particles from the

point of creation is 0.28 nm. It is only one tenth of the intermolecular distance of the methacrylic acid monomer [1].

When the irradiation doses to both cuvette parts were the same (2 Gy and 2 Gy), insignificant (0.20 mm) increase just behind the boundary was observed. Additional number of diffused free radicals contributed to faster polymerization saturation in higher dose part were responsible for the formation of polymerization transfer zone backwards to the 2 Gy zone. The measured response, which was estimated along longitudinal axis of 2 Gy irradiated sample part (from 15 mm to 25 mm) was varying insignificant from 0.12 a.u to 0.18 a.u. It shows that only 2 Gy irradiation contributed to response and there were no diffused radicals from 0.5 Gy, 1 Gy, 3 Gy, 4 Gy and 5 Gy irradiation in this gel volume.

**Scenario No. 3.** In order to find out the complete polymerization propagation profile to not irradiated volume the gels were irradiated to 4 Gy and 5 Gy doses in the middle of sample. The 0.5 cm long zone was chosen in the middle of measurements' window of the cuvette (Fig. 9). The expansion of polymerized zone was clearly seen in each irradiated sample.

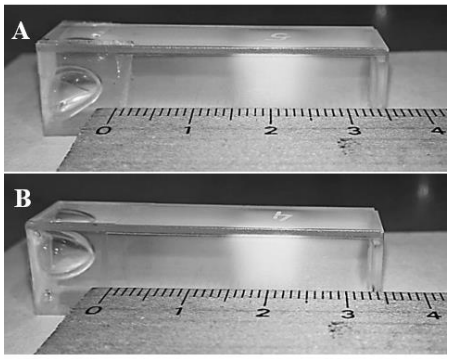


**Fig. 9.** A) 5 Gy, B) 4 Gy irradiated gel samples with no polymerization spread restrictions along the cuvette [5]

The cuvettes were scanned and the dose response profiles were established for the evaluation of polymerization propagation penumbra *ΔP*. The measured profiles (Fig. 10) had the same shape, but *ΔP* for 4 Gy and 5 Gy irradiated samples were different.

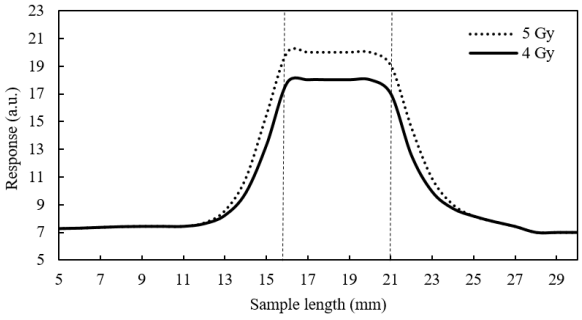


**Fig. 10.** The polymerization spread profiles of 5 and 4 Gy doses

The performed calculations revealed that *ΔP* was equal to 2 mm for 4 Gy dose and 5 mm for 5 Gy dose. Equal *ΔP* to both sides from the polymerized zone identified that the polymerization proliferates equally to both non-irradiated sides of gel if there are no restrictions within cuvette. No significant increase was observed in response between 5 to 11 mm and between 28 to 30 mm, which indicated existence of polymerization propagation ("dark polymerization" when no additional radiation dose is applied) to non-irradiated samples' side. In order to explain the polymerization spread to non-irradiated gel volume, the model that is clarifying polymer molecules' migration was presented [10]. The model indicates that the expansion of polymerized derivatives to non-irradiated volume could be explained by using "spur" propagation theory. The polymerization propagation kinetic model of the polymer molecules is defined as a localized microscopic area. As it was mentioned before, the radiolytic products appear in clusters that are called "spurs". They are produced along the path of an incident of ionizing irradiation and ejected secondary electron. The propagation of the "spurs" into a medium is simplified as a spread of the elementary wave. In this model, it was assumed that initial "spur" has constant size and the same number of radical. The radical inside the "spur" reacts only with neighbor "spur" when both spreading "spurs" interact with each other [10, 11]. The yields of radical depend on the localized energy loss in the interaction area of ionizing irradiation. When the energy is consumed, the interactions of radicals increase; therefore, the distance between the "spurs" decreases. Such a behavior of radicals affects the yield of polymerization and the propagation of produced polymers. When the radiation dose is higher, the higher amounts of "spurs" are formed in the same volume [12]. This effect leads to denser polymerized volume.

## 4. Conclusions

To sum up the experimental results of the polymerization proliferation in gel sample volume, it is important to mention that when there is no polymerization spread restrictions, the polymerization in all directions is possible.

It was found, that polymerization induced penumbra was increasing from 2 to 6 mm when 0.5–5 Gy doses were applied and may saturate at >5 Gy. The polymerization expansion at the boundary between two zones irradiated to different doses ranged from 3.2 mm (0.5 Gy, 1Gy) to 4.1 mm for sample's part, which was irradiated to 3 Gy, 4 Gy, 5 Gy doses. It was observed that the polymerization in cuvettes filled with nMAG gel propagated symmetrically; which allowed to detect the boundaries and intersection using photo-scanning method with a good accuracy.

The advanced nMAG gel showed promising results in dose response after low photon dose (0.5 – 5 Gy) irradiation. However, further studies are needed to improve the chemical composition of nMAG taking into account that a high spatial resolution is needed to detect radiation doses with 0.1 Gy accuracy.

## Acknowledgment

This study was supported by Research Council of Lithuania. Project S-MIP-17-104.

## 5. References


1. Baldock C. Polymer gel dosimetry. Physics in Medicine and Biology. 2010, p. 55, R1–R63. doi: 10.1088/0031-9155/55/5/R01.
2. Okay O. General properties of hydrogels. Hydrogel Sensors and Actuators. Springer Series on Chemical Sensors and Biosensors (Methods and Applications). 2009, p. 6.
3. Ahmed L.E. Hydrogel: Preparation, characterization, and applications: Natural-based polymers for biomedical applications. Journal of Advanced Research. 2015, 6(2), p.p. 105–121.
4. Mcauley K. Fundamentals of polymer gel dosimeters. Journal of Physics: Conference Series. 2006, 56, 35–44.
5. Seperiene N. The development of polymer gels and composites with the enhanced sensitivity to low-dose irradiation. Doctoral disertation, Kaunas, 2018. p.p. 49-52.
6. Zeidan O.A., et al. Dosimetric evaluation of a novel polymer gel dosimeter for proton therapy. Medical Physics. 2010, 37(5), p.p. 2145–2152.
7. Marini A., et al. Fricke gel dosimeters with low-diffusion and high-sensitivity based on a chemically cross-linked PVA matrix. Radiation Measurements. 2017, 106, p.p. 618–621.
8. Basfar A.A. and moftah B. Novel composition of polymer gel dosimeters based on N-(Hydroxymethyl) acrylamide for radiation therapy. Radiation Physics and Chemistry. 2015, 112, p.p. 117–120.
9. Andrews H.L., et al. Gel dosimeter for depth dose measurements. Review of Scientific Instruments. 1957, 28, p.p. 329–332.
10. Yoshioka M. Examination of fundamental characteristics of a polymer gel detector in a proton beam irradiation. Radiation Measurements. 2011, 46, p.p. 64–71.
11. Maitra J. and. Shukla V.K. Cross-linking in hydrogels — A review. American Journal of Polymer Science. 2014, 4(2), p.p. 25–31. doi: 10.5923/j.ajps.20140402.01.
12. Seiffert S. and Sprakel J. Physical chemistry of supramolecular polymer networks. Chemical Society Reviews. 2012, 41, p.p. 909–930.

*MEDICAL PHYSICS IN THE BALTIC STATES 13 (2019)*

Proceedings of International Conference "Medical Physics 2019"
November 2019, Kaunas, Lithuania

# POLYCHROMATIC X-RAY ATTENUATION PROPERTIES OF NORMOXIC POLYMERS GELS

Aleksandras ŠEVČIK, Diana ADLIENĖ
Department of Physics, Kaunas University of Technology, Kaunas, Lithuania

***Abstract*:** Monte Carlo (MC) model based on FLUKA code was used to calculate the mass attenuation coefficients of the widely used non-irradiated normoxic polymer gel dosimeters, namely nMAG and nPAG gels, in polychromatic X-ray field. First, monochromatic beam attenuation was modelled, and the results were validated with NIST reference data and discrepancy was found <1%. In the second part the simulation was repeated with polychromatic X-ray spectra used in the diagnostic and therapeutic medical physics and mass attenuation coefficient values were derived for normoxic polymer gels and water medium for the reference purposes. The data obtained by this work can be used for the analysis of gel dosimeter's behavior in polychromatic photon radiation fields.

***Keywords*:** interaction of photons with matter, polychromatic X-ray spectrum, Monte Carlo, modeling, Fluka program package, X-ray attenuation, polymer dose gels.

## 1. Introduction

Polymer gel dosimeters are made of radiation sensitive materials, which record three-dimensional dose distributions [1]. Radiation induced polymerization of gels occurs upon irradiation. The degree of polymerization is dose dependent.

The radiological properties, including attenuation, of polymer gels as well as other media are thoroughly analyzed by researchers using MC simulation [2-6]. Vahabi et al. [7] has recently performed MC simulation using MCNP code for the most popular polymer gels checking their mass attenuation coefficient values for the monochromatic energies and comparing them with XCOM database [8].

During polymerization the attenuation properties of the polymer gels are changed accordingly. In order to evaluate these polymerization related changes, the attenuation properties of materials irradiated to polychromatic photon beam must be carefully analyzed. Polychromatic X-rays are represented by a broad energy spectrum thus their attenuation in material cannot be described by a simple Beer-Lambert law which only pplies for monochromatic radiation.

To the best of our knowledge, there are no studies which would analyze the simulation-derived mass attenuation coefficients for modelled normoxic polymer gel media in the photon field of various polychromatic x-ray spectra. In this work, the authors used the MC simulation package to model and calculate the mass attenuation coefficients for the widely used normoxic polymer gels irradiated with 80, 100, 120, 150, 200, 6000 and 15000 kVp polychromatic X-ray beam. For the verification purposes, the attenuation coefficients of water medium in the monochromatic X-ray field were simulated and compared with XCOM [8] NIST Standard Reference Database 126 [9]

## 2. Instruments and methods

### 2.1. Theoretical framework

The mass attenuation coefficient $\mu/\rho$ (in terms of $cm^2/g$) defines the rate of intensity loss by a narrow beam of monoenergetic photons with an incident intensity $I_0$ when passes through a medium with thickness $x$ and density $\rho$ and emerges with intensity $I$:

$$\mu/\rho = x^{-1} ln(I_0/I), \qquad (1)$$

from which $\mu/\rho$ can be obtained from measured values of $I_0$, $I$ and $x$. The NIST Standard Reference Database 126 was used to compare the mass attenuation coefficients with the simulated results in the monochromatic photon field.

### 2.2 Simulation framework

Monte Carlo code FLUktuierende KAskade (FLUKA) is a fully integrated particle physics simulation package for simulating the interaction of radiation with matter covering a wide range of applications from radiation to medical physics [10, 11]. This code is one of standard tools used at CERN and NASA for dosimetry, radioprotection and high energy interaction studies [12, 13].

The data from the EPDL97 [14] photon data library have become the source for pair production, photoelectric and total coherent cross-section tabulations, as well as for atomic form factor data. The simulation physics set-up deals with transport of electrons, positrons and photons in addition to activated Rayleigh scattering and inelastic form factor corrections to Compton scattering and Compton profiles, detailed photoelectric edge treatment and fluorescence photons, multiple scattering, photon polarization considered for Compton, Rayleigh and photoelectric effects [15, 16]. An installed voxel geometry module allows to create the detailed 3D representations from CT scans for dosimetry or other research purposes.

A production threshold and kinetic energy transport cut-off is set to 1 keV for electrons and 1 keV for photons.

The Fluka simulation package allows to re-create a beam using a custom routine that can be sampled directly from the provided spectrum of any specific X-ray equipment. A computational toolkit SpekCalc [17-19] has been employed to generate orthovoltage X-ray spectra replicating the tungsten anode X-ray tube based GULMAY D3225 unit. The unit spectrum was carefully replicated modelling tungsten target angled at 20º relative to the beam axis, adding 0.8 mm inherent beryllium filtration and 2.44 mm aluminum added filtration.

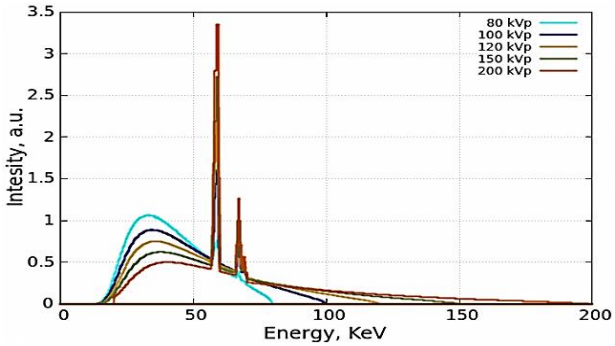


**Fig. 1.** The polychromatic spectra of orthovoltage machine simulated in MC simulation. The source data provided by SpekCalc

The 6 MV and 15 MV spectra was replicated using the data from clinical accelerators of the Varian Clinac C series [20]. The data of orthovoltage x-ray spectra generated by SpekCalk and megavoltage x-ray spectra of the linear accelerators was used as sampling distribution in Fluka to replicate the same spectrum in its environment (Fig.1 and 2).

The simulation geometry has been prepared in the following way: the pencil beam of chosen spectrum is directed into Z positive direction through 10 layers of water medium where each layer has a thickness of 1 cm (Fig.3).

The polychromatic photon beam is generated as a pencil beam source with no divergence. Only primary beam photon fluence is counted and the change of its intensity is calculated. The total attenuation with coherent scattering is evaluated and mass attenuation coefficient is derived.

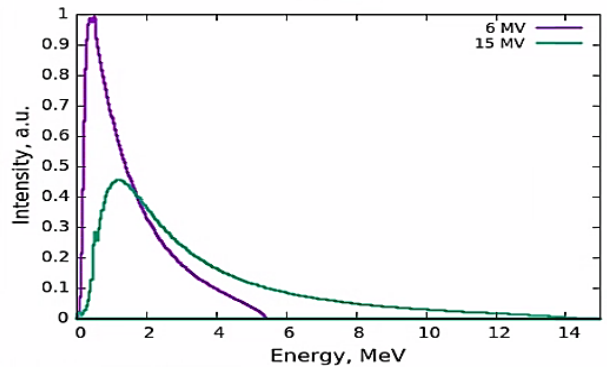


**Fig.2.** The polychromatic spectra of megavoltage machine simulated in MC simulation. The source data based on Varian Clinac C series

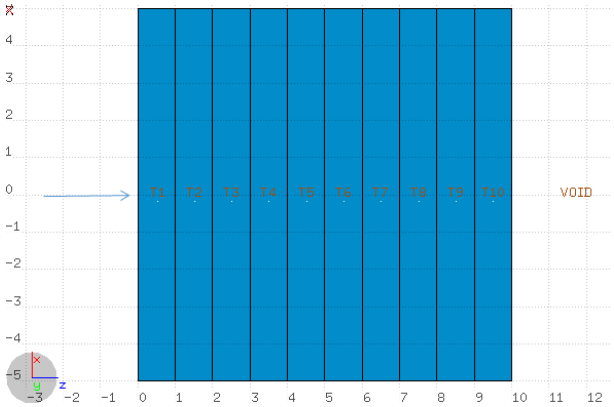


**Fig. 3**. The geometry of attenuation measuring simulation

The basis for media was modelled identical to the composition of normoxic methacrylic acid (nMAG) consisting of 5% methacrylic acid (MAA, $C_4H_6O_2$), 8% gelatin ($C_{102}H_{151}N_{31}O_{39}$), 0.5% of tetrakis-(hydroxymethyl)-phosphonium-chloride (THPC, $[(HOCH_2)_4PCl]$), 86.5% water ($H_2O$) and polyacrylamide (nPAG) gel consisting of 3% acrylamide (AAM, $C_3H_5NO$), 3% N,N' -methylene-bis-acrylamide (BIS, $C_7H_{10}N_2O_2$), 5% gelatin ($C_{102}H_{151}N_{31}O_{39}$), 2% of THPC, $[(HOCH_2)_4PCl]$ and 87% ($H_2O$) (Table 1).

**Table 1.** Composition by relative weight of modelled gels

| Element | Materials, mass % of elemental composition | | |
|---|---|---|---|
| | nMAG | nPAG | Water |
| | $\rho$ = 1.05 g/cm$^3$ | $\rho$ = 1.04 g/cm$^3$ | $\rho$ = 1.00 g/cm$^3$ |
| H | 10.56 | 10.58 | 0.182 |
| O | 80.90 | 80.52 | 0.818 |
| C | 6.94 | 6.18 | - |
| N | 1.43 | 2.03 | - |
| P | 0.08 | 0.33 | - |
| Cl | 0.09 | 0.37 | - |

FLUKA code calculates the statistical error (type A uncertainty) to estimate the standard deviation of the repeated simulations results. The simulation was performed in 10 batches each containing $10^6$ events. The statistical error was kept under 1% in all regions of importance.

### 3. Results and discussion

In the first part of the simulation the monochromatic beams were modelled and the attenuation in the water medium was simulated. The results were compared with NIST database reference values. Discrepancies did not exceed 1% which indicated that selected model parameters are suitable for such calculations (Table 2)

**Table 2.** Comparison of derived mass attenuation coefficient with NIST reference values in water medium

| Monochromatic Beam Energy, MeV | Simulated μ/ρ cm^2/g | NIST reference value [] | Difference |
|---|---|---|---|
| 0.01 | 5.327E+00 | 5.329E+00 | 0.04% |
| 0.02 | 8.063E-01 | 8.096E-01 | 0.41% |
| 0.03 | 3.761E-01 | 3.756E-01 | -0.13% |
| 0.04 | 2.663E-01 | 2.683E-01 | 0.75% |
| 0.05 | 2.292E-01 | 2.269E-01 | -0.99% |
| 0.06 | 2.058E-01 | 2.059E-01 | 0.05% |
| 0.08 | 1.824E-01 | 1.837E-01 | 0.71% |
| 0.10 | 1.716E-01 | 1.707E-01 | -0.52% |
| 0.20 | 1.369E-01 | 1.370E-01 | 0.11% |
| 0.30 | 1.193E-01 | 1.186E-01 | -0.62% |
| 0.40 | 1.062E-01 | 1.061E-01 | -0.10% |
| 0.50 | 9.649E-02 | 9.687E-02 | 0.39% |
| 0.60 | 8.926E-02 | 8.956E-02 | 0.33% |
| 0.80 | 7.787E-02 | 7.865E-02 | 0.99% |
| 1.00 | 7.020E-02 | 7.072E-02 | 0.73% |
| 1.50 | 5.724E-02 | 5.754E-02 | 0.52% |
| 2.00 | 4.973E-02 | 4.942E-02 | -0.64% |
| 3.00 | 3.980E-02 | 3.969E-02 | -0.29% |
| 4.00 | 3.393E-02 | 3.403E-02 | 0.28% |
| 5.00 | 3.058E-02 | 3.031E-02 | -0.89% |
| 6.00 | 2.758E-02 | 2.770E-02 | 0.44% |
| 8.00 | 2.411E-02 | 2.429E-02 | 0.74% |
| 10.00 | 2.225E-02 | 2.219E-02 | -0.27% |
| 15.00 | 1.933E-02 | 1.941E-02 | 0.42% |

Simulations with monochromatic beam were repeated in the modelled gel media and compared with the values obtained using XCOM tool for the reference. Similarly to the previous results, the discrepancies did not exceed 1% which further validates the selected simulation parameters and modelled media.

The simulations with polychromatic beams were processed in the same modelling setup. The spectra of these beams were scored and presented in Fig.1. The resulting mass attenuations coefficients are listed in the figures below as a function of penetration depth, starting with water medium (Fig. 3 and Fig.4). The results for nMAG are shown in Fig.5 and Fig.6 as well as for nPAG in Fig.7 and Fig.8 for each polychromatic spectrum.

Comparison of all three media for different polychromatic beam energies are provided in Fig. 9 to Fig. 15.

**Table 3.** Comparison of derived mass attenuation coefficient with XCOM reference values in nMAG medium

| Monochromatic Beam Energy, MeV | Simulated μ/ρ cm^2/g | XCOM reference value [] | Difference |
|---|---|---|---|
| 0.01 | 5.178E+00 | 5.162E+00 | -0.32% |
| 0.02 | 7.911E-01 | 7.901E-01 | -0.12% |
| 0.03 | 3.711E-01 | 3.692E-01 | -0.51% |
| 0.04 | 2.658E-01 | 2.650E-01 | -0.30% |
| 0.05 | 2.251E-01 | 2.248E-01 | -0.12% |
| 0.06 | 2.045E-01 | 2.042E-01 | -0.15% |
| 0.08 | 1.816E-01 | 1.824E-01 | 0.44% |
| 0.10 | 1.697E-01 | 1.696E-01 | -0.07% |
| 0.20 | 1.363E-01 | 1.362E-01 | -0.08% |
| 0.30 | 1.180E-01 | 1.180E-01 | -0.02% |
| 0.40 | 1.056E-01 | 1.055E-01 | -0.09% |
| 0.50 | 9.647E-02 | 9.632E-02 | -0.16% |
| 0.60 | 8.880E-02 | 8.905E-02 | 0.28% |
| 0.80 | 7.827E-02 | 7.821E-02 | -0.08% |
| 1.00 | 6.971E-02 | 7.032E-02 | 0.86% |
| 1.50 | 5.732E-02 | 5.721E-02 | -0.20% |
| 2.00 | 4.884E-02 | 4.913E-02 | 0.59% |
| 3.00 | 3.926E-02 | 3.945E-02 | 0.49% |
| 4.00 | 3.370E-02 | 3.382E-02 | 0.34% |
| 5.00 | 2.988E-02 | 3.012E-02 | 0.81% |
| 6.00 | 2.752E-02 | 2.752E-02 | 0.00% |
| 8.00 | 2.402E-02 | 2.412E-02 | 0.41% |
| 10.00 | 2.183E-02 | 2.203E-02 | 0.92% |
| 15.00 | 1.911E-02 | 1.925E-02 | 0.73% |

**Table 4.** Comparison of derived mass attenuation coefficient with XCOM reference values in nPAG medium

| Monochromatic Beam Energy, MeV | Simulated μ/ρ cm^2/g | XCOM reference value [] | Difference |
|---|---|---|---|
| 0.01 | 5.40E+00 | 5.403E+00 | 0.02% |
| 0.02 | 8.25E-01 | 8.218E-01 | -0.33% |
| 0.03 | 3.80E-01 | 3.786E-01 | -0.25% |
| 0.04 | 2.69E-01 | 2.690E-01 | 0.06% |
| 0.05 | 2.27E-01 | 2.268E-01 | 0.07% |
| 0.06 | 2.06E-01 | 2.054E-01 | -0.38% |
| 0.08 | 1.82E-01 | 1.829E-01 | 0.31% |
| 0.10 | 1.70E-01 | 1.699E-01 | -0.07% |
| 0.20 | 1.37E-01 | 1.363E-01 | -0.37% |
| 0.30 | 1.18E-01 | 1.180E-01 | 0.30% |
| 0.40 | 1.05E-01 | 1.055E-01 | 0.26% |
| 0.50 | 9.64E-02 | 9.632E-02 | -0.07% |
| 0.60 | 8.92E-02 | 8.905E-02 | -0.11% |
| 0.80 | 7.83E-02 | 7.821E-02 | -0.09% |
| 1.00 | 7.06E-02 | 7.032E-02 | -0.42% |
| 1.50 | 5.76E-02 | 5.722E-02 | -0.75% |
| 2.00 | 4.91E-02 | 4.914E-02 | 0.03% |
| 3.00 | 3.91E-02 | 3.946E-02 | 0.94% |
| 4.00 | 3.38E-02 | 3.383E-02 | 0.16% |
| 5.00 | 2.99E-02 | 3.014E-02 | 0.73% |
| 6.00 | 2.75E-02 | 2.754E-02 | 0.22% |
| 8.00 | 2.40E-02 | 2.415E-02 | 0.57% |
| 10.00 | 2.21E-02 | 2.206E-02 | -0.26% |
| 15.00 | 1.93E-02 | 1.929E-02 | -0.29% |

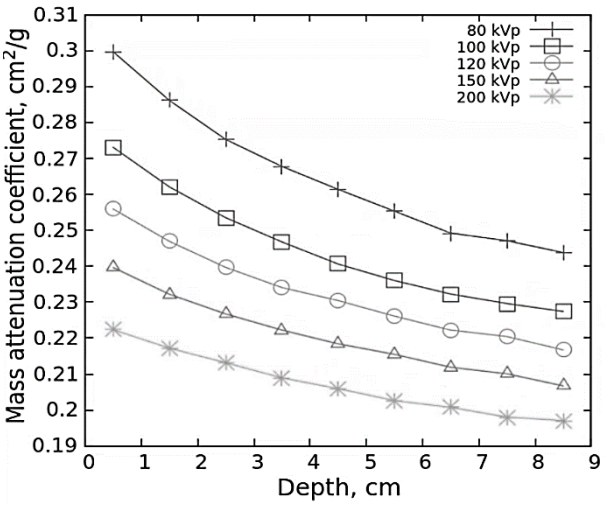


**Fig. 3**. Mass attenuation coefficient of water medium in the polychromatic orthovoltage photon field

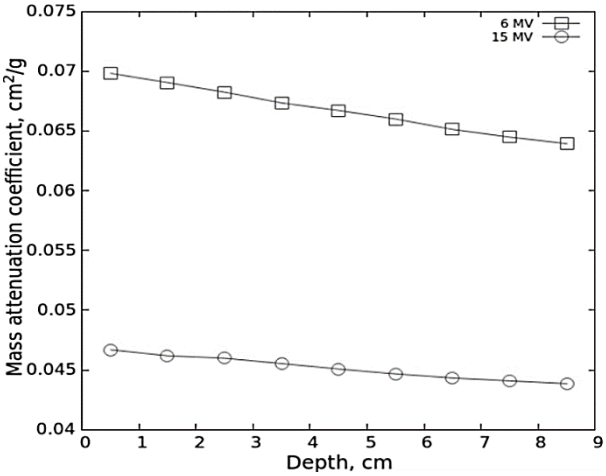


**Fig. 4**. Mass attenuation coefficient of water medium in the polychromatic megavoltage photon field

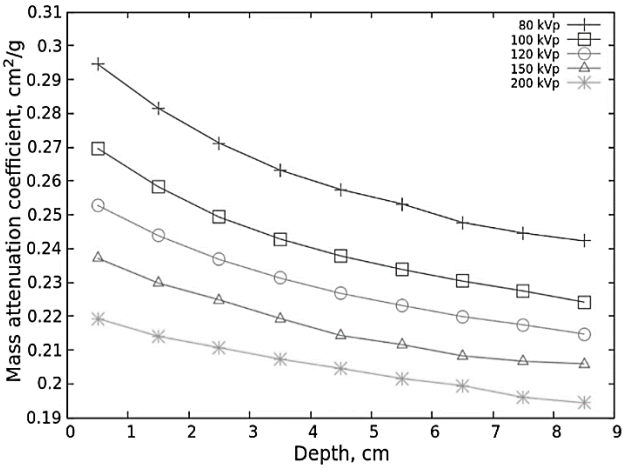


**Fig. 5**. Mass attenuation coefficient of nMAG polymer medium in the orthovoltage polychromatic photon field

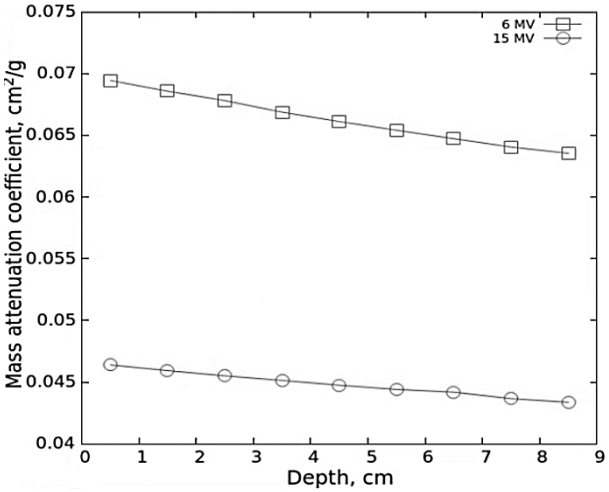


**Fig. 6**. Mass attenuation coefficient of nMAG medium in the polychromatic megavoltage photon field

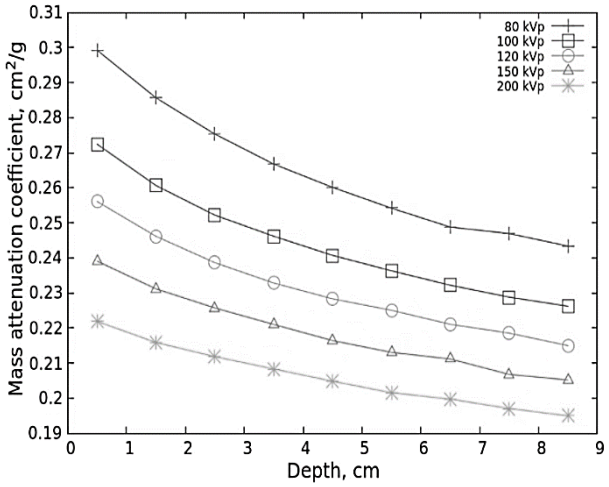


**Fig. 7**. Mass attenuation coefficient of nPAG medium in the polychromatic orthovoltage photon field

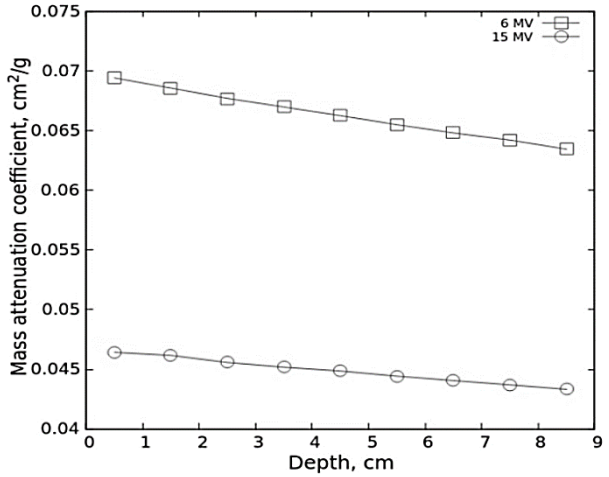


**Fig. 8**. Mass attenuation coefficient of nPAG medium in the polychromatic megavoltage photon field

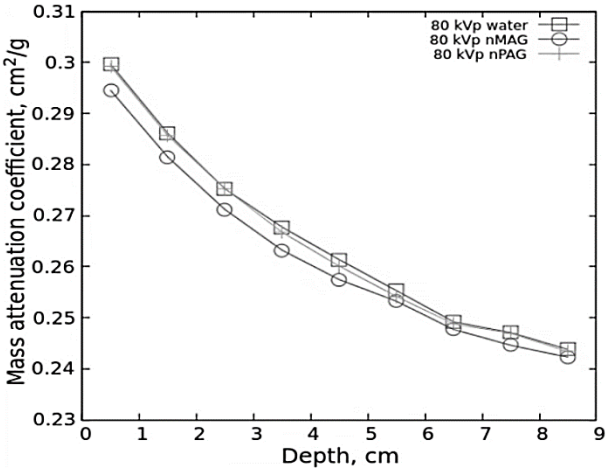


**Fig. 9**. Comparison of mass attenuation coefficient of nPAG, nMAG and water media in the 80 kVp photon field

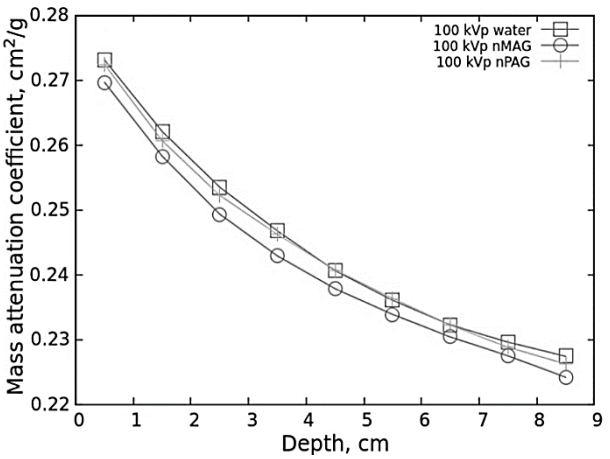


**Fig. 10**. Comparison of mass attenuation coefficient of nPAG, nMAG and water media in the 100 kVp photon field

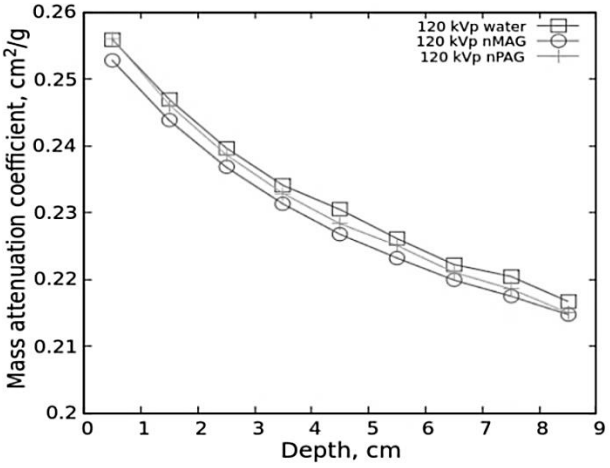


**Fig. 11**. Comparison of mass attenuation coefficient of nPAG, nMAG and water media in the 120 kVp photon field

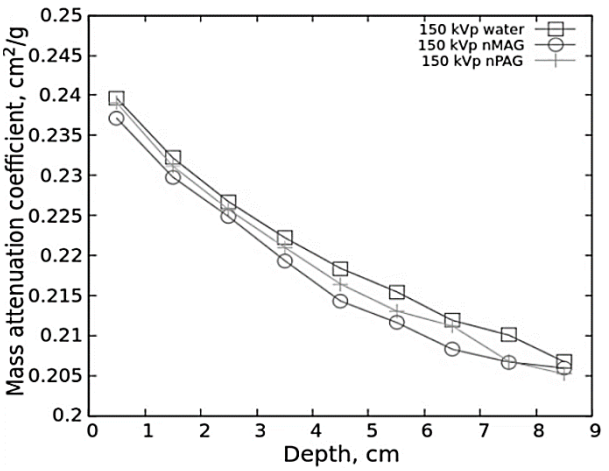


**Fig. 12**. Comparison of mass attenuation coefficient of nPAG, nMAG and water media in the 150 kVp photon field

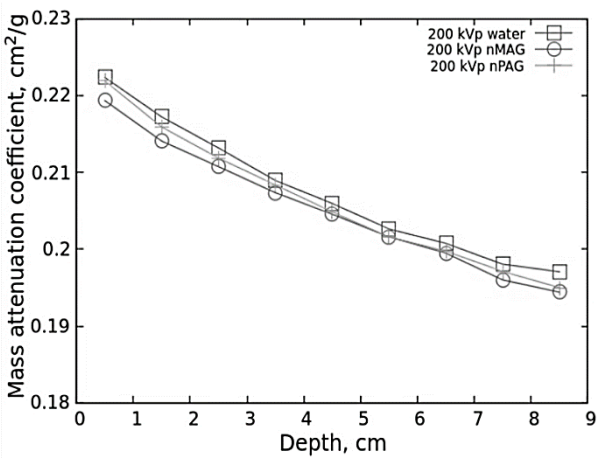


**Fig. 13**. Comparison of mass attenuation coefficient of nPAG, nMAG and water media in the 200 kVp photon field

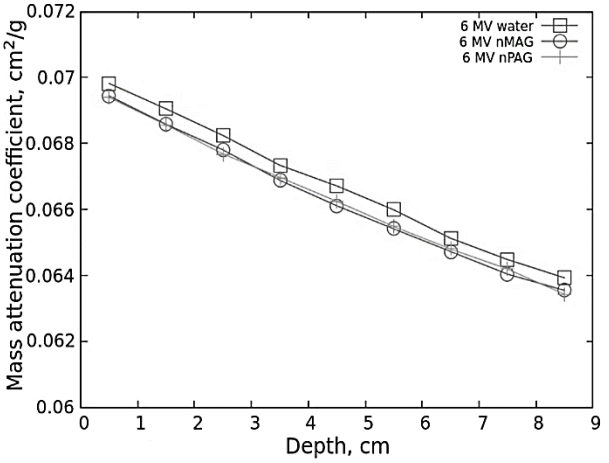


**Fig. 14**. Comparison of mass attenuation coefficient of nPAG, nMAG and water media in the 6 MV photon field

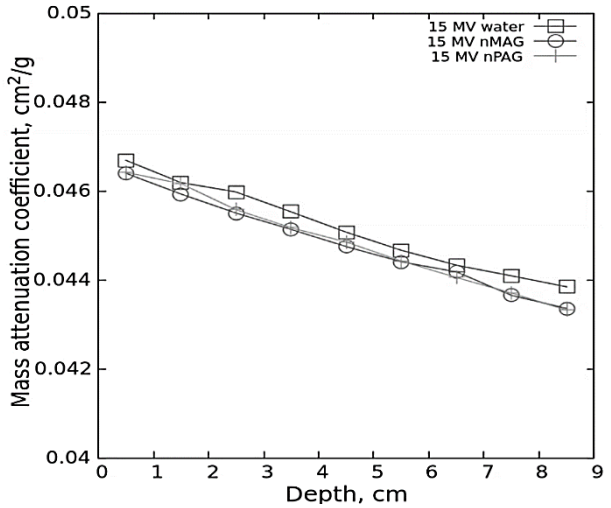


**Fig. 15**. Comparison of mass attenuation coefficient of nPAG, nMAG and water media in the 15 MV photon field

The mass attenuation coefficient of the media in the case polychromatic photon beam is used, depends on the photon penetration depth as low energy photons are being constantly absorbed by the medium. The effect is much greater in the orthovoltage range where the difference of the mass attenuation coefficient can range up to 4.5% per 1 cm of penetrated depth. Due to much higher initial photon energy, the attenuation coefficient differences are much lower ranging up to 1% per 1 cm of penetration depth when megavoltage beam is applied.

Both polymer gels are equivalent to the water in terms of the mass coefficient value in the polychromatic photon beam. The difference of this value does not exceed 1% in any given point for both of polymer gels.

## 4. Conclusions

The mass attenuation coefficient of non-irradiated polymer gels has been investigated in the presence of polychromatic photon beam. Taking into account that gels are tending to polymerize upon irradiation, the attenuation properties of the irradiated medium are changing. So it is essential to evaluate the impact of the polychromatic beam on attenuation properties. Mass attenuation coefficient as a function of photon penetration depth were determined for the widely used polychromatic beams in the ortho- and megavoltage range. It was found that the differences between attenuation coefficients calculated using monochromatic beam and polychromatic beam were in the range up to 4.5% per 1 cm in the orthovoltage field, and up to 1% per 1 cm in the megavoltage field.

The obtained values for polychromatic spectra were validated by running the same simulation setup in the monochromatic beams. The results were validated with NIST and XCOM reference data and discrepancy did not exceeded 1%.

The results of this work could be used for the evaluation of radiation energy transport parameters in polymer gel when polychromatic photon field is present.

## 5. References

1. Baldock, Clive, et al. Polymer gel dosimetry. *Physics in Medicine & Biology* 55.5R (2010):
2. Venning, A. J., et al. Radiological properties of normoxic polymer gel dosimeters. *Medical physics* 32.4 (2005): 1047-1053.
3. Gorjiara, Tina, et al. Radiological characterization and water equivalency of genipin gel for x-ray and electron beam dosimetry. *Physics in Medicine & Biology* 56.15 (2011): 4685.
4. Gorjiara, Tina, et al. Investigation of radiological properties and water equivalency of PRESAGE® dosimeters. *Medical physics* 38.4 (2011): 2265-2274.
5. Gorjiara, T., et al. Water equivalence of micelle gels for x-ray beams. *Journal of Physics: Conference Series*. Vol. 444. No. 1. IOP Publishing, 2013.
6. Souza, Luiza F., et al. Mass energy absorption coefficients and energy responses of magnesium tetraborate dosimeters for 0.02 MeV to 20 MeV photons using Monte Carlo simulations. *Applied Radiation and Isotopes* 148 (2019): 232-239.
7. Vahabi, S. M., Shamsaie Zafarghandi M., and Bahreinipour M. Monte Carlo simulation of some gel dosimeters' behaviour in photonic radiation field: research on attenuation coefficient. *Journal of Instrumentation* 14.08 (2019): P08001.
8. Berger, M. J., et al. Xcom: Photon cross sections database, nist standard reference database 8 (xgam). (2010).
9. Hubbell, J. H., and S. M. Seltzer. NIST standard reference database 126. *Gaithersburg, MD: National Institute of Standards and Technology* (1996).
10. Ferrari, A, Sala, P R, Fasso, A and Ranft, J. FLUKA: A Multi-Particle Transport Code. *(Program version 2005)*. No. INFN-TC-05-11.
11. Ballarini, F., Battistoni, G., Campanella, M., Carboni, M., Cerutti, F., Empl, A., Fassò, A., Ferrari, A., Gadioli, E., Garzelli, M.V. and Lantz, M. The FLUKA code: an overview. *Journal of Physics: Conference Series* (2006) 41(1) p. 151–160.
12. Herrera-Martinez, Adonai and Kadi, Yacine. Accelerator-Driven System Design FLUKA Exercise. [Accessed 19 September 2017]. Available from: http://indico.ictp.it/event/a04210/session/14/contribution/8/material/0/1.pdf
13. Mitaroff, A. and Silari, M. The CERN-EU High-energy Reference Field (CERF) Facility for Dosimetry at Commercial Flight Altitudes and in Space. *Radiation Protection Dosimetry* (2002) 102(1) p. 7–22.
14. Ferrari, A, Sala, P R, Guaraldi, R and Padoani, F. An improved multiple scattering model for charged particle transport. *Nucl. Inst. Meth*. [online] (1992) B71 p. 412–416.
15. Battistoni, G., Cerutti, F., Fasso, A., Ferrari, A., Muraro, S., Ranft, J., Roesler, S. and Sala, P.R. The FLUKA code: Description and benchmarking. *AIP Conference Proceedings (*2007) 896(1) p. 31–49.
16. Fano, U., Mcvoy, K. W. and Albers, James R. Sauter theory of the photoelectric effect. *Physical Review* (1959) 116(5)p. 1147–1156..
17. Poludniowski, Gavin G., and Philip M. Evans. Calculation of x-ray spectra emerging from an x-ray tube. Part I. Electron penetration characteristics in x-ray targets. *Medical physics* 34.6Part1 (2007): 2164-2174.
18. Poludniowski, Gavin G. Calculation of x-ray spectra emerging from an x-ray tube. Part II. X-ray production and filtration in x-ray targets. *Medical physics* 34.6Part1 (2007): 2175-2186.
19. Poludniowski, G., et al. SpekCalc: a program to calculate photon spectra from tungsten anode x-ray tubes. *Physics in Medicine & Biology* 54.19 (2009): N433.
20. Brualla, Lorenzo, et al. PENELOPE/PRIMO-calculated photon and electron spectra from clinical accelerators. *Radiation Oncology* 14.1 (2019): 6.

*MEDICAL PHYSICS IN THE BALTIC STATES 14 (2019)*

Proceedings of International Conference "Medical Physics 2019"
7 – 9 November 2019, Kaunas, Lithuania

# ZERO POINT ASSESSMENT OF THE RADIATION ENVIRONMENT – EXAMPLES OF A PROGRAM APPLIED IN SWEDEN (ESS) AND IN BELARUS (BELNPP)

Christian BERNHARDSSON[1], Kristina ERIKSSON STENSTRÖM[2], Sören MATTSSON[1], Mattias JÖNSSON[1], Guillaume PEDEHONTAA-HIAA[1,2], Christopher RÄÄF[1], Charlotta NILSSON[2], Vytenis BARKAUSKAS[2], Aliaksandr DVORNIK[3], Siarhei HAPONENKA[3], Vladislav NEKRASOV[4], Aleksandr VODOVATOV[4], Valery RAMZAEV[4]
[1]Medical Radiation Physics Malmö, Department of Translational Medicine, Lund University, Sweden; [2]Department of Physics, Division of Nuclear Physics, Lund University, Sweden; [3]Institute of Radiobiology National Academy of Sciences of Belarus, Belarus; [4]St Petersburg Research Institute of Radiation Hygiene named after Professor P.V. Ramzaev, Russia.
christian.bernhardsson@med.lu.se; kristina.stenstrom@nuclear.lu.se; aadvornik@yandex.ru; vodovatoff@gmail.com

***Abstract*:** Before commissioning of a nuclear facility it is important to determine the baseline of the radiation environment. Such baseline or Zero Point assessments can only, and uniquely, be made before start of operation of the facility and will serve several purposes when the facility is in operation. Here we report on the planning and implementation of such a Zero Point program for achieving high reproducibility and effectiveness of the assessments around two nuclear installations.

***Keywords*:** European spallation source, ESS, BelNPP, Astravets, activity concentration, dose rate, gamma emitters, $^{3}H$, $^{14}C$.

## 1. Introduction

When introducing activities involving an increased or decreased level of exposure to ionizing radiation, or risk of potential exposure, there are several factors and consequences to consider. The International Commission on Radiological Protection has defined three fundamental principles for radiation protection [1] in such a situation, namely justification, optimization, and the application of dose limits. In this report, we present a program for creating a basis to assure that the dose limits to the population are secured and accessible after commissioning a spallation source in Sweden and a nuclear power plant in Belarus. Although these two facilities have different purposes (research *vs* production of electricity), and will operate at completely different powers with different radionuclide inventories, they both have in common that radionuclides may be discharged into the environment during normal operation as well as at accidents. The program suggested here is intended to be an effective approach for determining the radiation environment prior to operation of the facilities. This is important for later comparisons and determinations of dose contributions to the public from future discharges when the facilities are in operation.

Within a few years, the European Spallation Source (ESS) will start to operate in the northeastern part of Lund, Sweden. When in operation, it will form a multidisciplinary research facility with one of the world´s most powerful (5 MW) spallation sources. Large amounts of radionuclides, the majority being short-lived, are going to be produced at ESS. Varying amounts of these radionuclides can potentially be released into the environment during normal operation [2]. For regulating the potential exposure to residents in the area, the Swedish Radiation Safety Authority (SSM) requires that these discharges should not exceed a corresponding annual effective dose of 0.1 mSv. In order to establish a baseline of the radiation environment around ESS prior to its operation, for later reference and dose estimates to the public, Lund University (on behalf of ESS) conducted a thorough survey of the area in 2017-2018 [3].

About 800 km directly to the east of ESS, the first nuclear power plant in Belarus (BelNPP) is being constructed outside Astravets in the Grodno region. The two water-water power reactors (VVER-1200) are estimated to start operation in the end of 2019 and in mid-2020, respectively, with a combined electrical power of about 2400 MW. Hence, the baseline of the radiation environment has to be determined prior to the operation of BelNPP. Such programs have already been carried out in the Astravets region (*e.g.* by Belhydromet, Minsk, Belarus). Our intention is to provide an

additional and complementary, independent assessment of the radiation environment baseline, using the same methodological approach as during the Zero Point assessment program around ESS. Unique with the suggested program is that the same small group, with representatives from Sweden, Belarus and Russia, perform all measurements and samplings. Furthermore, all samples are to be analyzed at Lund University for gamma emitting radionuclides as well as for $^{3}$H and $^{14}$C. In combination with the surveys, samples are also collected for intercomparison purposes between the involved laboratories and other interested institutions and laboratories.

## 2. Defining the Zero Point assessment program

The aim with the suggested Zero Point assessment program is to establish a baseline of the current levels of ionizing radiation and concentrations of various radionuclides, natural as well as artificial, prior to start of operation of ESS and BelNPP. Zero Point assessments are important for several future purposes, *e.g.* to provide:

- an independent baseline of the radiation environment and its variability,
- background data for identifying diffuse long-term discharges,
- data for reporting to authorities and the public,
- basis for measures/improvements as well as continued research and development.

Certainly, the Zero Point assessments must be carried out prior to the start of operation of the facility. The current radiation environment and its variability is location specific and is composed of historical as well as present sources such as fallout from Chernobyl and from nuclear weapons´ tests in the atmosphere during the 1950s and 1960s, discharges from hospitals and research, natural occurring radionuclides and cosmic radiation. The radiation baseline and its variability, including potential sources, must be established prior to start of operation of the facility in order to facilitate accurate future dose estimations, from contributions from the operation of the facility. For example, in the research intense northern part of Lund, close to ESS, elevated levels of $^{14}$C have been observed previously [4,5]. Varying contributions from gamma emitters are also expected from the generally low (*e.g.* [6, 7]) Chernobyl contamination (in both the Lund and Astravets areas) as well as discharges from hospitals and patients after nuclear medicine examinations and therapies. Although these sources compose a low contribution to the total exposure of the public, they must be carefully determined during the Zero Point assessment.

Special attention should be paid to the previously operated and now closed Ignalina NPP impact on the environmental contamination in the region [8].

The present Zero Point assessment program is based on the selection of reference locations to determine the present radiation environment. The program also includes sampling of important foodstuffs that are produced and consumed locally, as well as samples from various types of water bodies.

### 2.1. Defining and selecting the reference locations

The main part of the suggested Zero Point program is the measurements and samplings at the reference locations. These reference locations should be flat and open surfaces of at least 40×40 m$^2$, with a minimum of nearby houses, trees, stones *etc*. Furthermore, these reference locations are selected based on a few certain criteria: they should cover all directions around the facility; be representative and reflect the current population density in the area; be preserved over time and available for follow-up measurements in the future. The latter criterion is difficult to foresee and determine, as the areas around ESS, BelNPP and similar facilities are in continuous expansion and development, and the facilities are to be operated for several decades. Therefore, a large number of locations are selected to achieve some redundancy in case part of the locations are not available in the future. Fig. 1 shows the theoretical strategy for selecting reference locations around ESS (a similar pre-expedition approach has been applied for the selection of reference locations around BelNPP).

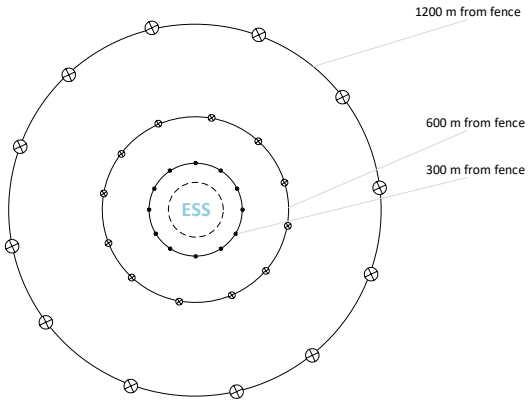


**Fig. 1.** At three different distances from the facility, 36 reference locations, evenly distributed, are selected for the Zero Point assessments today and for future measurements**.**

At each of the reference locations, several assessments are carried out to define today's radiation environment for future comparison. The assessments include:

- *In situ* gamma spectrometry (HPGe/NaI(Tl))
- Mobile gamma spectrometry (NaI(Tl))
- Measurement of the ambient dose equivalent rate (1 m above ground, plastic scintillator)
- Activity distribution in soil (down to 20-25 cm)
- Activity concentration in grass (1 m$^2$ surface)
- Long-term measurements with one dosemeter positioned 1 m above the ground (NaCl dosemeters read by optically stimulated luminescence, OSL) [9]

In Fig. 2 below is an illustration of the assessments carried out at each reference location.

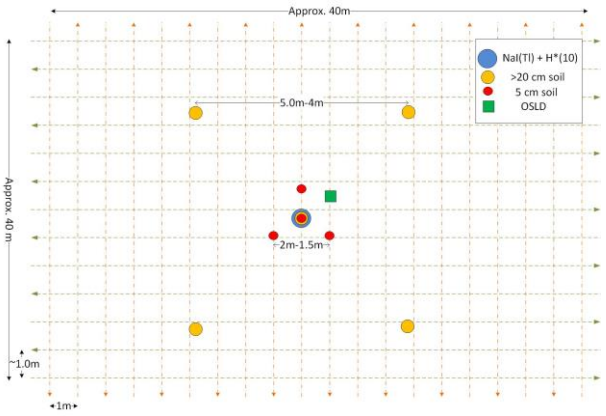


**Fig. 2.** Sampling approach at each reference location. In the center of each surface, *in situ* gamma spectrometry is carried out, as well as positioning of an OSL dosemeter, together with sampling of deep soil cores at five positions. Gamma spectrometry is also carried out with a backpack carried NaI(Tl) detector along the walking lines indicated by the grid in the figure.

### 2.2. Other measurements and samplings

Apart from the defined measurements and samplings at the reference locations, other assessments are carried out in the area between the reference locations in order to determine potential exposures and pathways to the people living in the area. These include determination of activity concentrations of gamma emitters in bioindicators, crops, forage, milk and sewage sludge. Included are also activity determinations of $^{3}$H in ground- and surface water, sewage sludge, bioindicators, crops and milk. $^{14}$C is measured in tree rings, grass, bioindicators, milk and in fullerene soot monitors. When possible, these assessments and samplings are carried out in connection to the reference locations.

Due to limited time, the sampling and measurements in the Astravets area had to be reduced in comparison to that in the Lund area. However, the amount of reference locations and samples of water is estimated to be the same as for the program applied around ESS.

## 3. Results

### 3.1. Zero Point assessment around ESS

Fig. 3 shows a map with the actual reference locations and other sites where samples were collected for the Zero Point assessment around ESS.

No unexpected gamma emitters were observed in the various samples collected. Small concentrations of $^{131}$I were observed in some samples of sewage sludge, as expected from clinical practices at the hospital in Lund. The activity concentrations of $^{3}$H were below the minimum detectable activity (29 Bq/l and 14 Bq/l). For the sampling sites included, there were no signs of local anthropogenic contamination of $^{14}$C.

A full description of each of the sites, the assessments carried out and the results may be found in the Zero Point report for ESS [3]. Apart from that report there is also a popular scientific folder, distributed to various stakeholders (mainly neighbors to ESS), that is also freely available [5].

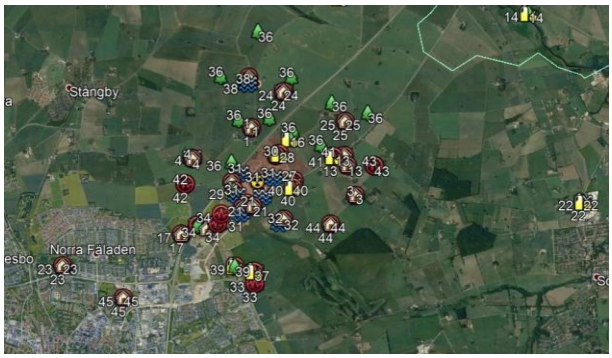


**Fig. 3.** Reference locations and sampling sites around ESS. Red points indicate reference locations, blue points where water was sampled, green points where crops were sampled, yellow points where bioindicators were sampled (see [3] for a full list of the sites and samples collected).

### 3.2. Zero Point assessment around BelNPP

A first expedition to the Astravets area was carried out 16-20 of September, 2019. During that expedition the group fulfilled the assessment measurements, as described above, at 29 selected reference locations around BelNPP (see Fig. 4). Water was collected in two rivers as well as in several wells in private gardens (for analysis of $^{3}$H). Tree rings were collected in a limited number of trees (for analysis of $^{14}$C). More than 200 soil samples were collected, that are soon going to be analyzed for activity concentration of gamma emitting radionuclides.

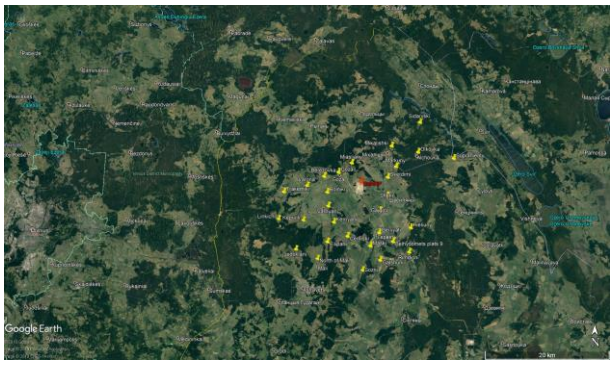


**Fig. 4.** Reference locations around BelNPP (as of the first expedition). BelNPP and the reference locations are marked on the map with red and yellow thumbtacks, respectively. The border to Lithuania is indicated by a yellow line.

A second expedition to the same area is planned in the period 15-17 of October 2019. The focus during that expedition is to include more reference locations and to sample various types of locally produced foodstuffs that are of importance to the inhabitants in the area.

A third expedition is planned to take place in the beginning of November, 2019. That expedition will cover sites in Lithuania, in an area along the border to Belarus. The aim of that expedition is to perform the Zero Point program at additionally 10-20 reference locations in Lithuania, as well as sampling of waters and foodstuffs in that area.

After the three expeditions and when all analyses have been completed, the results will be made publically available in a report. Similar to the Zero Point program

around ESS, a popular scientific summary will be made available in relevant languages as well.

## 4. Conclusions

The Zero Point assessment program has been successfully implemented around ESS and is currently being implemented around BelNPP. Indeed, this is a limited program but it still provides a careful overview of the radiation environment for some of the main important exposure sources for future operation of the facilities. However, one factor that also should be included and considered is the seasonal variations of the radiation environment. The intention is to perform a more thorough study of these changes around ESS by long-term studies of *e.g.* radionuclide concentrations in sewage sludge, water and air, as well as in other matrices of special interest (*e.g. Fucus* and other bioindicators).

## 5. Acknowledgement

The discussions with Belhydromet, Minsk, Belarus, and the Ministry of Health, Belarus, during the planning and implementation of the project around BelNPP is highly appreciated.
The Zero Point assessment around ESS was carried out as a one-year project, financially supported by ESS (contract ESS-0093103). The independent Zero Point assessments carried out around BelNPP are financially supported by SSM (project SSM2019-6032).

## 6. References

1. International Commission on Radiological Protection. Recommendations of the ICRP. Oxford: Elsevier; ICRP Publication 103; 2007.
2. Ene D., Avila R., Hjerpe T., Bugay D., Stenberg K. Assessment of environmental consequences of the normal operations of the ESS facility. 2018. IOP Publishing: Conf. Series 1046 (2018) 012018.
3. Bernhardsson C., Eriksson Stenström K., Jönsson M., Mattsson S., et al. Assessment of „Zero Point" radiation around the ESS facility. Internal report Ma RADFYS 2018:01 and BAR-2018/04, Lund University. 2018. Available (2019-09-29) at: https://portal.research.lu.se/portal/files/57600811/ESS_Zero_Point_public_190204.pdf
4. Skog G. Undersökning av förhöjda nivåer av $^{14}C$ i Lund 2009-2010. Report to SSM. Radiocarbon Dating Laboratory, Lund University, Lund, 2010.
5. Lunds universitet informerar om bakgrundsmätningar av strålningsnivån kring ESS [Folder], in Swedish, 2018. Availble (2019-09-29) at: http://www.nuclear.lu.se/fileadmin/nuclear/14C_AMS/2-viksfolder_web.pdf.
6. Isaksson M., Erlandsson B., Linderson ML. Calculations of the deposition of $^{137}Cs$ from nuclear bomb tests and from Chernobyl accident over the province of Skåne in the southern part of Sweden based on precipitation. Journal of Environmental Radioactivity 2000;49:97-112.
7. Atlas (2009). $^{137}Cs$ contamination maps of Belarus and Russia. In Russian: Atlas of modern and forward-looking aspects of the consequences of the Chernobyl disaster in the affected areas of Belarus and Russia. Issued by the joint program of activities to mitigate the Chernobyl catastrophe within the Union State for 2006-2010 from the budget of the Union State of Belarus and Russia.
8. Magnusson, A., Stenstrom, K., Adliene, D et al. (2007). Carbon-14 levels in the vicinity of the Lithuanian nuclear power plant Ignalina. 2006. Nucl. Instr.Meth. in Phys.Res. B. 259 (1) 530-535.
9. Waldner L. and Bernhardsson C. Physical and dosimetric properties of NaCl pellest made in.house for the use in prospective optically stimulated luminescece dosimetry applications. Radiation Measurements 2018;119:52-57.

*MEDICAL PHYSICS IN THE BALTIC STATES 14 (2019)*

Proceedings of International Conference "Medical Physics 2019"
7 – 9 November 2019, Kaunas, Lithuania

# MEASUREMENT OF RADON EXHALATION RATE USING LOCAL TECHNIQUE

Hussien EL-SAMMAN[1], Wafaa ARAFA[2], Ashry ASHRY[3], Lamiaa ABDELRAZIK[4]
[1]Minufiya University, [2]Ain Shams University, [3]Ain Shams University, [4]Minufiya University (Egypt)
hsamman@aucegypt.edu, wafaa.arafa@gmail.com, Lamiaa4reality@gmail.com

***Abstract:*** Radon concentration, exhalation, emanation rate for some Egyptian soil samples, different building materials and fertilizers has been measured by using a local radon chamber that was designed, constructed and tested in the laboratory. Two measurement methods (active and passive) were applied. It was found that the average of exhalation rate was lower than that defined by ICRP. The influence of humidity, temperature, grain size and surface area of samples on the radon parameters has also been discussed.

***Keywords:*** Radon Chamber, CR-39 D, AB-5, Leakage, Back Diffusion, Exhalation Rate, Emanation Rate.

## 1. Introduction

Soil and buildings materials contain various amounts of natural radionuclides of the uranium ($^{238}$U) and thorium ($^{232}$Th) series, and the radioactive isotopes of potassium ($^{40}$K). These radionuclides are sources of the external and internal radiation exposure in dwellings. Radon gas is produced by the disintegration of $^{226}$Ra, which is a decay product of $^{238}$U. After $^{222}$Rn is generated in the solid grains, it emanates through pores in gaseous or liquid form and then migrates a significant distance from the site of generation in rocks, soil or building materials into the atmosphere before being inhaled / exhaled by population. The exhalation rate provides a measure of the liberation of radon from inside a sample to outside the sample. Its value depends on emanation and on the concentration gradient between pore and ambient air. Since the soil and building materials are considered as mainly contributors for indoor radon concentration there is a need to estimate radon exhalation rate. Different techniques and methods can be used for this purpose: passive methods which employ nuclear track detectors, to measure radon exhalation rate, or active methods which employ active detectors such as scintillation cell monitor and pulse ionization chambers [1].
This paper discusses radon exhalation process and the main factors influencing this process, analyses different measurement techniques and provides measurement results.

## 2. Experimental Setup

### 2.1. Measuring System (Accumulation Chamber)

A new technique was established to measure radon emanation and radon exhalation rate from some of Egyptian soils and building materials. The constructed system consists of two chambers (the sample chamber and measuring chamber) with different volumes (Fig.1). The chambers are made of transparent polymethylmethacrylate, PMMA, with wall thickness of 5mm. The sample chamber is cubic of (40*40*40) cm$^3$ with a tight lid having a hole of ø5cm. A thick rubber glove is glued by its end around the inner circumference of the hole in such a way which permits the operator to handle and control samples inside the chamber when it is closed. The measuring chamber is cubic of (20*20*20) cm$^3$ with circular port of ø 5cm on the back side for the CPRD detector. The measuring chamber is equipped with tight lid having 30 holes with length (1.5cm) to insert and take out CR-39 detectors during the experiment. Each chamber part is glued using chloroform. The two chambers are connected by a vinyl tube (with 6cm diameter and 30cm length). The vinyl tube has a valve to allow the radon flow from sample chamber to measuring chamber. The whole system is sealed with silicon material to prevent leakage of radon gas. In order to change the environmental conditions inside the sample chamber, a thermo - hygrometer device ( TFA / Germany) with two separated digital LCD is used to measure temperature (from -10 °C to +60 °C) and relative humidity (from 10 % to 99 %). In order to vary the temperature inside the sample chamber, a heater is placed inside of the chamber and connected to a temperature controller (measurement accuracy ±1 C°).
In order to decrease the humidity $CaCl_2$ crystals were placed inside the chamber during the experiment to dry the air. The increase of humidity is achieved by locating of a small flask with water inside the chamber.

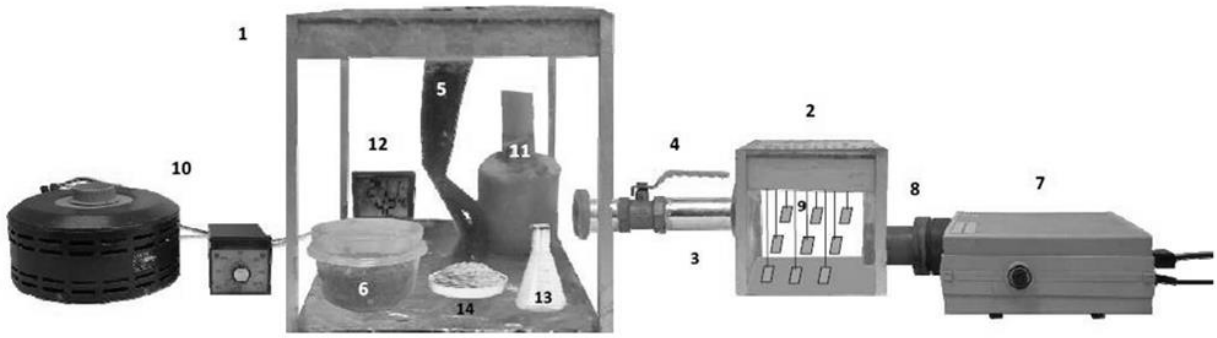


1. Sample Chamber
2. Measuring Chamber
3. Connection Tube between the two Chambers
4. Valve
5. Hole with rubber Gloves
6. Building Material Sample
7. AB-5 Monitor
8. CPRD Detector
9. CR-39 Detector
10. Temperature Controller
11. Heater
12. Thermo-Hygrometer
13. Flask with water
14. $CaCl_2$ Crystal

**Fig.1.** Constructed Measurement System

### 2.2. AB-5 monitor

The pylon model AB-5 portable radiation monitor is the most popular and versatile instrument for fast accurate measurement of environmental radiation levels. The AB-5 monitor is characterized by the automatic calculation of radon gas concentration in pci/l or $Bq/m^3$ and a memory function which automatically accounts each run, cycle and interval. Device can hold data of 675 intervals (which correspond to hourly counts during 25 days. Collected data and parameters can be recalled for displaying or for printing using Pylon PPT-1 printer).

### 2.3. SSNTD CR-39 detector

SSNTD CR-39 detector is Polyallyl diglycol carbonate film detector, is manufactured from diethylene glycol $C_{12}H_{18}O_7$ monomer The CR-39 sheets were cut to 0.5*0.5*0.01 cm pieces and hanged on the wires inside of measuring chamber for the assessment of radon exposure. If Alpha particles are released from soil or building materials samples due to radioactive decay, they will strike these films; causing damages in the films related to the leaving broken molecular chains. Latent tracks formed by alpha particles in CR-39 films are visualized using chemical etching (NaOH solution, 6 hours, 70C°). Applied etching allows for track visualization using conventional optical microscope, and separate tracks can be counted. Using optical microscope (40 x magnification) a number of tracks can be distinguished per image. Thirty fields were counted in each CR-39 film in our experiments.
The radon concentration in CR-39 films was estimated after background subtraction using equation (1):

$$Rn\ Conc. = T/K.t, \quad (1)$$

where T is the average number of tracks ($tracks/cm^2$), K is the calibration factor ($tracks.cm^{-2}\ d^{-1}$ // $Bq.m^{-3}$), t is the exposure period (day).

### 2.4. Collection of samples and their preparation for measurement

The soil samples were collected from two different areas of the Eastern Desert of Safaga area of Egypt (Gabal El-Misikat Gabal El-Majal). The samples were kept in suitable standard containers for more than one month. The building materials as white cement, black cement, sand, ceramic, marble and granite are the most common used materials in Egypt. These materials were collected from different areas. Collected samples were cleaned by removing the undesirable stones and dried in slow air flow for several days. The samples were weighed and sealed in suitable standard containers. Due to the fact that the raw materials which are used for production of some fertilizers contains various amounts of natural radioactive elements, two types of different fertilizers have been collected and sealed in suitable standard containers. Each container was carefully stored for three weeks to achieve the secular equilibrium between ($^{226}Ra$) and its daughter ($^{222}Rn$).

## 3. Measurements

### 3.1. Calculation of radon concentration and radon exhalation rate

The amount of radon formed in rocks and soils depends on their uranium content. However, this alone is not decisive in determining the radon concentration in air, it is also determined by the extent to which the radon atoms formed actually emanates from the mineral grains and whether radon can leave the pore space either by diffusion or together with a flow of air or water. In addition, radon concentration in the soil air is significantly affected by the occurrence of moisture/ water in the pores. Besides soil, construction materials may also significantly contribute toward the indoor radon. Permeability of the soil is a main factor affecting radon levels in dwellings. As the measurement of soil permeability is difficult, the exhalation rate, which is the number of radon atoms leaving the soil per unit surface

area per unit time from the ground, is thought to be a better indicator of radon risk. Also the exhalation rate provides a measure of the liberation of radon from inside a sample to outside the sample. Its value depends on emanation and on the concentration gradient between pore and ambient air [2]. The concentration of radon emanated from samples was allowed to build up with time. The buildup of radon concentration $C_{(t)}$ follows the following equation [3]:

$$C_{(t)} = C\,(1 - e^{(-\lambda t)}), \quad (2)$$

where C is the equilibrium radon concentration (Bq/m$^3$), λ is the radon decay constant =0.007553(h $^{-1}$).
The radon free exhalation rate can be calculated from the equation (3) [4]:

$$E_x = C\lambda V/ (1\text{-}e^{-\lambda t}), \quad (3)$$

where: V is volume of accumulation chamber (m$^3$) and t is the exposure time (h).
This equation is valid if there is no air exchange due to chamber leakage of radon out of the accumulation chamber [4] and if the concentration in the chamber is low compared to the concentration in the pore air of sample (i.e. no back-diffusion effects). Since the soil pore space have higher radon concentration than the open air atmosphere, radon atom will diffuse from the pore space into the open air. Radon gas atoms can escape to the atmosphere by diffusion process. The diffusion phenomenon occurs when there is a different gas concentration between two media. In a consequence, a flux from high concentration will move to low concentration. The values of leakage rate ($\lambda_{leak}$) and back diffusion ($\lambda_{back}$) can be determined using the equation proposed by Chao et al. [5], for the leakage rate (q, m$^3$h$^{-1}$) and the back-diffusion rate (D, h$^{-1}$), where $\lambda_{leak}$ =q/V and $\lambda_{back}$ = D.
The value of $\lambda_{leak}$, which presumably is not affected by radon loss due to permeation through the chamber, is determined by measuring for a period of 24h the decay of $^{222}$Rn gas which is still contained in the accumulation chamber when the sample is removed.

$$\lambda_{leak} = (M_f - M_l)/(C_b - Co), \quad (4)$$

where $M_f$ is the initial slope of natural decay curves (Bq/m$^3$h), $M_l$ is the slope of experimental decay curves (Bq/m$^3$h), $C_b$ is the initial radon concentration in the chamber during the leakage experimental (Bq/m$^3$), $C_o$ is the background radon concentration in the laboratory (Bq/m$^3$).
In a closed chamber that contains a sample, $^{222}$Rn concentration increases with the passage of time from zero to its maximum value. After reaching its maximum value, back diffusion of radon also takes place, which reduces the $^{222}$Rn concentration by a factor in the chamber. The value of time constant due to back diffusion ($\lambda_{back}$) can be calculated from the following equation [5]:

$$\lambda_{back} = (M_e/C) - (\lambda + \lambda_{leak}), \quad (5)$$

where $M_e$ is the initial slope of the radon growth curve in the accumulation chamber (Bq/m$^3$h).
If leakage and back-diffusion phenomena occur, the growth of radon concentration in the chamber follows an exponential trend, where the effective time constant ($\lambda_{eff}$, h$^{-1}$) is not the decay constant only, but is equal to:

$$\lambda_{eff} = \lambda + \lambda_{back} + \lambda_{leak}. \quad (6)$$

### 3.2. Calculation of emanation rate

The principal phenomenon that allows radon atoms to leave the grains of material is the recoil of a nucleus owing to alpha-particle emission in the generation process of radon from radium. The emanation rate can be calculated from the following equation [5, 6]:

$$E_o = [M_e - (q/v)\, C_o](\, v/A). \quad (7)$$

The radon emanation $E_o$ represent the radon emanation rate when C= $C_o$. The radon emanation is not constant as the amount of radon in the air will get back to the grain material. The radon emanation is found from the chamber radon concentration (C), so the emanation rate split into two terms ($E_o$) and (α C). The radon emanation rate ($E_m$) follows a linear relationship with the radon concentration inside the chamber and can be expressed by the following equation [5:

$$E_m = E_o - \alpha\, C, \quad (8)$$

where α is the specific radon back diffusion (α =DV/A, m/h)

### 3.3. Calculation of emanation coefficient

For mineral grains with a typical density, a radon atom can leave the grain if its distance from an exterior surface is less than 0.07 mm. The number of atoms which emerge from the soil grains is always less than the number of atoms generated. The emanation coefficient, F, is defined as the ratio of the number of radon atoms leaving the grains to the number generated in the sample [9]. We obtain the emanation coefficient from the ratio between the radon atoms accumulated in the chamber volume and the atoms generated in the soil sample. The radon in the chamber is measured when there is equilibrium between exhaled and decayed radon. The emanation coefficient is calculated from the ratio between the growth value and the radon specific activity in the soil sample [7 using the following relation [8]:

$$F = C_{Ra}^{\,eff} / C_{Ra}^{\,real} \quad (9)$$

where $C_{Ra}^{eff}$=(CV)/W, $C_{Ra}^{real}$=(CVλ)/A is the effective and real radium content respectively (Bq/kg), A is the sample surface area (m$^2$), C is the equilibrium radon concentration (Bq/m$^3$), V is the radon chamber volume (m$^3$), W is the sample mass (kg).

## 4. Results & Discussion

### 4.1. Determination of radon half-life time inside the chamber

The experimental half-life time of radon was measured by using a high activity sand sample and found to be 3.81 days, which is in perfect agreement of the known half-life time of radon.

### 4.2. Calibration of CR-39 detector for radon measurements

The calibration factor of CR-39 detector was measured and found to be 0.177 track.cm$^{-2}$.d$^{-1}$ per Bq.m$^{-3}$. This result is in good agreement with the previous studies [1,8-10] where the calibration factor is given as (0.18, 0.177, 0.17, 0.18) track.cm$^{-2}$.d$^{-1}$ per Bq.m$^{-3}$ respectively.

### 4.3. Test of the chamber

The chamber was tested for best performance and quality. It has been done by feeding the exposure chamber by radon from $^{226}$Ra source. Three radium sources of activity 5 µCi each were used. The radium sources produce a constant flow of radon. AB-5 monitor and CR-39 detectors were exposed to radon source in the same time for more than two weeks to achieve the equilibrium. After passing the first week, one of CR-39 detectors was removed every day and sealed in a plastic bag to keep it against the laboratory background radiation till chemical etching treatment occurred. The plotted Fig.2 shows the three stages build up, stability and decay process of radon.

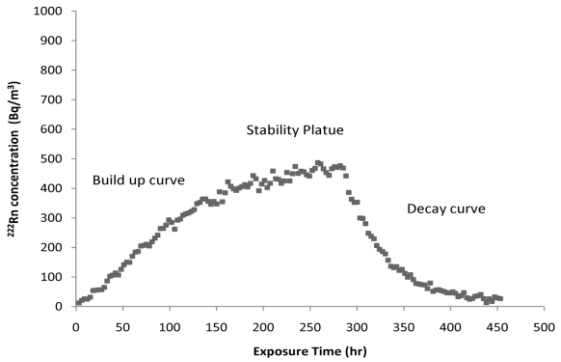


**Fig.2.** Radon behavior observed in testing chamber. $^{226}$Ra source was used to generate the radon..

Measurements performed within 15 days of high activity natural sand samples using AB-5 monitor and CR-39 detectors were in good agreement. Figure 3 shows a good correlation between the performance of the two detectors with correlation coefficient of 0.98, which means that the passive method (the cheapest and easiest method) provides reliable data.

### 4.4. Radon concentration as a function of accumulation time

Soil Sample from Gabel El Misikat has been enclosed in the sample chamber and left until the radon equilibrium was achieved. The radon equilibrium has been achieved in less than 20 days (about five times the half-life of $^{222}$Rn) due to the phenomena, other than decay, which are responsible for the decrease of radon concentration in the chamber air. These phenomena were reported and discussed before: this could be due to diffusion and back-scattering occurring in the chamber [4, 5]. In this study, leakage and back-diffusion effects were investigated as possible cause of an early equilibrium. , so the time constant due to leakage ($\lambda_{leak}$) and back diffusion ($\lambda_{diff}$) have been evaluated to achieve the correction for the radon concentration.

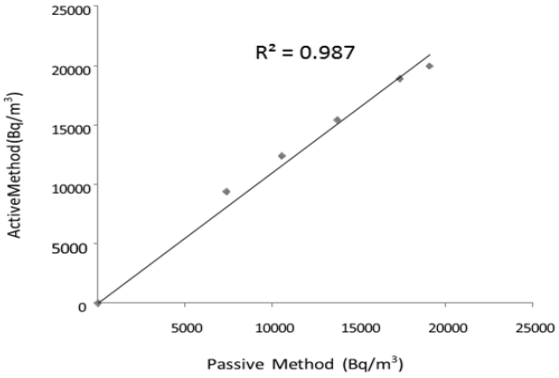


**Fig.3.** The variation of the radon concentration as it measured by active and passive detector.

### 4.5. Calculation of time constant $\lambda_{leak}$ , $\lambda_{diff}$ and $\lambda_{eff}$

As the chamber may be not completely airtight when it is closed, it is very important to take in consideration air exchange due to chamber leakage that effect on radon concentration and on other parameters. For this reason high activity sample was kept in the radon sample chamber to achieve equilibrium then the output valve of the chamber was closed to permit radioactive decay occurring. The buildup and radioactive decay process was plotted. The value of leakage rate can be calculated from slope of decay curve using equation (4). This process was repeated using another source to ensure the accuracy in the obtained value of leakage rate. The average value of $\lambda_{leak}$ was found to be (1.198*10$^{-2}$) h$^{-1}$. The value of $\lambda_{diff}$ was calculated for different types of samples. The sample was kept inside the chamber for more than one week according to the type of the sample. It is known that the Radon concentration in the chamber increases by time till it reaches its maximum value. Therefore back diffusion takes place after reaching its maximum value, which reduces the concentration of radon by a factor, $\lambda_{diff}$, in the chamber. From the slope of buildup curves of each sample and by using equation (5), the value of $\lambda_{diff}$ can be calculated. It ranged from (8.44 *10$^{-3}$ – 0.04 *10$^{-2}$) h$^{-1}$ for soil samples and different types of building materials samples respectively. It is clear that the variation in the back diffusion values was due to the different origin area where these samples were collected. Each area has its specific characteristics (grain size, porosity, radium contents) which effects on the radon concentration and consequently on the back diffusion process. The leakage and back-diffusion phenomena occur during experimental work where we cannot neglect their effects. In most samples the effect of leakage and back-diffusion will be appeared for sampling time larger than

30 hours. By obtaining the values of leakage $\lambda_{leak}$ and back diffusion $\lambda_{diff}$, the value of effect time constant $\lambda_{eff}$ can be calculated simply from equation (6). It ranged from ($1.15*10^{-1}$ - $9.9*10^{-2}$) $h^{-1}$. The buildup curves can be corrected by using these parameters ($\lambda_{eff}$, $\lambda_{leak}$ and $\lambda_{diff}$). Figure 4 shows the three types of growth curves for Gable El-Misikat sample No.1. Curve 1 shows slower growth and lower equilibrium value of the radon concentration with chamber leakage phenomena and back diffusion. Curve 2 shows the radon concentration without leakage effect (the value of back diffusion was neglected) while curve 3 shows the radon concentration without leakage and back diffusion.

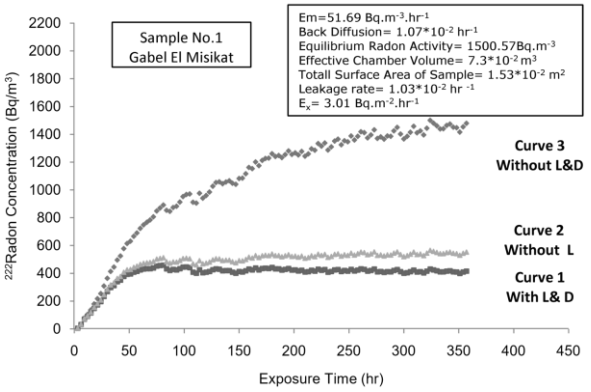


**Fig.4.** Correction of radon concentration by leakage and back diffusion factor for Gable El-Misikat (sample No.1).

### 4.6 Calculation of radon concentration, radon free exhalation rate and radon emanation rate

It was found that the radon concentration varied from (36.91 – 1754.77) $Bq/m^3$ for soil samples; (9.2 – 72.68) $Bq/m^3$ for building materials and (69.94 - 192.45) for fertilizer materials samples. The radon exhalation rates varied from (0.09 - 3.68) $Bq/m^2.h$ for soil sample; (0.02 -0.29) $Bq/m^2.h$ for building material samples and (0.1377 - 0.40) $Bq/m^2.h$ for fertilizer. The radon emanation rate ranged from (BDL value to 58.05) $Bq/m^2.hr$ for soil sample and from (BDL value to 10.06) $Bq/m^2.hr$ for building material sample. However the radon concentrations in all building material samples was below the world average and hence do not posed any health hazard. Also, the radon concentration in the fertilizers samples is below the allowed limit. The great variation of exhalation rates and emanation rate is expected to be due to the difference in radium amount in investigated samples. Good correlation between radon concentration and radon exhalation rate in soil samples was found. It was observed and plotted with a correlation coefficient of 0.996. This value is in agreement with the results provided by Shashikumar et al [11]. The laboratory measurements of real radium content and effective radium content and emanation coefficient were obtained from equation (9) for soil samples and building materials and fertilizer samples. It was found that the emanation coefficient depends on the radium concentration, porosity, temperature and water content, and also on the radium distribution in the internal structure of a material [12].

### 4.7 Factors affecting the radon concentration, exhalation rate and emanation rate (Humidity, Temperature, Surface Area and Grain size)

The factors that affect radon concentration, exhalation and emanation rates have been studied in relationship to temperature, humidity and grain size and surface area of samples (Table 1).

**Table 1.** Variations of $^{222}Rn$ concentration, exhalation and emanation rate with different parameters

| **Humidity %** | | **Conc. ($Bq/m^3$)** | **$E_x$ Rate ($Bq/m^2h$)** | **$E_m$ Rate ($Bq/m^2h$)** |
|---|---|---|---|---|
| 42 | | 1382.48 | 2.95 | 41.40 |
| 89 | | 1423.11 | 3.06 | 42.11 |
| 95 | | 1578.31 | 3.46 | 42.96 |
| **Temperature (˚C)** | | | | |
| **In** | **Out** | | | |
| 25 | 22-24 | 1478.13 | 3.63 | 55.11 |
| 40 | 25-27 | 1071.27 | 2.63 | 35.45 |
| 55 | 26-29 | 921.21 | 2.26 | 25.96 |
| **Surface Area ($m^2$)** | | | | |
| 0.0028 | | 1367.708 | 2.784 | 201.441 |
| 0.0153 | | 977.265 | 1.967 | 18.047 |
| 0.0415 | | 820.29 | 1.648 | 4.599 |
| **Grains Form** | | | | |
| Rock | | 32.00 | 29.04 | 8.14 |
| Stone | | 30.79 | 22.24 | 9.09 |
| Crushed | | 29.13 | 20.38 | 10.06 |

The effect of humidity may refer to the lower recoil distance of radionuclides in water-filled sample pores than in air-filled pores. This results in a higher probability of the recoil radon atoms to stay into water-filled pores and not being reabsorbed by the other grains, and in turn determines large exhalation rate from humid samples [11]. The emanation rate is expected to increase with increasing humidity because an increase in the amount of water in the pore spaces increases the probability of capturing radon atoms that could not be reabsorbed by other grains. The effect of grain size is present due to the fact that increase in pore space between grains provides more space for radon diffusion. The phenomenon of temperature effect may be due to the humidity decrease with increasing temperature. This also may be related to the fact that when the temperature inside the chamber is higher than the outdoor temperature the warm air with low radon concentration may flows out [13]. The effect of the surface area of sample can be explained by the equation of radon exhalation rate (equation 10) [14] and of radon emanation rate (equation 8) which shows a decrease of radon concentration, radon exhalation and radon emanation rate by the increase of the exposure surface area:

$$E_x = C\,\lambda\, V/[\,A(1-e^{-\lambda t})], \qquad (10)$$

where V is volume of accumulation chamber ($m^3$), A is the surface area of sample ($m^2$)

## 5. Conclusions

- A new radon chamber has been designed and constructed to control flow of radon, temperature and

humidity. The constructed radon chamber was tested and calibrated using radium sources.

- The radon half-life time inside the constructed chamber was measured. The calibration factor of CR-39 detector was established and compared to previously published values.
- Comparison between active and passive detectors was done to check the reliability of the proposed passive method.
- The radon free exhalation was measured for some soil samples that were collected from different plutons in the central part of the Eastern Desert of Egypt. It was found that the radon exhalation rate in the Gabal El-Misikat higher than Gabal El-Majal.
- It was found that the average value of radon free exhalation rates for Egyptian building materials and Egyptian fertilizers was below the safe limit recommended by the (ICRP). It was suggested that this material may be used in building constructions as it doesn't pose any health hazards due to low radon exhalation rate.
- The experiments presented in this study have shown that the evaluation of chamber leakage and back diffusion lead to a correction of radon exhalation rates of about 42 - 57%.
- It is recommended to properly fix and strictly respect the experimental conditions since the values of exhalation rates are strongly dependent on factors such as humidity, air temperature, sample surface area and sample grain size.

## 6. References


1. Hafez A.F., Hussein A. S. and Rasheed N.M., 2001, A study of radon and release from Egyptian building materials using polymeric nuclear track detectors. Appl. Radiat.Isot., 54, 291.
2. Martino S. De, Sabbarese C., and Monetti G.; 1998, Radon emanation and exhalation rates from soils measured with an electrostatic collector, Appl. Radiat. Isot., 49, 407–413.
3. Mohammed Al-Jarallah, Radon Exhalation from Some Saudi Rocks, P-1b-18.
4. Tuccimei P., MoronicM., Norica D., 2005. Simultaneous determination of 222Rn and 220Rn exhalation rates from building materials used in central Italy with accumulation chambers and continuous solid state alpha detector: influence of particle size, humidity and precursors oncentration, Appl. Radiat. Isot. 64, 254-263.
5. Christopher Y.H. Chao, Thomas C.W. Tung, Daniel W.T. Chan, John Burnett, 1997. Determination of radon emanation and back diffusion characteristic of building materials in small chamber tests. Building and environment 32(4), 355-362.
6. Bondansky D. 1987, “Indoor Radon and Its Hazard” University of Washington Press, Seattle and London.
7. Abo-Elmagd M., Metwally S.M., El-Fikib S.A., Eissa H..M., Salama E., 2007, Passive and active measurements of radon-related parameters inside ancient Egyptian tombs in Luxor, Radi. Meas. 42, 116 – 120.
8. Arafa W., Badran H. and El-Samman H., 2009, Determination of The Equilibrium Factor and Dose Equivalent from Radon and Its Progeny Using Active and Passive Techniques, Faculty of Women, Ain Shams University.
9. Nabil Mohammed Hassan, Abdel Fattah Hafez, Emad Ibrahim Khalil, 2004, Study Of Radon Emanation Rate From Some Egyptian Raw Materials Using Polymeric Track Detectors And Electronic Device (Alpha-Guard).
10. Mansy M., EL-Fiki S.A. and Abo-EL-Magd M., J., 1998, BioPhysics 4 (1), 91.
11. Shashikumar T. S., Ragini N., Chandrashekara M. S. and Paramesh L., 2008, Studies on radon in soil, its concentration in the atmosphere and gamma exposure rate around Mysore city, India, CURRENT SCIENCE, VOL. 94, NO. 9.
12. Salvatore De Martino, Carlo Sabbarese, Giuliam Monetti, 1996. Radon Emanation and Exhalation rates from soils measured with an electrostatic collector, Appl. Radiat. Isot. 49, 4, 407-413.
13. IAEA, 1989. Measurement of radionuclides in food and environment.
14. Arafa. W., 2004, Specific activity and hazards of granite samples collected from the Eastern Desert of Egypt. Journal of Environmental Radioactivity 75 (2004) 315–327.

*MEDICAL PHYSICS IN THE BALTIC STATES 14 (2019)*

Proceedings of International Conference "Medical Physics 2019"
7 – 9 November 2019, Kaunas, Lithuania

# X-RAY SCATTERED RADIATION INDUCED ROS GENERATION AND CELL VIABILITY CHANGE RELATED TO ABSORBED DOSE.

Tadas DIDVALIS[1,2], Paulius RUZGYS[1], Saulius ŠATKAUSKAS[1], Saulius MICKEVIČIUS[1]
[1]Vytautas Magnus University, K. Donelaičio 58, LT-44248, Kaunas, Lithuania
[2]Hospital of Lithuanian University of Health Sciences Kauno klinikos, Eivenių 2, LT-50161, Kaunas, Lithuania
[1]tadas.didvalis@fc.vdu.lt

***Abstract*:** In this study we present experimentally evaluated relative ROS generation with and without side scattering effect in affected media and in cells and out-of-field dose effect to cell viability. We found that due to the side scattering of X-ray photons the applied energy to the in-field cells differs significantly from the energy delivered to out-of-field cells, thus indicating differences in ROS generation and cell viability. Performed cell viability test revealed positive cell growth effect in media affected by side scattering of ionizing radiation

***Keywords*:** ROS, side scattering, cell viability, radiotherapy.

## 1. Introduction

The fundamentals of ionizing radiation induced ROS generation in irradiated biological tissues are clearly understood. However cell reaction to ionizing radiation is still not fully understood and is a subject for further investigations since it plays crucial role in clinical radiation therapy. Significant interest for cell response to low dosage was raised after it was shown that radiation induced energy side scattering effects indeed affect the healthy cells surrounding malignant tissues [1]. This less investigated and poorly controlled phenomenon may induce a secondary cancer as a result of cancer treatment using radiotherapy [2]. The feasibility of such prediction relies on the results of the complex multi-field radiotherapy techniques (IMRT, VMAT and SRS) that enable assessment of low dose impact on malignant as well as healthy tissues during the treatment of patient [3]. The poorly predictable side scattering effects during radiation treatment make low dose effects on cells more complicated. Furthermore, malignant and healthy tissue reactions to low doses are different due to non-homogenic histology as a result of non-homogenic histology, uneven vascularization or cellular growth rate. But it is already known, that the signals sent by apoptotic cell can change the behavior of the unaffected cells [4] and may lead to the death of at least part of the affected cells via pathway of apoptosis. These arguments indicate the need for broad range *in vitro* studies concerning cell irradiation to low doses. However to our bet knowledge there are no standardized experimental procedures evaluating side scatter effects to cells *in vitro*.

In this study we present a protocol, that allow the evaluation of ionizing radiation induced side scattering effect to cells *in vitro* by using materials that are common in cell culture laboratories. This protocol can be adapted for measurement of ROS generation induced by radiation side scattering effects, or for the assessment of affected cell viability as well as for its metabolic activity changes. Moreover, with a minor modification of presented protocol one can study the effect of affected apoptotic cell signaling to the affected cells.
In this paper we discuss the results of ROS generation in irradiated cells in the presence of side scattering effects in affected media or without as well as well as the influence of the irradiated growth medium on un-irradiated cells.

## 2. Materials and methods

96 and 24 well plates were irradiated with and without water in between in order to assess ROS generation and cell viability after replacing growth medium for cell colony assay with irradiated growth medium.

### 2.1 Cell culture

Chinese hamster ovary cells (CHO-K1) were cultured at 37°C in water-saturated air containing 5% $CO_2$. The cells were routinely passaged in growth medium (DMEM, Sigma-Aldrich) supplemented with 10 % of FBS (Sigma-Aldrich), 1 % of G-glutamin (Sigma-Aldrich) and 1 % of penicillin/ streptomycin (Sigma-Aldrich). The unaffected cell doubling time was approximately 12 h. CHO cell line was a generous gift of dr. D. Bagnard (Strasbourg University).

### 2.2 Irradiation procedure

Water was chosen as a scattering material between individual wells since significant fraction of scattered photons can be produced due to irradiation of medium. For this study black flat bottom 96 well plate (Thermo Fisher) for ROS evaluation and transparent flat bottom 24 well plate (Thermo Fisher) for the evaluation of the cell colony assay were placed between two 4 cm thick PMMA plates, which were necessary considering build up effect. Prepared experimental constructions were irradiated in linear accelerator Varian Clinac DMX to 8 Gy, applying 6 MeV photon beam and using 4x4 $cm^2$ irradiation field. This field size was sufficient enough to cover 96 well plate (Fig. 1) and 24 well plate (Fig. 2) arranged in a specific patterns.

In order to reduce dose distribution distortions induced by air gaps above medium. Irradiation was performed from the bottom side of plates. Monitor unit calculation and dose distribution simulation were performed using AAA algorithm on Varian Eclipse treatment planning system. Computed tomography scans of phantom and plate set with scatter material and without scatter material were used for dose planning. Simulated values for in-field and out-of-field doses were used for the comparison with experimental results

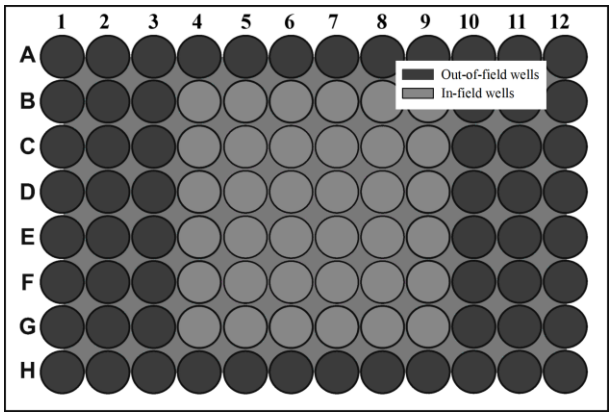


**Fig. 1**. 96 well plate with 36 centrally located and marked in-field wells. Water was used as a scattering media between wells.

### 2.3 Assessment of ROS in cells and growth medium

Our recent study [5] has shown that one of the parameters that correlates with a DNA damage and cell death and can be monitored is ROS generation during and after irradiation. Therefore DCFDA dye method for ROS evaluation has been used. Cells were incubated in 50 μM/ml of 2',7'-dichlorodihydrofluorescein diacetate (H2DCF-DA) for 60 min prior to the irradiation and then distributed 50 μl per each well. After irradiation the 50 μl of 96 % ethanol was added to cell suspension in order to equally disperse DCF dye. After 30 min of incubation the DCF induced fluorescence was measured by using spectrophotometer (TECAN Genios Pro 96/384).

Performing scattering experiments 100 μl of water was added between each well.

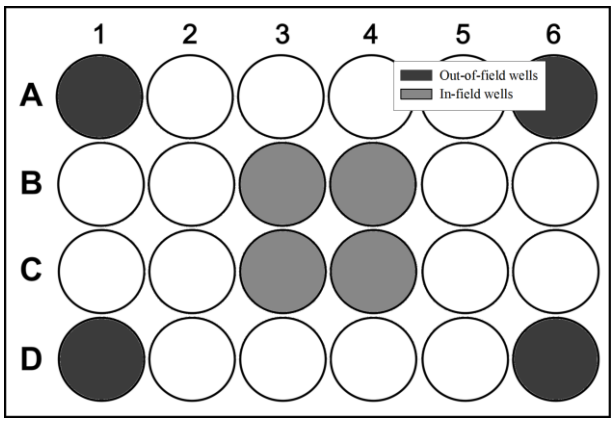


**Fig. 2**. 24 well plate with marked in-field wells and out-of-field wells.

### 2.4 Assessment of irradiated growth medium effect on cells viability

For the investigation of cell viability assay 24 well plate was used. Cell suspension with growth medium (106 cells/ml) was prepared and 500 μl of suspension was poured into 4 centrally located wells (in-field) and 4 wells located at the corners of well plate (out-of-field). The same irradiation procedure was applied as for the case of ROS assessment. After irradiation the growth medium of each well was removed, centrifuged and placed onto Petri-dishes with 400 cells per dish. Cell colonies were counted after 7 days.

## 3. Results

We found a significant ($p < 0.001$) increase of generated ROS in wells with scattering media in between. The increase of generated ROS by 28.18 % for in-field wells and by 45.07 % for out-of-field wells as compared to ROS generation without scattering material was observed (Fig.3). It is notable that application of scattering material increases relative in-field and out-of-field ROS concentration by 4.6 %. The experimental results were comparable with those, obtained from dose distribution simulation.

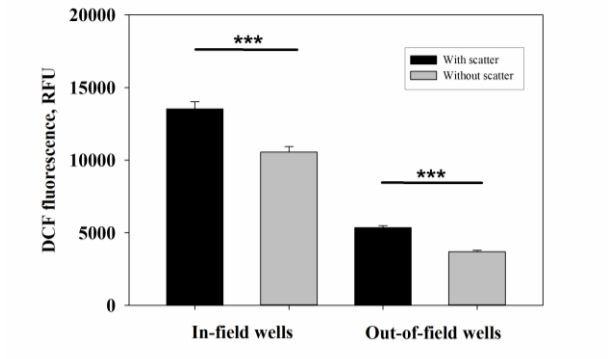


**Fig. 3**. Comparison of average values of DCF fluorescence between in-field wells and out-of-field wells with and without scatter material between wells. Two-tailed T-test for independent samples was used to test for significance. *** signifies $p < 0.001$.

We also found significant ($p < 0.001$) difference between cell numbers in colonies that grew in growth

medium in out-of-field located wells and of colonies grown in field located wells (Fig. 4). The increasing tendency of colony counts of cells was clearly identified. Also, the significant ($p < 0.05$) difference between colony counts of cells that grew in irradiated growth medium previously populated with cells and growth medium without cells. There was no significant difference observed between the colony counts of cells grown in fresh media.

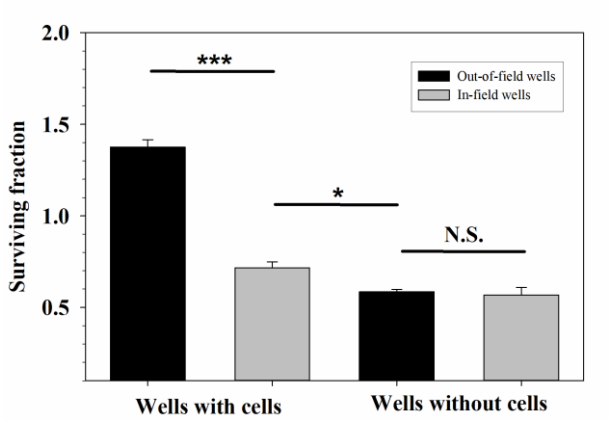


**Fig. 4**. Comparison of surviving fraction of cells after irradiation between in-field wells and out-of-field wells with and without cells. Results are normalized to 400 colonies. N.S. signifies p values > 0.05, * signifies p values < 0.05, *** signifies $p < 0.001$.

## 4. Discussion

The results presented here have tree issues to address. Firstly, a new protocol has been developed which enables monitoring of side scattering effects induced by irradiation. Secondly, ROS generation related to side scattering effects has been investigated. Thirdly, cell proliferation effect as a result of irradiated cell signaling has been shown.

The usage of 24 well plate in irradiation experiments allows to "turn on" or "turn off" side scattering effects since one can fill the air gaps between wells in the plate and investigate direct effect on generation of ROS. "Turned on" side scattering allowed for generation of the significant amount of ROS in out- of-field wells as compared with "turned off" setup. Evidently, side scattering effects also significantly increased ROS generation in infield wells. This lead to conclusion, that side scattering effect must be considered when evaluating cells behavior after irradiation. The next step was to evaluate a side scattering ROS effect to cell viability. A colony forming test was chosen to be performed for cell viability evaluation. As expected, direct irradiation of ionizing radiation had a substantial viability decrease. But the cell viability was not changed once cells were exposed to side scattering. Therefore, we have not observed a "Bystander" effect in cell viability by using our setup. Nevertheless, the cells were indeed affected by the side scattering. The proof of this is shown in Fig. 4. During this experiment the irradiated in- and out-of-field cells were kept for 3 hours. Then the irradiated media with the cells was centrifuged in order to take out the floating cells and put on unirradiated cells that were already prepared for clonogenic assay. This viability test revealed a positive cell growth effect in media which was affected by side scattering radiation. It was estimated that the side scattering effect had a major impact of the cell viability, which was not changed in this case.

According to the literature analysis [6, 7] the cells "communicate" with each other via signaling molecules that are present in the extracellular matrix. In our experiments the extracellular matrix was media taken from side scattering irradiated cells and applied to unirradiated cells (cell growth in irradiated media). We have not evaluated exactly which and how many signaling molecules were present in the media, however we have shown a significantly positive viability change in cell growth when applying side scattering irradiated cell growth media for the growth of unirradiated cell colonies.

## 5. Conclusions

Radiation induced side scattering effects affect in-field and out-of-field located cels, thus altering ROS generation. Since cell death after irradiation is a result of DNA damage generated radiation induced ROS, evaluation of ROS generation is crucial for the evaluation of out of field located cells viability. Significant radiation induced out-of-field ROS generation was observed performing our investigations which was contributing to the viability changes of the affected cells.

## 5. References

1. Kadhim, M., Salomaa, S., Wright, E. et al. (2012). Non-targeted effects of ionising radiation—Implications for low dose risk, Mutation Research/Reviews in Mutation Research. 84-94.
2. Harrison, R. (2017). Out-of-field doses in radiotherapy: Input to epidemiological studies and dose-risk models. Phys.Med. 239-246.
3. Lazzari, G., Terlizzi, A., Leo, M.G., Silvano, M. (2017). VMAT radiation-induced nausea and vomiting in adjuvant breast cancer radiotherapy : The incidental effect of low-dose bath exposure, Clinical and Transl. Rad. Onc. 43-8.
4. Marín, A., Martin, M., Linan, O. et al. (2015). Bystander effects and radiotherapy. Reports of practical oncology and radiotherapy. 12-21.
5. Didvalis, T., Ruzgys, P., Šatkauskas, S. et al. (2018). Assessment of ROS production using DCFH-DA dye in CHO cells after application of ionizing radiation, 2nd International Conference SmartBio, 34.
6. Timothy, M., Pawlik, M., Keyomarsi, K. (2004). Role of cell cycle in mediating sensitivity to radiotherapy. Int. J. Rad. Onc. Biol. Phys. 928-942.
7. Matsuya, Y., McMahon, S., Tsutsumi K. et al. (2018). Investigation of dose-rate effects and cell-cycle distribution under protracted exposure to ionizing radiation for various dose-rates. Scientific reports.

*MEDICAL PHYSICS IN THE BALTIC STATES 14 (2019)*

Proceedings of International Conference "Medical Physics 2019"
7 – 9 November 2019, Kaunas, Lithuania

# APPLICATION OF DICENTRIC ASSAY FOR TRIAGE DOSE ESTIMATION IN CASE OF LARGE-SCALE RADIATION EMERGENCIES

Antonio JREIJE, Diana ADLIENE
Kaunas University of Technology, Lithuania
antonio.jreije@ktu.edu, diana.adliene@ktu.lt

***Abstract:*** In case of large scale radiation emergencies, exposure dose of the victims should be estimated quickly to distinguish between individual with no exposure and those requiring urgent medical treatment. The manual dicentric assay is the most widely used assay for individual dose estimation since it s able to detect low exposure doses (≥ 0.1 Gy) and can differentiate between whole and partial body exposures. However, the so called "gold standard" assay cannot be used in case of mass casualty events because it is laborious and time consuming. Therefore, to decrease the turnaround time of the assay, the automatic dicentric assay was established for preliminary dose estimation. The automatic dicentric assay includes automatic metaphase finding (with a 10x objective), capturing image acquisition (with a 63x magnification) and automatic detection of dicentrics which are validated by an experienced human scorer. The aim of this study was to further increase the throughput of the automatic dicentrics assay by capturing images with a 40x objective instead of a 63x objective.

***Keywords*:** Radiation accidents, triage dose estimation, dicentric assay

## 1. Introduction

In the last few decades, there has been a worldwide increase in the use of radioactive materials and ionizing radiation in medicine as well as in other fields (i.g. industry, military…) and consequently, the number of radiation accidents have increased. For instance, 99 radiation exposures related to nuclear power plant accidents were reported between 1952 and 2009 [1]. Nevertheless, Chernobyl disaster (1986) and Fukushima Daiichi disaster (2011) remains the most devastating nuclear incidents in the history during which a large number of victims were exposed to an unknown dose of radiation [1].
Clinical signs and symptoms (e.i. nausea and vomiting) and fluctuations in blood cell count can serve as a first indicator of radiation over-exposure. However, symptoms are subjective parameters that differ in intensity between victims and can be the result of intense anxiety that occurs in these overwhelming events [2]. Therefore, an independent parameter should be available in emergency radiation accidents in order to provide information about radiation doses received to the blood of each victim and therefore to identify the "worried well" public otherwise known as extremely anxious peoples who didn't received any radiation [3].
In the case of radiation accidents, biological dosimetry serves as a tool to estimate the dose received by exposed individuals. Cytogenetic damages induced by ionizing radiation in the peripheral blood lymphocytes are the most commonly used indicator for biodosimetry purposes [4]. The dicentric chromosome assay is considered until the present day as the "goal standard" in biological dosimetry [5]. Dicentric chromosomes result from the abnormal fusion of two different chromosome segments (each with a centromere) following a radiation exposure induced DNA double strand breaks (Fig.1) [6].


**Fig. 1.** Lymphocyte cells in metaphase with two dicentrics and two acentric fragments [6].

One drawback of the manual dicentric assay is the prolonged time required for the results to be available (approximately 3-4 days). This makes the dicentric assay not useful in case of mass casualty where the exposure status of a large number of victims should be

reported in a timely manner. To increase the throughput of this assay, the conventional manual scoring method has to be adapted to large scale radiation emergencies**.** Thus, new scoring techniques which involve either the reduction of the number of cells analysed or the detection of dicentrics with the help of software have been implemented [7].

The aim of this research was to optimize the automatic scoring of the dicentric assay currently employed in biodosimetric laboratories. The automatic dicentric assay involves different steps including the automatic capturing of metaphase images at 63x magnification which is the most time consuming step. In order to increase the throughput of the assay, the automatic dicentrics scoring with a 40x objective instead of the 63x objective was investigated.

## 2. Methods

### 2.1. Irradiation

Whole blood samples (10 ml heparinized tubes) withdrawn from a healthy female donor were irradiated using $^{137}$Cs source at the dose rate of 0.495 Gy/min in a HWM D2000 unit (Wälischmiller Engineering GmbH, Markdorf, Germany). The irradiation covered 11 different dose ranges between 0 and 6 Gy (i.e. 0.1; 0.25; 0.5; 0.75; 1; 1.5; 2; 3; 4; 5 and 6 Gy). Afterwards, the blood aliquots were incubated for 2 h at 37°C.

### 2.2. Cell cultures

Blood cultures were performed according to the IAEA recommendations [8] and the ISO standards [9]. Whole blood was transferred to tubes (10 ml) containing RPMI-1640 culture medium (Biochrom, Berlin, Germany) supplemented with Fetal Calf serum 10% FCS, the mitogen Phytohemagglutinin 2% PHA and antibiotics (Penicillin/Streptomycin). After 24 h of cell culturing, mitotic block was induced by the addition of colcemid (Roche, Mannheim) with a final concentration in culture of 0.08 mg/ml. Blood cells were cultured for 48 h in total. After this the cells were treated with a hypotonic solution of 75mM KCl. Then cells fixation in methanol:acetic acid (3:1) was performed three times. Overnight storage of the fixed cells in the freezer was possible. Finally, prepared slides were stained in Giemsa-solution containing 20 ml Giemsa and 230 ml PBS buffer for 5 min before being rinsed 3 times in distilled water. The slides were dried overnight and then covered with a mounting medium and coverslips. Before analysis, the slides were stored to dry for an additional day.

### 2.3. Scoring methods

Analysis of slides was performed with the automatic scoring system Metafer 4 developed by MetaSystem (Altlussheim, Germany). For each of the 11 dose points, three different slides were scored. Automatic dicentric scoring involved 3 steps: metaphase finding (Msearch), automatic image acquisition (Autocap) and finally dicentric detection by the software (DCScore) (Fig.2).

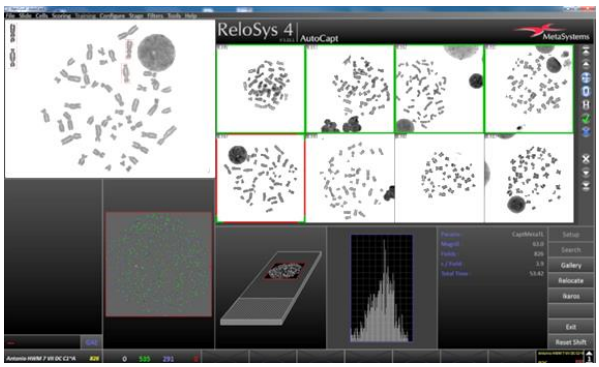


**Fig 2.** Captured metaphases for the detection of dicentric candidates with DCScore software.

In order to compare the performance of both 63x objective (with oil) and 40x objective (without oil) images of the same cells were auto-captured with both magnifications. Then, an experienced human scorer quickly evaluated the chromosomes detected and marked by the software as possible dicentrics and decided to either validate them as true dicentric or reject them. From a pool of 41168 captured images, 27992 cells were accepted for analysis with the 63 x magnification and 23224 cells were scored using the 40 x objective (Table 1).

For the 40x magnification, the DCScore software tool was not fully developed. Consequently, the software was unable to mark the detected dicentric chromosomes at the time when the study was performed. To overcome this problem, the scoring technique was adjusted for both objectives. All the cells that were identified by the software as having aberrant chromosomes were evaluated by the human scorer for the presence of dicentrics and the number of dicentric chromosomes detected by the human scorer was noted as confirmed dicentrics (CDics).

## 3. Results

### 3.1. Comparison of the total time required for dicentric analysis with 63x and 40x objectives

The time required for dose estimation was compared for automatic dicentric scoring with the currently used 63x objective and the 40x objective. When a 63x objective with oil was used for image acquisition, a total time of approximately 8 minutes was required to analyze 100 metaphases (Fig.3).

The majority of this total time (6.49 minutes/ 100 images) was devoted to the auto-capturing of high resolution images because metaphases should be focused twice by fine and coarse focus. However, the time necessary for image acquisition was drastically reduced to 2.93 minutes when a lower magnification was used since the 40x objective had a high depth of focus and consequently, the captured imaged were focused in only one step. In addition, immersion oil, which was applied with the 63x objective, added few seconds to the slides scanning time. (Oil immersion is used with higher magnification (63x and 100x) in order to improve the microscopes resolving power). Consequently, when a 40x objective was used for image

acquisition, approximately 45% of the total analysis time (4.4 minutes/100 metaphases) was saved.

### 3.2. Establishment of dose effect curves for automatic scoring with 63x and 40x objectives

The dose–effect curves for the yield of automatically detected dicentrics using both 63x and 40x objectives are calculated using following equation:

$$Y = C + \alpha D + \beta D^2 \quad (1)$$

where *Y* is the yield of dicentrics, *D* is dose, *C* is a background frequency, $\alpha$ is linear coefficient, $\beta$ is dose squared coefficient) [27]. Estimated values of these coefficients are provided in the Table2 as well as calculated dose-effect curves are shown in Fig.4.

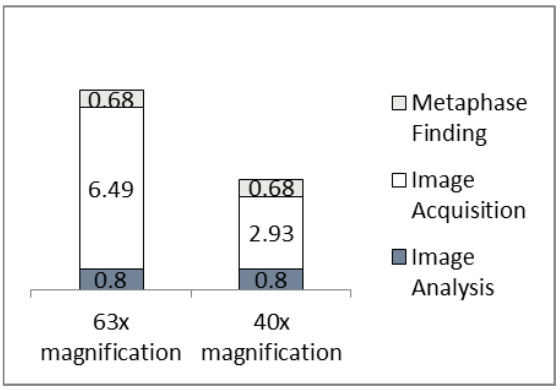


**Fig.3.** Time required for automatic dicentrics scoring for the analysis of 100 metaphases when a 63x or 40x objective is used for image acquisition.

**Table 1.** Number of analyzed images and observed yield of dicentrics following automatic dicentric scoring with 63x and 40x objectives.

| | Dose (Gy) | Captured images | Scored cells | Rejected cells | Rejected cells % | DA | DC | Dic/cell | SE |
|---|---|---|---|---|---|---|---|---|---|
| Semi-automatic (63 x) | 0 | 3145 | 1931 | 1214 | 38.6 | 110 | 8 | 0.004 | 0.001 |
| | 0.1 | 5207 | 3164 | 2043 | 39.2 | 288 | 17 | 0.005 | 0.001 |
| | 0.25 | 5075 | 3414 | 1661 | 32.7 | 171 | 15 | 0.004 | 0.001 |
| | 0.5 | 5993 | 4268 | 1725 | 28.8 | 342 | 57 | 0.013 | 0.002 |
| | 0.75 | 5807 | 3789 | 2018 | 34.7 | 350 | 89 | 0.023 | 0.002 |
| | 1 | 4150 | 2731 | 1419 | 34.2 | 291 | 126 | 0.046 | 0.004 |
| | 1.5 | 2610 | 1869 | 741 | 28.4 | 251 | 193 | 0.103 | 0.007 |
| | 2 | 2179 | 1527 | 652 | 29.9 | 299 | 253 | 0.166 | 0.01 |
| | 3 | 2896 | 2018 | 878 | 30.3 | 719 | 760 | 0.377 | 0.014 |
| | 4 | 1839 | 1449 | 390 | 21.2 | 822 | 1032 | 0.712 | 0.022 |
| | 5 | 877 | 704 | 173 | 19.7 | 459 | 676 | 0.96 | 0.037 |
| | 6 | 1390 | 1128 | 262 | 18.8 | 1087 | 1549 | 1.373 | 0.035 |
| Semi-automatic (40 x) | 0 | 3145 | 1611 | 1534 | 48.8 | 88 | 2 | 0.001 | 0.001 |
| | 0.1 | 5207 | 2658 | 2549 | 48.9 | 213 | 13 | 0.005 | 0.001 |
| | 0.25 | 5075 | 2800 | 2275 | 44.8 | 130 | 17 | 0.006 | 0.001 |
| | 0.5 | 5993 | 3058 | 2551 | 42.6 | 212 | 45 | 0.015 | 0.002 |
| | 0.75 | 5807 | 3318 | 2489 | 42.9 | 268 | 99 | 0.03 | 0.003 |
| | 1 | 4150 | 2242 | 1908 | 46 | 209 | 101 | 0.045 | 0.004 |
| | 1.5 | 2610 | 1601 | 1009 | 38.6 | 200 | 134 | 0.084 | 0.007 |
| | 2 | 2179 | 1351 | 828 | 38 | 262 | 230 | 0.17 | 0.011 |
| | 3 | 2896 | 1712 | 1184 | 40.9 | 483 | 485 | 0.283 | 0.013 |
| | 54 | 1839 | 1265 | 574 | 31.2 | 669 | 800 | 0.632 | 0.022 |
| | 5 | 877 | 565 | 312 | 35.6 | 350 | 475 | 0.841 | 0.039 |
| | 6 | 1390 | 1043 | 347 | 25 | 894 | 1351 | 1.295 | 0.035 |

DA: automatically detected dicentrics, DC: confirmed dicentrics, RD: rejected dicentric candidates.

**Table 2.** Estimated values of the coefficients of the dose effect curves obtained after semi-automatic scoring using 63x and 40x objectives

| | | Estimate | SE | P-value |
|---|---|---|---|---|
| Semi-automatic (40 x) | C | 0.0025 | 0.0009 | 0.0089 |
| | α | 0.0082 | 0.0033 | 0.0137 |
| | β | 0.3389 | 0.0011 | <0.0001 |
| Semi-automatic (63 x) | C | 0.0036 | 0.0009 | <0.0001 |
| | α | 0.0007 | 0.0031 | 0.8120 |
| | β | 0.4004 | 0.0011 | <0.0001 |

**Table 3.** Statistical comparison of the model coefficients based on Z-Scores

| | Z-Score | P-value |
|---|---|---|
| C | 0.873 | 0.383 |
| α | -1.627 | 0.104 |
| β | 4.014 | <0.0001 |

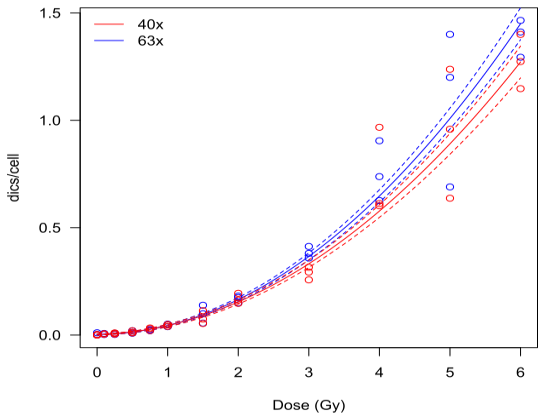


**Fig.4.** Dose-effect curves of semi-automatic dicentric analysis for two different objectives.

At low exposure doses up to 2 Gy, the dose- effect curves resulting from dicentrics scoring with both 63x and 40x objectives merge.
In addition, a statistical comparison of the linear coefficients suggests no statistically significant difference between the two curves (table 3).
This indicates that the yield of dicentrics is similar for both objectives at lower doses. However, at doses higher than 2 Gy, the curve derived from dicentric scoring with the 40x magnification is lower than the 63x magnification. The quadratic coefficient (β) is significantly lower for the 40x objective (p-value <0.0001). Therefore, at higher doses and when scoring was performed with the 63x objective, a higher number of dicentric chromosomes were marked by the software and confirmed as true dicentrics by the human scorer. The lower yield of dicentrics obtained with the 40x objective can be explained by the fact that the software has a difficulty in detecting dicentrics when images are acquired at this lower magnification. Moreover, captured with the 40x objective chromosomes were smaller in size, and therefore, the human scorer failed to confirm some true dicentric chromosomes in the validation step. All of these factors contributed to the signifiantly lower curve derived from scoring with the 40x objective.

## 4. Conclusions

The results obtained in our study represent a first step toward the optimization of the automatic dicentric assay. In case of large-scale radiation emergencies, the throughput of the automatic dicentric assay can be drastically increased when scoring with 40x objective. Image acquisition with the 40x magnification results in the reduction of the turnaround time for individual dose assessment by approximately 45% in case of mass casualty incident. Moreover, the established dose-effect curves are almost similar for both objectives; although the curve derived from scoring with 40x objective is significantly lower for radiation doses higher than 2 Gy. It is important to perform further investigation and validation of this scoring technique before implementing the automatic dicentric scoring with 40x objective in biodosimetric laboratories. Future validation should involve the dose estimation of single-blind irradiated blood samples with the newly established dose response curve. Furthermore, in order to assure the reproducibility of this new assay in case of mass casualty scenarios, inter-comparison should be performed between different biodosimetry laboratories.

## Acknowledgment

Autors express their gratitude to the staff the Biological dosimetry unit of the Bundesamt für Strahlenschutz (BfS), Munich, Germany where all investigations have been performed.

## 5. References

1. Benjamin K. Sovacool (2010). A Critical Evaluation of Nuclear Power and Renewable Electricity in Asia, *Journal of Contemporary Asia*, 40 (3) 393–400.
2. Willems P, August L, Slabbert J, et al. (2010) Automated micronucleus (MN) scoring for population triage in case of large scale radiation events. *International Journal of Radiation Biology*. 86(1) 2-11.
3. Kulka U et al. (2017). RENEB - Running the European Network of biological dosimetry and physical retrospective dosimetry. International J Radiat Biol. 93(1):2-14.
4. Ainsbury EA, Bakhanova E, Barquinero JF, Brai M, Chumak V, Correcher V et al. (2011). Review of retrospective dosimetry techniques for external ionising radiation exposures. RPD 147, 573–592.
5. Hartwell, L., Hood, L. Goldberg, M., Reynolds, A., Lee, S. (2011). Genetics From Genes to Genomes, 4e. New York: McGraw-Hill.
6. Lloyd, A. A., Edwards, J. E. Moquet, Y. C. Guerrero-Carbajal (2000). The role of cytogenetics in early triage of radiation casualties. APRADISO, 52(5), 1107–1112.
7. Buglova E, Roy L. Presentation of some activities of IAEA in the field of emergency preparedness. In: *Proceedings of BioDose 2008*. Hanover, NH.
8. ISO 21243. Radiation protection - Performance criteria for laboratories performing cytogenetic triage for assessment of mass casualties in radiological or nuclear emergencies - General principles and application to dicentric assay, International Organization for Standardization, Geneva, Switzerland, 2008.

*MEDICAL PHYSICS IN THE BALTIC STATES 14 (2019)*

Proceedings of International Conference "Medical Physics 2019"
7 – 9 November 2019, Kaunas, Lithuania

# MULTISCALE MODELING AND ANALYSIS OF LIPID MEMBRANES INTERACTION WITH ANTIBIOTICS: A CASE STUDY ON GRAM-NEGATIVE BACTERIA

Sridhar HARIHARAPUTRAN, Arul MURUGAN Natarajan, Zilvinas RINKEVICIUS
Kaunas University of Technology, Studentų str. 50, LT-51368 Kaunas, KTH Royal Institute of Technology, Stockholm, Sweden.
murugan@theochem.kth.se, zilvinas.rinkevicius@ktu.lt

***Abstract*:** Bacterial infections are a major concern responsible for several million deaths every year. Our work and paper describe computational methods to develop multi-scale models and coarse grain molecular dynamic simulations of cell envelopes of gram-negative bacteria and its interactions with nano particles by studying its binding free energies and optical properties using QM/MM methods.

***Keywords*:** multiscale modeling, chemical physics, bacteria, infection,

## 1. Introduction

Gram-negative bacteria, the superbugs are already attaining resistance to broad range of antibiotics leading to chronic infections and increase in the cost of healthcare worldwide and biofilm associated infections. It is crucial to understand the interactions of bacterial cell with its surroundings to design novel antibiotics and develop antimicrobial coatings. Along with healthcare, bacteria also causes economic losses to the industry. Previous works both experimental and theoretical methods investigated the properties of bacteria and nanoparticles as well. Gram-negative bacteria has an outer membrane that makes it impermeable to lipopolysaccharide molecules and intrinsically resistant. Various factors govern the entrance of these molecules and multiple mechanisms are associated with the production of their cell walls.

Bacterial adhesions onto the solid surfaces of industrial applications lead to economic loss due to biofilm formation that is critical to microbiology and biomedical research. It is also important to understand the interacttion of bacterial cell envelope to its surroundings that serve as a corner stone in the design of new antibiotics and antimicrobial coatings.

Lipids are an important component of lipid bilayers and has a crucial role in several cell signaling and physiological processes. In the the outer leaflet of the outer membrane of the Gram-negative bacteria lipopolysaccharides (LPS) are a major component acting as a barrier to multple threats and protecting the bacterium.

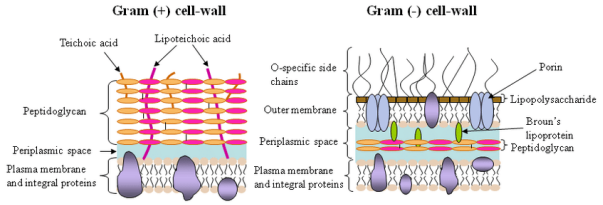


**Fig. 1**. Schematic represenation of Gram-postive and Gram-negative bacterial cell wall. (Atanasova, 2010)

Previous and ongoing works prove it is important to study the shape and structure of outer membrane becuase the strucutre of LPS can provide information in ouuter membrane protein biogenesis and help in antibiotic design. And the shape and stability are beleived to play a signficiant role in the insertion and folding of proteins in the outer membrane. And also to develop a rational way to design new antibiotic drugs. Understanding and then manipulating the structure and stability of LPS is essential that makes the outer membrane to be more impermeable. (5)

Various diseases are caused due to membrane abnormalities. It is proved that biological membranes are good targets for therapy.[1] Bacterial interaction with their surroundings are decided through the membranes that is a part of the cell envelopes. These envelopes are highly complex strcutures though bacteria can be simple organims [2]. In patients with cancer, blood stream infections are responsible for major complications due to the delays in chemotherapy along with many others. Gram-negative bacteria is assoicated with the etiology of BSI [3].

Molecular dynamics' (MD) simulations help in deriving structural and dynamic descriptions of mebrane than it is possible by conducting experiments. Even though it is highly essential to validate the results in agreement with the available experimental data (6).

Nanoparticles as such are being used as carrier for transporting the antibiotics to a specific target site to deliver the drugs or compounds used against gram-negative bacteria. Recent studies have proved the use of nanomaterials as a technique that can be adopted for drug delivery systems.

## 2. Materials and Methods

This work involves computational approaches for building the systems and analysis. Membrane systems are built using CHARMM-GUI web-based platform and using membrane builder for building bilayer model for molecular dynamics simulations. Based on the literature studies the combinations of the heterogenous lipids are chosen. Several models were built for simulations and analysis. These models are then subjected to molecular dynamics simulations using Amber software suite and using high performance computing (HPC) facilities in Sweden.

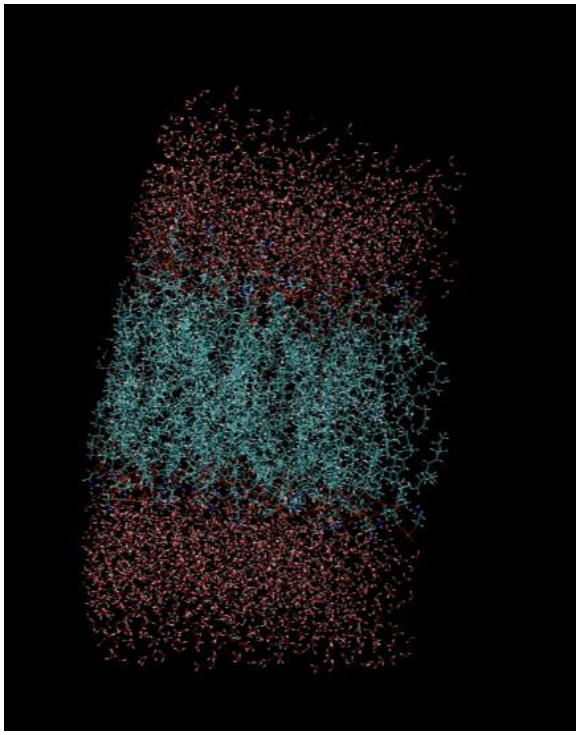

**Figu. 2.** Strucutre of 3:1 ratio bilayer systems generated using VMD.

Results from the previous works and literature review helped in decision making processes for introducing ligands into these systems. Various parameters were assessed. Results analyzed and plots generated show a positive direction to introduce nanoparticle into the systems. We present only our preliminary results in this paper that are generated, analyzed in the recent past using these methods.

Vancomycin is an antibiotic used for the treatment of bacterial infections. Outer membrane of the Gram-negative bacteria makes it difficult and impermeable to large glycopeptide molecules. Whereas in Gram-positive it is able to inhibit proper synthesis of cell wall.

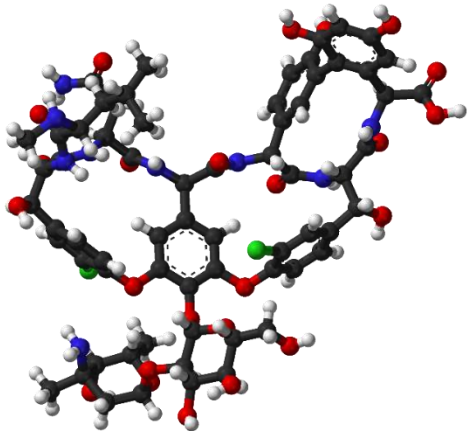

**Fig. 3.** 3D structure of Vancomycin

Based on other researchers, lipid contents and possible combinations in different ratio as previously discussed are presented in Table 1.

**Table 1.** Lipids, composition and ratio

| Lipids | Ratio |
|---|---|
| POPE:POPG | 1:1 |
| POPE:POPG | 3:1 |
| POPE:POPG | 5:1 |

Calculated Number of Lipids: 1:1

| Lipid Type | Upperleaflet Number | Lowerleaflet Number |
|---|---|---|
| POPE | 21 | 21 |
| POPG | 21 | 21 |

Calculated XY System Size:

| | Upperleaflet | Lowerleaflet |
|---|---|---|
| Protein Area | 0 | 0 |
| Lipid Area | 2536.8 | 2536.8 |
| # of Lipids | 42 | 42 |
| Total Area | 2536.8 | 2536.8 |

Average Area 2536.80

A 50.37 B 50.37

## 3. Results and Discussion

Simulations were carried out using Amber software suite for different time scales. Results were analyzed using more software packages and in-house programs, algorithms.

Molecular dynamics' simulations results help in understanding the interaction of small molecules with gram-negative bacteria and form the seed for the analysis using QM/MM methods and for understanding the energy profiles of penetration of small molecules using steered molecular dynamics simulations or in understanding the selective behavior and analysis of organic molecules and permeability of membranes. Using the results, it is now possible to proceed further with the molecular dynamics simulations of TiO2 and TiO2/Au nanoparticles in multiple solutions and using

appropriate force fields. Interaction of nanoparticles with the Gram-negative bacteria will be deciphered using the molecular dynamics simulations and Monte-Carlo methods.

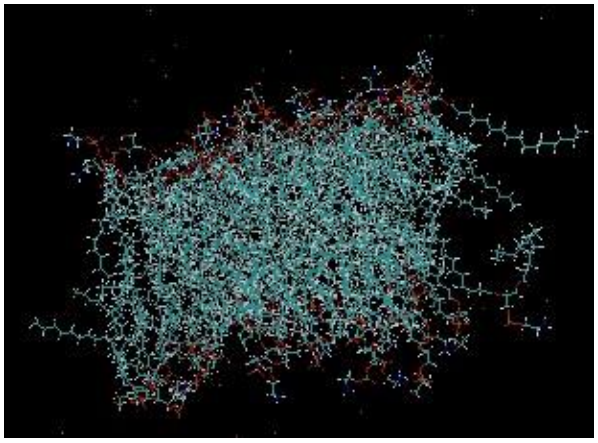

**Fig. 3.** Molecular Dynamics Simulations results generated from 1:1 system

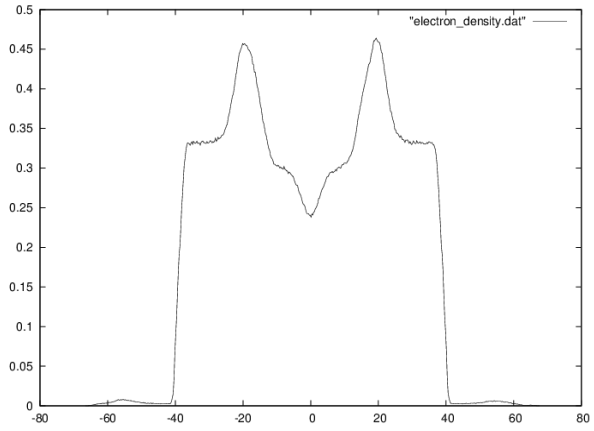


**Fig. 4.** Electron density map generated for 1:1 ratio system
X axis – Distance from the Lipid Bilayer Center (Angtroms)
Y axis – Normalized Electron Density

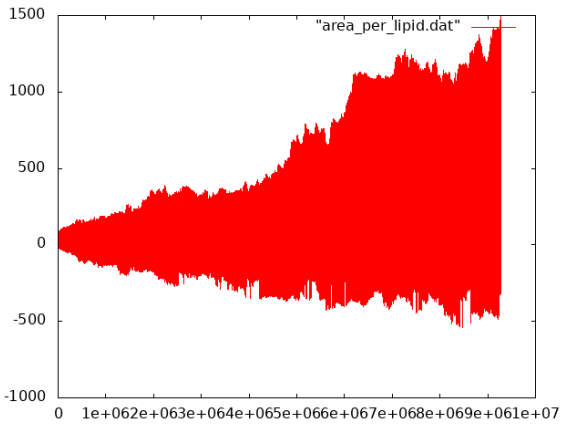


**Fig. 5.** Area per lipid for heterogeneous lipid systems with vancomycin

Electron density profile give the information of density of electrons through the lipid bilayer by measuring the average over a period of time. Data is further analyzed with previous works and compared with other researchers' from experimental studies.

In order to gain information on the fundamental property of the lipid bilayer and to know the equilibrium status of the lipid bilayer in the simulations the area per lipid is assessed. Once the value reaches a stable state it confirmed that the strucutre of the lipid bilayer do not change. Experimentally it will be a daunting process.

## 4. Conclusions

Gram-negative bacteria are associated with infectious diseases and are a threat to healthcare world-wide and causes loss in industrial applications. Our work and preliminary results show computational methods and simulations paves the way for the effective use of nanoparticles as carriers and drug delivery systems to the specific target site. Further it will also contribute to the development of antibiotics against multi-drug resistant bacteria.

## 5. Acknowledgements

Kaunas University of Technology, Studentų str. 50, LT-51368 Kaunas, KTH Royal Institute of Technology, Stockholm, Sweden. Swedish National Infrastructure for Computing (SNIC).

## 6. References

1. NA Murugan, R Apostolov, Z Rinkevicius, J Kongsted, E Lindahl, H Ågren. Association dynamics and linear and nonlinear optical properties of an n-acetylaladanamide probe in a popc membrane**.** Journal of the American Chemical Society, 2013.
2. J Parkin, M Chavent, S Khalid. Molecular simulations of Gram-negative bacterial membranes: a vignette of some recent successes. Biophysical journal, 2015.
3. Islas-Muñoz, B., Volkow-Fernández, P., Ibanes-Gutiérrez, C., Villamar-Ramírez, A., Vilar-Compte, D., & Cornejo-Juárez, P. (2018). Bloodstream infections in cancer patients. Risk factors associated with mortality. *International journal of infectious diseases : IJID : official publication of the International Society for Infectious Diseases*, *71*, 59-64 .
4. Kalina R. Atanasova**.** Interactions between porcine respiratory coronavirus and bacterial cell wall toxins in the lungs of pigs. 2010.
5. S. Kim, D.S. Patel, S. Park, J. Slusky, J.B. Klauda, G. Wid malm, W. Im. Bilayer properties of lipid a from various gram-negative bacteria. Biophys J, 111 (2016), pp. 1750-1760
6. Braun, A. R., Brandt, E. G., Edholm, O., Nagle, J. F., & Sachs, J. N. (2011). Determination of electron density profiles and area from simulations of undulating membranes. *Biophysical journal*, *100*(9), 2112–2120. doi:10.1016/j.bpj.2011.03.009
7. Hariharaputran S, Natrajan AM, Rinkevicius Z. (2019). Multiscale Modelling of Phospholipid Membranes Interactions with Nanoparticles. *Proceedings of Lietuvos nacionalinė fizikos konferencija (LNFK 43.,October 3-5, PP. 198.*

*MEDICAL PHYSICS IN THE BALTIC STATES 14 (2019)*

Proceedings of International Conference "Medical Physics 2019"
7 – 9 November 2019, Kaunas, Lithuania

# ENVIRONMENTAL AGEING AND ITS EFFECT ON COMPRESSIVE PROPERTIES OF DENTAL COMPOSITE

Ksenija PRILADIŠA[1], Jurģis SILIŅŠ[2], Tatjana GLASKOVA-KUZMINA[3], Jevgenijs PROSKURINS[4], Sandra BĒRZIŅA[5], and Elizabete JAUNOZOLA[6]
[1]Riga Stradins University, Faculty of Dentistry, Riga, Latvia; [2]Riga Stradins University, Faculty of Dentistry, Riga, Latvia; [3]Riga Stradins University, Faculty of Medicine, Department of Physics and University of Latvia, Institute for Mechanics of Materials, Riga, Latvia; [4]Riga Stradins University, Faculty of Medicine, Department of Physics; [5]Riga Stradins University, Faculty of Dentistry, Department of Conservative Dentistry and Oral Health, Riga, Latvia; [6]Riga Stradins University, Faculty of Dentistry, Department of Conservative Dentistry and Oral Health, Riga, Latvia
k.priladish@gmail.com; jurgissilins@gmail.com; Tatjana.Glaskova-Kuzmina@rsu.lv; Jevgenijs.Proskurins@rsu.lv; Sandra.Berzina@rsu.lv; Elizabete.Jaunozola@gmail.com

***Abstract*:** Dental composite materials (CM) are widely used in dentistry for restorations. The aim of this study was to determine how compressive properties of commercially available dental CM change in simulated intraoral conditions. The investigated material was 3M ESPE Filtek™ Ultimate A2 Enamel Shade that is widely used in dental clinic and preclinical studies for anterior and posterior restorations. First, the compressive properties of dental composite were determined in uncondensed state. The compressive modulus, strength and maximal deformation were evaluated from the stress-strain curves obtained for the prismatic CM specimens. The specimens were immersed in distilled water (pH = 6), water and vinegar solution (pH = 4), and alkaline mineral water (pH = 8) at 50 °C until equilibrium moisture content. Then, the mechanical testing in compression was repeated. It was experimentally confirmed that the storage in simulated intraoral conditions caused a significant reduction of compressive properties of the dental CM, which can negatively influence the lifespan of the restoration. The strength and compressive modulus of the moistened samples were reduced by 27% and 25%, accordingly, but the maximal deformation was increased by 0.4% in comparison with the unconditioned samples. The CM stored in solution with pH = 8 had the highest elastic modulus and strength and the lowest maximal deformation in comparison with the CM stored in more acidic solutions (pH is 4 and 6), indicating to lower inner degradation phenomena of the dental CM.

***Keywords*:** dental composite, compressive properties, environmental ageing, moisture and temperature effects, pH factor

## 1. Introduction

Mechanical performance in harsh intraoral environment of the dental composite material has been a concern to dentistry specialists and material suppliers – both want a persisting positive outcome of material usage. Mechanical characteristics, chemical factors, temperature and pH fluctuations play an important role in materials lifespan. Water, food and drink particles, saliva and humidity contact with fillings surface in the oral cavity cause degradation by erosion, solubility and absorption [1].

Since the nature of polymer resins used in dental composites is polar, they are prone to absorbing water. Thus, water absorption may cause structural changes within a material, which accelerate the rate of degradation by abrasive wear or fatigue [1].

In fact, many solvents may cause surface softening of dental composite, which stimulates their wear. There is a wide range of conditions that may exist in the mouth: the pH of oral fluids varies from pH = 4 to pH = 8.5, highly acidic soft drinks and the use of chalk-containing toothpastes extend this range from a lower end of pH = 2 up to pH = 12. Dental CM is quite resistant to liquids having neutral pH values but erode rapidly at extremes of either acidity or alkalinity. It partially explains why certain materials perform adequately with some patients but not others [1].

It was experimentally verified that distilled water and hot drinks (e.g., tea) had the same destructive effect on the CM surface [2] resulting in increased surface roughness of the test specimens due to erosion, comparing to "unaged" specimens in initial state. Moreover, it was found that the surface roughness of dental composite increased greatly after hydrothermal ageing in 96%

ethanol comparing to environmental ageing in distilled water in one-year study [3].

Liquids in outer layers of the surface do not only affect dental CM, but upon moisture absorption, partial solubility takes place. Due to leaching of some components, the material loses from 0.31 to 10.26 μg/mm³ resulting in structural changes, destruction in polymer matrix and subsequent decrease of mechanical performance intra orally [4]. Water sorption was increased in acidic environment (e.g. pH = 3.1) [5] compared to distilled water with pH = 7. The equilibrium of moisture content in acidic environment may decrease, because of increased desorption, although sorption and desorption processes depend on material chemical structure and its reaction with the liquid. It may be due to microstructural changes in the material during the water uptake process that made paths for water to vaporize [1, 6].

On the other hand, it was found that after storing dental CM and glass ionomer cement in distilled water for 30 days there was an increase in compressive strength [7, 8], which was explained by post-curing of the composite expressed as increase in cross-linking density of polymer chains [7]. It is typical for polymer resins that in the case of non-complete curing, especially at high temperatures, post-curing phenomena can occur during water absorption leading to no change or even increase of mechanical and thermophysical properties proving that post-curing process dominates over plastization [9-11]. Due to different composition (types and content of mineral filler and polymer resin), storage time and processing conditions moisture uptake can increase, decrease or even not affect the fracture toughness of CM [4].

Moreover, polymer-based dental composites to high extent are affected by temperature changes. In the oral cavity the maximum temperature reached in vivo was 76.3 °C for hot beverage and about 50 °C for hot food [12]. The glass transition temperature (Tg) for dental CM, that have dimethacrylate monomers Bis-GMA, TEGDMA, UDMA, Bis-EMA and PCDMA base is about 40–45 °C [13]. Upon immersion in distilled water $T_g$ was negatively affected by water, which acted as plasticizer leading to increase in softness and flexibility, and reduction of its brittleness making composites rubberier [13]. Nowadays, dental CM differ in structure and composition that make them stable to survive and withstand the environmental factors in the mouth successfully. Although, fluctuations in temperature, levels of pH factor and food particles negatively affect the mechanical properties of dental composites and may lead to their degradation and decrease of the lifetime.

The aim of the study was to determine how compressive properties of commercially available dental CM change in simulated intraoral conditions at different pH factor. For this purpose, the test specimens were prepared in the form of prisms as closely as possible to the realistic conditions of restauration processing conditions and environmentally "aged" in liquid solutions having different pH factor: distilled water (pH = 6), mineral water (pH = 8), and water and vinegar solution (pH = 4). The test specimens of dental composite were fully immersed in the liquids at 50 °C, and the moisture kinetics was observed. After reaching the equilibrium moisture content mechanical properties in compression were tested before and after hydrothermal ageing to investigate its effect on compressive properties of the dental CM.

## 2. Materials and methods

The investigated material was Filtek™ Ultimate A2 enamel shade (3M ESPE, Germany) which is widely used in dental clinic and preclinical studies for anterior and posterior restorations. According to material datasheet the matrix material consists of bis-GMA, UDMA, TEGDMA, and bis-EMA resins which has 78.5 wt.% of inorganic filler which consists of silica and zirconia with particles sized in the range 0.6-10 μm.

The test specimens were prepared according to ASTM D695 in the form of prisms with sizes 5×5×10 mm. Each specimen was made in the silicon moulds (Zhermack Elite HD plus putty and Zhermack Elite HD plus light body) according to the size of prisms. Moulds were taken of pre-made 3D printed prisms (Fig. 1).

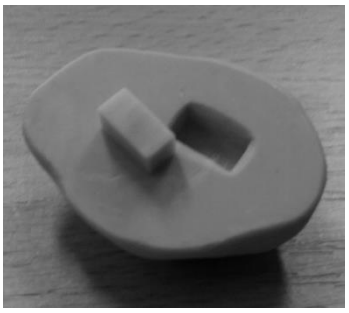

**Fig. 1**. Pre-made prism in a silicon mould.

Composite material was layered in the moulds using dental spatula, and each layer was cured with MegaDenta Megalux CS curing lamp for 40 sec according to the instructions. Each composite prism consisted of 11-13 layers of the dental CM. After final layer was cured, the prism was taken out of the mould and polished with composite polishing discs (Sof-Lex™ countering discs). The test specimens were conditioned in the glass bottles as shown in Fig. 2, which were filled with according liquid solution having certain pH factor.

**Fig. 2**. Test specimens before environmental ageing.

First the mechanical properties of dental composite were determined in uncondensed state. The mechanical testing in compression was performed by using servo-hydraulic testing system MTS 5T at a speed rate 1 mm/min until failure. The compressive modulus, strength and maximal

deformation were evaluated from the stress-strain curves obtained for five CM specimens.

Then for the investigation of environmental effects, three groups of five specimens were immersed in the following solutions at 50 °C: 1) distilled water (pH = 6), 2) water and vinegar solution (pH = 4), and 3) alkaline mineral water (pH = 8) until equilibrium moisture content. For the investigation of the moisture absorption kinetics, the test specimens were periodically removed from the desiccator, air dried for 5 min, and then weighed by using a Mettler Toledo XS205DU (USA) balance with accuracy 0.05 mg. At least five specimens were used for each material type, and the averaged values are presented in the paper. After that, the mechanical tests in compression were repeated at the same conditions to reveal the effect of absorbed moisture on the compressive properties of the CM.

## 3. Results and discussion

### 3.1. Moisture absorption

The peculiarities of moisture absorption of the dental CM in the solutions with different pH factor and temperature 50 °C were studied. According to Fig. 3 the overall behaviour was similar in all following classical Fick's law for three-dimensional moisture diffusion

$$w(t) = w_\infty - (w_\infty - w_0) \times \frac{8}{\pi^6} \sum_{k=1}^{\infty}\sum_{n=1}^{\infty}\sum_{m=1}^{\infty} \frac{\left[1-(-1)^k\right]^2\left[1-(-1)^n\right]^2\left[1-(-1)^m\right]^2}{k^2 n^2 m^2} \times \times \exp\left[-\lambda^2_{k,n,m} D t\right] \quad (1)$$

where

$$\lambda^2_{k,n,m} = \lambda_k^2 + \lambda_n^2 + \lambda_m^2 = \left(\frac{\pi k}{a}\right)^2 + \left(\frac{\pi n}{b}\right)^2 + \left(\frac{\pi m}{l}\right)^2 \quad (2)$$

and $w_0$ and $w_\infty$ are the initial and the equilibrium moisture contents in the specimen, while $a$, $b$ and $l$ are the thickness, width and length of the specimen, respectively. There are two independent parameters in Eq. (1): diffusion coefficient or diffusivity $D$ and equilibrium moisture content $w_\infty$. The equilibrium moisture content is usually evaluated as maximally achieved moisture content over the sorption test, while time-varying moisture content (in %) is obtained by using following expression:

$$w(t) = \frac{m(t) - m_0}{m_0} \cdot 100, \quad (3)$$

where $m(t)$ is time-varying mass of the specimen at time $t$, $m_0$ is the mass of the specimen in initial state ($t = 0$).

Then the diffusion coefficient can be calculated from the initial slope of the curve $w$ vs. $\sqrt{t}$ [14]:

$$D = \frac{\pi h^2}{16 t}\left(\frac{w(t) - w_0}{w_\infty - w_0}\right)^2. \quad (4)$$

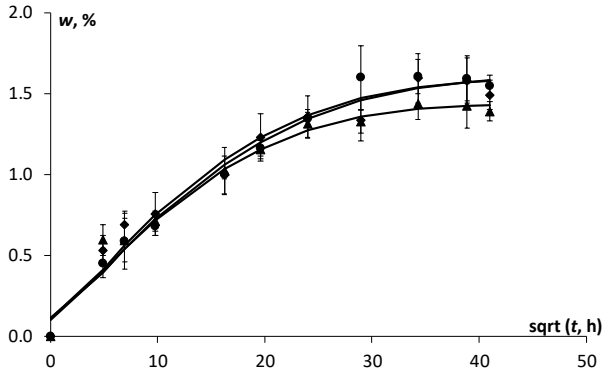


**Fig. 3**. Moisture uptake in solutions with different pH level (● - 4, ♦ - 6, and ▲ – 8). Dots – experimental data, lines – calculation by Eq. (1).

According to Fig. 3 the dental CM immersed in the solution having pH = 8 had the lowest equilibrium moisture content (1.44 ± 0.05) % in comparison with the rest solutions (1.61 ± 0.09) % (pH = 4) and (1.59 ± 0.11) % (pH = 6)). Nevertheless, the diffusivity of the dental CM was slightly increased with the increase of pH factor: (2.36 ± 0.24) × $10^{-4}$ mm$^2$/h (pH = 4), (2.63 ± 0.26) × $10^{-4}$ mm$^2$/h (pH = 6) and (3.06 ± 0.30) × $10^{-4}$ mm$^2$/h (pH = 8) revealing the increase of the rate of water absorption with the increase of pH factor.

### 3.2. Compressive properties

Generally dental composites are subjected to cyclic compressive loadings and the compressive strength of the dental composite resins (250−350 MPa) should be close to enamel and dentin, but the tensile strength of composite resins is much lower (50−90 MPa) [15].

According to ASTM D695 the compressive strength is considered as the maximum compressive stress carried by a test specimen during the test and is calculated by dividing the maximum compressive load by the original minimum cross-sectional area of the specimen [16]. The compressive modulus was calculated by drawing a tangent to the initial linear portion of the stress-strain curve and dividing the compressive stress represented by the point on the tangent line by the corresponding strain. Finally, the maximal deformation is the maximal deformation of test specimens at the end of the test.

The representative stress-strain curves for the test specimens are provided in Fig. 4 before and after the environmental ageing in all solutions. Obviously, the CM specimens, which were stored in simulated intraoral conditions with different pH factor, have reduced compressive properties in comparison with the CM specimens tested in initial conditions. The strength and compressive modulus of moistened samples were maximally (in solution with pH = 4) reduced by 27.4% and 24.9%, accordingly, in comparison with the samples in initial conditions.

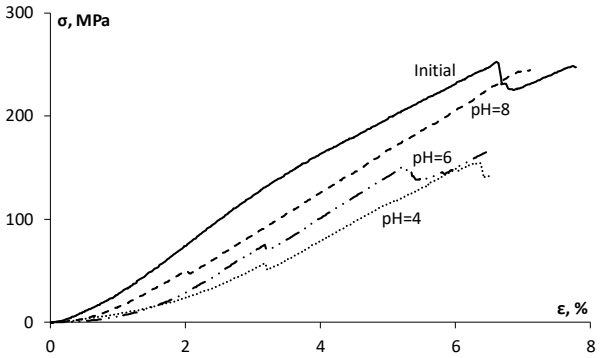


**Fig. 4**. Representative stress-strain curves for the dental CM in initial conditions and stored in solutions with different pH factor (indicated on the figure).

As seen from Fig. 4 the CM stored in solution with pH = 8 had the highest elastic modulus (4.3 GPa), the highest strength (211.7 MPa) and the lowest maximal deformation (7.3%) in comparison with the results obtained for the samples stored in more acidic solutions (pH = 4 and pH = 6), indicating to lower inner degradation phenomena of the dental CM.

## 4. Conclusions

It was experimentally confirmed that the CM specimens, which were stored in different simulated intraoral conditions (water absorption at 50 °C in three solutions with pH was 4, 6, and 8) until equilibrium water content (app. 70 days), have reduced compressive properties in comparison with the CM specimens tested in initial conditions.

Moisture and temperature caused significant degradation of compressive properties of the dental composites, which can lead to the reduction of the lifetime of dental restorations. Based on experimental results it can be concluded that the CM stored in solution with pH = 8 had the highest compressive characteristics in comparison with more acidic solutions (pH = 4 and pH = 6), as well as the lowest equilibrium moisture content revealing the lowest degree of environmental ageing of the dental CM.

## Acknowledgements

This work was partly funded by ERDF project No. 1.1.1.2/VIAA/1/16/066 for the support of post-doctoral research "Environmental effects on physical properties of smart composites and fibre-reinforced plastics modified by carbonaceous nanofillers for structural applications". The participation in the *14th conference Medical Physics in the Baltic States* was funded by Riga Stradins University.

## References

1. McCabe J. F., Angus W. G. Applied Dental Materials. 9th edition, Walls John Wiley & Sons, 2013, 312 p.
2. Draughn R. A. Effects of temperature on mechanical properties of composite dental restorative materials. Journal of Biomedical Materials Research, 1981, 15(4), p. 489-495.
3. Hahnel S., Henrich A., Bürgers R., Handel G., Rosentritt M. Investigation of mechanical properties of modern dental composites after artificial aging for one year. Operative Dentistry, 2010, 35 (4), p. 412-419.
4. Alrahlah A. Physical, Mechanical and Surface Properties of Dental Resin-composites, 2013, PhD thesis, the University of Manchester, Manchester, UK, 195 p.
5. Rahim T. N., Mohamad D., Akil H. M., Rahman I. A. Water sorption characteristics of restorative dental composites immersed in acidic drinks. Dental Materials, 2012, 28 (6), p. 63-70.
6. Santos C., Clarke R. L., Braden M., Guitian F., Davy K. W. M. Water absorption characteristics of dental composites incorporating hydroxyapatite filler. Biomaterials, 2002, Vol. 23, p. 1897-1904.
7. Chen S., Ohman C., Jefferies S. R., Gray H., Xia W., Engqvist H. (2016). Compressive fatigue limit of four types of dental restorative materials. Journal of the Mechanical Behavior of Biomedical Materials, 2016, 61, p. 283-289.
8. Zakir M., Kheraif A. A., Asif M., Wong F. S., Rehman, I. U. A comparison of the mechanical properties of a modified silorane based dental composite with those of commercially available composite material. Dental Materials, 2013, 29 (4), p. 53-59.
9. Sousa J. M., Correia J. R., Cabral-Fonseca S. Durability of an epoxy adhesive used in civil structural applications. Construction and Building Materials, 2018, 161, p. 618-633.
10. Prolongo S. G., Gude M. R., Ureña A. Water uptake of epoxy composites reinforced with carbon nanofillers. Composites Part A, 2012, 43, 2169-2175.
11. Glaskova-Kuzmina T., Aniskevich A., Sevcenko J., Borriello A., Zarrelli M. Cyclic moisture sorption and its effects on the thermomechanical properties of epoxy and epoxy/MWCNT nanocomposite. Polymers, 2019, Vol. 11 (9), 1383, p. 1-14.
12. Feuerstein O, Zeichner K, Imbari C, Ormianer Z, Samet N, Weissm EI. Temperature changes in dental implants following exposure to hot substances in an ex vivo model. Clinical Oral Implants. Research 2008, 19, p. 629–633.
13. Sideridou I., Achilias D. S., Kyrikou E. Thermal expansion characteristics of light-cured dental resins and resin composites. Biomaterials, 2004, 25, p. 3087–3097.
14. Loos A. C., Springer G. S. Environmental effects on composite materials. Westport: Technomic Publishing Co 1981, p. 1.
15. Petronijević B., Marković D., Šarčev I., Anđelković A., Jeremić Knežević M. Fracture resistance of restored maxillary premolars. Contemporary Materials, 2012, III-2, p. 219-225.
16. ASTM D695. Standard Test Method for Compressive Properties of Rigid Plastics. International. 2015.

*MEDICAL PHYSICS IN THE BALTIC STATES 14 (2019)*

Proceedings of International Conference "Medical Physics 2019"
7 – 9 November 2019, Kaunas, Lithuania

# EFFICIENCY AND COLOUR STABILITY OF A COMBINED IN-OFFICE AND TAKE-HOME WHITENING WITH PHILIPS ZOOM: A RETROSPECTIVE STUDY

Giedrė MORKŪNAITĖ, Dr. Rimantas OŽIŪNAS
Lithuanian University of Health Sciences (LSMU) MA Faculty of Odontology Department of Prosthodontics
m.giedre@yahoo.com

***Abstract***. This retrospective study aimed to evaluate colour efficiency immediately after teeth whitening, to validate colour stability after 12–15 months and to evaluate teeth sensitivity. 111 patients received combined in-office and take-home whitening with 6% of hydrogen peroxide and Philips Zoom WhiteSpeed system. Study showed that Philips Zoom whitening system were effective, permanent for up to 12–15 months post-whitening and nearly sensitivity-free.

***Keywords:*** teeth whitening, philips zoom, sensitivity, colour stability, bleaching, 6% hydrogen peroxide

## 1. Introduction

### 1.1. Teeth whitening

Teeth bleaching is one of the most conservative and effective dental treatments to improve or enhance a patient's smile. In-office teeth whitening can be done using different concentrations of hydrogen peroxide (HP) or carbamide peroxide (CP), between 5% and 40% [1] with additional light source such as light emitting diode (LED), LED plus lasers, lasers, ultraviolet lamp, halogen curing lights, non-thermal atmospheric pressure plasmas (NAPP) [2] [3] [4] [5]. Supplementary light source allows to use lower gel concentration and improve whitening of vital teeth [6]. Grazioli, Valente et al. (2018) concluded that HP concentration above the 15% level does not increase bleaching effectiveness, and may increase the possibility for alteration of enamel hardness, surface morphology, and acidity of the medium [7]. Additionally, Soares, Diana Gabriela et al. (2019) summarised that high amount of HP concentrations (35–40%) cause in vitro and vivo toxicity to pulp cells [8]. Philips Zoom in-office kit contains 6% HP gel which, according to the General Dental Council (GDC), is the highest concentration allowed in the European market.

The LED lamps are characterised by colour and wavelenght and they are supplied with filter that decreases the temperature of pulp [9]. Violet light has a slightly shorter wavelength than blue LED, greater frequency and lower penetrability and this leads to a significant pulp protection during whitening [10]. Philips Zoom WhiteSpeed LED is blue and its wavelength is 465 nm and it is absorbed fairly quickly by the chromophore bond (molecules that are located within enamel and dentin). When the molecules absorb the energy from the LED they become energised and this energy absorption makes it easier for the HP to break the bonds apart and as a result those smaller uncoloured chromophores fragments are converted into water and carbon dioxide [11] [12]. Consequently, the colour yellow is removed from the teeth.

### 1.2. Colour stability

Longevity of remarkable whitening effect depends on various aspects. Avoidance of any dark staining drinks, foods and smoking after whitening procedure is essential for 14 days due to considerably higher staining in bleached teeth compared with non-bleached teeth. [13] Furthermore, it is meaningful to refrain from eating for a couple of hours after bleaching. This gives the teeth time to re-hydrate before they are subjected to staining foods. By re-hydrating first it is thought that teeth are slower to re-stain. Nonetheless, after 2 weeks these stains that are formed from food and drinks are extrinsic so they can be quickly removed by professional cleaning [14]. Wearing individual trays with Philips Zoom DayWhite 6% HP for 12 days after bleaching ensure the stability of achieved colour during whitening and helps to enhance further whitening results. Further, DayWhite 6% HP has three desensitisers – ACP, potassium nitrate and fluoride which ensure that the superficial enamel microhardness and ultramorphology do not change [15]. Professional dental hygiene should be accomplished two times a year. Moreover, excellent and meticulous individual dental hygiene plays a crucial part to maintain a white smile. It incorporates cleaning of interdental spaces with brushes and floss, brushing teeth with non-abrasive

toothpaste everyday and with abrasive toothpaste once a week. This regimen contributes to the stability of achieved colour during whitening.

### 1.3. Teeth sensitivity

Teeth sensitivity, also known as hypersensitivity, is a sharp, short, sudden pain that can affect one or more teeth [16]. It can be caused by thermal changes, tactile, osmotic, temporarily chemical changes like whitening or when the dentin and dentinal tubules are exposed from thinning enamel or recession [17]. The more dentinal tubules are exposed the greater fluid movement irritates the tooth's nerve centre sending the pain signal to the brain [16] [17].

Whitening gels containing potassium nitrate, amorphous calcium phosphate (ACP) and fluoride minimise sensitivity during and after procedure. ACP remineralises teeth resulting in an increased hardness of the tissues, increased fluoride efficacy and obstruction of the dentin tubules. It helps to leave enamel smooth and shiny which offsets the effects of a low pH gel. Other products that do not have ACP can often leave the teeth looking chalky or rough. This desensitiser is absorbed fairly quickly and remains on the tooth structure even after it's been removed but it will dissipate fairly quickly if the patient eats or drinks immediately after using it. Potassium nitrate ($KNO_3$) is a highly effective agent used to reduce sensitivity. It works by penetrating into enamel and dentin making its way to the dental pulp where the nerves are located. The Potassium ions interrupt the transmission of pain signals the nerves send to the brain creating a calming effect on the sensory nerve by averting the nerve from repolarizing after it has depolirized in a pain cycle [18] [19]. Fluoride is a beneficial desensitiser which forms a calcium fluoride layer on the enamel. This layer is later dissolved and diffuses into the enamel, saliva or pellicle resulting in stimulating remineralisation and decreasing teeth sensitivity [20] [21]. Kutuk, Zeynep B. et al. (2018) concluded that ACP, potassium Nitrate and fluoride did not affect the color change during whitening [22].

Bleaching agent's pH also plays an important part in teeth sensitivity. Ideally pH should be fairly neutral/alkaline and most of the whitening gels are typically much lower in pH making them acidic for the reason that HP is more stable at lower pH and also as an avoidance of its decomposing and significantly lower dissociation into free radicals. [23] [24] [25]. Decreased pH cause temporary roughening of the enamel [26] and damage to the pulp chamber, due to affection of HP excess [24]. Acidic HP whitening gels tend to dissociate into free radicals considerably less than neutral/alkaline pH gels. L. Balladares (2019) concluded that the amount of HP neutral/alkaline pH gels that reach the pulp chamber was lower than acidic pH gels [24]. Philips Zoom in-office 6% HP gel combined with pH-booster (Philips) has approximately 8.5 pH and take-home DayWhite 6% HP is 7.5–8.5 pH.

The findings of this study are necessary due to lack of whitening researches with 6% HP that investigate efficiency, colour stability and teeth sensitivity.

**Objective**: This retrospective study aimed to evaluate teeth whitening effectiveness and sensitivity after procedure. **Tasks**: 1) to evaluate colour efficiency immediately after teeth whitening; 2) to validate colour stability after 12–15 months; 3) to evaluate teeth sensitivity.

## 2. Method and materials

Lithuanian University of Health Sciences and the Bioethics centre approved this retrospective study (Nr. BEC-OF04). A total of 111 patients from A. Morkunas dental clinic from 2016 to 2019 were recruited for in-office teeth whitening treatment using 6% HP (Philips Zoom) with additional Philips Zoom WhiteSpeed light (blue LED 456 nm, 190 mW/cm$^2$, WhiteSpeed LED Accelerator), plus 12 days of at-home whitening with 6% HP (Philips Zoom DayWhite). The data of whitening results were analysed from patients medical/dental history records. All of the patients, who received teeth whitening were selected by the inclusion and exclusion criteria listed in Table 1. 82 female and 29 male were enrolled in this retrospective study. All subjects were scheduled for three visits as described below.

**Table 1.** Inclusion and exclusion criteria for patients

| Inclusion | Exclusion |
|---|---|
| • Adults (18+ years old).<br>• Good general health.<br>• No active caries.<br>• No restorations on anterior teeth.<br>• Healthy gums.<br>• Stain-free surface (surface should be polished with soda and a prophy brush with prophylaxis paste).<br>Opportunity to follow a white diet before (after professional dental hygiene) and after whitening for 2 weeks. | • Allergies to teeth bleaching products.<br>• Pregnant or lactating women.<br>• Those currently treated by their physician for a serious illness or disorder e.g. immune compromised, AIDS and uncontrolled diabetes etc.<br>• Light sensitive individuals, including those on PUVA (Psoralen + UV Radiation) or other photo chemotherapy.<br>• Patients taking any photo-reactive drugs or substances, whether over-the-counter (O.T.C.), prescription or homeopathic.<br>• Moderate or severe sensitivity.<br>• Advanced periodontal disease.<br>• Undergoing treatment for caries, gingivitis, periodontitis.<br>• Visible supragingival calculus.<br>• Orthodontic treatment.<br>Currently using chlorhexidine mouth rinse. |

### 2.1. First visit

Patients signed an informed consent about the services that are provided in the clinic, medical/dental history records and teeth whitening agreement. Prior to whitening procedure professional dental hygiene was performed to all subjects. It consists of three parts: removal of hard and soft plaque above and under the gums safely by hand instruments, removal of pigmented plaque with soda powder (KaVo PROPHYpearls™, calcium carbonate) and finishing by polishing teeth with prophy-paste (VOCO Clean Joy (coarse (red) RDA = 195, fine (green) RDA = 16) and ApaCare polishing paste RDA = 150). The accurate impressions using alginate material (Cavex Cream Alginate) were taken after dental hygiene procedure and sent to laboratory. The trays were made following the recommendations by dental technicians that the thickness of them should be 1mm. This allows sufficient flexibility of the trays when the patient is inserting and removing it from their mouth. Patients were informed to avoid any dark staining drinks, foods and smoking before whitening procedure. This allows to obtain maximum stain-free surfaces and to get remarkable results.

### 2.2. Second visit

All patients brushed their teeth with a toothbrush and a toothpaste. Teeth were not polished in office before whitening by reason of dental pellicle provides a natural protection from extrinsic acid challenges and as consequence HP is capable of to penetrate to the enamel and bleach the chromophores. The colour of teeth was evaluated at baseline and immediately after the whitening session using the digital Easyshade V spectrophotometer (Vita, Zahnfabrik, Germany) that provides statistically more reliable colour measurements. The spectrophotometer was used with VITA classical A1–D4 shade system for the reason that it was frequently used in the clinic and it was the principal shade system used in Philips Zoom whitening. The VITA Classical Shade Guide includes 16 tabs from lightest to darkest as follows: B1, A1, B2, D2, A2, C1, C2, D4, A3, D3, B3, A3.5, B4, C3, A4, C4 (Table 2).
Teeth sensitivity was assessed immediately after the procedure.
All subjects were provided with custom made trays and at-home whitening gel (Philips Zoom DayWhite 6% HP). At-home whitening was prescribed for 12 days starting 24 hours after in-office whitening. DayWhite with 6% HP wear time: 60 minutes daily. Patients were informed to avoid any dark staining drinks, foods and smoking after whitening procedure for 14 days.

### 2.3. Third visit

Clinical colour stability of the whitening system was obtained by colour change in the spectrophotometer after 12–15 months.

**Table 2.** Shade ranging from 1 to 16 (brightest to darkest) according to VITA Classical Shade Guide, VITA Zahnfabrik, Bad Säckingen, Germany

| Shade | Value |
|---|---|
| B1 | 1 |
| A1 | 2 |
| B2 | 3 |
| D2 | 4 |
| A2 | 5 |
| C1 | 6 |
| C2 | 7 |
| D4 | 8 |
| A3 | 9 |
| D3 | 10 |
| B3 | 11 |
| A3.5 | 12 |
| B4 | 13 |
| C3 | 14 |
| A4 | 15 |
| C4 | 16 |

## 3. Results

Medical/dental history records of 111 patients were assessed and the mean mean age was 32.08 (range of 18–64 years) with standard deviation of 8.9 participated in this research.
Figure 1 depicts that teeth colour was assessed before whitening and more than three fifths (67.5%) of patients shade value was A2 (29.7%), A3 (21.6%), A1 (16.2%). Alternative shade value vary from 7.2% to 0.9%. Shade value B1 and D2 were not investigated in this research. Figure 1 shows that 99,1% of patients teeth after whitening reached maximum values of B1 (80.2%) and A1 (18.9%). Only 0.9% of patients teeth reached A2 shade value.
In accordance with Kolmogorov-Smirnov and Shapiro-Wilk results do not match normality while comparing teeth colours assessment before and after whitening. Therefore results were analysed by Wilcoxon test. There was a significant difference between teeth colour before and after whitening ($p < 0.001$).
Only 1.8% of patients reported teeth sensitivity immediately after whitening (Table 3).

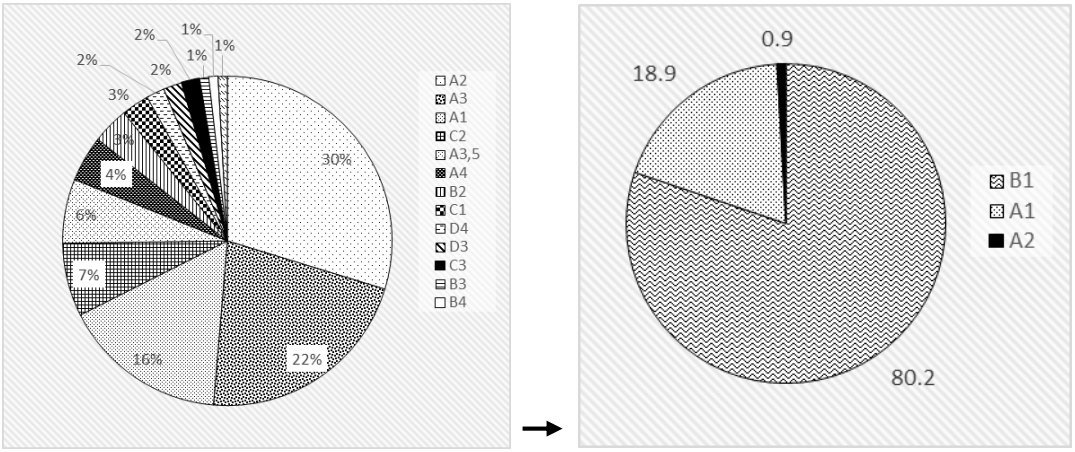


**Fig. 1.** Colour before whitening and after whitening was evaluated at baseline and immediately after the whitening session

**Table 3.** Teeth sensitivity

| Sensitivity | | Frequency | Percent | Valid Percent | Cumulative Percent |
|---|---|---|---|---|---|
| Valid | | | | | |
| | Not sensitive | 108 | 97.3 | 98.2 | 98.2 |
| | Sensitive | 2 | 1.8 | 1.8 | 100.0 |
| | Total | 110 | 99.1 | 100.0 | |
| Missing system | | 1 | 0.9 | | |
| | Total | 111 | 100 | | |

### 3.1. Colour stability

Colour stability was assessed to those who had whitening during 2016–2018 for the reason that 12–15 month period was passed. Teeth whitening with Philips Zoom system was performed to 11 patients in 2016, to 22 patients in 2017 and to 39 patients in 2018. Nonetheless not all of the patients returned to the clinic for teeth shade evaluation. 7 patients, who had whitening procedure in 2016, teeth shade B1 value after 3 years decreases nearly to A1 and A2 values. 17 patients who had the procedure in 2017 have the same tendency: B1 shade value reduces to close A1 and A2 values. Further, 34 patients who had whitening in 2018, have the same trend of decreasing from B1 to A1 and A2.

All patients were divided into two groups: the ones who have no significant darkening occurred for at least 1 year recall and others whose whitening effectiveness decreased dramatically. Data were analysed using Fischer's exact test. There was a significant association between teeth whitening and colour stability (Fisher's Exact $p < 0.001$).

## 4. Conclusions

1) In-office whitening with low concentration of HP (6%) activated by Philips Zoom WhiteSpeed LED light was effective because the maximum values of B1 and A1 was reached for the majority of the patients.

2) Colour stability after in-office whitening combined with take-home whitening gel of 6% HP (DayWhite) used with individual trays for 12 days after the procedure was permanent for up to 12–15 months post-whitening.

3) The results indicated that teeth whitening with Philips Zoom system is nearly sensitivity-free.

## 5. References

1. Kwon S. R. and Wertz P. W. Review of the mechanism of tooth whitening. J Esthet Restor Dent. 2015; 27(5): 240-257.
2. Mondelli, R. F. L., Soares A. F., Pangrazio, E. G. K., Wang L., Ishikiriama S. K. and Bombonatti J. F. S. Evaluation of temperature increase during in-office bleaching. Journal of Applied Oral Science. 2016; 24(2):136-141.
3. Alqahtani M. Q. Tooth-bleaching procedures and their controversial effects: a literature review. Saudi Dent J. 2014; 26(2):33-46. doi: 10.1016/j.sdentj.2014.02.002.
4. Baroudi K. and Hassan N. A. The effect of light-activation sources on tooth bleaching. Niger Med J. 2014; 55(5):363-368. doi: 10.4103/0300-1652.140316.
5. Mondelli R. F., Azevedo J. F, Francisconi A. C., Almeida C. M. and Ishikiriama S. K. Comparative clinical study of the effectiveness of different dental bleaching methods – two year follow-up. J Appl Oral Sci. 2012; 20(4):435-443. doi: 10.1590/s1678-77572012000400008.
6. Kwon S. R., Kurti S. R., Oyoyo U. and Li Y. Effect of light-activated tooth whitening on color change. J Esthet Restor Dent. 2015; 27:S10-S17. doi: 10.1111/jerd.12142.
7. Grazioli G., Valente L. L., Isolan C. P., Pinheiro H. A., Duarte C. G. and Munchow E. A. Bleaching and enamel surface interactions resulting from the use of highly-concentrated bleaching gels. Arch. Oral Biol. 2018; 87:157-162.
8. Soares D. G., Marcomini N., Duque C. Caroline de Oliveira, Bordini E. A. F., Zuta U. O., Basso F. G., Hebling J. and Costa C. Alberto de Souza. Increased whitening efficacy and reduced cytotoxicity are achieved by the chemical activation of a highly concentrated hydrogen peroxide bleaching gel. Journal of Applied Oral Science, 27, e20180453. Epub August 12, 2019. https://dx.doi.org/10.1590/1678-7757-2018-0453
9. Lo Giudice R., Pantaleo G., Lizio A. et al. Clinical and spectrophotometric evaluation of LED and laser activated teeth bleaching. Open Dent J. 2016; 10:242-250. Published 2016 May 31. doi: 10.2174/1874210601610010242.

10. Santos A. E. C. G. D., Bussadori S. K., Pinto M. M. et al. Evaluation of in-office tooth whitening treatment with violet LED: protocol for a randomised controlled clinical trial. BMJ Open. 2018; 8(9):e021414. Published 2018 Sep 4. doi: 10.1136/bmjopen-2017-021414.
11. Coceska E., Gjorgievska E., Coleman N J., Gabric D., Slipper I. J., Stevanovic M. et al. Enamel alteration following tooth bleaching and remineralization. J. Microsc. 2016; 262:232-244. doi: 10.1111/jmi.12357.
12. Kwon S. R. and Wertz P. W. Review of the mechanism of tooth whitening. J Esthet Restor Dent. 2015; 27(5): 240-257.
13. Shereen S. A., Anne L. H. and William M. J. Effect of bleaching on tooth discolouration from food colourant in vitro. Journal of Dentistry, Volume 39, Supplement 3, 2011, Pages e52-e56.
14. Tay L. Y., Kose C., Herrera D. R., Reis A. and Loguercio A. D. Long-term efficacy of in-office and at-home bleaching: A 2-year double-blind randomized clinical trial. Am J Dent. 2012; 25(4):199-204.
15. Lilaj B., Dauti R., Agis H., Schmid-Schwap M., Franz A., Kanz F., Moritz A., Schedle A. and, Cvikl B. Comparison of bleaching products with up to 6% and with more than 6% hydrogen peroxide: whitening efficacy using BI and WID and aide effects – an in vitro study. Journal Frontiers in Physiology, Volume 10, 2019, Pages 919, doi: 10.3389/fphys.2019.00919, ISSN 1664-042X.
16. Haneet, R. K. and Vandana, L. K. Prevalence of dentinal hypersensitivity and study of associated factors: a cross-sectional study based on the general dental population of Davangere, Karnataka, India. Int Dent J. 2016; 66:49-57. doi: 10.1111/idj.12206.
17. Marto C. M., Baptista P. A., Nunes T. et al. Evaluation of the efficacy of dentin hypersensitivity treatments – a systematic review and follow-up analysis. J Oral Rehabil. 2019; 46:952-990.
18. Nanjundasetty J. K. and Ashrafulla M. Efficacy of desensitizing agents on postoperative sensitivity following an in-office vital tooth bleaching: a randomized controlled clinical trial. J Conserv Dent. 2016; 19(3):207-211. doi: 10.4103/0972- 0707.181927
19. Maran B. M., Vochikovski L., de Andrade Hortkoff D. R., Stanislawczuk R., Loguercio A. D. and Reis A. Tooth sensitivity with a desensitizing-containing at- home bleaching gel – a randomized triple-blind clinical trial. J Dent. 2018; 72:64-70.
20. Alencar C. D. M., De Paula B. L. F., Araújo J. L. N., Alves E. B., De Albuquerque Jassé F. F. and Silva C. M. Effect of low-level laser therapy combined with 5000 parts per million fluoride dentifrice on postbleaching sensitivity: A clinical, randomized, and double-blind study. J Esthet Restor Dent. 2018; 30:352-359.
21. Bollineni S., Janga R. K., Venugopal L., Reddy I. R., Babu P. R. and Kumar S. S. Role of fluoridated carbamide peroxide whitening gel in the remineralization of demineralized enamel: An in vitro study. J Int Soc Prev Community Dent. 2014; 4(2):117-121. doi: 10.4103/2231-0762.137638.
22. Kutuk Z. B., Ergin E., Cakir F. Y. and Gurgan S. Effects of in-office bleaching agent combined with different desensitizing agents on enamel. J Appl Oral Sci. 2018; 27:e20180233. Published 2018 Nov 8. doi: 10.1590/1678-7757-2018-0233.
23. Bersezio C., Martín J., Prieto M. V. et al. One-year bleaching efficacy using two HP products with different pH: a double-blind randomized clinical trial. J Esthet Restor Dent. 2019; 1-7.
24. Balladares L., Alegría-Acevedo L. F., Montenegro A., Arana-Gordillo L. A., Pulido C., Salazar-Gracez M. T., Reis A. and Loguercio A. D. (2019). Effects of pH and application technique of in-office bleaching gels on hydrogen peroxide penetration into the pulp chamber. Operative Dentistry. 10.2341/18-148-L.
25. Torres C. R., Crastechini E., Feitosa F. A., Pucci C. R. and Borges A. B. Influence of pH on the effectiveness of hydrogen peroxide whitening. Oper Dent. 2014; 39( 6): E261-E268.
26. Ito Y., Otsuki M. and Tagami J. Effect of pH conditioners on tooth bleaching. Clin Exp Dent Res. 2019; 5(3):212-218. Published 2019 Feb 19. doi: 10.1002/cre2.172.

*MEDICAL PHYSICS IN THE BALTIC STATES 14 (2019)*

Proceedings of International Conference "Medical Physics 2019"
7 – 9 November 2019, Kaunas, Lithuania

# MAIN PIEZOELECTRIC PARAMETERS OF BONE MEASURED BY INTERFEROMETRIC METHODS

Virgilijus MINIALGA
Department of Physics at Kaunas University of Technology
Virgilijus.minialga@ktu.lt

***Abstract*:** Piezoelectric bone parameters have been studied by other authors using various methods and states. In the case of direct piezoelectric testing, there is a charge lack of electrical resistance of the bone.
The electric field applied to the test sample redistributes charges in inverse piezoelectric phenomenon and causes sample geometrical changes.
The Michelson laser interferometer was adapted to measure submicron bone specimen shifts in our experiments. The resulting bone piezoelectric coefficient values were about 30 pC / N.

***Keywords*:** Piezoelectricity, bone piezoelectricity, Michelson laser interferometer

## 1. Introduction

Piezo-materials have a direct piezo effect, when an electrical charge is produced when mechanically stressed. The opposite may also be true: the reverse piezo effect occurs when the applied voltage changes the dimensions of the piezo material. Such materials include quartz, Segnet salt, lead zirconium titanate ceramic, polyvinylidene difluoride **(**PVDF**)** and bone. Piezo-ceramics are very widely used in a variety of devices because they are compact and easy-to-control. Piezoelectricity is also a beneficial property of the bone, as this feature allows bone to regenerate and be treated more effectively.
Bone piezoelectric properties are not as expressed when compared to the best-known piezoelectric materials. Therefore, sensitive mechanical displacement measurement methods should be used. Laser interferometric techniques are well suited for such research.
Michelson laser interferometer was used to measure specimen shifts in inverse piezoelectric phenomenon experiments.
Laser interferometer has its lowest sensitivity limits. Therefore the lowest values of experiment conditions should be evaluated.
Michelson interferometer with He-Ne laser was used in this experiment to measure the displacement factor $\Delta h$ and piezoelectric coefficient $d_{33}$ for the reverse piezoelectric effect of pig and ox bones. Other parameters were calculated using displacement factor: Young's modulus, relative dielectric permeability.

### 1.1. Main piezoelectric parameters

Dimensional changes can be calculated by the following formulas, when electrical voltage $U_3$ is connected to the piezoelectric plate in the vertical direction [1]:

$$\Delta l = d_{31} \cdot U_3 \cdot l/h, \quad (1)$$
$$\Delta w = d_{32} \cdot U_3 \cdot w/h, \quad (2)$$
$$\Delta h = d_{33} \cdot U_3, \quad (3)$$

where $l$ and $\Delta l$ are length and its change, $w$ and $\Delta w$ are the width and its change, $h$ and $\Delta h$ are thickness and its change of the rectangular specimen, $d_{ik}$ are corresponding piezoelectric coefficients.
Force generated by the piezo-material depends on the voltage applied to the plate, the relative dielectric permeability, the piezoelectric constant, plate's surface area, and the thickness of the plate [1]. Force $F_3$ generated by the piezo specimen can be calculated using the formula:

$$U_3 = \frac{d_{33} F_3 h}{\varepsilon_0 \varepsilon_r S_3} \quad (4)$$

where $\varepsilon_0$ - vacuum dielectric permeability; $\varepsilon_r$ is the relative dielectric permeability of the specimen; $S_i$ - specimen surface area.
Relative dielectric permeability is given by the formula

$$\varepsilon_r = \frac{Ch}{\varepsilon_0 S_3} \quad (5)$$

where C is the electrical capacity of specimen,
Young's modulus $E$ is found by the formula

$$\sigma = E \frac{\Delta h}{h} \quad \text{or} \quad E = \frac{F/S}{\Delta h/h} \quad (6)$$

where $\sigma$ is the mechanical stress.

### 1.2. Structure of the bone

Bone tissue is made up of bone cells and solid mineralized extracellular material. The extracellular matrix is also called the bone matrix and contains organic and inorganic elements. Organic part is Type I collagen and its parent material, as well as proteoglycans, proteins and osteopontin. The inorganic part is hydroxyapatite; this part is amorphous [2].
Biological processes in all bones are accompanied by the electrical phenomena that are related to piezoelectric properties. Japanese scientists Fukada and Yasuda were the first to prove this by examining human bone. They have experimentally found a direct and inverse piezoelectric effect in bone [3]. Later, these scientists studied animal tendons, which are piezoelectric and contain almost pure collagen [4]. Bone walls themselves contain many thin layers in which collagen fibrils form a helical configuration around the bone axis (Fig. 1)

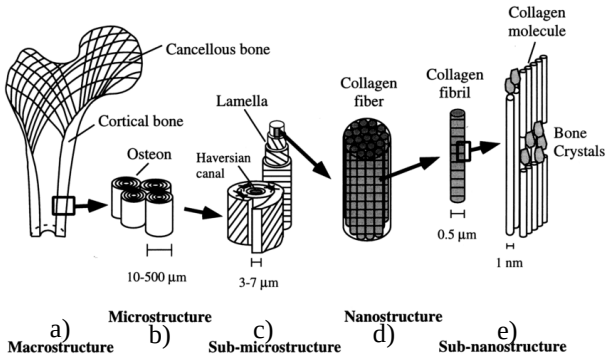


**Fig. 1**. Hierarchical structural organization of bone:(a) cortical and cancellous bone; (b) osteons with Haversian systems; (c) lamellae; (d) collagen fiber assemblies of collagen fibrils; (e) bone mineral crystals, collagen molecules, and non-collagenous proteins [2]

Piezoelectric properties of the bone are generally attributed to collagen fibrils (Fig. 1). Because collagen molecules contain charge carriers, when bone is mechanically exposed, electric dipoles are formed and thus a direct piezoelectric effect occurs [5].
M. Otter and other researchers studied three different samples: healthy bone, non-mineralized bone (hydroxyapatite removed), and inorganic bone (removed collagen) by measuring their electrical potential. They found that the potential was highest in those samples that did not have collagen removed [6].
Israeli scientists have studied the human tibia with a piezo-force microscope (PFM), a modified atomic force microscope. Alternating current was applied to the tip of the microscope probe and the displacement of the specimen was recorded accordingly, showing this inverse piezoelectric effect. A linear relationship between the applied voltage and the piezo phenomenon was observed during the study [7].
Fukada and Hara researchers found in their investigations of dependence the piezoelectric phenomenon on heating, that it disappears when samples were heated above 150 ° C, because this temperature irreversibly changes the structure of collagen in the bone.

Also after bone fractures, various bone components, including collagen fibers, are destroyed. As a result, electrical phenomena in the bone are disrupted. Therefore, the use of an artificial external variable electromagnetic field can promote bone healing (Fig. 2). Prior to this, it is very important to match the generated field so it to be similar to the electric field generated by natural bone [8].

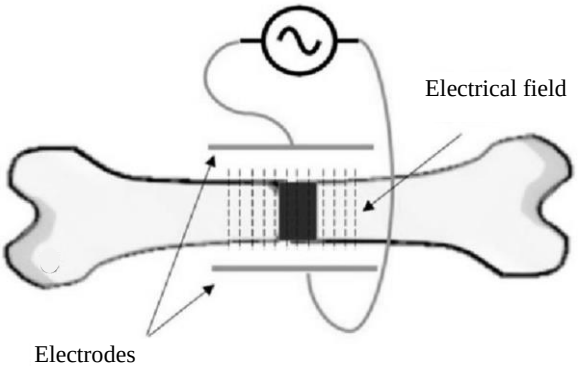


**Fig.2**. Electrical stimulation of bone healing diagram [8]

### 2.1. Laser interferometer

Michelson laser interferometer was prepared for the mechanical displacement measurements (Fig.3). It consisted of a He - Ne laser, a coherent light source with a wavelength $\lambda$ = 633 nm, a stationary fixed mirror, a piezo-material mirror and a photo sensor. Experiments were performed with the PC Scope 500 computer oscilloscope and the PC Labs 2000 Velleman software.

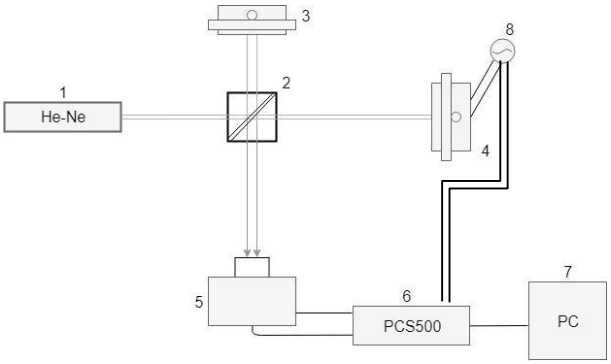


**Fig. 3**. Diagram of applied Michelson interferometer; 1 is laser, 2 is light beam divider, 3 is stable mirror, 4 is mirror with piezo-material, 5 is photo-sensor, 6 is oscilloscope block, 7 is personal computer, 8 is source of variable electrical voltage

After division by beam divider (2) two beams reflected from the mirrors (3) and (4) go to photo-sensor (5). This photo-sensor produces electrical voltage which is measured by PC scope (6). The result of the interference depends on the change in the position of the mirror (4) which is displaced by the change in the thickness of the piezo-material. Thus, a change in the interferometer signal indicates a change in sample thickness. Beams of light go forward and back to the mirrors. Therefore displacement of moveable mirror can be calculated according to formula

$$\Delta h = N\frac{\lambda}{4} \qquad (8)$$

where $N$ is number of maximum-minimum light intensity changes on photo-sensor.
A moveable mirror (4) was attached to piezo-material and fixed in the Michelson interferometer using mounting arrangement shown in Fig. 4.

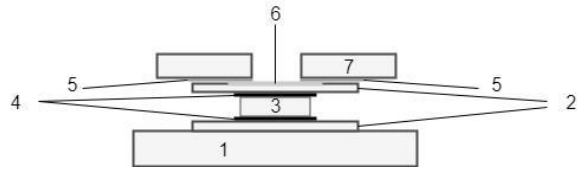


**Fig. 4**. Piezo-material attachment unit: 1 is- base; 2 are Teflon layers (PTFE film); 3 is piezo-material; 4 are electrodes; 5 is rubber layer; 6 is mirror; 7 is the oppressor

### 2.2. Measurement procedure

Required value of displacement for measurements in Michelson interferometer used should be about 300nm. Value of required voltage was calculated using approximate values of piezoelectric constants of piezo-materials. Voltage value of about 1000 V was obtained for bone specimens. Such voltage was fed from high DC voltage supply. This voltage was turned on for one second or less to piezo-material in attachment unit. Changes of applied voltage and of photo-sensor voltage were observed on oscilloscope screen. Typical view of obtained oscilloscope curves is presented in Fig. 5.

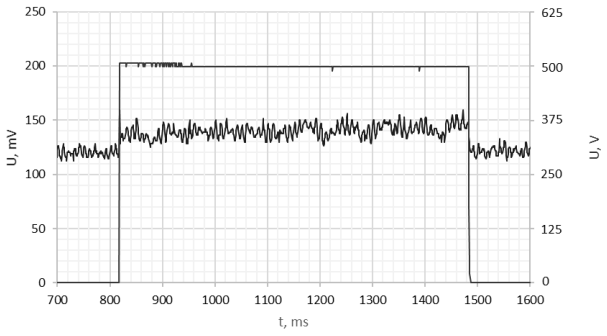


**Fig. 5**. Typical oscilloscope curves obtained in experiment: rectangular curve shows change of applied voltage to piezo-electric material; noisy curve means electrical signal from photodiode

The rectangular curve shows changes of applied voltage to piezoelectric material. Its value can be measured using right hand scale. Initially the voltage was not turned on, then it was connected for approximately one second and then turned off again.
The noisy curve is electrical signal from photodiode. It can be seen that it changes simultaneously with connected driving voltage. Its value can be measured using left hand scale. To evaluate amount of optical signal change in particular case the full voltage change from minimum to maximum values should be measured in advance.

## 3. Results

Five specimens of different type of pig and ox bones were prepared for investigations. Dimensions of the materials were measured before testing. Electrical capacity of the materials was measured simultaneously with the Mastech MY6243 multimeter. Geometrical and electrical parameters of specimens are presented in Table 1.

**Table 1**. Geometrical and electrical parameters of specimens

| Speci-men | Thick-ness, m | Width, m | Length, mm | S, $m^2$ | C, pF |
|---|---|---|---|---|---|
| 1 | $5\ 10^{-3}$ | $9\ 10^{-3}$ | $7\ 10^{-3}$ | $6{,}3\ 10^{-5}$ | 11 |
| 2 | $5\ 10^{-3}$ | $8\ 10^{-3}$ | $17\ 10^{-3}$ | $14\ 10^{-5}$ | 17 |
| 3 | $6\ 10^{-3}$ | $10\ 10^{-3}$ | $7\ 10^{-3}$ | $7\ 10^{-5}$ | 12 |
| 4 | $5\ 10^{-3}$ | $9\ 10^{-3}$ | $5\ 10^{-3}$ | $4{,}5\ 10^{-5}$ | 9 |
| 5 | $5\ 10^{-3}$ | $10\ 10^{-3}$ | $6\ 10^{-3}$ | $6\ 10^{-5}$ | 10 |

Specimen 1 was the part of pig rib, the specimen 2 was part of bull rib, the specimen 3 was pig rib heated at temperature 100 ºC, the specimen 4 was pig rib heated at temperature 120 ºC, the specimen 5 was pig rib heated at temperature 150 ºC for half hour.
After measurements of specimens thickness changes in Michelson interferometer and calculations the resulting table of piezoelectric parameters was obtained. They are presented in Table 2.

**Table 2.** Piezoelectric parameters of specimens.

| Speci-men | *Δh, nm* | $d_{33}$, *pm/V* | $\varepsilon_r$ | *F, N* | *E, GPa* |
|---|---|---|---|---|---|
| 1 | 15 | 30 | 95 | 174 | 8 |
| 2 | 40 | 80 | 65 | 100 | 9 |
| 3 | 30 | 50 | 100 | 130 | 3 |
| 4 | NA | NA | NA | NA | NA |
| 5 | NA | NA | NA | NA | NA |

Errors of results can reach as high as 50% because of noisy signals as can be seen in Fig. 5.

## 4. Conclusions

Measured piezoelectric coefficients were slightly higher than those of other authors. This may be due to the absence of electrical charge leakage when measured by the reverse piezoelectric effect and no reduction of electric field influence on the piezoelectric material lattice.
Specimens heated at temperatures higher than 100 ºC show no piezoelectric effect.
Similar results were obtained by scientists who studied thermally affected tendons and bones. Fukada first examined the tendons (composed of pure collagen) heated at various temperatures and found that collagen thermal contraction occurred above 120 °C and measurements were no longer possible [9].

## 5. References


1. Piezoelectricity [05-08-2019] Internet resorce: <http://www.pitt.edu/~qiw4/Academic/MEMS1082/Lecture%208-1.pdf>.
2. Rho, Jae-Young, Kuhn-Spearing, Liisa ir Zioupos, Peter. *Mechanical properties and the hierarchical structure of bone.* Medical Engineering and Physics 20. 1998, p. 92-102.
3. Fukada, Eiichi; Yasuda, Iwao. *On the Piezoelectric Effect of Bone*. Journal of the physical society of Japan. 1957, p. 1158-1162.
4. Fukada, Eiichi; Yasuda, Iwao. *Piezoelectric Effects in Collagen.* Japanese Journal of Applied Physics. 1964, p. 117-121.
5. Wang, Jessie. Piezoelectricity in Bone – Piezoelectric Effect and Bone Density. [06-21-2019 ]. Internet resorce: <https://www.bjultrasonic.com/piezoelectricity-in-bone/>.
6. Otter, Mark, Goheen, Susanna ir Williams, Wendell S. Streaming potentials in chemically modified bone. [06-21-2019]. Internet resorce: <https://onlinelibrary.wiley.com/doi/abs/10.1002/jor.1100060306>.
7. Halperin, C and others. Piezoelectric Effect in Human Bones Studied in Nanometer Scale. [06-21-2019]. Internet resorce: [<https://pubs.acs.org/doi/full/10.1021/nl049453i>.
8. Khalifeh, Jawad M. Electrical Stimulation and Bone Healing: A Review of Current Technology and Clinical Applications. [06-21-2019]. Internet resorce: <https://www.semanticscholar.org/paper/Electrical-Stimulation-and-Bone-Healing%3A-A-Review-Khalifeh-Zohny/53702bd1799972a7f0040dca8e05885812ccd484>.
9. Behari, Jitendra. *BIOPHYSICAL BONE BEHAVIOR Principles and Applications.* Singapore : John Wiley & Sons (Asia), 2009. 53-70 p. ISBN 978-0-470-82400-9.

*MEDICAL PHYSICS IN THE BALTIC STATES 14 (2019)*

Proceedings of International Conference "Medical Physics 2019"
9 - 11 November 2019, Kaunas, Lithuania

# DESIGN OF OPTICAL IMAGING SYSTEM FOR POLYMER GEL DOSIMETRY

Mantvydas MERKIS, Stevan VRBASKI, Benas Gabrielis URBONAVIČIUS, Leonas JAKEVIČIUS
Physics Department of Kaunas University of Technology, Lithuania;
mantvydas.merkis@ktu.edu;

***Abstract*.** Polymer gel dosimetry has substantial advantages when compared to other dosimetry techniques: polymer gel dosimetry allows the acquisition of dose distribution in three dimensions, boasts relatively good spatial accuracy, chemical composition of the gel dosimeters makes them biological tissue equivalent, which vastly improves the uncertainty of the measurements. However, existing gel scanning techniques, such as magnetic resonance imaging, are expensive and complicated, or affects the gel during read out, such as X-ray computed tomography [1]. In this article design of a simple open-source dose mapping optical scanning system for polymer gel dosimetry is described. Designed system consists of two main components – optical spectrometer and cuvette positioning system. MAGAT polymer gel was used for pilot testing of the system. Calibration and dose mapping experiments were performed.

***Keywords*:** gel dosimetry, polymer gels, polymer gels readout, MAGAT.

## 1. Introduction

Polymer gel dosimeters are made sensitive to radiation due to their chemical composition that changes its physical properties when irradiated. Scientists attracted attention to this area due to unique characteristics of polymer gels: they allow to evaluate 3D dose distribution, also, polymer gels are flexible, tissue equivalent and have good spatial accuracy [1].

However, readout of the polymer gels to acquire dose distributions is a complicated task. Expensive and sophisticated magnetic resonance imaging (MRI) is most frequent technique nowadays. However, there are several other approaches: computed tomography (CT), optical scanning and ultrasound. Each technique has its own advantages and disadvantages [1].

During magnetic resonance imaging relaxation rate of water molecules is measured. When polymer gel is irradiated, monomers are converted to polymers and mobility of water molecules as well as relaxation rate changes. MRI is considered as a gold standard in polymer gel dosimetry, however, it is complicated and expensive [2].

CT imaging can also be used for acquiring 3D dose distribution, because polymerization induces density changes in the gel. Unfortunately, CT imaging has significant drawbacks: low sensitivity of dose, also, the gel is irradiated with additional dose during imaging [3].

Ultrasound imaging of gels is perspective technique: ultrasound scanners are low cost and compact. During imaging time of flight of acoustic wave in the gel or amplitude difference between received and transmitted signals are registered. However this approach is still in development stage by several researchers [1,2].

Optical imaging can be alternative to expensive MRI. During optical scanning light transmission through the gel is measured because polymerisation induces scattering centres in the gel. Various systems can be used to scan whole volume of the gel: stepper motors, rotating mirrors. Optical imaging has significant advantages comparing to other measurement techniques: it has good resolution, high sensitivity, technique is simple. However, commercially available 3D optical scanning systems for polymer gels do not exist [1, 4].

In this work, design of dose mapping optical imaging system for polymer gel dosimetry is described. Optical imaging allows to achieve results comparable with MRI though implementation of the system is less sophisticated [4]. This makes optical imaging an ideal tool for gel characteristics investigation during gel development phase.

## 2. Materials and methods

Developed open-source optical imaging system for polymer gel imaging consists of several major components: Ocean Optics USB650 spectrometer, cuvette positioning system and a specialized in-house developed control software.

**Positioning system.** To achieve dose mapping capabilities a specialized sample positioning system was developed. Measured step size in a vertical direction is 0.15 mm. Step size in horizontal direction - 0,125 mm.

Other researchers consider a resolution of 0,5 mm to be sufficient [4].
Such resolution is achievable by using a set of stepper motors with a step resolution of 1/3600º and torque value of up to 2 Nm. System uses two separate stepper motor drivers to optimise the power requirements, so that the system could be power through the USB interface, which is also used for the control commands from the computer. This feature makes the system highly mobile for in-situ measurements, if needed. Block diagram of the systems' electronics are shown in figure 1. A general view of completed system is shown in figure 2.
Optical system consist of an Ocean Optics spectrometer and a specialized optical fiber adapter setup (Fig. 2).
Structural components were designed and manufactured in house using 3D printing and CNC laser cutting techniques.

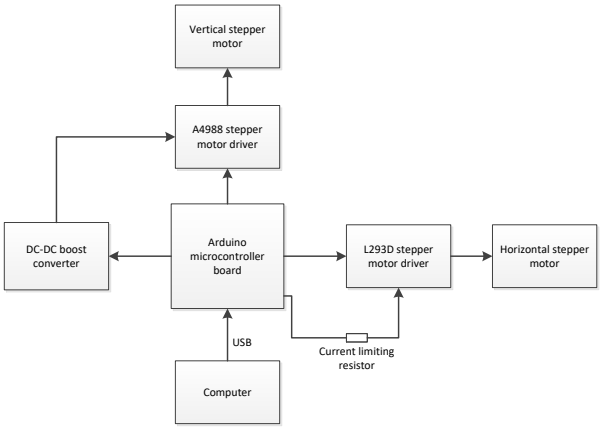


**Fig. 1.** Block diagram of the electronics of the positioning system

**Fig. 2.** USB650 spectrometer with the sample positioning system

A specialized firmware for the microcontroller was developed along side the PC control software for manipulating the sample and data acquisition from the spectrometer. Software and firmware was developed using Processing v3 programming language.

**Polymer gel.** Optical imaging system was tested with MAGAT polymer gel. Constituent parts of the MAGAT gel:

- distilled water
- gelatin
- methacrylic acid (MAA)
- tetrakis (hydroxymethyl) phosphonium chloride (THCP)

MAGAT polymer gel was prepared by the following procedure:
At the first stage 300 bloom gelatin (purchached from Sigma Aldrich) and destilated water were mixed together. Concentration of 8% (w/w) of gelatin was mixed with half of the required volume of distilled water. After that, this mixture was heated up to 45 ºC until clear solution is formed. At the same time, MAA is added in the 30% of the remaining water and THPC in the remaining 20%. All the solutions are then mixed together and allowed to cool down.
6MeV photons were used for irradiation of the samples in the dose range of 1 Gy to 7 Gy, with 1 Gy step. Irradiated gel was scanned using developed optical imaging system three days after irradiation. Transmitted light spectrum was acquired in 56 different points in the sample cuvette with gel and absorption spectrum was calculated. Measurement points were equally distributed across the surface of the sample: 8 slices were used with 7 measurement points at each slice. Data processing on gathered data was implemented. Outliers in the data were eliminated and average spectrum from multiple points was calculated.

## 4. Results and discussion

Using the developed optical scanning system several readout experiments were performed with irradiated MAGAT gel samples.
Dose mapping. Using acquired data is was possible to perform dose mapping of the samples in 2D. This is a valuable tool for determining the viability to use different dosimetric gel formulations in high gradient radiation fields, such as used in brachytherapy. An example of obtained dose mapping results with used MAGAT gel is shown in figure 3.

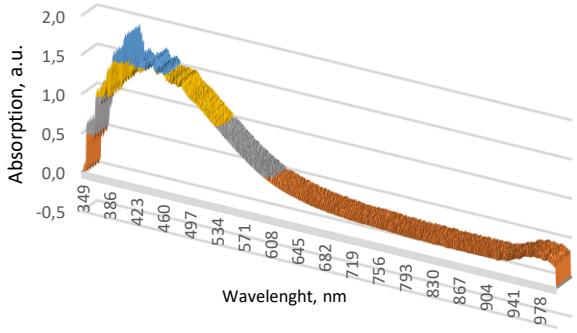


**Fig. 3.** 2D dose map for 3 Gy irradiated MAGAT dosimetic gel sample

Obtained dose maps for different irradiation doses were consistent (ex. Fig. 3). Calculated highest deviation form the average was no more than 3%. This correlates well with the fact that samples were irradiated in a uniform radiation field. Because of this observed consistency, an average spectrum was used for further data analysis. Average spectral data for different irradiation doses is shown in figure 4.

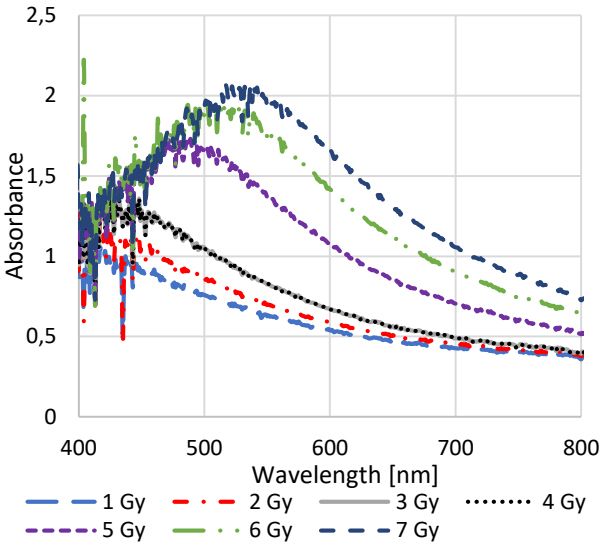


**Fig. 1.** With designed imaging system acquired absorption spectrum

Analysing this integral spectral data it is possible to determine the most optimal readout wavelength for the specific dosimetric gel formulation. At this wavelength the calibration curve with have the highest derivative value. Using the obtained experimental data it was determined that this wavelength is 582 nm. Graphically a calibration curve for the determined optimal wavelength is shown in figure 5. This curve can be approximated using linear dependency with $R^2$=0,9198.

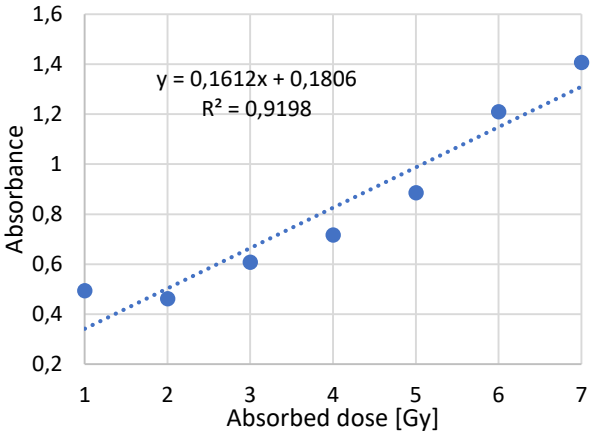


**Fig. 2.** MAGAT dosimetric gel calibration curve based on the obtained experimental data with the optical scanning system

To compare this results with a measurement from a single point on a sample, another set of measurements were performed with Ocean Optics USB 2000+ spectrometer. In these measurements only a single point on a sample was measured due to the construction of the measurement system. Graphically the calibration curve is shown in figure 6.

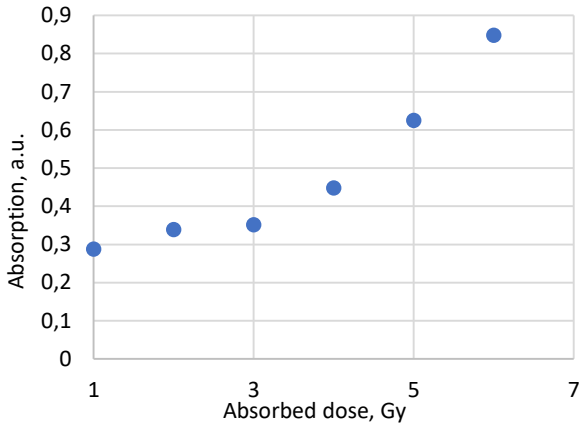


**Fig. 3.** With Ocean Optics USB 2000+ spectrometer acquired calibration curve

Interestingly using this spectrometer optimal wavelength for measurement was determined to be 660 nm. This difference in the optimal wavelength for the calibration curve shows that single point absorption measurements might not give the most reliable result, mainly due to thigh impact of possible measurement uncertainty, which is reduced in the case of 2D scanning of the sample (as previously discussed). It is also clear that linear function will not approximate obtained data points.

## 5. Conclusions

Developed optical imaging system for polymer gel dosimetry has great potential to acquire accurate dose distribution data. With designed device physical scanning point resolution in the vertical direction is 0,15 mm, in horizontal direction - 0,125 mm.

Optical imaging system was tested by performing MAGAT polymer gel dosimetric measurements. These experiments showed that the most optimal wavelength for reading out used MAGAT gel for dosimetric purposes is 580 nm. Comparing obtained data with another readout method showed that dose mapping capabilities are promising, although improvements are needed for data acquisition and processing algorithms used.

## Acknowledgement

This work was partly supported by research grant No MIP-S-17-104 of Lithuanian Research council

## 6. References

1. Baldock, Clive, et al. Polymer gel dosimetry. Physics in Medicine & Biology, 2010, 55.5: R1.
2. De Deene, Yves. How to scan polymer gels with MRI?. In: Journal of Physics: Conference Series. IOP Publishing, 2010. p. 012015.
3. Jirasek, A.; Hilts, M. An overview of polymer gel dosimetry using x-ray CT. In: J. Phys.: Conf. Ser. 2009. p. 10.1088.
4. Oldham, Mark, et al. Optical-CT gel-dosimetry I: Basic investigations. Medical physics, 2003, 30.4: 623-634.
5. Ocean Optics Icn, USB-650 Red Tide Spectrometer Manual. 2008.

*MEDICAL PHYSICS IN THE BALTIC STATES 14 (2019)*

Proceedings of International Conference "Medical Physics 2019"
7 – 9 November 2019, Kaunas, Lithuania

# ENHANCEMENT OF RADIOSENSITIVITY OF DOSE GELS

Stevan VRBASKI[1], Judita PUIŠO[1], Diana ADLIENĖ[1], Marija KAZIUKAITIENĖ[2]
[1]Kaunas University of Technology, Kaunas, Lithuania
[2]JSC "Affidea" Medical diagnostic imaging center in Kaunas, Lithuania
steva.vrbaski@gmail.com

***Abstract:*** Development of new radiotherapy techniques requires new and effective dose registration methods in radiotherapy. Dose gel dosimetry as only one possible 3D dose assessment method was used for the dose distribution verification in radiotherapy during the years, however due to the sensitivity issues it loses its positions. Among possible approaches how to improve the sensitivity of dose gels introduction of metal nanoparticles into gel solution is one of possible solutions.
The aim of this work was to perform comparative analysis for sensitivity of modified MAGAT dose gels without and with silver salt additives.
Investigation of gel samples was performed using UV-VIS spectroscopy method and MRI image processing using MRI.
It was shown, that silver nanoparticles/nanoclusters produced direct in irradiated gels contribute to some extent to the enhancement of gel sensitivity to irradiation, however in order to understand complex polymerization and radiolysis process more detailed analysis is needed.

***Keywords:*** dose gels, radiolysis of nanoparticles, dose sensitivity.

## 1. Introduction

Dose gels are known for decades as reliable dosimeter for the assessment of 3D dose distributions in irradiated volume [1]. Usually dose gels consist of one or two monomers that are tending to polymerize upon irradiation and form polymer networks. Polymerization level is the main parameter which is directly related to the absorbed dose at the spot. Most of these gels are water based thus indicating possible tissue equivalency which is requested applying dose gels for dose verification in radiotherapy [2].
There are many different chemical formulations of dose gels, depending on which and also on irradiation conditions the properties of these gels may vary significantly. Gels sensitivity to irradiation is a key issue when discussing their applicability as a dosimeter, however dose evaluation method sensitivity is also very important, since different method for the "read out" might be applied: MRI, X ray CT, optical CT, ultrasound, UV-VIS and many others [3-5] Since relative sensitivity of commonly used dose gels is low and varies between 0.9 for nPAG to 1.6 for VIPET [1, 6] there is a need to improve it. There are several methods that allow for the improvement of dose gel sensitivity: modification of gel's chemical content, admixing of specific additives or metal nanoparticles into gel solution [7-9] or addition of salts with the aim to produce nanoparticles inside the gel solution [10, 11].
It is well-known that metal Pt, Au, Ag, Cu and Al nanoparticles undergo a strong interaction with light because conduction electrons on metal surface may have collective oscillation when being exposed to specific wavelengths. A range of electromagnetic spectrum where light absorption dominates is called plasmon resonance absorption band. Exploration of this phenomenon enables possibility to reach higher registration sensitivity [12] and therefore distinguish smaller changes in absorbed dose inside the gel.
On other hand, metal nanoparticles with high atomic mass number are characterized by high cross-section for photoelectric effect, which is dominant at low photon irradiation energies. In this case the energy of ejected electron might not be very large with questionable ionization ability. Therefore, the size and shape of nanoparticles play an important role in the gels. Larger particles or formation of clusters leads to auto-absorption of electrons. As photon energy increases, Compton effect becomes dominant. Depending on their energy scattered photons might also be able to initiate photoelectric effect in another atom.
It is to point out that in some cases nanoparticles are introduced directly into the tumor with the aim to achieve higher than usual energy absorption in the irradiated target which is necessary for cancer treatment. In such a case application of dose gels containing nanoparticles is an elegant solution to reproduce dose distribution in irradiated volume.

## 2. Materials and methods

### 2.1. MAGAT gel

MAGAT gel is one of the most popular normoxic polymer gels [13, 14]. It consist of Methacrylic acid, MAA) (Sigma Aldrich), gelatin (300 bloom, Sigma Aldrich), distilled water and oxygen scavenger (hydroxymethyl) phosphonium chloride (tetrakis, THCP).

Prior to start gel preparation gelatin was admixed to a small amount of water and left for 15 min to swell. Then the rest of water was added and the solution was heated up to 45ºC under continuous stirring until the whole amount of gelatin was dissolved and the solution became clear. The solution was cooled down to 30ºC and the MAA was added drop by drop continuing to stir. Finally oxygen scavenger was added and prepared solution was poured into 4 ml standard PMMA cuvettes and immediately sealed. Samples were left for at least 6 hours in the room temperature for solidification. Prepared samples were covered with Al foil and left in dark place for 24 hours. Chemical content of prepared gels is provided in Table1.

**Table 1.** Chemical composition of MAGAT gels

| | **MAGAT** |
|---|---|
| Water | 88% |
| Gelatin | 5% |
| MAA | 7% |
| THPC | 10 mM |

### 2.2. Silver containing gels

Two batches of silver containing gels have been prepared. One of batches contained 4% (w/w) gelatin water solution with admixed 150 mM, 200 mM and 250 mM of 1M $AgNO_3$ solution in water respectively. Another batch was prepared by adding of small amount of $AgNO_3$ to the prepared MAGAT gel solution. Both types of gels were prepared and kept following the above disrobed procedure.

The irradiation of prepared gel samples sets was performed in Oncology Hospital of the Lithuanian University of Health Sciences. 6MeV photon beam of linear accelerator Clinac DMX (Varian) was used for irradiation. Other irradiation parameters were as follows: max dose depth was 1.5 cm; SSD was set to 100 cm; field size was10×10 cm2; dose rate was 3 Gy/min. Irradiation doses ranged from 1Gy to 9 Gy.

One sample from each different batch was not irradiated and kept for the reference.

### 2.3. Readout of gels

Two methods were applied for the analysis of irradiated dose gels and for estimation of dosimetric gel's sensitivity. Optical characteristics of gels were analyzed in the interval of wavelength between 250nm and 850nm using UV-VIS spectrometer Ocean Optics USB 4000. Absorbance and transmittance spectra were measured and corresponding gel's sensitivity to irradiation dose was evaluated using OriginPro and Microsoft Excel program packages.

Siemens MAGNETOM Altea 1.5 T MRI scanner was used for imaging of the irradiated gels. Images were processed using ImageJ and MathLab program packages and the dose gel sensitivity to the absorbed dose related to MRI read out method was evaluated.

## 3. Results

### 3.1. MAGAT gels

Polymer gels change their optical properties upon irradiation. Radiation induced crosslinking of monomers is responsible for color changes in irradiated polymer gel, which can be assessed by UV-VIS analysis method. The UV-VIS absorbance spectra for MAGAT gel samples irradiated to different doses are provided in Fig.1. The red shift of the absorbance maximum and appearance of the shoulder in spectrum which records formation of polymer clusters with the increasing absorbed dose can be clearly observed.

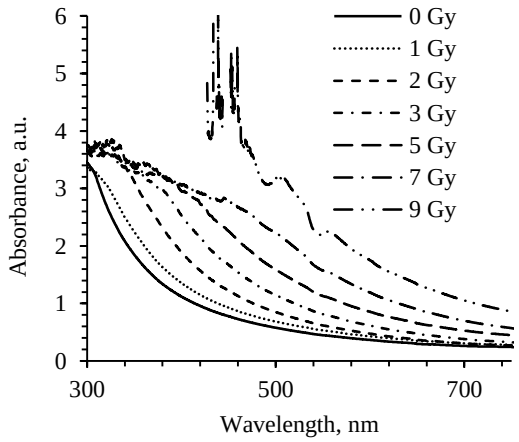


**Fig. 1** .Absorbance UV-VIS spectra of MAGAT

Relative MAGAT gel sensitivity to the irradiation dose can be estimated from the slope of the dose calibration curve, which is provided in Fig.2. At the wavelength of 600 nm estimated sensitivity value of MAGAT gel was 0.16 and was comparable with the sensitivity of other gels [1].

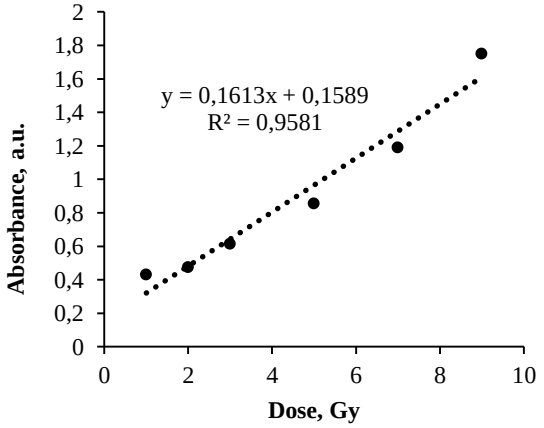


**Fig.2.** Dose calibration curve of MAGAT gel.

The same batch of MAGAT samples was scanned in MRI unit MAGNETOM Altea applying 1.5 T field. T2

MR weighted image of irradiated MAGAT gel samples is shown in Fig.3.

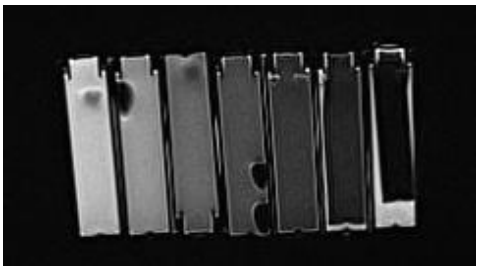

**Fig.3.** T2 MR weighted image of MAGAT gel samples irradiated to different doses.

Using ImageJ simple statistics MR images of the separate cuvettes were processed. The results of calculations are provided in a Table 2.

**Table 2.** Staistics of T2 MR image

| Dose [Gy] | Mean | Std. Dev. | Min | Max | Median |
|---|---|---|---|---|---|
| 0 | 189.606 | 4.327 | 176 | 206 | 190 |
| 1 | 150.736 | 3.917 | 139 | 161 | 151 |
| 2 | 101.094 | 4.226 | 85 | 111 | 102 |
| 3 | 72.601 | 5.100 | 58 | 103 | 73 |
| 5 | 53.848 | 3.597 | 43 | 66 | 54 |
| 7 | 37.256 | 3.455 | 23 | 46 | 37 |
| 9 | 12.299 | 2.851 | 5 | 21 | 12 |

The tendency of saturation was observed analyzing the MRI response, in irradiated MAGAT gel samples when the irradiation dose was increased to > 6 Gy (Fig.4). However in the interval of lower doses relative dose sensitivity value of 0.3 was achieved.

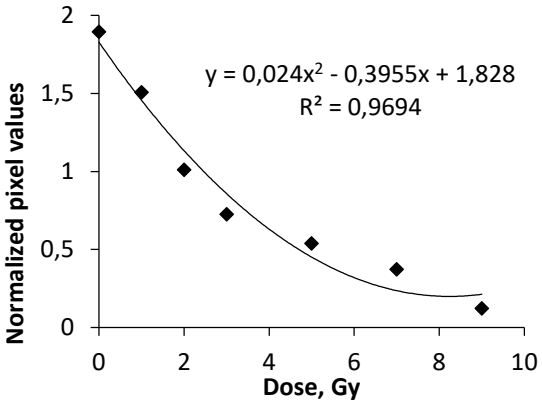


**Fig.4.** Normalized gel response to different irradiation doses.

### 3.2. AgNO3 gels

The main obstacle for application of gels containing silver salt for dosimetry purposes is their high photo sensitivity. This means that short after the gel preparation its color becomes yellowish, which indicates formation of silver structures inside the gel. To avoid this just after preparation gels were covered with Al foil and put in dark place. However we have not succeed to fully protect our gels from daily light impact.

Nevertheless the yellowish color of gels was changed significantly after irradiation in linear accelerator. The color became more brownish till red depending on the irradiation dose as it can be seen in the Fig.5.

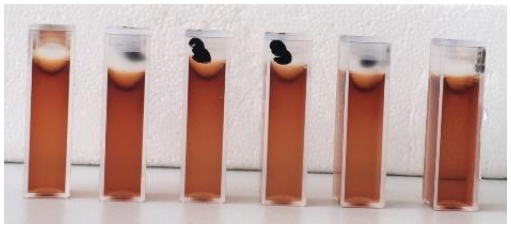

**Fig. 5.** $AgNo_3$ containing gel samples after irradiation to different doses.

Color changes in irradiated $AgNO_3$ containing gels is the first indicator that atomic silver nanoparticles or nanoclusters are formed in the gels. This hypothesis was supported by the results of UV-VIS spectroscopy. A small, however well expressed surface plasmon resonance peak was observed in all investigated absorbance spectra of the irradiated silver salt containing gel samples. UV-VIS spectra of gel samples containing 150 mM of $AgNO_3$ are provided in Fig.6.

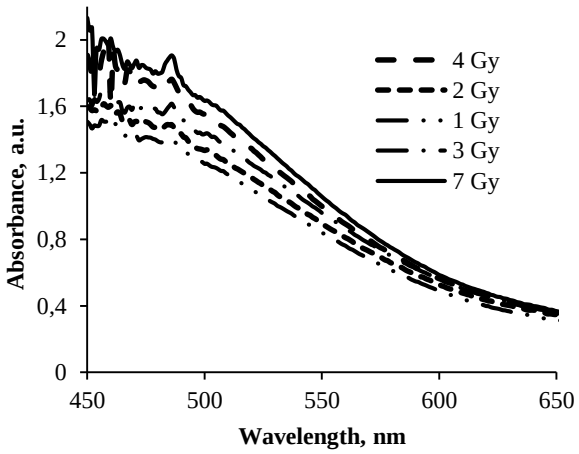


**Fig.6.** UV-VIS spectra of gel samples containing 150mM of $AgNO_3$ and irradiated to different doses.

More detailed analysis revealed that there were 2 peaks on each absorbance spectrum observed. This is direct approval that Ag nanoclusters were formed in the gels due to irradiation. The results of more detailed peak analysis are provided in Fig.7.

Taking into account that surface plasmon resonance was absorbed at 486 nm, it was roughly estimated that silver clusters of 70 nm in size were formed. Since the interval of irradiation doses was relative small, no peak red shift was observed with the increased dose, which indicated that no clusters or nanoparticles having other size or shape have been formed. However increasing peak intensity indicated the increase in the number of clusters/nanoparticles with the increased dose.

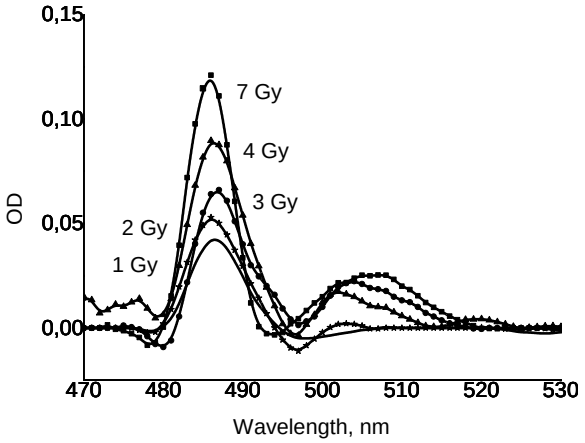


**Fig.7.** Surface plasmon resonance peak analysis for irradiated gels containing silver nitrate.

### 3.3. MAGAT gels +$AgNO_3$

The irradiation experiments performed with MAGAT gels containing small amount of silver nitrate failed. Prepared gels were already polymerized after 48 h of storage in dark place thus it was impossible to find any differences between gel samples irradiated to different doses (Fig.8.)

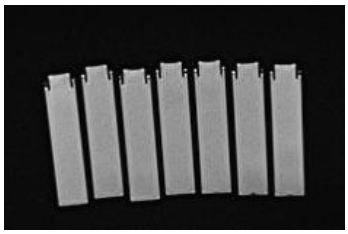

**Fig. 8.** T2 MR image of MAGAT gels with admixed small amount of $AgNO_3$ irradiated to different doses.

The issue was explained by the fact that dose gels are very sensitive to interaction with oxygen species that initiate immediate gel polymerization. Usually small amount of oxygen scavenger is added to the prepared gels to avoid molecular interactions with oxygen. We have used tetrakis as oxygen scavenger, however it contained Cl which most probably was reacting with $AgNO_3$ thus decreasing the possibility to avoid interaction of oxygen species in gels.

## 4. Conclusion

Dosimetry gels have no competition in terms of experimental verification of clinical 3D radiotherapy procedures applied for the treatment of cancer patients. Linear dose response of dose gels was estimated when optical UV-VIS method was applied for gel evaluation. MRI evaluation performed on gels didn't show linear dose response, however the sensitivity of MRI method was almost twice higher as compared to optical method in low dose region.

Possibility to sensitize gel adding silver nitrate to the water solution of gelatin has been investigated. It was shown that due to formation of silver nanoclusters in irradiated gels it is possible to enhance gel sensitivity by at least two times.

Experiments with adding of silver nitrate to MAGAT gel solution failed generally due to the interaction of oxygen scavenger with $AgNO_3$, since the gels were already polymerized after 48 h of storage.

## 5. References

1. Baldock C. Polymer gel dosimetry. Physics in Medicine and Biology. 2010, p. 55, R1–R63.
2. Silveira, M.A. Pavoni, J.F, Ba, O. (2017). Three-dimensional quality assurance of IMRT prostate plans using gel dosimetry, Phys Med. 34.1-6.
3. Lee, H., Roed1, Y., Ibbott, S. (2018). Dose rate and fractionation dependence of methacrylic acid based polymer gels using optical and MRI techniques, Department of Radiation Physics, UT MD Anderson Cancer Center, Houston, TX, 2018
4. Matrosic, C. et al (2017). Dosimetric comparison of DEFGEL and PAGAT formulae paired with an MRI acquisition. J. Phys.: Conf. Ser. 847. 012012
5. Urbonavicius, B., Adliene, D. (2018). In situ assessment of X-ray induced changes in polymerized gels using surface plasmon resonance detector. Nucl Instr. Meth. B. 435. 236-241.
6. De Deene, Hurley, Y., Venning, C., Vergote, A., Mather, Healy, K.., Baldock, C. (2002). A basic study of some normoxic polymer gel dosimeters. Phys. Med. Biol. 47, 3441–3463.
7. Vedelago, J., Mattea, F., Valente, M. (2018). Integration of Fricke gel dosimetry with Ag nanoparticles for experimental dose enhancement determination in theranostics, App. Rad. Isot. 141, 182-186.
8. S Ebenezer Suman Babu et al. (2017). Cerium nanoparticle effect on sensitivity of Fricke gel dosimeter: Initial investigation, IOP: Conference Series. 847 012053.
9. Khadem-Abolfazli, M., Mahdavi, M.Mahdavi, S.R.M, Ataei, Gh. (2013). Dose enhancement effect of gold nanoparticles on MAGICA polymer gel in mega voltage radiation therapy, Int. J. Rad. Res. 11(1): 55-6.
10. Torres, L, Slipping, J., Restuccia, N., Cuzzocre, S., Cutroneo, M., Barreca, M, Fazio, B., Marco, G.Di., Guglielmino, S. (2018)., Laser-generated bismuth nanoparticles for applications in imaging and radiotherapy. J. Phys. Chem. of Solids, 119, 62-70
11. Soliman, Y.S., (2014). Gamma-radiation induced synthesis of silver nanoparticles in gelatine and its application for radiotherapy dose measurements, J. Phys. and Chem. of Solids, 102, 60-67
12. Puišo, J., Adlienė, D., Guobienė, A., Prosyčevas, I., Plaipaitė-Nalivaiko, R. (2011). Modification of Ag-PVP nanocomposites by gamma irradiation. Mat. Sci. and Eng. B. 176 (19), 1562-1567.
13. Hurley, C., Venninga, A., Baldock, C.(2005). Study of a normoxic polymer gel dosimeter comprising methacrylic acid, gelatin and tetrakis (hydroxymethyl) phosphonium chloride (MAGAT), Appl. Rad. Isot. 63. 443–456.
14. Nik Noor Ashikin Nik Ab Razak. (2016) Optimization of the MAGAT gel dosimeter compositions. Iranian Journal of Radiation Research. 14(4). 305-311.

*MEDICAL PHYSICS IN THE BALTIC STATES 14 (2019)*

Proceedings of International Conference "Medical Physics 2019"
7 – 9 November 2019, Kaunas, Lithuania

# 3D PRINTED BOLUSES USAGE IN RADIOTHERAPY

Lali KESHELAVA[1], Artūras ANDREJAITIS[2],
Reda ČERAPAITĖ-TRUŠINSKIENĖ[3] Todorka DIMITROVA[4], Jurgita LAURIKAITIENĖ[1,2]
[1]Kaunas University of Technology, The Faculty of Mathematics and Natural Science, Kaunas, Lithuania;
[2]Oncological Hospital of Kaunas Clinics, Radiotherapy Department, Kaunas, Lithuania;
[3]Lithuanian University of Health Sciences, Physics, Mathematics and Biophysics Department, Kaunas, Lithuania;
Plovdiv University "Paisii Hilendarski", Plovdiv, Bulgaria
kkeshelava@gmail.com, jurgita.laurikaitiene@ktu.lt, andrejaitis@gmail.com, redcera@gmail.com, tldimitrova@abv.bg

***Abstract*:** Build-up material (bolus) appliance in radiotherapy gives the possibility to use bolus as an additional body for uneven and concaved surfaces, improving treatment procedure's outcome. Even if flexible silicone bolus is used the air gaps between bolus and patient's body are present. This has impact on the homogeneity and conformity of the dose distribution and respectively diminished absorbed dose to the patient's surface, e.g. skin. Using 3D printing techniques, it is possible to create individualized boluses, eliminating the impact of the air gaps, so assuring an accuracy of the treatment procedure.
In this work we introduce 3D printed patient related individualized bolus and the results on phantom surface dose measurements performed using the bolus.

***Keywords*:** Bolus, 2D film dosimetry, 3D printed PLA bolus

## 1. Introduction

Irradiation of the irregular (uneven and concaved) surfaces (for example, head and neck) [1] and tumours located near or at the surface (skin, scar and etc.) using high energy (MeV) photons, generate a lower dose on the irradiated surface ("skin sparing" effect) [2-4]. Due to this fact boluses as an additional body layer, which results in a better homogeneity and conformity of the dose to the body surface are used [2]. This leads to the better treatment outcome and also avoiding the risk of possible recurrences. It is known, that even if the standard flexible silicone bolus is used during treatment procedures, in the most cases it would be impossible to avoid air gaps between the patient's body and the bolus [4, 5], and the changes in an absorbed dose and dose distribution will be present. Possible solution of this problem is fixation of the bolus on the patient's surface using so called „sticking boluses" [5] or production of the individualized bolus, like 3D printed boluses might be [1, 6]. Using 3D printed technique it is possible to create patient related individualized boluses, which allow for avoiding or minimization of the air gaps between bolus and the patient surface, so eliminating the impact of the air gaps on the dose absorbed at the surface, so assuring the quality of the treatment procedure.
The aim of this work was to measure and analyse the irradiation doses on the phantom's surface using individualized 3D printed polylactic acid plastic (PLA) bolus and evaluate is suitability for further application in radiotherapy. evaluating their suitability for the usage in radiotherapy.

## 2. Methodology

*Irradiation procedure*. Linear accelerator "Varian DMX" was used for irradiation of experimental setup with the high energy photons ($E_{max}$ = 6 MeV) (Fig.1). Standard PMMA computed tomography (CT) head phantom [7] was used in experimental measurements to imitate rounded shape of any anatomic structure.

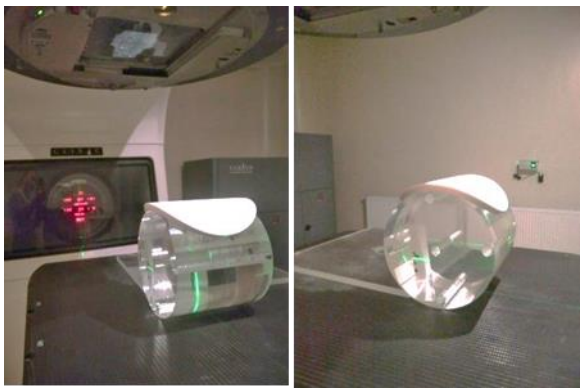

**Fig. 1.** Experimental setup: individualized 3D printed PLA bolus on the standard CT PMMA head phantom.

### 2.1. Printing of individualized 3D printed polylastic acid (PLA) bolus

Open code program package "3DS Max" was used to create a virtual curve-shaped bolus (Fig.2) which was later printed using 3D printer Zortrax M300 (Fig.3).

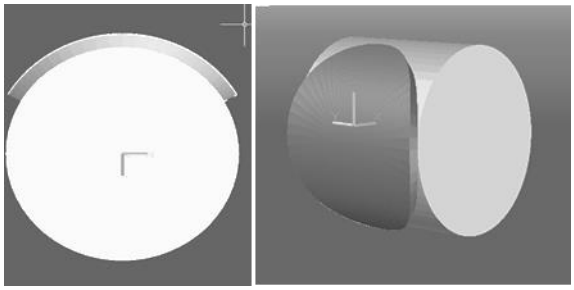

**Fig.2.** 3D visualization of head phantom and bolus development process in "3DS Max"

Individualized boluses were printed out of polylactic acid plastic (PLA) material, which is almost tissue equivalent material and can represent an additional body layer [8]. Different polymer infill ratio (90% and 100% was chosen for printing of boluses in order to evaluate the impact of this parameter on measurement results. The thickness of the 3D printed bolus was 1 cm due to the fact that the ordinary silicone bolus has the same thickness.

**Fig. 3**. Standard CT PMMA head phantom and 3D printed polylactic acid plastic (PLA) bolus.

### 2.2 GafChromic film dosimetry

Doses on a surface of the phantom were investigated using 2D GafChromic films EBT2, which were located under the bolus on the CT PMMA head phantom's surface. Prior to start experimental measurements GafChromic films were calibrated. For this reason sheets of Gafchromic films were cut into 1.5 cm x 1.5 cm pieces and irradiated in Linear accelerator to different doses from the range between 0 Gy and 3.0 Gy. 6 MeV photon beam was used for irradiation. The specific dose range was chosen due to the fact, that 2 Gy/ fraction are used to treat the patients in a standard external radiotherapy procedure. Irradiated GafChromic films were scanned 48 hours after irradiation procedure using HP Office Jet Pro 8600 scanner and analysed using red component mode. The image of irradiated pieces of GafChromic films used for calibration are provided in Fig 4,

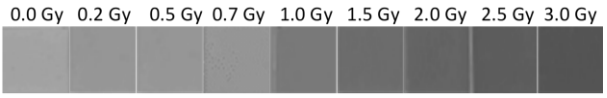


**Fig. 4.** Irradiated pieces of Gafchromic films EBT2 (red component).

All the irradiated films were analysed and evaluated using program "ImageJ", which allows for measuring of grayscale pixel values, that are used for recalculation of the optical density [9]:

$$OD = log_{10} \frac{PV_{unirradiated}}{PV_{afterirradiation}}, \qquad (1)$$

where $PV_{unirradiated}$ is the pixel value of film, which was not irradiated (0 Gy), and $PV_{afterirradiation}$ - pixel value of the film which was irradiated to specific dose (Fig.4).
Using recalculated optical densities derived from measured pixel values calibration curve was constructed (Fig.5).

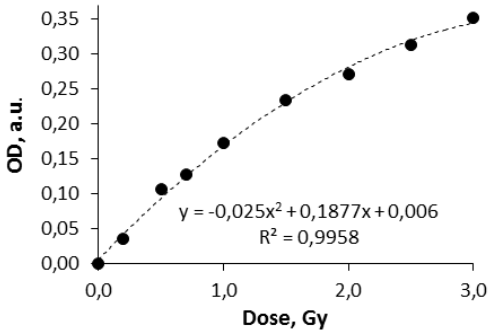


**Fig. 5.** Calibration curve of Gafchromic film EBT2.

### 3. Results and discussion

It is known, that application of boluses in high energy radiotherapy may increases the surface (skin) dose to the patient [3], while for the uneven and concaved surfaces it is possible to get more homogeneous dose distribution at the surface or in a volume [1]. The main problem for the uneven patients' surfaces which remains even if flexible standard silicone bolus is used, is the air gaps between the patient and bolus what results the reduction of the dose [4, 6]. Due to this application of patient related individualized boluses is of advantage. Creation of individualized boluses is possible using 3D printing technique. Analysis of the irradiation doses measured using individualized PLA bolus which was printed with 100 % infill, showed that the results could be comparable with the results of our previous study, where so called "sticking" bolus was used [6]. It was found that the difference between the results was 3.34 % when comparing the results of measurements performed with "sticking" bolus (estimated mean dose 2.02 Gy/fraction) with 2D film dosimetry measurements using individualized 3D printed PLA bolus with 100 % infill ratio (estimated mean dose 2.09 Gy/fraction). Observed discrepancies between 2D film dosimetry and treatment planning system settings could be related to possible calibration uncertainties introduced performing film calibration [10].

GafChromic film irradiation experiments performed with a 3D phantom printed with 90 % infill reviled, the the infill plays an important role when printing phantoms and boluses for radiation medicine applications. The printing pattern structure was clearly seen in the irradiated film, indicating patterned dose delivery to the skin in the case when bolus is printed with < 100% infill. The photographs of GafChromic films irradiated under the 3D boluses printed with different infills are provided in Fig.6.

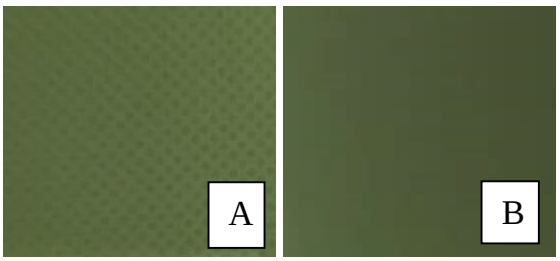


**Fig. 6.** The photographs of GafChromic films irradiated under PLA boluses: A - under "patterned" bolus, printed with 90% infill ratio; B - under bolus with 100% infill ratio.

Due to patterned delivery of dose in the case of bolus with 90% infill ratio application, it was decided to analyse absorbed doses at the dark and light spots on the film separately (Fig.7).

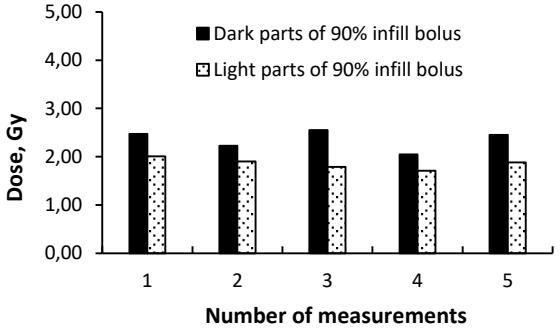


**Fig. 7.** Irradiation doses measured under the 3D printed PLA bolus with 90% infill ratio, analysing dark and light spots separately.

Evaluation of the doses at the dark spots showed good agreement (with a deviation of 4.06 %) between the results provided by treatment planning system when "sticking" bolus was used (mean dose 2.02 Gy) and the results of 2D films dosimetry using individualized 3D printed PLA bolus with 90 % infill (mean dose 2.10 Gy) The difference between the doses measured with differently printed boluses: with 90 % infill ratio and with 100 % infill ratio was rather small - only 0.21 % as it can be seen in Fig. 8. However it should be noted that "patterned" dose delivery may have additional uncertainties in dose delivery to the patient. So it is recommended to use boluses printed with 100% infill ratio, thus assuring more accurate dose registration using 2D film dosimetry.

Performed investigation indicates, that the individualized 3D printed PLA bolus with 100 % infill ratio could be successfully used in radiotherapy field, since it secures avoiding the air gaps, which usually influence changes in absorbed doses and their distribution, diminishing the quality of irradiation procedure. However for the case of the individualized 3D printed PLA bolus with 90 % infill ratio detailed analysis is still needed.

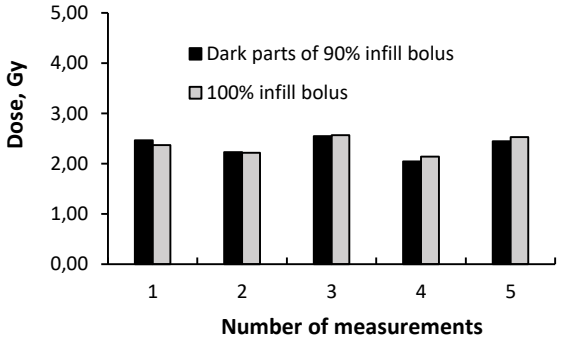


**Fig. 8.** Irradiation doses measured under the 3D printed PLA bolus with 90% infill ratio (dark) and 100 % infill ratio (grey).

## 4. Conclusions

Two PLA boluses with different infill ratios (90 % and 100 % correspondingly) have been printed and used in radiotherapy procedure to cover the surface of the rounded phantom without air gaps. Absorbed doses were evaluated using 2D GafChromic film dosimetry. It was found that the results obtained using 3D printed phantoms are comparable with those obtained from the standard treatment planning system when the "sticking" bolus is applied. The deviation from the planning system was 3.34% in the case of bolus printed with 100% infill rate and 4.06% in the case when bolus with 90% infill rate was used. Application of the bolus with 90% infill revealed that the dose might be "patterned" when delivered to the patient surface, which was clearly seen on GafChromic film. This clearly indicates, that application of patterned boluses (<100% infill) needs very detailed investigations before it can be recommended for clinical use.

However performed in vitro investigation has shown, that the patient related individualized bolus printed with 100% infilling successfully could cover the shaped surface (without air gaps) and might be used for dosimetry purposes in radiotherapy.

## Acknowledgement

This work was partly supported by research grant No. MIP-S-17-104 of Lithuanian Research council.

## 5. References

1. Michiels S., Barragán A.M., Souris K., Poels K., Crijns W., Lee J.A., Sterpin E., Nuyts S., Haustermans K., Depuydt T. Patient-specific bolus for range shifter air gap reduction in intensitymodulated proton therapy of head-and-neck cancer studied with Monte Carlo based plan optimization. Radiotherapy and Oncology, Vol. 128, 2018, p. 161–166.
2. Park S.Y., Choi C.H., Park J.M., Chun M, Han J.H., Kim J.I. A patient-specific Polylactic Acid Bolus Made by 3D Printer for Breask Cancer Radiation Therapy. PLoS One, 2016, 2016, Vol. 11 no. 12:e0168063.
3. Fuse H.; Shinoda K.; Inohira M.; Kawamura H.; Miyamoto K.; Sakae T.; Fujisaki T. Note: Utilization of

polymer gel as a bolus compensator and a dosimeter in the near – surface buildup region for breast – conserving therapy. Review of Scientific Instruments. Vol. 86, No. 9, 2015: 096103.

4. Khan Y., Villarreal-Barajas J. Eduardo, Udowicz M., Sinha R., Muhammad W., Abbasi Ahmed N., Hussain A. Clinical and Dosimetric Implications of Air Gaps between Bolus and Skin Surface during Radiation Therapy Journal of Cancer Therapy, Vol. 4, 2013, p. 1251-1255.
5. Laurikaitienė, J., Tzirkalov, T., Dimitrova, T.L., Laurikaitis, M. Evaluation of skin dose under the bolus for post-operative breast cancer treatment. Medical physics in the Baltic States: proceedings of the 13th international conference on medical physics, Kaunas, Lithuania, 9-11 November, 2017. Kaunas: Kaunas University of Technology. ISSN 1822-5721. 2017, p. 69-72.
6. Canters R.A., Lips I.M., Wendling M., Kusters M., van Zeeland M., Gerritsen R.M., Poortmans P., Verhoef C.G. Clinical implementation of 3D printing in the construction of patient specific bolus for electron beam radiotherapy for non-melanoma skin cancer. Radiother Oncol., Vol. 121, No. 1, 2016, 148-153.
7. Capintec, Inc. CT Head and Body Dose Phantom. http://www.capintec.com/product/ct-head-and-body-dose-phantom/.
8. Adlienė, D., Jaselskė, E., Rudžianskas, V., Šeperienė, N. First approach to ionizing radiation based 3D printing: fabrication of free standing dose gels using high energy gamma photons. Nuclear instruments and methods in physics research, Section B: Beam interactions with materials and atoms. Amsterdam: Elsevier. ISSN 0168-583X. eISSN 1872-9584. Vol. 435, 2018, p. 246-250.
9. Sim G.S., Wong J.H.D., Ng K.H. The use of radiochromic EBT2 film for the quality assurance and dosimetric verification of 3D conformal radiotherapy using Microtek ScanMaker 9800XL flatbed scanner. Journal of applied clinical medical physics, Vol. 14, No. 4, 2013, p.85-95.
10. Nakano M., Hill R.F., Whitaker M., Kim J.H., Kuncic Z. Study of surface dosimetry for breast cancer radiotherapy treatments using Gafchromic EBT2 film. Journal of Applied Clinical Medical Physics, Vol. 13, No 3, 2012, p. 83-97. .

*MEDICAL PHYSICS IN THE BALTIC STATES 14 (2019)*

Proceedings of International Conference "Medical Physics 2019"
7 – 9 November 2019, Kaunas, Lithuania

# QUALITATIVE ANALYSIS OF HEAD AND NECK TREATMENT PLANS FOR INTENSITY MODULATED RADIATION THERAPY

Justė JANKEVIČIENĖ[1], Jurgita LAURIKAITIENĖ[2,3], Jurgita ČYVIENĖ[2], Rūta NEDZINSKIENĖ[4]
[1]Lithuanian Energy Institute Laboratory for Renewable Energy and Energy Efficiency, Kaunas, Lithuania;
[2]Kaunas University of Technology, The Faculty of Mathematics and Natural Science, Kaunas, Lithuania;
[3]Oncological Hospital of Kaunas Clinics, Radiotherapy Department, Kaunas, Lithuania;
[4]Kaunas University of Technology, Accounting Department, Kaunas, Lithuania
justelaz@gmail.com; jurgita@medicinosfizika.lt; jurgita.cyviene@ktu.lt; ruta.nedzinskiene@ktu.lt

***Abstract***: Modern radiotherapy technologies, like intensity modulated radiotherapy (IMRT) allows to irradiate tumor with a higher dose per treatment, at the same time reducing exposure to the critical organs, thus avoiding acute reactions, like dry mouth, swallowing problems, and etc. Therefore, still the main challenge of external beam radiotherapy for head and neck cancer is to protect irradiation of organs at risk, within limits of the tolerance dose level, determining the possible risks of early and late reactions, while evaluation irradiation of the tumour let us to determine efficiency of the treatment outcome, assuring local tumor control. A brief analysis of critical organs and tumor irradiation processes determines patient's quality of life and survival.

***Keywords:*** IMRT, head and neck cancer, tolerance dose levels, homogeneity, conformity.

## 1. Introduction

According to the World Health Organization (WHO) over the world yearly every sixth person dies from the oncological disease. According to the Lithuanian Register data last year 846 new cases of head and neck tumors were registered, of which 663 deaths were reported [1]. Although this number represents 4.77 % of all cancer cases, while the mortality for head and neck cancer is more than 78 %. External beam radiotherapy using high energy photon beams are mostly used for the head and neck cancer irradiation. The most important issue of head and neck cancer (HNC) irradiation is protection of the critical organs (spinal cord, brain stem, chiasma, salivary or parotid glands, larynx and etc.), which are close or are in the region of irradiation and are influenced by acute, delayed side effects and/or even possible severe complications, which determines patient's quality of life [2-4]. Due to this reason modern radiotherapy technologies such as volumetric arc therapy, intensity modulated radiotherapy (IMRT) and etc. are recommended, because allows to irradiate tumor with a higher dose per treatment, at the same time reducing or keeping the same exposure to the healthy tissues and critical organs [5]. In such way could be prolonged patient's survival and improved quality of life, avoiding early and late reactions, like dry mouth, swallowing problems, and etc. [6]. So during the external beam radiotherapy of HNC the main challenge is to avoid or protect irradiation of healthy tissues and organs at risk within limits of the tolerance dose level, simultaneously without reduce of the maximum prescribed dose to the tumor. Therefore, irradiation of the critical organs, even if, is used modern 3D treatment techniques, has to be evaluated in compare with the tolerance dose levels, determining the possible risks of early and late reactions.

The aim of this study were to create a fast and simple qualitative analysis of head and neck IMRT treatment plans, determining the possible risks of early and late reactions, assuring local tumor control, and so defining the outcome of radiotherapy procedure.

## 2. Materials and methods

Qualitative analysis was done for 20 randomly chosen plans. Two different "protocols" were used for qualitative analysis of IMRT plans: QUANTEC (Quantitative Analysis of Normal Tissue Effects in the Clinic) guidelines [7] and ONTARIO Head and Neck IMRT protocol [8]. The main difference between these guidelines is tolerance dose levels for organs at risk and tumor, which are presented in Table 1.

Tolerance dose levels, according to QUANTEC and ONTARIO guidelines, for the most treatment cases delineated critical organs (spinal cord, parotid glands, and oesophagus) were "recalculated" to the "points", which are presented in Table 2. Such kind (using "points' scale") of the IMRT plans evaluation using ONTARIO protocol was introduced in the 2017

Radiation Knowledge Competition for Head and Neck Nasopharynx case [9].

**Table 1**. Tolerance dose levels for two different "protocols": QUANTEC and ONTARIO.

| Organ | Dose parameter | QUANTEC Dose, Gy | ONTARIO Dose, Gy |
|---|---|---|---|
| Brain | $D_{max}$ | 60 | 60 |
| Brain stem | $D_{max}$ | 54 | 54 |
| Optic chiasm | $D_{max}$ | 55 | 50 |
| Spinal cord | $D_{max}$ | 50 | 48 |
| Cochlea | $D_{mean}$ | 45 | 50 |
| Parotid | $D_{mean}$ | 25 | 26 |
| Pharynx | $D_{mean}$ | 50 | - |
| Larynx | $D_{max}$ | 66 | 45 |
| Oesophagus | $D_{mean}$ | 34 | 45 |
| Planning tumor volume (PTV) constraints | | | |
| PTV/ "target" | | 95 – 107 % | 95 – 115 % |

**Table 2**. Tolerance dose levels of organs at risk/ critical organs relation to the points.

| Organ | Lower dose limit, Gy | | | Upper dose limit, Gy | | |
|---|---|---|---|---|---|---|
| | 1* | 2* | Points | 1* | 2* | Points |
| Spinal cord, $D_{max}$ | ≤48 | ≤46 | 3 | ≥50 | ≥48 | 0 |
| Parotid gland, $D_{mean}$ | ≤20 | ≤20 | 2 | ≥25 | ≥26 | 0 |
| Oesophagus, $D_{mean}$ | ≤30 | ≤40 | 3 | ≥34 | ≥45 | 0 |
| Planning tumor volume (PTV) constraints | | | | | | |
| PTV* | ≤ 92 % | | 0 | ≥ 95 % | | 5 |
| 1* – QUANTEC, 2* – Ontario H&N IMRT Protocol | | | | | | |

Evaluation using the "points' scale", for example, for one of the organs at risk, like parotid gland, could be explained as follows: the maximum recommended tolerance mean dose level for parotid gland following guidelines is 25 Gy (QUANTEC) or 26 Gy (ONTARIO), if this organ exceeds recommended maximum tolerance mean dose level, it respectively will be equated to 0 points, if it is less than 20 Gy, it will be equated to 2 points, if the tolerance mean dose level differs in the range from 20 Gy to 25 Gy or 26 Gy (depending on "protocol"), the points differs from 2 to 0 respectively, i.e. if the parotid gland mean dose was 22.2 Gy, the point value of such critical organ will be 1.27 points out of a possible 2.0 points (figure 1).

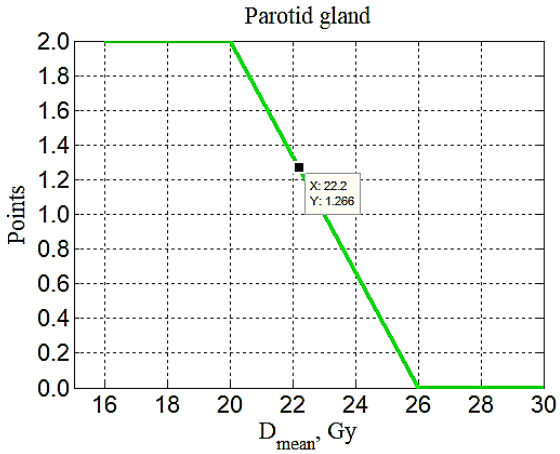


**Fig. 1.** The "points' scale" usage for the parotid gland: planned parotid gland mean dose per whole treatment for one of the IMRT plans were 22.2 Gy, what corresponds to 1.27 points, following QUANTEC guidelines.

So these graphical dependencies for qualitative evaluation of the randomly chosen IMRT plans were obtained using clinically treated patients' data (table 3). For the faster evaluation and prediction of possible early and late reactions for the treated patients were created the program "IMRT Plans Analysis" (figure 2).
Evaluation of IMRT plans were done using the data about the doses of the main critical organs, like parotid glands, spinal cord, oesophagus, which were contoured in all randomly chosen investigated plans and due to which the most common and the most "visible" early and late reactions usually occurs, influencing quality of the patient.

**Table 3.** The main parameters of the IMRT plans used for qualitative evaluation.

| Critical organs, *D*, Gy | IMRT plan No. | | | | | | | | | | | | | | | | | | | |
|---|---|---|---|---|---|---|---|---|---|---|---|---|---|---|---|---|---|---|---|---|
| | PTV + boost | | | | | | | PTV + boost1 + boost2 | | | | | | | | | | | | |
| | 1 | 2 | 3 | 4 | 5 | 6 | 7 | 8 | 9 | 10 | 11 | 12 | 13 | 14 | 15 | 16 | 17 | 18 | 19 | 20 |
| Right parotid gland, $D_{vid}$ | 19.7 | 18.5 | 24.4 | 32.7 | 11.2 | 14.3 | 15.7 | 23.0 | 19.3 | 22.2 | 30.1 | 19.8 | 25.9 | 31.9 | 21.0 | 43.4 | 21.8 | 21.6 | 17.9 | 26.1 |
| Left parotid gland, $D_{vid}$ | 21.6 | 21.4 | 27.7 | 10.6 | 13.6 | 14.1 | 20.2 | 34.7 | 20.6 | 21.2 | 30.1 | 34.1 | 26.2 | 29.0 | 15.1 | 38.1 | 19.7 | 34.0 | 26.0 | 14.7 |
| Spinal cord, $D_{max}$ | 19.1 | 37.1 | 41.5 | 45.4 | 43 | 41.0 | 39.2 | 42.8 | 42.8 | 39.5 | 43.8 | 44.9 | 41.1 | 42.9 | 45.2 | 45.9 | 41.4 | 45.9 | 35.7 | 41.1 |
| Oesophagus, $D_{vid}$ | 41.2 | 12.6 | 20.4 | 30.1 | 24.2 | 30.0 | 25.1 | 40.7 | 38.8 | 44.6 | 26.0 | 43.9 | 13.4 | 27.6 | 21.7 | 5.2 | 35.7 | 18.8 | 12.5 | 29.9 |
| | | | | | | | | | | | | | | | | | | | | |
| PTV $D_{95}$, Gy | 62.1 | 57.2 | 62.5 | 64.3 | 55.9 | 62.6 | 56.3 | 65.8 | 65.8 | 66.2 | 64.4 | 65.5 | 67.3 | 66.2 | 65.9 | 65.7 | 66.9 | 65.9 | 65.4 | 66.8 |
| $D_p$, Gy | 66 | 60 | 66 | 66 | 60 | 66 | 60 | 70 | 70 | 70 | 70 | 70 | 70 | 70 | 70 | 70 | 70 | 70 | 70 | 70 |

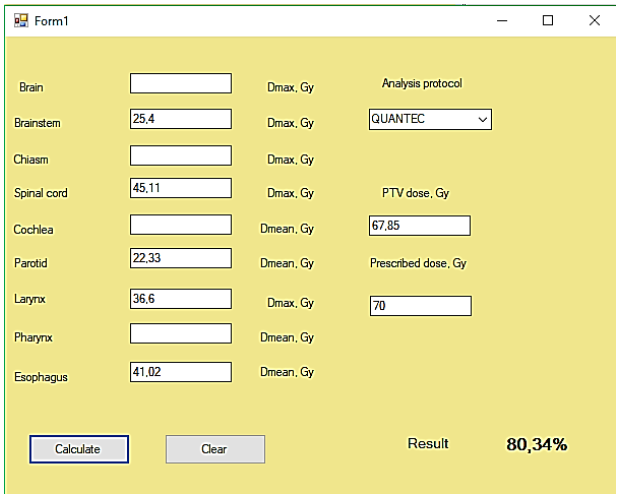


**Fig. 2.** The main window of the program "IMRT Plans Analysis".

For the qualitative analysis of the treatment plans were also used planning tumour volume (PTV) evaluation (irradiation of the target), using homogeneity (HI) and conformity (CI) indices, which usually shows the uniformity of dose distribution in the irradiated target volume. The main equations used for homogeneity and conformity calculations in this study:

$$HI = \frac{D_{max}}{D_p} \text{ [10]} \quad (1)$$

$$CI = \frac{V_{95}}{V_{PTV}} \text{ [11]} \quad (2)$$

where $D_{max}$ is the maximum dose; $D_p$ is the prescribed dose; $V_{95}$ is the PTV volume covered by 95 % isodose; $V_{PTV}$ – total volume of PTV.

## 3. Results and discussion

3D IMRT treatment planning, like and other external photons' beam therapy techniques are limited due to healthy tissues and critical organs tolerance dose levels. Even if, it is a modern IMRT technique with which is possible to reduce the dose to the critical organs, at the same time increasing dose to the tumor, still the basic problem and challenge for the medical physicists is protection of critical organs in the irradiation area or near the target of irradiation. According to the tolerance dose levels for critical organs, using the guidelines, like QUANTEC and ONTARIO, it is an option to evaluate treatment outcome, predicting possible early and late reactions. Therefore, using created program "IMRT Plans Analysis" analysis of 20 randomly chosen treatment plans for the head and neck patients were done faster. This investigation showed, that due to QUANTEC and ONTARIO guidelines, even if the risk of early and late reactions are possible to reduce, however to avoid a higher irradiation of some critical organs, like parotid glands and oesophagus is impossible. Especially, it were significantly seen comparing results depending on the total prescribed dose per treatment (60, 66 Gy and70 Gy). Even, if the prescribed dose per whole treatment were increased for 4 Gy (from 66 Gy to 70 Gy), the mean tolerance dose level for oesophagus was exceeded ~45 % for 70 Gy/whole treatment and just ~12.5 % for 66 Gy/whole treatment. These results confirmed clinically registered dysphagia, and even parotid glands function reduction up to 25 % and/or esophagitis risk [12] for 38 % patients', like it was observed following to QUANTEC recommendations. Due to higher tolerance dose level for oesophagus due to ONTARIO protocol, the percentage risk was twice lower. So evaluating the possible late and early reactions for the oesophagus it could be recommended to follow QUANTEC recommendations, according to clinically registered reactions like dysphagia and/or esophagitis risk. The same tendency was observed and for the parotid glands, but due to similarities of the tolerance dose levels for the parotid glands following QUANTEC and ONTARIO guidelines the results could be comparable: ~54 % for 70 Gy/whole treatment and just 25 % for 66 Gy/whole treatment, observing possible reactions of xerostomia, chewing and swallowing problems [13-15]. Using already mentioned "points' scale" for the plans evaluation, were observed, if the plans percentage evaluation of the points were more than 65 % the possibility clinically to register early and late reactions of evaluated plans significantly decreases.
According to the evaluation results of QUANTEC and ONTARIO, even if, for some cases, like oesophagus, it could not be comparable, however they could complement each other, and ONTARIO head and neck IMRT protocol could be used as an additional data.

During this study additional analysis of homogeneity (HI) and conformity (CI) indices were used for irradiation of the tumor and efficiency of the treatment outcome evaluation. According to the results, which as it is seen in a figure 3 A) (HI) and B) (CI) the calculated values are in close proximity to the 1 (differs less than 10 %), what shows a sufficient and assured local control of the tumour (figure 3). Thus the plans for which homogeneity and conformity indices were the closest to the one or even equal to one showed as already mentioned a sufficient and assured control of the tumor, but at the same time were clinically observed higher toxicity to the critical organs.

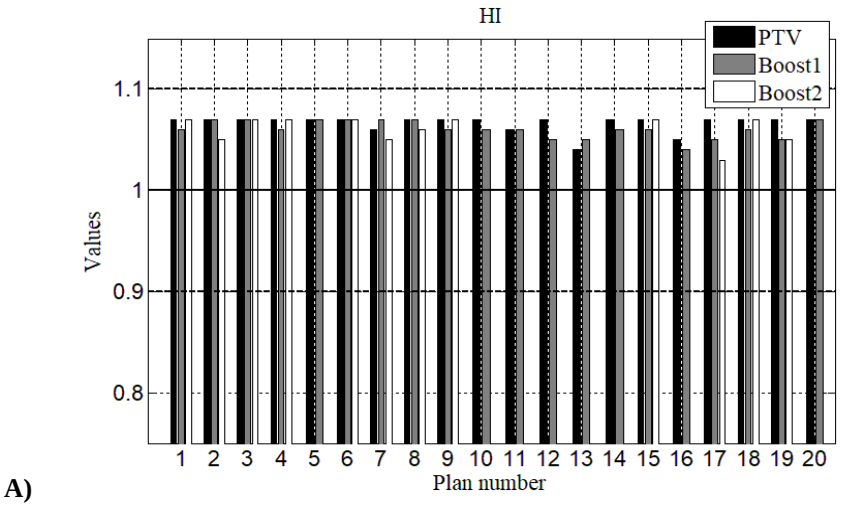


**A)**

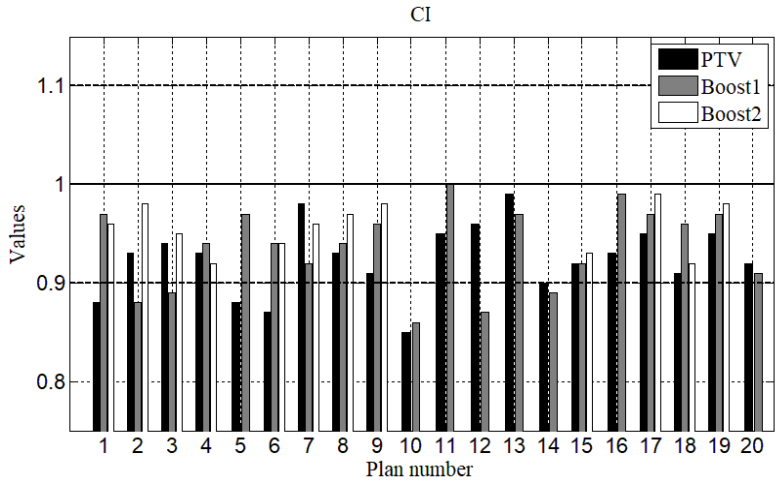


**B)**

**Fig. 3.** Distribution of: A) homogeneity indices of analysed IMRT plans and B) conformity indices of analysed IMRT plans.

## 4. Conclusions

3D IMRT treatment planning, like and other external photons' beam therapy techniques are limited due to healthy tissues and critical organs tolerance dose levels, which usually are evaluated using guidelines or recommendations, like QUANTEC. According to analysis of the results, using QUANTEC and ONTARIO guidelines, were evaluated treatment outcome, predicting possible early and late reactions. For the faster evaluation and prediction of possible early and late reactions of the randomly chosen IMRT plans for head and neck patients, were created the program "IMRT Plans Analysis". Analysis of the results showed, that following to the QUANTEC and ONTARIO guidelines, even if, the risk of early and late reactions is possible to reduce, but to avoid a higher irradiation of some critical organs, like parotid glands and oesophagus is impossible, due to PTV and critical structures regions intersection. According to this, for some of the patients were observed such late reactions, like xerostomia, dysphagia and even parotid glands function reduction up to 25 %.

Using "points' scale" for the IMRT plans evaluation, were noticed, if the plans percentage evaluation recalculated from the points' data to the percentage value is more than 65 %, the possibility to observe early and late reactions of evaluated plans significantly decreases.

Analysis of homogeneity (HI) and conformity (CI) indices were used as an additional evaluation of the tumor irradiation and efficiency of the treatment outcome. According to the results calculated HI and CI values were in a close proximity to the 1, what showed a sufficient and assured local control of the tumor.

## Acknowledgement

This work was partly supported by research grant No MIP-S-17-104 of Lithuanian Research council.

Special thanks to Danas Gutaravičius who helped on the programming with endless patience.

## 5. References

1. www.nvi.lt/uploads/pdf/Vezio%20registras/Vezys_lietuvoje_2018.pdf
2. Taberna M, Rullan A. J, Hierro C., Navarro V., Vázquez S., Lozano A., Vilajosana E., Maños M., Marí A., Viñals J., Mesía R. Late toxicity after radical treatment for locally advanced head and neck cancer. Oral Oncology 51, 2015, 795–799.
3. Nasr A., Habash A. Dosimetric analytic comparison of inverse and forward planned IMRT techniques in the treatment of head and neck cancer. Journal of the Egyptian National Cancer Institute, 2014, 26, p. 119–125.

4. Rudzianskas, V.; Inciura, A.; Juozaityte, E.; Rudzianskiene, M.; Kubilius, R.; Vaitkus, S.; Kasėta, M.; Adliene, D. Reirradiation of recurrent head and neck cancer using high-dose-rate brachytherapy // Acta otorhinolaryngologica Italica. Pisa: Pacini editore. ISSN 0392-100X. Vol. 32, no. 5, 2012, p. 297-303.
5. Cheung K., Intensity modulated radiotherapy: advantages, limitations and future developments. Biomed Imaging Interv J. 2(1): e19. Epub 2006 Jan 1. PubMed PMID: 21614217; PubMed Central PMCID: PMC3097603.
6. Mcdonald M., Liu Y., Moore M., Johnstone P. Acute toxicity in comprehensive head and neck radiation for nasopharynx and paranasal sinus cancers: cohort comparison of 3D conformal proton therapy and intensity modulated radiation therapy. Radiat Oncol. 2016.
7. Bentzen, S.M., et al., Quantitative Analyses of Normal Tissue Effects in the Clinic (QUANTEC): an introduction to the scientific issues. Int J Radiat Oncol Biol Phys, 2010. 76 (3 Suppl): p. 3-9.
8. Recommendation Report Dose Objectives for Head and Neck IMRT Treatment Planning A project developed by the Head and Neck Community of Practice of the Radiation Treatment Program of Cancer Care Ontario for circulation to Regional Cancer Programs. Report Date: February 2014 Head and Neck Community of Practice of the Radiation Treatment Program of CCO Universal Date: 2014-02-01
9. https://radiationknowledge.org/competition2017/
10. Van'triet A., Mak A., Moerland M., Elders L. A conformation number to quantify the degree of conformality in brachytherapy and external beam irradiation: Application to the prostate. Int J Radiat Oncol Biol Phys. 1997; 37:731–6.
11. Govardhan H., Khaleel I., Sentihil K., Comparison of Intensity Modulated Radiation Therapy (IMRT) and Three Dimensional Conformal Radiotherapy (3DCRT) In Supratentorial Astrocytic Series WHO Grade III-IV Primary Malignant Brain Tumors. J Nucl Med Radiat Ther 2018, Vol 9(4): 368.
12. Dease J., Moiseenko V., Marks L., Chao C., Nam J., Eisbruch A. Radiotherapy dose – volume effects on salivary gland function. Int. J. Radiation Oncology Biol. Phys., Vol. 76, No. 3, Supplement, 2010, p. S58–S63.
13. Werner-Wasik M., Yorke E., Deasy J., Nam J., Marks L. Radiation dose – volume effects in the esophagus. Int. J. Radiation Oncology Biol. Phys., Vol. 76, No. 3, Supplement, 2010, p. S86–S93.
14. Peponil E., Glanzmann C., Willi B., Huber G., Studer G. Dysphagia in head and neck cancer patients following intensity modulated radiotherapy (IMRT). Radiation Oncology 2011, 6:1.
15. Richards T.M., Hurley T., Grove L., Harrington K.J., Carpenter G.H., Proctor G.B., Nutting C.M. The effect of parotid gland-sparing IMRT on salivary composition, flow rate and xerostomia measures. Oral Dis. No. 23, Vol. 7, 2017, p. 990–1000.

*MEDICAL PHYSICS IN THE BALTIC STATES 14 (2019)*

Proceedings of International Conference "Medical Physics 2019"
7 – 9 November 2019, Kaunas, Lithuania

# COMPREHENSIVE END-TO-END TEST OF TREATMENT PLANNING SYSTEM ACCORDING TO IAEA METHODOLOGY: HEAD & NECK CASE WITH VMAT DELIVERY

Aurimas KRAULEIDIS, Dainius BURDULIS, Vanda ANDRIJAITIENĖ
Klaipėda University hospital
aurimas.krauleidis@gmail.com; dainius.burdulis@gmail.com; vanda.andrijaitiene@gmail.com

***Abstract*:** Efficacy of radiotherapy is directly related to the accuracy of the delivered dose to the patient that in turn is dependent on the accuracy of beam data used in the treatment planning process. For the treatment technologies such as intensity-modulated radiation therapy (IMRT) to compare the delivered doses and dose distributions of treatment plan phantoms are used with pseudo-anatomic geometries. The purpose of this study was to show that quality assurance (QA) in all of the steps of the radiation treatment process is essential to ensure accurate dose delivery to the patient and to minimize the possibility of accidental over or under exposure. Performing comprehensive end-to-end tests is necessary part of a comprehensive QA programme in radiation oncology.

***Keywords*:** IMRT, QA, end-to-end test, Shane.

## 1. Introduction

Technology of radiotherapy has developed significantly over the last decade. New techniques such as intensity-modulated radiation therapy are becoming common practice in most radiation therapy institutions. At the same time, it is recognized that a significant number of institutions are not able to deliver IMRT treatment protocols within defined criteria of acceptability [1].
Usually the radiation fields in the radiation therapy is from 4x4cm up to 40x40 cm. However, in advanced and specialized radiotherapy, such as IMRT, gamma knife, SRS, extremely small fields of a few millimeters are used [2]. Problems in the dosimetry of small field is due to lack of lateral electronic equilibrium, overlap of the geometrical penumbra due to the size of detector, change in energy spectrum and associated dosimetric parameters, and stopping power ratio. A few problems and trends in the dosimetry of small field have been examined by other authors [3, 4]. Small volume detectors should be used that have minimum energy, dose, and dose rate dependency. Micro ion chambers are best suited for small field dosimetry. Output of such dosimeters is very sensitive to the position of the detector itself. Thus, verification of the positioning of the detector is of high importantance [5].
There are multiple challenges in designing and running effective dosimetry audits, with new techniques and new equipment combined with increasingly high expectations from both patients and professionals in outcomes and safety. There are different types of audits from postal to an on-site visit and from basic measurements in reference conditions through to a full end-to-end audit where an anthropomorphic phantom takes the place of the patient and follows the full pathway from imaging, through planning and to complex dose distribution delivery [6].
Head and Neck End-to-End Verification Phantom (SHANE, Figure 1) is designed for end-to-end testing of treatment planning systems. This phantom can be used for every step in the process from imaging acquisition to dosimetry verification and patient-specific QA during head-and-neck VMAT and IMRT procedures [7]. Phantom receives ion chambers, which can be positioned in four parallel holes drilled through the phantom in inferior-superior direction. High-fidelity anthropomorphic design contains complex internal anatomy with equivalent of normal tissues, bone, teeth and air cavities, that provides a realistic clinical simulation to evaluate the challenging effects of intra- and extra-cranial anatomies.

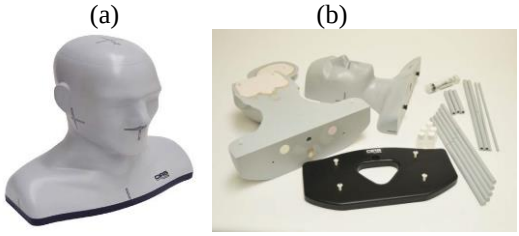


**Fig. 1.** Anthropomorphic CIRS SHANE phantom: (a) assembled SHANE, (b) SHANE components.

Measurement of beam output is the most fundamental measurement which confirms whether the machine has been correctly calibrated. Existing errors will create a

systematic error for every patient treated on the machine and therefore have the potential to create systematic differences in treatment outcomes.

Point dose and non-scanned integrated measurements, such as output factors, surface dose, leakage/transmission, wedge and tray factors, etc., can be measured in a water phantom, solid phantoms that mimic water may be used for convenience [8]. Other plastic material such as acrylic or polystyrene should be used with caution, as data collected with these materials may result in values that may require additional corrections due to differences in electron density. It was pointed out that solid phantoms do not truly represent the radiological properties of water [9]. A solid phantom should have an appropriate cavity drilled for tight fit of the detector which should be verified with a radiograph taken with low kVp with the detector inserted in the phantom. Different slabs of phantom should be used for different designs of the detector to ensure that a tight fit is maintained for each detector. When the detectors are placed in a solid phantom, enough time should be given to reach thermal equilibrium in the structure. Quality of the phantom material should be checked with a computed tomography CT scan for any artifacts and inhomogeneity in electron density via CT number. Note that these CT numbers may differ from water if the solid materials are designed to be water equivalent at megavoltage energies [10].

## 2. Methods and materials

This research was carried out at Klaipeda University Hospital, using a VARIAN linear accelerator UNIQUE equipped with 6 MeV photon beam energy, Millennium multileaf collimator (MLC-120) and electronic portal imaging device (EPID). Eclipse (version 10.0) treatment planning system with AAA dose calculation algorithm was used for dose calculation. SHANE phantom scanning was performed with 40 slice Siemens Somatom Sensation Open CT scanner. Calibrated Semiflex PTW 31010 ion chamber, PTW T10002 UNIDOS electrometer, PMMA slabs were used for dosimetric measurements.

To mimic a realistic patient procedure, this test uses an anthropomorphic phantom combined with a set of contours representing the target volumes and organs at risk (Figure 2).

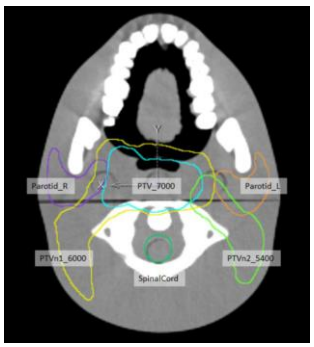


**Fig. 2.** Target volumes and organs at risk.

Phantom set-up was close to real patient set-ups using the technology normally used in the radiotherapy department such as the use of image-guidance procedures. Contours were electronically imported and superimposed on the computed tomography (CT) scans of the phantom. Dose prescriptions and normal tissue constraints are provided such that a treatment plan can be developed. Treatment plan was transferred to the treatment machine and the dose was delivered to the phantom. Appropriate dosimeters were used to determine both doses at specific reference points. Comparisons was made between the calculated and delivered doses.

Figure 3 shows a CT scan of the phantom indicating the location of the ion chamber channels. For each anatomical location, a specific insert is used to position the ion chamber.

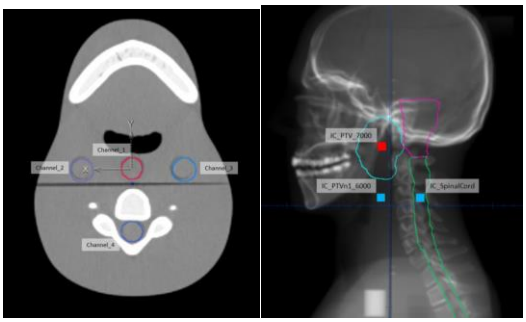


**Fig. 3.** Positions of the ion chamber channels

Shoulders of the phantom accommodate five electron density plugs: cortical bone, trabecular bone, lung inhale, lung exhale and a vial with water. In addition, anatomical structures such as spinal cord and the phantom body (soft tissue) can be used for electron density analysis (Table 1). Location of plugs is shown in Fig. 4.

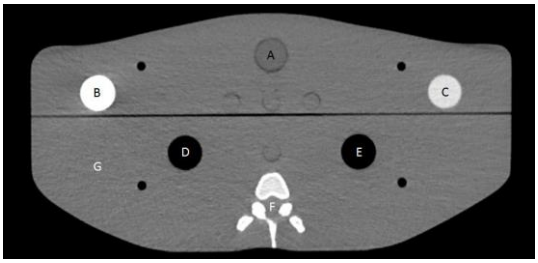


**Fig. 4.** CT image of the SHANE shoulder region with electron density plugs: A – water, B – cortical bone, C – trabecular bone, D – lung exhale, E – lung inhale, F – spinal cord, G – soft tissue

**Table 1.** Electron density data

| Phantom structures | Mass density g/cm$^3$ | Electron density x 10^23 /cm$^3$ | Electron density relative to water |
|---|---|---|---|
| water | 1.000 | 3.340 | 1.000 |
| cortical bone | 1.930 | 5.956 | 1.783 |
| trabecular bone | 1.200 | 3.863 | 1.156 |
| lung exhale | 0.500 | 1.648 | 0.493 |
| lung inhale | 0.205 | 0.668 | 0.200 |
| spinal cord | 1.070 | 3.488 | 1.044 |
| soft tissue | 1.055 | 3.434 | 1.028 |
| air | 0.001 | 0.003 | 0.001 |

Additionally, small field output factors, small field profiles and MLC tests were performed with the measured dosimetric data. All measurements were performed using a clinically commissioned algorithm for

H&N IMRT treatment planning with usual calculation settings.

To calculate the output factors for small fields 5 MLC-shaped field sizes were used (10 × 10 cm, 6 × 6 cm, 4 × 4 cm, 3 × 3 cm and 2 × 2 cm) and irradiated with 10 Gy on axis at 10 cm depth, 100 cm source-to-surface distance in water using the TPS.

For the calculation of MLC-shaped small field profile 2 × 2 cm MLC-shaped field was created in a water phantom and calculated the number of MUs to deliver 6 Gy to the isocenter at 10 cm depth, 100 cm source-to-axis distance using the TPS.

Dose distribution was computed with a calculation grid resolution of 1 mm. Cross-plane (in the direction of MLC movement) and in-plane (perpendicular to the MLC leaf movement) profiles generated at 10 cm depth as a line profile.

Picket fence test (Figure 5) was performed on the EPID device.

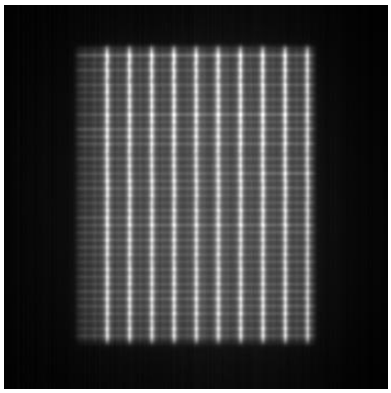

**Fig. 5.** Picket fence test

EPID device positioned at the isocenter (SID 100 cm) of the beam. Images from EPID in DICOM format were analyzed with the specialized program – EPIQA. EPIQA is a comprehensive tool for Quality Assurance with Electronic Portal Imaging Devices.

To measure the output factors of the TPS, 30x30x30 cm digital water phantom were virtually created and with a 10x10 cm field size at 100 cm SAD and 10 cm depth 2 Gy dose was delivered for monitor units' (MU) calculation.

30x30x30 $cm^3$ PMMA solid slab phantom with ionization chamber was irradiated in a 10 x 10 cm field at 100 cm SAD and 10 cm depth by the virtually in TPS calculated amount of monitor units. Procedure room temperature and air pressure were also measured.

SHANE phantom was scanned with CT scanner using typical head and neck CT scan protocol for radiotherapy. Phantom was positioned on the CT couch and aligned according to the LAP lasers lights. After scanning DICOM images transferred to the TPS. Hounsfield units (HU) versus electron density was evaluated. Targets and organs at risk (OAR) structures were copied to the scanned H&N phantom for treatment plan calculation. Treatment plan was calculated by using Vmat technique (2 full arcs). Plan prescription was 70 Gy in 30 fractions to the PTV. Plan was generated to achieve the dose constraints and the resulting plan should be clinically acceptable by ICRU-83.

Priority order of planning aims was:

1. Sparing of spinal cord and brainstem;
2. Coverage of PTV_7000;
3. Coverage of PTVn1_6000;
4. Coverage of PTVn2_5400;
5. Sparing of the Parotid_L (contralateral);
6. Sparing of the Parotid_R (ipsilateral);

Calculated plan was verified according to patient - specific QA procedure with SHANE phantom in LINAC treatment room.

SHANE phantom was positioned and aligned on the treatment couch. Treatment Dose plan delivery to phantom performed with Semiflex PTW 31010 ion chamber. Ion chamber was inserted into one of four Shane measurements channels, to the predefined position using the corresponding chamber cavity rod. Ion chamber positions have been:

- IC_PTV_7000
- IC_PTVn1_6000
- IC_PTVn2_5400
- IC_SpinalCord

Ion chamber measurements for all fields, has been acquired and repeated twice.

For the evaluation of the measured and TPS calculated values the following equation was used:

$$\text{Deviation } (\%) = (D_{cal} - D_{meas})/D_{meas} \cdot 100 \qquad (1)$$

where $D_{meas}$ is the dose value measured at the measurement point. Additionally, the ratio $D_{meas}/D_{cal}$ will be reported.

TPS calculated targets and OAR dose volume histograms (DVH) mean, minimum and maximum doses were compared with measured doses in the SHANE phantom.

## 3. Results and discussion

**Calculated and measured small field output factor.** Calculated MLC shaped small field output factors on treatment planning system are shown in table 2. Tolerance level for output factors is ± 3 % for 2 x 2 cm field and ± 2% for larger fields. According to our results, calculated output factors does not exceed tolerance level. Maximum deviation (2,22 %) observed in smallest MLC field (2 x 2 cm). Measured output factor was out of tolerance with 3.4 % deviation.

**Table 2.** Small field output factors data

| TPS calculated output factor | | | | | Measured output factor | | | |
|---|---|---|---|---|---|---|---|---|
| Field size, $cm^2$ | MUs to deliver 10 Gy to prescription point | Calculated Output factor | Reference data | Deviation, % | MUs to deliver 2 Gy to prescription point | Measured dose | Calculated Output factor | Deviation, % |
| 10 | 1518 | 1,000 | 1,000 | 0,00 | 256 | 1,934 | 0,967 | 3,4 |
| 6 | 1616 | 0,939 | 0,938 | 0,14 | | | | |
| 4 | 1701 | 0,892 | 0,886 | 0,72 | | | | |
| 3 | 1759 | 0,863 | 0,851 | 1,41 | | | | |
| 2 | 1847 | 0,822 | 0,804 | 2,22 | | | | |

**MLC shaped small field profile for 2 x 2cm.** Using TPS a virtual water phantom was created and dose distribution for cross-plane (Figure 6) and in-plane (Figure 7) profiles was calculated. Field size and the penumbra width (20%-80%) were calculated from submitted profiles and compared to measured baseline data. For in-plane profile calculated left and right penumbra difference from reference was 0,44 mm, 50 % of field size difference was 0,21 mm. For cross-plane profile calculated left penumbra difference from reference was 0,51 mm, right penumbra 0,43 mm, 50 % of field size difference was 0,10 mm. No greater differences than ±3 mm was observed of in-plane and cross-plane penumbra and results have not exceeded ±2 mm differences for field size. Reference data was taken from IAEA small field profiles.

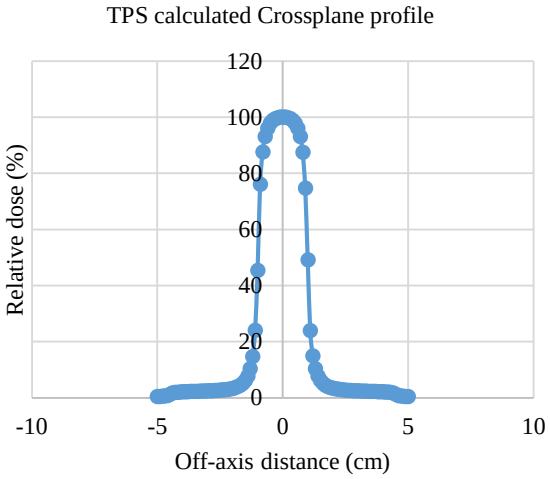


**Fig. 6.** MLC shaped small field cross-plane profile for 2 x 2cm

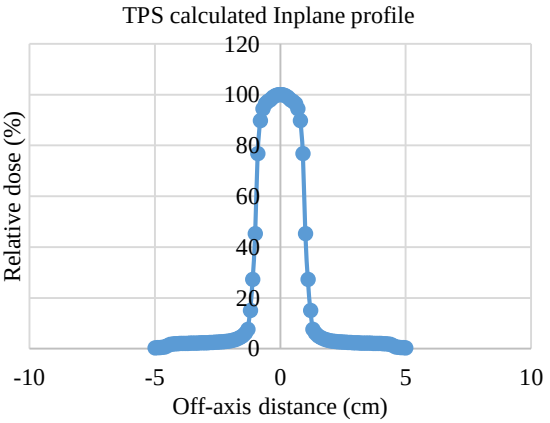


**Fig. 7.** MLC shaped small field in-plane profile for 2 x 2cm

**Picket fence test.** MLC dosimetry test with EPID was performed. Linac output for gantry angles 0°, 180°, 90° and 270° with 4x10 cm DMLC sliding window field and 0.5 cm slit have been tested to measure gravity influence for leaf position. Deviations from reference values for gantry angle 0° was 0,328 %, 90° – 0,036 %, 180° – -0,37 %, 270° – 0,005 %. For this test the values of a central ROI, as well as the deviation from the reference value, defined as the average over the four images ROI value.

**Accurate control of dose rate and Gantry speed during Vmat delivery test.** This test uses seven combinations of dose-rate, gantry range and gantry speed to give equal dose to seven 1.8 cm wide strips in a single Vmat field. For Linac performance analysis in delivering correct dose with variable dose rate and gantry speed we acquire open field image to compensate for beam profile. In Figure 8 pre-defined ROIs are displayed together with their values. Deviations from the reference value, defined as the average value of all the ROIs are shown in Table 3. Recommended tolerance value is 2%.

**Table 3.** Dose rate and gantry speed during Vmat delivery test ROI data

| ROI number | Deviation from reference value (%) |
|---|---|
| 1 | 1,29 |
| 2 | -0,2 |
| 3 | -0,31 |
| 4 | -0,03 |
| 5 | -0,3 |
| 6 | -0,32 |
| 7 | -0,14 |
| Tolerance (%) | 2 |
| Reference average value | 0,1511 ± 0,0009 |

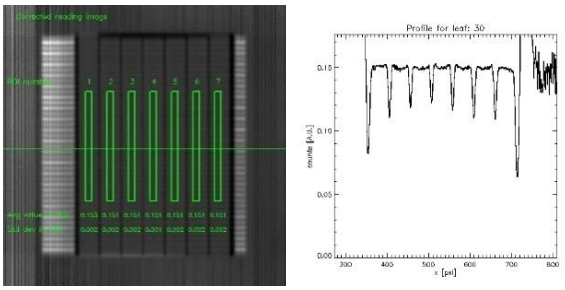

**Fig. 8.** Dose rate and gantry speed ROI analysis and measured profile

**Accurate control of leaf speed during Vmat delivery.** This test uses four combinations of leaf speed and dose-rate to give equal dose to four strips in a single Vmat field that to analyze linac and MLC performance in delivering correct dose with variable leaf speed and dose rate. Additionally, was acquired open field image to compensate for beam profile. ROIs are displayed together with their values (Table 4). Deviations from the reference value, defined as the average value of all the ROIs are shown with the recommended tolerance value of 2%

**Table 4.** Leaf speed during Vmat delivery test ROI data

| ROI number | Deviation from reference value (%) |
|---|---|
| 1 | 1,72 |
| 2 | -0,56 |
| 3 | -0,63 |
| 4 | -0,53 |
| Tolerance | 2 |
| Reference average value | 0,1432 ± 0,0016 |

**CT numbers to Relative Electron Density calibration.** Electron density of Shane phantom structures, measured CT calibration data, CT calibration data from TPS are shown in Table 5. Tolerance level for water is ± 5HU, for all other materials ± 20 HU. Out of tolerance are composite plug D (Figure 4) with 30 HU difference and plug B (Figure 4) difference 117 HU.

**Table 5.** Measured CT calibration data

| | Measured CT calibration data | | CT calibration data from TPS | | |
|---|---|---|---|---|---|
| Phantom structures | Relative electron density | Measured HU | Relative electron density | HU | HU difference |
| Air (H) | 0,000 | -1000 | 0,000 | -1050 | 50 |
| lung inhale (E) | 0,200 | -824 | 0,200 | -822,4 | -2 |
| lung exhale (D) | 0,493 | -560 | 0,493 | -529,8 | -30 |
| water (A) | 1,000 | -2 | 1,000 | -4,9 | 3 |
| solid water (G) | 1,028 | 27 | 1,028 | 25,7 | 1 |
| spinal cord (F) | 1,044 | 40 | 1,044 | 27,3 | 12 |
| trabecular bone (C) | 1,157 | 280 | 1,157 | 292,5 | -12 |
| cortical bone (B) | 1,783 | 1348 | 1,783 | 1230,6 | 117 |

**Treatment structures volumes verification and treatment planning results.** Measured all 9 structures used for treatment planning and calculated differences between references and calculated volumes (Table 6). All treatment volumes are within tolerances. Considering dosimetric treatment planning priorities, 15 goals have been reached, only mean dose for structure Parotid_L is higher (Table 6).

**Table 6.** Treatment structures volumes and treatment planning data

| | Volumes used for treatment planning | | | | Treatment planning results | | |
|---|---|---|---|---|---|---|---|
| Structure | Reference volume ($cm^3$) | Calculated volume ($cm^3$) | Volume deviation, % | Tolerance (%) | Volume | Dose (Objective) | Calculated Dose (Gy) |
| PTV_7000 | 88,5 | 87,99 | 0,60 | 1,0 | 98% | >90% (63.0 Gy) | 66,06 |
| | | | | | 95% | >95% (66.5 Gy) | 66,81 |
| | | | | | 50% | =100% (70.0Gy) | 70,26 |
| | | | | | 2% | <107% (74.9 Gy) | 72,57 |
| PTVn1_6000 (involved nodes) | 411,6 | 410,3 | 0,30 | 3,5 | 98% | >90% (54.0Gy) | 56,97 |
| | | | | | 95% | >95% (57.0Gy) | 58,04 |
| | | | | | 50% | 60.0-62.0 Gy | 61,44 |
| PTVn2_5400 (elective nodes) | 260,3 | 258,13 | 0,80 | 6,0 | 98% | >90% (48.6Gy) | 50,55 |
| | | | | | 95% | >95% (51.3Gy) | 51,82 |
| | | | | | 50% | 54.0 - 56.0 Gy | 55,19 |
| SpinalCord | 24,9 | 24,99 | -0,40 | 8,5 | 2% | <45Gy | 43,43 |
| SpinalCord_03 | 55,1 | 57,71 | -4,70 | 9,0 | 2% | <50Gy | 46,53 |
| BrainStem | 43,9 | 43,16 | 1,70 | 3,0 | 2% | <50Gy | 48,78 |
| BrainStem _03 | 72,5 | 72,03 | 0,60 | 1,5 | 2% | <55Gy | 52,24 |
| Parotid_L | 19,7 | 19,17 | 2,70 | 4,0 | **Mean** | **<24Gy** | **26,78** |
| Parotid_R | 23,4 | 22,07 | 5,70 | 4,0 | Mean | ALARA | 56,26 |

**Calculated and measured dose.** Table 7 shows the results of calculated and measured treatment volume doses and evaluated differences between TPS calculated 1 fraction mean dose ($D_{cal}$) and Measured 1 fraction mean dose ($D_{meas}$) in 4 different ion chamber positions. Calculated and Measured differences between all 4 ion chamber positions are within tolerance limits.

**Table 7.** Calculated and measured treatment volume doses analysis

| Structure associated with position of chamber | TPS calculate mean dose (Gy) | Homogeneity Index (HI) | TPS calculated 1 fraction mean dose, $D_{cal}$ (Gy) | Measured 1 fraction mean dose, $D_{meas}$ (Gy) | $D_{meas}/D_{cal}$ | Deviation (%) | Tolerance, % |
|---|---|---|---|---|---|---|---|
| PTV_7000 (nasopharynx), isocenter, red channel no 1 | 68,28 | 0,02 | 2,276 | 2,329 | 1,023 | -2,3 | 5 |
| PTVn1_6000 (involved nodes) 5 cm inferior to isocenter, blue channel no 2 | 59,55 | 0,03 | 1,985 | 2,029 | 1,022 | -2,2 | 5 |
| PTVn2_5400 (elective nodes), 5 cm inferior to isocenter, blue channel no 3 | 53,7 | 0,05 | 1,789 | 1,781 | 0,996 | 0,4 | 5 |
| IC_SpinalCord, 5 cm inferior to isocenter, blue channel no 4 | 39,1 | 0,07 | 1,301 | 1,349 | 1,037 | -3,6 | 7 |

## 4. Conclusions

Results of the end-to-end tests with the SHANE phantom demonstrates that the radiotherapy processes, with the physical components included in the tests, deliver dose distributions as planned with spatial and dosimetric accuracy appropriate for Vmat delivery in external beam radiotherapy. Calculated output factor for all tested field sizes does not exceed tolerance level, but measured dose for 10 x 10 cm field needs more investigation, since not meeting the output factor tolerances. Results also shown that CT numbers to relative electron density calibration is needed for two positions. MLC shaped small field profile, Picket fence test, Accurate control of dose rate, leaf and gantry speed during Vmat delivery test, calculated and measured dose in ion chamber positions, test results were within tolerance limits.

This study showed that end-to-end tests remain relevant and can identify fundamental global and local problems that affects radiotherapy treatments.

## 5. References

1. IAEA Supported National "End-to-End" Audit Programme for Dose Delivery Using Intensity-Modulated Radiation Therapy through On-Site Visits to Radiation Therapy Institutions Draft 08 to 10 October 2014 rev. 25-29 June 2015, rev. 10-14 July 2017, rev. October 2017, rev. November 2017, rev. February 2018
2. Das IJ, Ding GX, Ahnesjo A. Small fields: Nonequilibrium radiation dosimetry. Med Phys. 2008;35:206–15.
3. Wrya Parwaie, Soheila Refahi, Mahdieh Afkhami Ardekani, and Bagher Farhood., Different

Dosimeters/Detectors Used in Small-Field Dosimetry: Pros and Cons, J Med Signals Sens. 2018 Jul-Sep; 8(3): 195–203

4. S. D. Sharma., Challenges of small photon field dosimetry are still challenging, J Med Phys. 2014 Jul-Sep; 39(3): 131–132
5. Henry Finlay Godson, M. Ravikumar, S. Sathiyan, K. M. Ganesh, Y. Retna Ponmalar, and C. Varatharaj., Analysis of small field percent depth dose and profiles: Comparison of measurements with various detectors and effects of detector orientation with different jaw settings, J Med Phys. 2016 Jan-Mar; 41(1): 12–20
6. Gershkevitsh E., Pesznyak C., Petrovic B., Grezdo J., Chelminski K., Do Carmo Lopes M., Izewska J. Results of the IAEA project on TPS audit in radiotherapy in Europe. PD-0336, Radioth.Oncol.(Supplement 1), 103, (2012) S138
7. Ibbott G.G., Molineu A., Followill D.S. Independent evaluations of IMRT through the use of an anthropomorphic phantom, Technol. Cancer Res. Treat., 5, (2006) 481-487.
8. R. Kaderka, D Schardt, M Durante, T Berger, U Ramm, J Licher,C La Tessa. Out-of-field dose measurements in a water phantom using different radiotherapy modalities 2012 Institute of Physics and Engineering in Medicine. Physics in Medicine & Biology, Volume 57, Number 16
9. Palm A1, LoSasso T. Influence of phantom material and phantom size on radiographic film response in therapy photon beams. Med Phys. 2005 Aug;32(8):2434-42.
10. Dale W. Litzenberg, Hanan Amro, Joann I. Prisciandaro, Eduardo Acosta, Ian Gallagher, Don A. Roberts. Dosimetric impact of density variations in Solid Water 457 water-equivalent slabs. 2011, J Appl Clin Med Phys.

*MEDICAL PHYSICS IN THE BALTIC STATES 14 (2019)*

Proceedings of International Conference "Medical Physics 2019"
7 – 9 November 2019, Kaunas, Lithuania

# MCNP MODEL OF MEDICAL LINEAR ACCELERATOR TREATMENT HEAD

Simona BREIDOKAITE[1], Gediminas STANKUNAS[2]
Kaunas University of technology, Department of Physics[1]; Lithuanian Energy Institute[2]
simona.breidokaite@lei.lt; gediminas.stankunas@lei.lt

***Abstract*:** This work analyzes the construction of linear accelerator treatment head. Ways of photon interaction with the material heads' material are discussed, such as: photoelectric effect, Compton effect, pair creation as well as photon absorption properties of the materials used in the treatment head structures. MCNP-VIS and MCNP6 software packages are proved to be capable of describing the necessary Linac treatment head model aspects such as: description of geometry, source information, libraries used to describe cross-sections of photon interactions, and factors of flux to dose power.

***Keywords*:** Linac, MCNP, photons, treatment head

## 1. Introduction

It is important for clinical dosimetry manufacturers and experts to know accurate photon spectrum emitted from linear medical accelerators (LINAC) used radiotherapy. Major companies that develop and improve medical line accelerators are Varian [1] and Elektra [2]. This study analyzes the photon fluxes obtained in the Tungsten target.

Monte Carlo method is the most commonly used tool for investigating and modeling particle transmission through various materials. This complex method takes into account all possible physical phenomena occurring during the interaction between radiation and matter [3].

In the radiation therapy, high-energy photons (> 10 MeV) are produced, that possibly results in neutron production thus increasing the dose rate to the patient and can be affected by the materials used in the equipment production [4]. These neutrons are formed by photon beam interaction with the filters, targets and collimator materials

LINACs analyzed in this study are similar to those analyzed by J. S. Estepa Jiménez:

Varian Clinac 2100 C / D was modeled operating at 15 MV and photon spectra was calculated. Figure 1 shows treatment head geometry that includes main parts and what materials they are made of. The second model is made by Shaun CLARKE: In it there is a different concept of linear accelerator. It is mobile, in a vehicle (see figure 2)

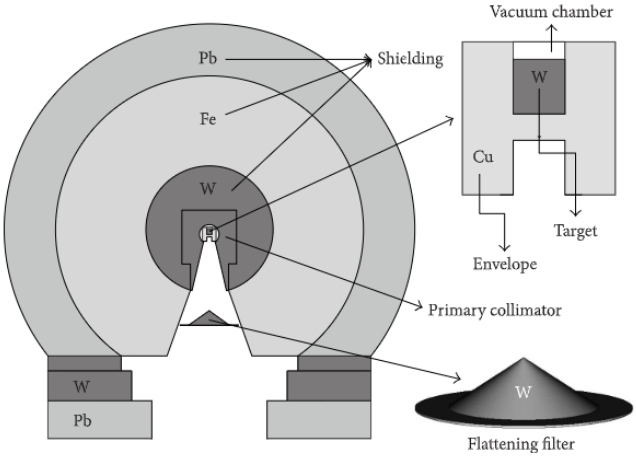


**Fig. 1.** Linear Accelerator Head model with shielding materials [5]

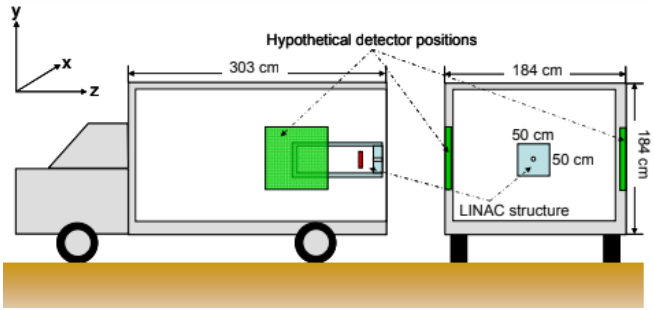


**Fig. 2.** Linear Accelerator model with shielding materials [6]

Purpose of this work: Using MCNP-VIS software package create linear accelerator treatment head model and with MCNP6 software perform photon transport calculations.

## 2. Model creation

### 2.1. Geometry

In the Monte Carlo method codes for the Cartesian coordinate system are used. Surfaces are described with themost common 3D surfaces equation as f (x, y, z) = 0

e.g. cones, spheres, cylinders, ellipsoids Some examples of surfaces equations:
Plane:

$$Ax + By + Cz - D = 0 \quad (1)$$

Sphere:

$$(x - A)^2 + (y - B)^2 + (z - C)^2 - R^2 = 0 \quad (2)$$

Cylinder:
On X-axis

$$(y - B)^2 + (z - C)^2 - R^2 = 0 \quad (3)$$

More complicated 3D geometries are created by using Boolean algebra element AND and OR and if the area is above or right of surface it is noted as ”–“ and if it is below or on the left side - “+”.

$$P_1^- \cap P_2^+ \cap C_1^-, P_1^+ \cup P_2^- \cup C_1^+ \quad (4)$$

Where $P_n$ is plane surfaces, $C_n$ is cylinder.
Space surrounded by these surfaces is called a cell. The cell may be: vacuum or any homogeneous material. The entire space should be subdivided into cells where there are no holes. Cells cannot overlap. [7].

### 2.2. Radiation source

Sources described by MCNP codes can be localized in one cell or distributed in many cells, or described as a point, line or plane. Emitted energy from the source may be discrete (usually gamma rays) or have spatial distribution.
While one source emits radiation isotopically, others may be anisotropic. In order to track a particle which has left the source, it is needed to get the information about the distribution of space, energy, and angles, which either must be calculated or described in the input file. Usually these three variables are related.[8]
The probability of a particle being released at a certain angle and direction is:

$$p(\Omega)d\Omega = \frac{d\Omega}{4\pi} = \frac{d\psi}{2\pi}\frac{d\omega}{2} \quad (5)$$

where ω = cosθ.

### 2.3. Photon interactions and their cross - sections

Analyzed physical processes are: photoelectric effect, pair creation, Compton scattering. General scattering cross section includes inconsistent scattering regardless of the use of simple or detailed physics. Thus, the total cross section $\sigma_t$ is taken as the sum of the three components**:**

$$\sigma_{ben} = \sigma_p + \sigma_{pp} + \sigma_s \quad (6)$$

Where: photoelectric photon, pair creation, Compton scattering cross section [9].
*Photoelectric effect*: This is treated as absorption. It causes the reduction of the number of tracked particles. Mostly it is used to generate other types of interactions (pair production or Compton scattering) [10].
*Pair production*: During this type of interaction, electron-positron pair is created after a photon absorption. The pair emits thermal energy which equal to 1.022 MeV. Electron is emitted in one direction with the energy of 0.511 MeV in a positron with the energy of 0.511 MeV is emitted in the opposite direction. The relatively rare triplet production is ignored in the MCNP code.
*Compton scattering*: In the MCNP code Compton scattering is important to determine the energy E, of the scattered photon and the angle of deflection from the plane of flight. Immediately at the point of collision, energy is determined and a new scattered photon is tracked further. Energy stored at the point of collision can then be used to obtain the Compton recoil electron and thus used for further transport calculation [8].
This interaction cross-section is described by Klein-Ninsin formula:

$$K(\alpha,\mu)d\mu = \pi r_0^2\left(\frac{a'}{a} + \frac{a}{a'} + \mu^2 - 1\right)d\mu \quad (7)$$

MCNP code photon interaction cross sections are described in different ACE tables in the form ZZZ000.nnP. There are currently four interaction data libraries: nn equals 01, 02, 03, 04: [8]
The newest library "04p" contains new data using the ENDF/B-VI.8 library. It has non-coherent and coherent, photoelectric and pair-creation interaction cross-sections at energies of 1keV-100GeV and Z = 1-100. These data tables have been reviewed and validated, which is why they are used in the MCNP software package. [11]

### 2.4. Photon spectra

Photons spectra lines are obtained when electrons in the outer layers of an atom enter the inner layers. Such transitions are generally prohibited because the lower states are already filled. However, if the inner layer is free (the inner electron is missing, perhaps not a high-speed electron is missing), one of the outer layer electrons can reduce the amount of energy to fill the vacancy. The energy difference for such a transition is quite large, so the wavelength of the emitted photon is quite short.
Photons can be obtained by bombarding a metal target with high-energy electrons. Using Janis software and ENDF/B-VIII library, Tungsten spectrum was calculated (Fig. 3) [12].

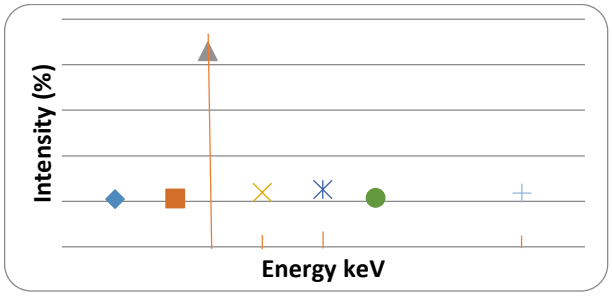


**Fig. 3.** Discrete photons spectrum of Tungsten

### 2.5. Flux to dose rate conversion factors

MCNP software package can count photon fluxes, but it cannot provide dose rate, but by entering conversation coefficients into grid parameters, we can calculate dose rate for calculated particle fluxes.

**Table. 2.** Conversation factors [8]

| Energy, Mev | Dose rate, rem/h | Dose rate, Sv/h |
|---|---|---|
| 0.01 | 2.78E-06 | 6.10E-02 |
| 0.015 | 1.11E-06 | 8.30E-01 |
| 0.02 | 5.88E-07 | 1.05 |
| 0.03 | 2.56E-07 | 0.81 |
| 0.04 | 1.56E-07 | 6.40E-01 |
| 0.05 | 1.20E-07 | 5.50E-01 |
| 0.6 | 1.11E-07 | 5.10E-01 |
| 0.08 | 1.20E-07 | 5.30E-01 |
| 0.1 | 1.47E-07 | 6.10E-01 |
| 0.15 | 2.38E-07 | 8.90E-01 |
| 0.2 | 3.45E-07 | 1.20E+00 |
| 0.3 | 5.56E-07 | 1.80E+00 |
| 0.4 | 7.69E-07 | 2.38 |
| 0.5 | 9.09E-07 | 2.93E+00 |
| 0.6 | 1.14E-06 | 3.44E+00 |
| 0.8 | 1.47E-06 | 4.38E+00 |
| 1 | 1.79E-06 | 5.20E+00 |
| 1.5 | 2.44E-06 | 6.90E+00 |
| 2 | 3.03E-06 | 8.60E+00 |
| 3 | 4.00E-06 | 1.11E+01 |
| 4 | 4.76E-06 | 1.34E+01 |
| 5 | 5.56E-06 | 1.55E+01 |
| 6 | 6.25E-06 | 1.76E+01 |
| 8 | 7.69E-06 | 2.10E+01 |
| 10 | 9.09E-06 | 2.56E+01 |

There are various conversion factors, but the medical physicist communities agree that the difference is not fundamental, and most often the differences in the coefficients result from different assumptions about source anisotropy, direction and model geometries.
These factors are often recalculated and modified by various national and international organizations such as: the National Commission on Radiation Protection, the American National Institute for Standards, and so on. Changes may be based on the results of new experimental calculations [8].
Conversion coefficients reported in the literature allows to convert the most common energies (MeV) to (rem/h). However, we can make further calculations and express the data in Sv/h
Conversion factors used in this work are the conversion table ICRP213 created in 1977 (table 2).

### 2.6. Shielding materials

Main parameters characterizing the absorptive properties of photons are the linear and mass attenuation coefficients. When the radiation consists of photons with monochromatic energy, then material linear attenuation coefficient is the same at all points through a layer of x-thickness. So number of photons that penetrate is [13]:

$$N(x) = N_0 e^{-\mu x} \tag{9}$$

Where: $N_0$ is the initial number of photos entering the material, x – thickness of the material, μ is the linear attenuation coefficient. Instead of the linear attenuation coefficient μ - mass attenuation coefficient $\mu_m$ is often used [14]:

$$\mu_m = \frac{\mu}{\rho}. \tag{10}$$

Mostly used materials as shielding in the Linacs' treatment head is Lead, Tungsten and stainless steel.
*Lead:* is the most commonly chosen shielding material because of it density, high atomic number, stability, easy production, high flexibility. Surfaces of lead are smooth, which makes it less likely to get contaminated with other substances, which in turn can become radioactive [15].
Lead mass attenuation coefficient when photon energy varies from 1-30MeV is about 0.12$cm^2g$, and the linear attenuation coefficient decreases as the energy varies from 1MeV to 4MeV from 0.79$cm^{-1}$ to 0.48$cm^{-1}$ and as the energy increases to 30MeV it reach 0.807$cm^{-1}$.[9]
*Tungsten*: alloys are very dense, so because of good absorption properties it makes them ideal for radiation protection in nuclear medicine or the nuclear industry. Radiation absorption properties also vary depending on the radiation energy. Mass attenuation coefficient of tungsten is about 0.112 $cm^{2}{\cdot}g$ in the energy range 1-30 MeV. [9].
*Stainless steel*: Steels contain heavy elements such as Cr, Fe, Ni and Cu, which have good shielding properties in the medium energies. Therefore, these materials are widely used in radiation protection in medicine. As the photon energy varies from 1-6MeV, the linear attenuation coefficient varies from 0.46 to 0.23 $cm^{-1}$ [17]

## 3. Software

### 3.1. MCNP-VIS

Monte Carlo N-Particle Visual Editor is internationally recognized as the best code for visually creating MCNP input files. This project improved the capabilities of the visual editor by allowing models to be scanned from computer design (CAD) files, allowing the user to modify and view the CAD file and then electronically generate and print valid MCNP input geometry [17].

### 3.2. MCNP

MCNP particle transfer code was developed by the Los Alamos National Laboratory in the United States. It was software code written using FORTRAN and C programming languages. MCNP can be used to perform heavy nuclear transfer calculations and is widely used in many areas such as nuclear fusion/fission reactor design,

radiation safety and dosimetry calculations in medical physics. Code allows simulate neutrons which energy range from 10-5 eV to 150 MeV and photons with energy range 1keV to 100GeV [8].

### 4. Results

Two models found in the literature, based on the first source, were used to develop a treatment head model. It was created using the MCNP-VIS software package visedX_23Z_740. This version allows for easier model creation, but later the model was created using version vised61_24j.23. Because MCNP6 is a newer and more reliable version than MCNPX.

Source is in the middle of this model. It is a square with a dimensions of 40x48 mm and is made of tungsten. In the upper part of the target there as a 1 cm empty space left where electrons interact with the target. The primary collimator is a sphere with a radius of 43 cm made out of tungsten. LINACs' radiation shielding was created using spheres with a radius of 95 cm and 120 cm. Each of the spheres contains a high atomic number materials such as stainless steel (SS-316L).

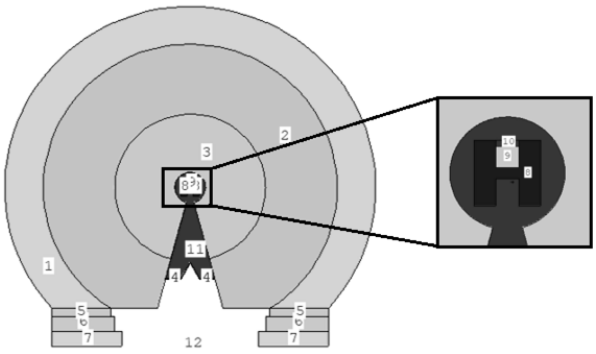

**Fig. 4**. Created linear accelerator treatment head model in the Y-Z plane.

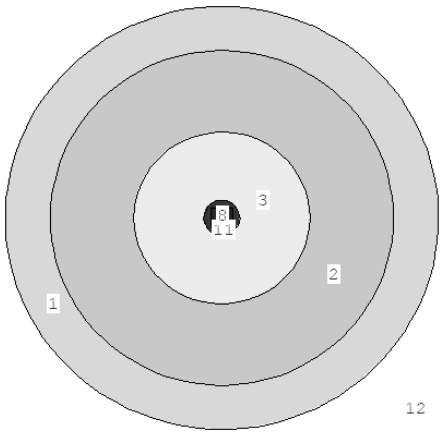

**Fig. 5**. Created linear accelerator treatment head model in the Y-X plane.

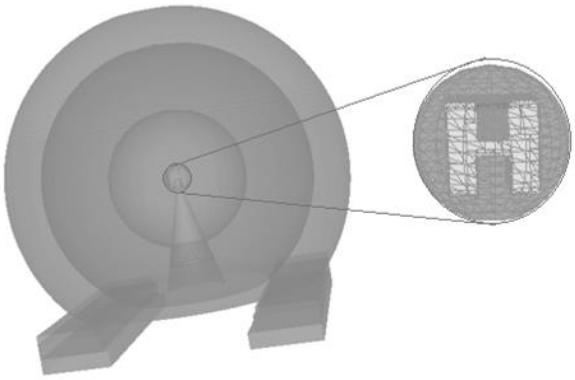

**6 Pav**. Created linear accelerator treatment head 3D model

Calculation of photon flux and dose rate was made using MCNP software. There were a total of $10^7$ calculated particle stories. Using MCNP-VIS, the occurrence and distribution of particles in space were recorded.

**Table 3** Information regarding the occurrence and loss of photons

| Photons occur | Amount | Energy MeV |
|---|---|---|
| Source | 1000010 | 25 |
| Bremsstrahlung | 28248718 | 9,4831 |
| Photon fled away | 2824646 | 1,44 |
| Single fluorescence | 11920712 | 0,5 |
| Double fluorescence | 1574960 | 0,1 |
| total | 45569046 | 36,4 |
| **Photon lost** | **Amount** | **Energy MeV** |
| Go away from mesh | 17445 | 0,05 |
| Energy loss | - | 0,0046 |
| Compton scattering | - | 6,84 |
| Electron capture | 44139011 | 4,26 |
| Pair creation | 1412323 | 25,296 |
| total | 45568779 | 36,441 |

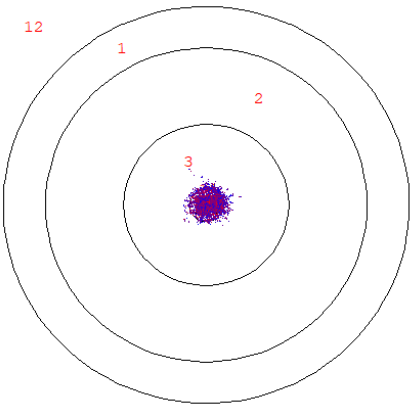

**Fig. 7.** in the Y-X plane. Minimum Energy: 0.001MeV, Maximum Energy: 26,248MeV

As can be seen from Figures 7 and 8 the photons are distributed locally around the selected point source. However, a few photons were tracked both inside cell 11 and outside the filter (cell 4).

For dose rate calculations, $10^7$ particle transfer calculations were performed, and we see that the dose rate varies from $1.7 \cdot 10^{-9}$ Sv/h to 0.4 Sv/h. As can be seen in Figure 9, most of the dose rate is in the source area and

has not spread throughout the treatment head in all directions, indicating that the photon absorbers are well selected. Propagation is only visible towards the filter through the airspace, but towards the filter, photons penetrate the structure. This may result in an additional dose for the patient.

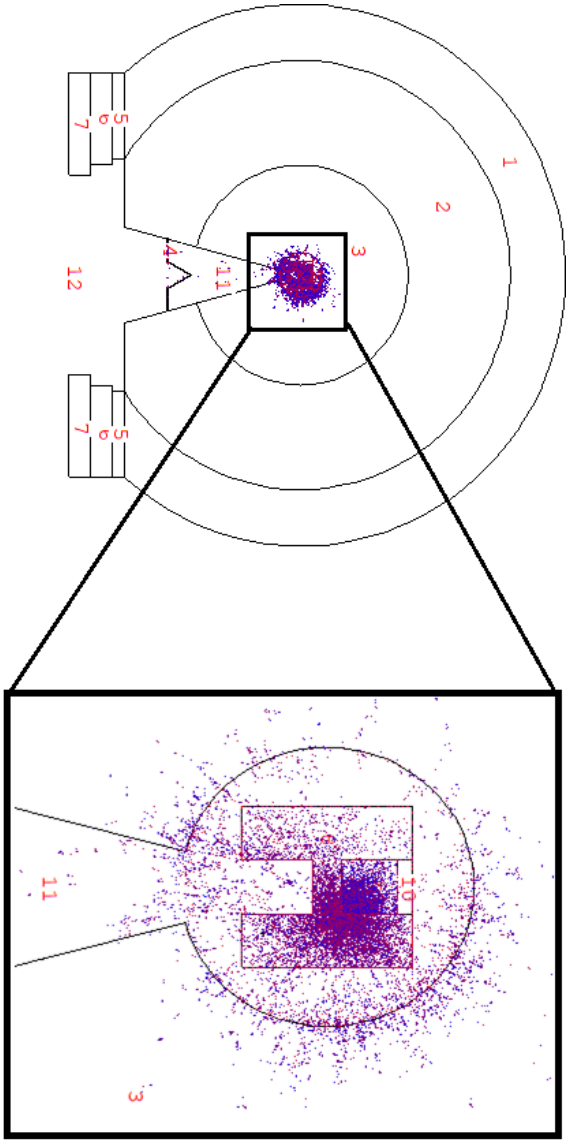


**Fig. 8.** Particle distribution in medical treatment head in the Y-Z plane. Minimum Energy: 0.001MeV, Maximum Energy: 26,248MeV

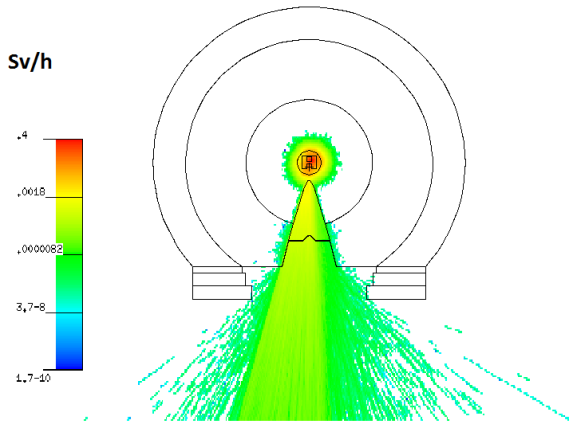


**Fig. 9.** Distribution of the dose rate of the created linear accelerator treatment head in the Y-Z plane

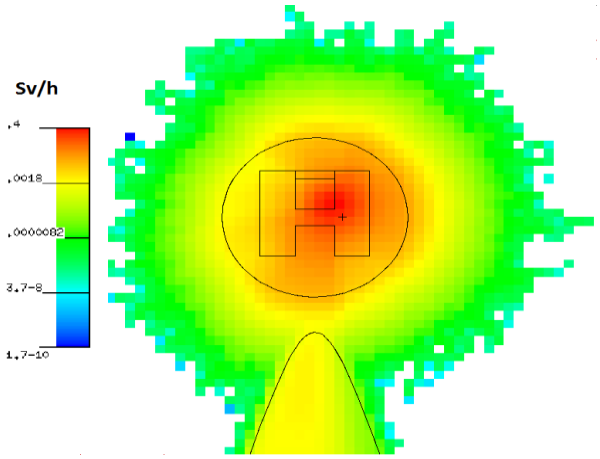


**Fig. 10**. Distribution of the dose rate of the created linear accelerator treatment head in the Y-Z plane near source

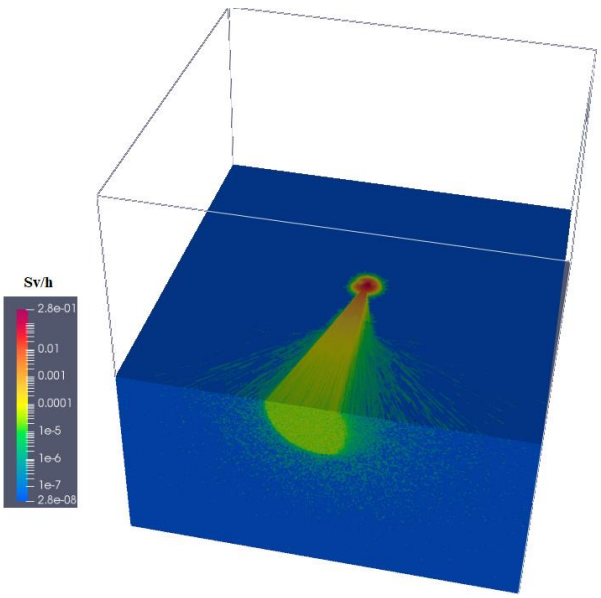


**Fig. 10**. 3D distribution of the dose rate in the created treatment head.

## 5. Conclusions

Using the MCNP6 software package, $10^7$ particle transfer calculations were performed and using MCNP-VIS photon distribution in device geometry was modeled. MCNP- VIS analysis showed that generated photons are located in the cells near the source and in air-filled space. For dose rate calculations, $10^7$ particle transfer calculations were performed, which showed that the dose rate varied from $1.7 \cdot 10^{-10}$ Sv/h to 0.4 Sv/h. Most of the dose rate is in the source area and the distribution is down streaming direction.

Despite that LINACs' treatment head uses high atomic number shielding materials, with high density, it was shown that some penetration happens nonetheless and that this may cause some additional dose to the patient.

## 6. References


1. Retrieved from. https://www.varian.com/.
2. Retrieved from http://www.elekta.com/.
3. A. Baumgartner, A. Steurer, and F. Josef Maringer, "Simulation of photon energy spectra from Varian 2100C and 2300C/D Linacs: simplified estimates with PENELOPE Monte Carlo models," , (2009) Applied Radiation and Isotopes, vol. 67, no. 11, pp. 2007–2012.
4. S. A. Martínez-Ovalle, et.al, "Neutron dose equivalent and neutron spectra in tissue for clinical linacs operating at 15, 18 and 20 MV," Radiation Protection Dosimetry, vol. 147, no. 4, Article ID ncq501, pp. 498–511, 2011.
5. JIMENEZ J. S, M. Díaz Lagos, and S. A. Martinez-Ovalle, "A Monte Carlo Study of the Photon Spectrum due to the Different Materials Used in the Construction of Flattening Filters of LINAC," Computational and Mathematical Methods in Medicine, [interactive]. 2017.article id 36216631. p 8. Retrieved from doi: .https://doi.org/10.1155/2017/3621631.
6. CLARKE Shaun, et al., "Monte Carlo Simulation for LINAC Standoff Interrogation of Nuclear Material"., 2017 OAK RIDGE NATIONAL LABORATORY (2007)
7. WILLIAM L. Dunn and J.Kennetth Shultis Exploring Monte Carlo Methods (2011) ISBN: 978-0-444-51575-9
8. X-5 MONTE CARLO TEAM, MCNP- a General Monte Carlo N-particle transport code, version 5, 2003m
9. HUBBEL, J. H. Photon Cross Section, Attenuation Coefficients and Energy absorption Coefficients. From 10 keV to 100GeV [interactive] 1969. Retrieved from: https://www.govinfo.gov/content/pkg/GOVPUB-C13-d79ab365252ddc7cff96dd333b3e2277/pdf/GOVPUB-C13-d79ab365252ddc7cff96dd333b3e2277.pdf
10. P. Oblozinsky, et. Atl., "Handbook on Photonuclear Data for Applications: Cross-Sections and Spectra," IAEA-TECDOC-1178, International Atomic Energy Agency: Vienna, Austria (2000).
11. D. E. Cullen, J. H. Hubbell, and L. D. Kissel, "EPDL97: The Evaluated Photon Data Library, '97 Version," (1997), UCRL-50400, Vol. 6, Rev. 5, Lawrence Livermore National Laboratory.
12. Retrieved from: https://www.sbir.gov/sbirsearch/detail/
13. SNOVER K A. Giant Resonances in Excited Nuclei Annual Review of Nuclear and Particle Science [Interactive] vol. 36:545-603 Retrieved from doi: https://doi.org/10.1146/annurev.ns.36.120186.002553
14. WEIBER, Joshep Properties of Metals Used for RF Shielding [interactive] 1993, Retrieved from:https://mri-q.com/uploads/3/4/5/7/34572113/lindgren_metals_used_for_rf_shielding.pdf
15. A guide to the use of lead for radiation shielding [Interactive] 2016 Retrieved from: https://www.canadametal.com/wp-content/uploads/2016/08/radiation-shielding.pdf
16. Retrieved from https://www.astm.org/BOOKSTORE/DS68/pg53.pdf
17. Retrieved from http://www.mcnpvised.com/visualeditor/visualeditor.html

*MEDICAL PHYSICS IN THE BALTIC STATES 14 (2019)*

Proceedings of International Conference "Medical Physics 2019"
7 – 9 November 2019, Kaunas, Lithuania

# EVALUATION OF LEAD EQUIVALENT IN LEAD-FREE MATERIALS

Ieva MASIULYTĖ[1], Marius LAURIKAITIS[2]
[1]Kaunas University of Technology, Faculty of Mathematics and Natural Sciences;
[2]Hospital of Lithuanian University of Health Sciences Kaunas Clinics, Oncology Hospital, Radiotherapy Department.
iev.masiulyte@gmail.com; marius@medicinosfizika.lt

***Abstract:*** During radiology procedures, when it is used ionising radiation, the staff should wear the protective cloths, protecting them from scattered radiation. Today the most popular material used for protection is lead, which has a lot of advantages, but also disadvantages, like lead is known as a toxic material, all wearable protection is heavy, aprons can cause back pains or even traumas, and etc. In the last decade it is offered many various types of materials, which could be used instead of lead (tungsten, bismuth, tin, antimony, copper, and etc.). Replacing lead with these materials it is possible to make protections lighter and more comfortable. However, the basic problem of lead-free protections is that it is not always fulfil manufacturer's requirements.

***Keywords:*** Attenuation, lead equivalence, lead-free materials, shielding.

## 1. Introduction

The staff during radiology procedures when using X-rays should wear protective cloths protecting them from scattered X-rays. The most popular material used for protection is lead, as lead has high radiation absorption rate. From this point of view, it has a lot of advantages, but from health side it is not so great option. Lead is known as a toxic material, also because of its high atomic mass it is heavy metal. It means that all wearable protection is heavy, aprons can cause back pains or even traumas, caps are too heavy to properly wear it, with gloves we cannot reach high precision. Scientists in the last decade offered many various types of materials to use instead of lead. For this purpose we are able to use other materials such as tungsten [1], bismuth, tin, antimony, copper, and etc., also various polymers. By replacing lead we can make it lighter what helps to reduce chances to get health disorders, also it will be more comfortable [2]. The main problem of these lead-free protections is that it is not always fulfil requirements, and not meet lead equivalence which is stated by manufacturers.
The aim of this work is to measure attenuation properties and determine lead equivalent for non-leaded materials, which can be used for personal radiation protection.

## 2. Materials and methods

Attenuation properties of the materials used to protect against radiation were determined using the diagnostic X-ray machine Siemens MULTIX PRO. For the measurement methodology were chosen narrow beam configuration [3]. Experimental setup is shown in figure 1. The Fluoro Unfors Multi-O-Meter with external dose probe was used to perform dose measurement. The specimen was placed between X-ray unit and dose meter in a primary beam. The distance between the focal spot and the detector was 1000 mm and the specimen was placed in between. The attenuation properties determination experiments were performed using 81 kVp energy, the HVL of the system was 4.0 mm Al. The field size were collimated that to cover the dose detector.
The attenuation of the material was calculated after measuring exposure without sample and with sample, using equation 1.

$$Attenuation(percent) = \left(1 - \frac{expose\ with\ sample}{expose\ without\ sample}\right) x100 \quad (1)$$

The lead equivalence were determined and compared with the values declared by material manufacturer. The pure lead (99.9 %) attenuation curve was measured for lead equivalency determination. The specimen lead equivalency was found from this curve.
There were used different samples for determination of attenuation properties – KI-ARMOR Bi-Layer Lead-Free material (0.25 mm LE); KI-ARMOR Bi-Layer Lead-Free material (0.35 mm LE), Leaded Thyroid Shield (0.3 mm Pb).

## 3. Results and discussion

The measurement of attenuation curve is shown in figure 2. Using this curve and plotting measured attenuation of samples, we found the lead equivalent of each sample. Comparison of the results and manufacture stated lead equivalents is shown in table 1.

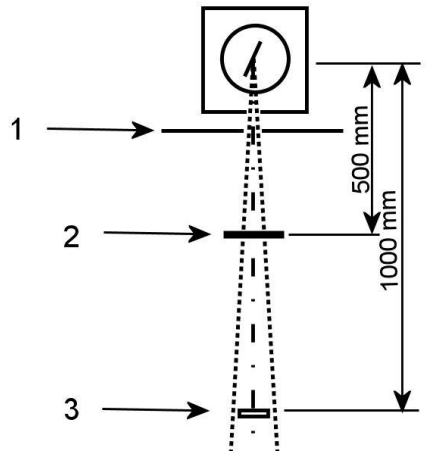


**Fig. 1.** Experimental setup. 1 – beam limiting device; 2 – sample; 3 – detector.

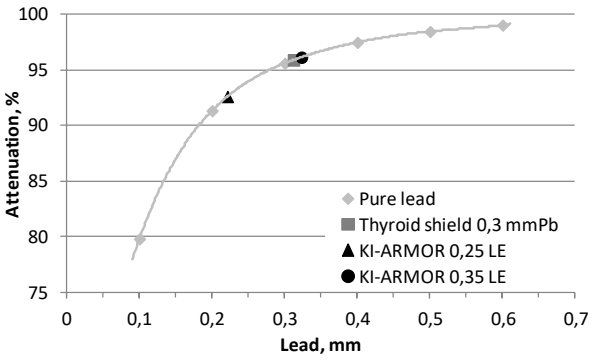


**Fig. 2.** Attenuation curve from lead thickness at 81 kVp (HVL 4 mm Al) and determination of lead equivalence of samples.

**Table 1.** Comparison of the results and manufacture stated lead equivalents.

| Sample | Manufacturer stated lead equivalence, mm | Determined lead equivalence, mm |
|---|---|---|
| Thyroid shield | 0.30 | 0.31 |
| KI-ARMOR 1 | 0.25 | 0.22 |
| KI-ARMOR 2 | 0.35 | 0.32 |

The leaded material (Thyroid shield) represents good agreement of stated and measured lead equivalence. The determined lead thickness is 4 % higher than declared value. Both KI-ARMOR lead free materials showed less lead equivalence values than stated manufacturer. The difference were 11.6 % for KI-ARMOR 1 and 7.7 % for KI-ARMOR 2.

The measurement methodology is used to determine the attenuation properties of materials used for primary beam shielding. The lead free materials uses high-Z elements such as Sn, Sb, Ba and W, whose K-edge absorption and photoelectric interactions can attenuate incoming radiation [4]. Due to lower attenuation of lead free materials were registered. The lead free materials are designed to use in scattered radiation, so the attenuation properties should be measured in different methodology, simulating real usage conditions. Also lead free materials should not be used to protect from primary X-ray beam and should not be used for patient's protection.

## 4. Conclusions

The KI-ARMOR free lead materials shows lower lead equivalence comparing with manufacture stated values due to the fact, that it is measured in primary beam experimental setup. For this reason should be used another methodology evaluating the lead equivalency, like it is described in [5].

## 5. References

1. Adlienė D., Griškonis E., Vaičiūnaitė N., Plaipaitė-Nalivaiko R.,. Evaluation of new transparent tungsten containing nanocomposites for radiation protection screens. Radiation protection dosimetry. Oxford : Oxford University Press. Vol. 165, Iss. 1-4, 2015, p. 406-409.
2. Miller D.L., Vano E., Bartal G., Dixon R., Padovani R., Schueler B., Cardella J. F., de Baere T. Occupational radiation protection in interventional radiology: a joint guideline of the Cardiovascular and Interventional Radiology Society of Europe and the Society of Interventional Radiology. Cardiovascular and Interventional Radiology, Vol. 33, No. 2, 2009.
3. ASTM International, F2547-06: Standard Test Method for Determining the Attenuation Properties in a Primary X-ray Beam of Materials Used to Protect Against Radiation Generated During the Use of X-ray Equipment, 2006.
4. Yucel H., Gulluoglu E., Cubukcu S., Uncu Y.A., Measurement of Attenuation Properties of the Protective Materials Used as a Thyroid Guard and Apron for Personnel Protection against Medical X-rays. Journal of Physical Science, Vol. 27(1), 2016, p.111-128.
5. ASTM International, F3094-14: Standard Test Method for Determining Protection Provided by X-ray Shielding Garments Used in Medical X-ray Fluoroscopy from Sources of Scattered X-Rays, 2014.

*MEDICAL PHYSICS IN THE BALTIC STATES 14 (2019)*

Proceedings of International Conference "Medical Physics 2019"
7 – 9 November 2019, Kaunas, Lithuania

# ESTIMATION OF $^{99m}Tc$ LEVELS IN URINE SAMPLES FOR NUCLEAR MEDICINE WORKERS

Simas JANKAUSKAS[1], Jurgita LAURIKAITIENĖ[1,2], Irina GINEIKIENĖ[3]
[1]Kaunas University of Technology, The Faculty of Mathematics and Natural Science, Kaunas, Lithuania;
[2]Oncological Hospital of Kaunas Clinics, Radiotherapy Department, Kaunas, Lithuania;
[3]The Hospital of Lithuanian University of Health Sciences Kaunas Clinics, Radiology Department, Kaunas, Lithuania
simas.jankauskas@yahoo.com, jurgita.laurikaitiene@ktu.lt, irina.gineikiene@lsmu.lt

***Abstract:*** The usage of a wide variety of radionuclides in nuclear medicine usually results in a significant risk of long-term exposure to a low-level radiation for the workers. $^{99m}Tc$ is the most frequently used radioisotope for medical purposes, due to its application for various diagnostic procedures, to diagnose various malignant tumors and other diseases. Such wide usage of radionuclide creates a demand for effective methodologies, which could be helpful to perform occupational monitoring.

***Keywords:*** nuclear medicine, $^{99m}Tc$, occupational exposure, gamma spectroscopy.

## 1. Introduction

One of the biggest hazards working in a department of nuclear medicine is the possibility of long-term exposure effects to low-level radiation that follows biological effects, due to specifications of un-sealed sources usage and possible exposure of the staff. A lot of attention has been paid in recent years for radiation protection in nuclear medicine department, due to use of short half-life radiopharmaceuticals like $^{99m}Tc$ (half-life of 6.01 hours) [1-3].

Occupational whole-body workers' exposure are effectively controlled by the use of lead shielding between the worker and radioactive sources, but internal exposure may occur, if handling of radionuclides is enough frequent or the protection of working environment is insufficient. Evidence of genotoxic effects during periods of long-term radiation exposure has been reported [1-2]. While biological effects of moderate and high doses are evident, there are considerable considerations regarding the biological effects due to low-dose exposures as well [1]. However, individual monitoring of internal exposure to short-lived radionuclides could be challenging, because these radionuclides rapidly vanish from the body. According to this reason, quantitative dosimetry addressing the internal doses from the short-lived radionuclides, like $^{99m}Tc$ is often overlooked [4]. Anyway, assuring that the level of the internal contamination is not exceeding the accepted limits, various dosimetry techniques should be used. For example, *in vitro* tests of urine samples are often used for individual monitoring of internal occupational exposure. Pros of *in vitro* tests are: inexpensive in compare with the *in vivo* assay, utilising whole-body counters, it can be applied for alpha, beta and gamma emitter, and the samples for analysis can be done outside the institution [2].

The aim of this study was to analyse detection of $^{99m}Tc$ radionuclide in urine samples for nuclear medicine department personnel, using gamma spectrometry.

## 2. Methods and materials

### 2.1. Sampling

Sixteen samples of urine were collected from nuclear worker, who was working with $^{99m}Tc$ radionuclide in nuclear medicine department.

Samples were collected into sterile plastic urine sampling bottles for 4 weeks period: on mondays before work with $^{99m}Tc$ (to measure the balance of radionuclide remaining after weekend), on mondays after work with $^{99m}Tc$ (to measure level of radionuclide after one working day) and on fridays after 5 working days period with $^{99m}Tc$. Also one bottle of plastic urine sampling was used for background measurements.

### 2.2. Measurements of $^{99m}Tc$ spectroscopy

Ten millilitres of each urine sample were taken and poured into test-tubes (figure 1). Then test–tubes were put into gamma spectrometer "CompuGamma 1282" and spectrum of each radionuclide were measured for 100 000 s.


**Fig. 1.** Gamma spectrometer "CompuGamma 1282" test-tubes.

Gamma spectrometer "CompuGama 1282" (figure 2) is a device that can operate as a counter of impulses to measure samples activity and as a gamma spectrometer to determine composition of radionuclides. Automatic micro-computer manages universal gamma counter, which counts gamma photons emitted by radionuclides in range of energy 10-2000 keV.

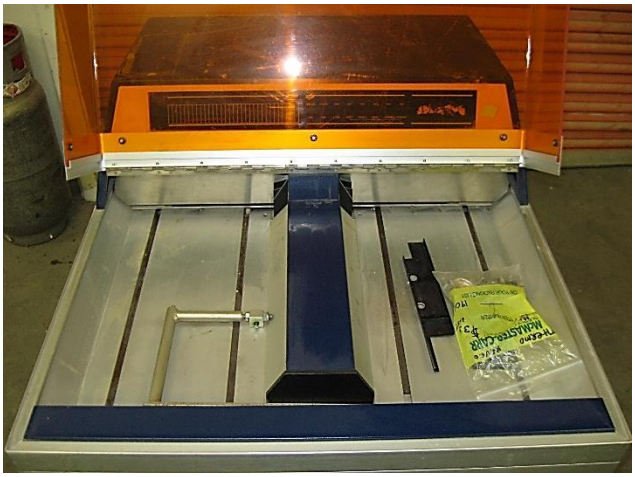

**Fig. 2.** Gamma spectrometer "CompuGamma 1282" spectrometer.

Using histogram of the measurement, channel number was recalculated to an energy using formula:

$$E = 10 \cdot 200^{\frac{k}{256}}, \quad (1)$$

where k – channel number and E – photon energy, keV.

It is known, that an average energy of $^{99m}Tc$ is 140.53 keV, according to 1.4 % of 142.60 keV energy and 98.6 % of 140.50 keV energy:

$$E = 0.014 \cdot 142.6 + 0.986 \cdot 140.5 = 140.53\ keV \quad (2)$$

Registered counts were recalculated into activity (Bq) using formula:

$$A = \frac{CPM}{60s}\ [Bq], \quad (3)$$

where CPM means counts per minute.

## 3. Results and discussion

Every day (5 days per week) before starting dilutions of $^{99m}Tc$, worker measures the activity of radionuclide, which is "taken" from technetium–molybdenum generator (table 1).

**Table 1.** Activity of $^{99m}Tc$ taken from technetium–molybdenum generator per 4 weeks.

| Weeks | Activity on monday, MBq | Activity on friday, MBq | Total activity/5 days, MBq |
|---|---|---|---|
| 1 | 8520 | 2800 | 29820 |
| 2 | 8340 | 2700 | 25190 |
| 3 | 8430 | 2670 | 25450 |
| 4 | 8460 | 2760 | 25430 |
| Average activity, MBq | 8437.5 | 2732.5 | 26472.5 |

Total average activity per all 4 weeks investigation with which worker had worked was 26472.5 MBq, which differed from 25190 MBq to 29820 MBq per one working week (5 days/week). According to a short half-life (6.01 hours) of $^{99m}Tc$, due to decay processes, during whole working week, the generator must be renewed every week, that's why activity on monday is higher than on friday. Due to this reason, if it is possible, it is recommended to make some sort of replacements between co-workers, during a working week, so trying to minimize the worker's exposure.

Analysing registered data of urine samples with gamma spectrometer "CompuGamma 1282" the total number of counts were recalculated into activity (table 2) Measurements of the background sample showed, that in this sampleactivity of $^{99m}Tc$ were not registered. The main difference of the registered results were observed just analysing the urine samples taken on monday before work and after work (table 2), then the registered average activity increased ~0.24 % from 0.00095 Bq (before work) to 0.00126 Bq (after work), while F. Araújo and etc. [3] showed, that using liquid $^{131}I$ in one millilitre of urine sample were registered activities from 1.2 Bq to 46 Bq. So registered percentage difference (~0.24 %) of this increase was not so significant in evaluated urine samples, due to the main $^{99m}Tc$ characteristic: solid phase. Differently as $^{131}I$ registered enough high activities in urine samples [3], which could be in a liquid phase and could be

inhaled [4-5], $^{99m}Tc$ registered activities were so low, due to possible absorbtion through the arms, as it is direct contact with a radionuclide.
Also, from the registered data it is not seen any significant difference in determined activity between the measurements after work on monday and friday (what could have be expected) and it could be related to the lower activity of radionuclide on fridays in compare with an activity on mondays (table 2).

**Table 2**. Activity of $^{99m}Tc$ in urine sample and background radiation registered on monday before work and after work and on friday after work with radionuclide.

| Weeks | Monday (before work) | |
|---|---|---|
| | Activity, Bq | Total no. of counts |
| 1 | 0.00097 | 97 |
| 2 | 0.00094 | 94 |
| 3 | 0.00094 | 94 |
| 4 | 0.00095 | 95 |
| Average values | 0.00095 | 95 |
| Background activity | 0.00000 | |
| Weeks | Monday (after work) | |
| | Activity [Bq] | Total no. of counts |
| 1 | 0.00128 | 128 |
| 2 | 0.00125 | 125 |
| 3 | 0.00125 | 125 |
| 4 | 0.00126 | 126 |
| Average values | 0.00126 | 126 |
| Background activity | 0.00000 | |
| Weeks | Friday (after work) | |
| | Activity [Bq] | Total no. of counts |
| 1 | 0.00098 | 98 |
| 2 | 0.00093 | 93 |
| 3 | 0.00095 | 95 |
| 4 | 0.00094 | 94 |
| Average values | 0.00095 | 95 |
| Background activity | 0.00000 | |

Even, if a gamma spectroscopy is methodology normally used for occupational exposure monitoring of $^{131}I$ [5-6], depending on activity of the day, some significant changes could be registered using and $^{99m}Tc$ radionuclide.

## 4. Conclusions

Activity of $^{99m}Tc$ in urine samples of the worker were determined using gamma spectroscopy. Results showed, that even if, $^{99m}Tc$ is used in a solid phase, anyway it is possible to register very low activities changes, but due to low activities it is not recommended to use this method as a dosimetry or routine monitoring for $^{99m}Tc$ radionuclide.

## 5. References

1. Noh S., Jeong S., An M., Jang H.K., Kwon T.E., Lee J.I., Park T.J., Lee J.K..International Dosimetry for Inkate of $^{18}FDG$ Using Spot Urine Sample. Radiat Prot Dosimetry, Vol. 168, No. 3, 2016, p. 343-9.
2. Al-abdulsalam A., Brindhaban A. Occupational Radiation Exposure among the Staff of Departments of Nuclear Medicine and Diagnostic Radiology in Kuwait. Med Princ Pract. Vol. 23, No. 2, 2014, p.129-33.
3. Araújo F., Corbo R., Dantas A. L. A., Dantas B. M., Lucena E. A., Rebelo A. M. O., Sousa W. O. Evaluation of Internal Exposure of Nuclear Medicine Staff Through *in vivo* And *in vitro* Bioassay Techniques. Radiation Protection Dosimetry, Vol. 127, No. 1-4, 2007, p. 465-468.
4. Bangvirunrak J., Nukultham A., Peekhunthod D., Pukkhaw T., Sansakon S. Baseline Quantity of $^{131}I, ^{137}Cs, ^{134}Cs$ and $^{40}K$ in Urinary Excretions from Thai People and Internal Exposure Dose. IOP Conf. Series: Journal of Physics: Conf. Series 860, 2017, 012038.
5. Bitar A., Doubal A. W., Maghrabi M. Assessment of Intake And Internal Dose From Iodine-131 for Exposed Workers Handling Radio-pharmaceutical Products. Appl Radiat Isot. Vol.82, 2013, p. 370-5.
6. Kol R., Pelled O., Canfi A., Gilad Y., German U., Laichter Y., Lantsberg S., Fuksbrauner R., Gold B. The Interference of Medical Radionuclides With Occupational *in vivo* Gamma Spectrometry. Health Phys. Vol. 84, No. 6, 2003, p. 756-63.

*MEDICAL PHYSICS IN THE BALTIC STATES 14 (2019)*

Proceedings of International Conference "Medical Physics 2019"
7 – 9 November 2019, Kaunas, Lithuania

# ELECTRON IRRADIATION AS A METHOD OF INCREASING EFFICACY OF SOME WATER SOLUBLE DRUGS IN ONCOLOGY

L.I. ASLAMOVA[1], M.A. ZABOLOTNYY[1], G.I. DOVBESHKO[2], G.I. SOLYANIK[3]
[1]Taras Shevchenko National University of Kyiv, Ukraine; [2]Institute of Physics of NASU, Kyiv, Ukraine; [3]R.E. Kavetsky Institute of Experimental Pathology, Oncology and Radiobiology of NASU, Kyiv, Ukraine
aslamova258@gmail.com; fedcba137@ukr.net; gd@iop.kiev.ua; gsolyanik@gmail.com

***Abstract:*** The effect of pre-irradiation with high-energy electrons of a physiological solution on the absorption spectra and therapeutic characteristics of the Conium and Doxorubicin drugs dissolved in it was investigated.

***Keywords:*** Conium, Doxorubicin, electrons irradiation, absorbed dose of irradiation, oncology.

## 1. Introduction

To date, there is a steady tendency towards individualization of treatment of cancer patients, which is associated with the individual sensitivity of the body to therapeutic agents (which may vary 10-40 times) and the selectivity of their antitumor activity. The latter manifests as a small difference between the dose of antitumor drugs, which provides effective inhibition of the tumour process, and the dose that causes significant damage to normal organs and tissues of the body. It is also important that malignant tumour resistance makes a significant contribution to the variability of the body's sensitivity to antitumor drugs. Actuality of the research is due to the necessity to create non-destructive physical methods of modification of antitumoral preparations for the increase of their therapeutic efficiency [1, 2].
Main research objective described in this paper - is the study and analysis of influence of previous electrons irradiation of solvent on optical and therapeutic properties of solution of medicinal preparations of anthracycline and alkaloid rows for the increase of their efficiency [2].

## 2. Materials and methods

Experiments were performed with doxorubicin ("Pharmacia Italia SpA", Italy) and Conium (Weleda, Germany). Conium, contains a number of alkaloids, the main of which are Coniin ($C_8H_{17}N$), N-Methylconiin ($C_9H_{19}N$), γ-Conitsiin ($C_8H_{15}N$), Conhydrin ($C_8H_{17}NO$) and Pseudoconhydrin ($C_8H_{17}NO$) [3]. As a solvent, a physiological solution of 0.9% NaCl ("Novofarm-Biosynthesis", Ukraine) was used.

All samples for recording IR spectra were prepared in KBr tablets. IR spectra were recorded using a Bruker IFS 66 IR Fourier spectrometer (Germany) in transmission geometry. Accuracy of the determination of the wave number was 0.2 $sm^{-1}$, the accuracy of determining the transmittance - 0.1%. Measurement was carried out no later than 10 days after irradiation of the physiological solution. Sample temperature was within the range of 20-25 °C. Registration and processing of the spectra was carried out using the OPUS 5.5 program.

## 3. Results

Calculations of the dipole moments and the energy of the ground states of the alkaloid's molecules (Table 1) showed that three alkaloids (γ-Conitsiin, Conhydrin, Pseudoconhydrin), of the six studied, have higher dipole moments' values, which can probably lead to the formation of adducts involving these molecules. Of particular interest is γ-Conitsiin, the only of the alkaloids that make up the Conium, which has a double bond connecting the N and C atoms.

**Table 1.** Dipole moments and the energy of the ground state of alkaloids that are part of the Conium

| The name of alkaloid | Dipole moment, D (Debye) | Energy of the basic state, Eh (Energy Hartree) |
|---|---|---|
| Coniin | 0.84 | -371.8857 |
| N-Methylconiin 1 | 0.4628 | -411.7231 |
| N-Methylconiin 2 | 0.4713 | -412.1554 |
| γ- Conitsiin | 1.83 | -369.2145 |
| Conhydrin | 1.30 | -448.1843 |
| Pseudoconhydrin | 2.39 | -451.1421 |

The presence of a double bond in the γ-Conitsiin may indicate the possibility of the formation of stable chemical complexes.
For the molecules of each of the alkaloids, geometry optimization was performed and the IR spectra were

calculated, scale factor of 0.9720 was used for the spectra Fig.1.

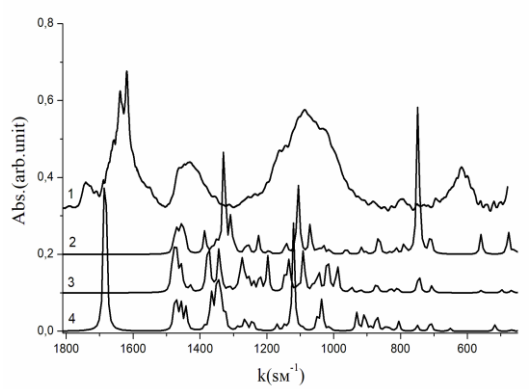


**Fig. 1.** IR spectra. 1- experimental spectrum of the drug Conium, 2 - the calculated data for the Coniin molecule, 3 - the calculated data for the N-Methylconiine molecule, 4 - the calculated data for the molecule of γ-Conitsiin.

Spectral dependences of absorption (A) in the infrared light range, of solutions of therapeutic drugs in non-irradiated and previously irradiated by electrons, was measured. Spectra were determined in the wave vector range (k) $[4{\cdot}10^2–2{\cdot}10^3]$ $sm^{-1}$. Energy of the irradiating electrons was 2.0 MeV. Analysis of the absorption spectra of solutions of alkaloids obtained using irradiated and non-irradiated solvents showed that the addition of an irradiated solvent affects the positions of the maxima of the absorption bands of the Conium. Such a displacement of the absorption lines in the oscillating region of the IR spectrum is evidence of a change in its confirmation state, due to interaction with the molecules of the irradiated solvent. Values of the dose of absorbed (I) irradiation were 10, 20, 40, 60, 80 kGy.

**Table 2.** Characteristics of the used irradiation by electrons are given

| Fluence of the electron flux, $sm^{-2}$ | Irradiation time, s | Absorbed dose of irradiation, kGy |
|---|---|---|
| $6{*}10^{13}$ | 60 | 10 |
| $1{*}10^{14}$ | 76 | 20 |
| $2{*}10^{14}$ | 307 | 40 |
| $4{*}10^{14}$ | 445 | 60 |
| $4{*}10^{14}$ | 580 | 80 |

Correlation analysis of Pearson [4] was used in the comparative analysis of absorption (A (k, I)) of solutions of antitumor drugs. Interval ε is evenly divided by 1200 points.

Study of the ability of high-energy electron irradiation of a physiological solution, as a solvent of a drug, to modify the pharmacological activity of the antitumor drug doxorubicin was investigated in vitro using the line of cancer cells of the lung carcinoma of Lewis (LLC). It was recorded that LLC incubation for 24 hours in the presence of doxorubicin, dissolved in a non-irradiated saline solution, resulted in a concentration-dependent decrease in the number of living cells. This behavior is due to inhibition of proliferation of tumor cells (cytostatic action) and/or their death (cytotoxic action) caused by the antitumor drug. At the same time, doxorubicin, dissolved in an irradiated saline solution, leads to an increase in cytotoxic/cytostatic effects, which is most pronounced at low concentrations: so, the number of LLC live cells at concentrations below 3 μM decreased by an average of 20% ($p < 0.05$) compared with the action of doxorubicin, dissolved in a non-irradiated physiological solution. Similar results were obtained in the study with Conium.

## 4. Conclusions

1. Irradiation of the solvent, without substantially changing the medications (in all cases, the correlation coefficient exceeds the critical value), changes some of its properties in the oscillation range, which significantly depends on the conformational state of the molecules.
2. Ability to increase the pharmacological activity of the antitumor drugs Conium and Doxorubicin (especially in the range of low concentrations) with high-energy electron irradiation of a solvent was established. Low variability of cell survival rates after incubation with Doxorubicin and Conium in irradiated physiological saline as compared to the corresponding indices with non-irradiated solvent was registered.
3. By determining the pharmacological activity of the cytotoxic/cytostatic action of aqueous solutions of antitumor drugs (with and without irradiation) in relation to LLC cells in vitro, it has been established that irradiation of aqueous solutions of Doxorubicin and Conium leads to an increase in their cytotoxic/ cytostatic action, most pronounced in relatively low concentrations.
4. Structural forms were determined, the values of the dipole moments and the energy of the ground state of alkaloids included in the Conium were calculated: Coniin, N-Methylconiine, γ-Conitsiin, Conhydrin and Pseudoconhydrin. It has been established that the conformations of the molecules of alkaloids with the lowest energy have the maximum possible linear dimensions and the smallest values (for stable states) of the dipole moment.

## 5. References

1. Ambili Remesh, Toxicities of anticancer drugs and its management, International Journal of Basic & Clinical Pharmacology. – July-August 2012. – Vol. 1. – № 1 – p. 2-12.
2. Заболотний М.А., Куліш М.П., Дмитренко О.П., Соляник Г.І., Прилуцький Ю.І., Драпіковський М.А., Кузьменко М.О., Полуян Н.А., Кияшко В.А., Спосіб модифікації водорозчинних протипухлинних препаратів за допомогою радіаційного опромінення, Патент на винахід № 116 227, Зареєстровано 26.02.2018.
3. Stephen T. Lee, Benedict T. Green, Kevin D. Welch, James A. Pfister and Kip E. Panter, Stereoselective Potencies and Relative Toxicities of Coniine Enantiomers, Chem. Res. Toxicol. – 2008. – Vol. 21. – № 10. – p. 2061-2064.
4. A.G. Asuero, A. Sayago, A.G. Gonzalez, The Correlation Coefficient: An Overview, Critical Reviews in Analytical Chemistry. – 2006. – Vol. 36. – № 1. – p. 41-59.

*MEDICAL PHYSICS IN THE BALTIC STATES 14 (2019)*

Proceedings of International Conference "Medical Physics 2019"
7 – 9 November 2019, Kaunas, Lithuania

# RADIOTHERAPY OF PREGNANT PATIENT – PROCEDURES AND THEIR IMPROVEMENTS TO STRENGTHEN RADIATION SAFETY CULTURE IN MARIA SKŁODOWSKA-CURIE INSTITUTE – ONCOLOGY CENTRE IN WARSAW

Agnieszka KUCHCIŃSKA[1], Elżbieta LAMPKA[2], Wojciech BULSKI[3], Maryna RUBACH[4], Jacek LAMPKA[1], Dorota KIPRIAN[5]

[1] Radiotherapy Department, Maria Skłodowska-Curie Institute-Oncology Centre, Warsaw, Poland.
[2] Lymphoid Malignancies Department, Maria Skłodowska-Curie Institute-Oncology Centre, Warsaw, Poland.
[3] Medical Physics Department, Maria Skłodowska-Curie Institute-Oncology Centre, Warsaw, Poland.
[4] Chemotherapy Day Ward, Maria Skłodowska-Curie Institute-Oncology Centre, Warsaw, Poland.
[5]Leader of Radiotherapy Team of the Maria Skłodowska-Curie Institute – Oncology Centre, Warsaw, Poland.

## 1. Introduction

Radiotherapy of a pregnant patient is a very sensitive topic. In pregnancy, Hodgkin Lymphoma is one of the most common type of tumour after breast cancer. Our Institution is one of the biggest in Poland. Warsaw branch of the Institute has a long experience with successful therapy of pregnant patients (266 patients in period 1988-2018) mostly with breast cancers, sarcomas and lymphomas, including the largest group of 147 patients with Hodgkin Lymphoma, 131 children delivered by this group of patients. Patient treatment schemes included chemotherapy, radiotherpy, surgery performed either alone or combined according to the type of cancer and clinical indication.

## 2. Purpose/Objective

Creation of a proper working environment to promote and build Radiation safety culture is crucial in order to assure patient safety (both mother and child), and therefore all 10 factors (personal accountability, questioning attitude, effective safety communication, leadership safety and actions, decision making, respectful work environment, continuous learning, problem identification and resolution, environment for rising concerns, work process), mentioned by the IAEA during competition called 'towards strong radiation safety culture', are strongly supported by the Director of our institute, and by the relevant involvement of the Leader of Radiotherapy Team whose duty is to oversee and accept all standard medical procedures.

## 3. Materials and methods

All necessary radiation safety procedures have been implemented so far. Nevertheless, due to constant improvement of radiation safety culture, better procedures are under investigation. Project, submitted as a part of the IAEA competition, aimed at strengthening radiation safety culture during the treatment of pregnant patients, was positively evaluated and got through the selection of the first stage.

## 4. Results

Our approach supports all 10 IAEA/WHO BONN calls for actions. Over time treatment approach has developed due to technological and clinical changes. One of the biggest change is that currently the ISRT (Involved site radiation therapy) has replaced MANTEL fields approach, which has significantly contributed to the lower radiation treatment long term toxicity.

## 5. Conclusion

Sharing experience concerning successful therapy of pregnant patients is crucial to contribute to better understanding when treatment (including radiotherapy) during pregnancy is safe for the foetus and for the mother. To support communication and to strengthen the risk-benefit dialogue we closely cooperate with patient organizations, in order to promote and explain among public when treatment of pregnant patients is safe.

*MEDICAL PHYSICS IN THE BALTIC STATES 14 (2019)*

Proceedings of International Conference "Medical Physics 2019"
7 – 9 November 2019, Kaunas, Lithuania

# CORRUPTION PREVENTION IN MEDICINE: LEGAL ASPECTS

Egidijus NEDZINSKAS[1], Rūta NEDZINSKIENĖ[2]
[1]Lithuania Business University of Applied Sciences; [2]Kaunas University of Technology
egidijus.nedzinskas@ltvk.lt; ruta.nedzinskiene@ktu.lt

***Abstract*:** The fight against corruption is one of the main goals of each state. Corruption in medicine is extremely dangerous phenomenon, as the greatest risk is associated with patients' health. The article aims to define the concept of the corruption and to analyse the legal regulation of the corruption prevention in the field of medicine. The results of this article are based on analysis of the scientific literature and legal documentation.

***Keywords*:** Corruption, Corruption prevention, Corruption in medicine, Legal regulation of corruption.

## 1. Introduction

There is a phenomenon of corruption in every state and the aspiration to reduce corruption in the country faces great challenges. According to the Corruption Perceptions Index published by Transparency International in 2018, Denmark is considered the most transparent country in the world, while Lithuania ranks 38 out of 180 in terms of transparency [1].

Corruption has enormous social and economic consequences [2]. It takes place in different sectors – health, education, justice and different places [3]. There are several channels through which corruption hinders economic development including the disproportionate increase in government spending, the distortion of the composition of government spending away from education, health and maintenance of infrastructure toward less-efficient public projects that have a greater scope for manipulation and opportunities for bribes [4].

Corruption is a particularly serious problem in the Lithuanian medical system. The medical system and the services it provides are extremely necessary to the society and indispensable to the people, but corruption in the medical system, compared to other Lithuanian institutions, is increased significant. It is paradoxical, that corruption flourishes in the medical field because the physician, who solemnly has assumed Hippocratic Oath, swears that "I will seek the welfare of the patient, avoid any inhumane steps, misguiding of the patient, and corruption" [5], thus, he/she should completely distance himself / herself from the corrupt acts. However, the increase in corruption in medicine is caused by such factors as low salaries of employees, worsening demographics of the Lithuanian population and emigration of young prospective specialists. Corruption is also stimulated by the perfunctory attitude of the Government and the passive involvement of the society in anticorruption activities. As a result, we face with grand corruption (bribing of the pharmacists by the representatives of the public authorities and the public sector) and petty corruption (when people express their gratitude to the physician for provision of the services with a box of chocolates or a gift).

Medicine is an important link of the public policy because it affects everyone, and corruption in medicine is therefore a major public concern. A big attention to corruption in medicine is paid in different studies [6-12]. Scientists have researched corruption in medicine, highlighting its different forms related to bribery of patients [6-8], unethical promotion of medication [9-10], activities of private medical institutions [10-12].

However, it is important to emphasize that corruption in medicine is one of the most dangerous social phenomena, as the greatest risk is associated with patients' health. Unethical activities in medicine field lead to the factors that disturb patient's quality of life via drug resistance, health compromise and financial burden [13].

Thus the medical field is particularly vulnerable to corruption, and proper legal regulation of the corruption prevention in this area is especially important.

**The goal** of this article is to define the concept of corruption and to analyse the legal regulation of the corruption prevention in the field of medicine. Objectives of the research: 1) to perform the analysis of the concept of corruption; 2) to disclose the forms of corruption in the medical system; 3) to carry out the analysis of the legal regulation of corruption prevention in Lithuania. In this article, the concept of corruption and its forms in medicine there are analysed using the method of the analysis of the scientific literature. The legal basis was analysed using the method of analysis of legal documentation.

## 2. The concept of corruption

Corruption is a global problem which threatens the legal, political, social and economic system. Scientists describe corruption as one of the oldest forms of crime acts [14-16]. Corruption is varying while adjusting to changes in the environment and, due to the complexity of the phenomenon of corruption, there are more than 300 definitions of corruption [15].

Many scientists state that corruption is an abuse of power and authority. [17-19], others highlight that by corruption there is sought a personal benefit [18, 20-22]. Ionescu states that the personal benefit is ensured by the expense of society [21]. Buinickienė emphasizes the benefiting as performing / non-performing of her / his duties in an unlawful and / or unfair manner [22]. Raudonienė highlights that corruption is a deliberate act of a person [23].

The concept of corruption encompasses all spheres of social activity - private, public, as well as the persons performing private and public functions, if they gain the benefits of performing those functions [24]. There are distinguished the most common forms of corruption: 1) bribery; 2) abuse of office; 3) trade in influence; 4) protectionism; 5) nepotism; 6) tax evasion; 7) fraud; 8) cartel agreements [25].

According to the level of the corruption there is determined petty and grand corruption**.** Petty corruption is manifested in making small payments, such as giving a bribe to a policeman or a doctor, expecting a favourable solution. Meanwhile, the grand corruption is trading in laws, court decisions, of public procurements. It manifests in the highest levels of the government where it can be influenced perspectives of the development of the legislation, politics, state and social affairs [7].

Klitgaard points out, that corruption is stimulated by a monopoly on public services, discretion in decision-making (the right to decide a matter at his/her own discretion) and a lack of responsibility for wrongful decisions [26]. Ackermann points out that corrupt relationship is beneficial to both the bribe recipient and the bribe giver, and thus their relationship violates government policy [25]. According to Gavelis, corruption is often the fastest, cheapest and most effective competitive tool to achieve a specific goal [27]. However, corruption is a widespread latent crime which often consists of the crime without victims, which makes investigation of corruption very difficult [28].

In order to evaluate and analyse the phenomenon of corruption, it is important to combine macro and micro level of theoretical perspectives, to take into account the time perspective and the ever-changing and complex forms of corruption and the peculiarities of the context in international, regional, national and local levels [29].

As corruption is the result of the failure of standardized laws to regulate social life [30], it is important to mention that there is a relationship between trust in the legal system and social trust [31].

Thus, corruption is a global problem which causes a serious threat to the rule of law, democracy, human rights, and violates the principles of social justice and competition. It is important to take a full picture of corruption in a much wider political, social, economic and legal context.

## 3. Corruption in medicine

The medical field is particularly vulnerable to corruption. Corruption phenomena in medicine are the most dangerous social phenomena, endangering human rights, distorting social justice and endangering public morality. One of the main reasons for this is the information asymmetry between physicians and patients i.e. patients do not know when they fall ill, when they will seek for medical advice, or whether they are treated properly, or prescribed medication is appropriate [12].

Scientists point to various forms of corruption in medicine. Corruption is defined as bribery of patients in order to obtain quality personal health care services and bribery in order to receive certain procedure, non-sequential treatment [6]. People who use healthcare services are afraid of risking their health and they seek the best possible health care services, making corruption in medicine difficult to avoid and bribing the doctor as a matter of course for receiving better and faster services [7, 8].

However, the main identified risk is related to the health of patients when prescribing not the most appropriate, non-essential medications [32, 33]. In order to protect the use of certain medications or a special company providing healthcare services, corruption can appear in many forms, such as prescribing an inappropriate treatment, prescribing inappropriate, ineffective, and more expensive medications; performing unethical, non-compliant with the legislation advertising of medicines to the patients [8-9]. Corruption is also considered to be the sale of samples of medicinal products which should be distributed free of charge to the patients [10].

A lot of medical personnel work in more than one workplace, mostly in the public and the same time in the private institutions. This gives a rise to additional conflicts of interest and opportunities for corruption, for example, in a public hospital, the physician recommends that the patient would continue treatment or rehabilitation in a private (sometimes owned by the same physician or where he/she works) institution [11].

There can be also distinguished other forms of corruption involving private medical institutions, such as the illicit use of state-owned devices and instruments for the private care of patients [10]. After the patient paid for certain services, he/she is specifically provided with lower quality, lower level services in order to save the resources of the private company [12].

Due to the corrupt activities of the private personal health care institutions the overall public confidence in the healthcare system is decreasing [11].

In general, corruption in medicine has a negative impact on the availability and quality of the healthcare. Thus, appropriate legal regulation is needed to ensure effective prevention of corruption in the country.

## 4. Legal aspects of the corruption prevention

The purpose of the corruption prevention is to minimise influence of corruption to the economy, democracy,

social welfare, national security, and to increase the quality of public service delivery.

In Lithuania, the President of the Republic of Lithuania (hereinafter - LR), the Seimas of the LR, the Government of the LR, the Commission on Professional Ethics and the main institution, the Special Investigation Service (STT), play a key role in the fight against corruption. The purpose of the STT is to detect and investigate corruption-related offenses and to develop and implement measures to prevent corruption [34].

On 28/05/2002 the Seimas of the LR adopted the Law on Prevention of Corruption [35], which states that the prevention of corruption is the disclosure and elimination of causes and conditions of corruption by establishing and implementing a system of appropriate measures, as well as impact on individuals in order to deter them from corruption-related crimes. According to this law by the corruption prevention it is sought to minimise influence of corruption to the economy, democracy, social welfare, national security, and to increase the quality of public service delivery.

According to the Criminal Code of the Republic of Lithuania [36], there are defined corruption offences such as bribery, trading in influence, graft, and other offences, if they are committed in the public administration sector or providing public services seeking the benefit of themselves or others.

One of the most important documents in the fight against corruption is the United Nations Convention against Corruption of 31/10/2003 [37]. The Convention states that corruption is no longer a domestic problem but an international phenomenon affecting the societies and economies of all countries, and that international cooperation is needed to prevent and control it, and that the prevention and eradication of corruption is the responsibility of all States. The Convention entered into force in Lithuania on 20/01/2007. Lithuania has transposed many of the anti-corruption measures of the Convention into its national legislation.

On 02/09/2010 the EU signed the Agreement Establishing an International Organisation - the Anti-Corruption Academy. The purpose of the Academy is to promote effective and efficient prevention of corruption and fight against it [38]. To achieve this purpose, there are organised anti-corruption education, sponsored research, provided technical assistance in the field of corruption and applied other measures. On 21/05/2013 Lithuania joined the International Anti-Corruption Academy.

In Lithuania corruption prevention in the field of medicine is carried out by a direct institution subordinate to the Government of the LR - the Ministry of Health of the LR. In 2005, the Ministry of Health, considering the fact that corruption in the health system is gradually taking on an international form, became a permanent member of the International Anti-Corruption Network - the European Healthcare Fraud and Corruption Network (EHFCN).

On 17/11/2009 the programme "On Prevention of Corruption in the Healthcare System" was approved by the Order No. V-773 of Minister of Health [39]. The purpose of the programme is to ensure long-term, effective and purposeful prevention and control of corruption in the Lithuanian health system.

On 07/07/2014 the Rules "On the conduct of staff of personal health care institutions who are exposed to possible corruption offence" were approved by the Order No. V-773 of Minister of Health [40]. These rules contains details how a health care worker should behave when faced with or informed about a potential corruption offence in a health care institution.

On 10/03/2015 the programme "On the National Anti-corruption Programme of the Republic of Lithuania for 2015-2025" was approved by the order No. XII-1537 of the Seimas of LR [41]. The purpose of the programme is to ensure a long-term, effective and purposeful system of the prevention of corruption and its control in the Republic of Lithuania in 2015-2025.

On 17/06/2015 a plan “On Inter-institutional Activities for the Implementation of the National Anti-Corruption Programme 2015-2025 of the Republic of Lithuania for 2015–2019” was approved by the resolution of the Government of the LR [42]. It states that one of the prioritized activities is the reduction and elimination of the corruption risk in health care and social protection systems - the reorganisation of the coordination system of health care institutions by increasing transparency of health care institutions; the establishment of a mechanism in order to support the healthcare institutions.

On 10/12/2015 the programme “On the Prevention of Sectoral Corruption in the Health Care System 2015-2019” was approved by the order of Minister of Health [43], which aims to ensure a long-term, effective and purposeful system of the corruption prevention and its control in the healthcare system 2015–2019. The purpose of the programme is to reduce the scale of corruption, increase transparency, openness, and to reduce and eliminate the prerequisites for corruption in the healthcare system.

Taking into account above discussed documents it can be stated that Lithuania has a sufficiently extensive regulation of international and national legislation in the fight against corruption. Nevertheless, there are major challenges faced when implementing anti-corruption policy in Lithuania.

## 5. Conclusions

Corruption is a global problem which causes a serious threat to the rule of law, democracy, human rights, undermines the principles of social justice and competition, inhibits economic growth, and reduces people's confidence in the state as it changes to adapt to environmental change. Corruption is a systematic, deliberate act of a person in the form of an abuse of power and authority which is primarily aimed at seeking the personal gain at the expense of society through unlawful and / or fraudulent conduct in the performance / non-performance of his / her duties. Corruption can occur in the highest levels of the government, trade in laws, judgments, public procurements and prospects for social development.

Medicine is distinguished as one of the most vulnerable to corruption areas. People are afraid of risking their

health and seeking the best possible medical care. That is why corruption in medicine is difficult to avoid and bribing a physician is a matter of course. There is a lack of public anti-corruption education about the damage caused by corruption, however a lack of public spirit is another problem when implementing public anti-corruption policy in Lithuania.

It is to point out that Lithuania has a separate institution to fight against corruption - the STT, it has adopted the Law on Prevention of Corruption, and after becoming a full member of the EU Lithuania acceded to the UN Convention and EC Treaty documents. Based on this, Seimas of the LR approved a national anti-corruption programme, which was the key issue for Minister of Health to approve the programme on the Prevention of Sectoral Corruption in the Health Care System. Nevetherless, it is clear that no one legal instrument can protect the society against corruption if it is treated formally and is not followed.

## 6. References


1. Corruption Perceptions Index 2018. Transparency International. https://www.transparency.org/cpi2018 [Retrieved on 2019-09-30].
2. Peltier-Rivest D. A model for preventing corruption. Journal of Financial Crime, Vol. 25 No. 2, 2018. p. 545-561.
3. Graycar A. Mapping corruption in procurement. Journal of Financial Crime, Vol. 26 No. 1, 2019. p. 162-178.
4. Monteverde V. The cost of corruption. Journal of Financial Crime, Vol. 26 No. 2, 2019. pp. 568-582.
5. Ter Meulen R.H.J., Van Leeuwen E. Medicinos etika. Vilnius, 2003. p. 77.
6. Ensor T., Duran-Moreno A. Corruption as a challange to effective regulation in health sector. In ed. Saltman, Richard B., Busse, Reinhard, Mossialos, Elias, Buckingham: Open University Press. Regulating entrepreneurial behaviour in European health care system, 2002. p. 106-124.
7. Palidauskaitė J. Korupcija viešuosiuose pirkimuose: nuo teorinės apibrėžties iki atvejo studijos (I dalis). Viešoji politika ir administravimas, Nr. 32, 2010. p. 74-84.
8. Raipa A. Naujoji viešoji vadyba, Kaunas, Technologija, 2007. p. 233-276.
9. Zaksaitė S. Korupcijos privačiame sektoriuje kriminalizavimo, kvalifikavimo ir įrodinėjimo problemos: kai kurių praktinių pavyzdžių analizė. Teisės apžvalga, No. 2 (9), 2012. p. 36-54.
10. Vian T. Review of corruption in the health sector: theory, methods and interventions. Health Policy Planning, No. 23 (2), 2008. p. 83-94.
11. Ecorys. European Healthcare Fraud & Corruption Network. Study on Corruption in the Healthcare Sector, 2013. Luxembourg, Publications Office of the European Union, https://ec.europa.eu/home-affairs/sites/homeaffairs/files/what-is-new/news/news/docs/20131219_study_on_corruption_in_the_healthcare_sector_en.pdf [Retrieved on 2019-07-15].
12. Savedoff William D., Hussmann K. Kodėl sveikatos sistemoms būdinga korupcija? In Sergej Muravjov. Korupcijos mįslės, Eugrimas, Vilnius, 2009. p. 91-110.
13. Umar M. Pharmaceutical promotional activity and patient's quality of life. International Journal of Pharmaceutical and Healthcare Marketing, Vol. 13 No. 3, 2019. p. 246-263.
14. Eigen P. Korupcijos tinklas: kaip pasaulinio masto judėjimas kovoja su papirkinėjimu, Vilnius, Dialogo kultūros institutas, 2007. p. 11.
15. Palidauskaitė J. Korupcijos ir atsakomybės problema viešojo administravimo sistemoje. Viešoji politika ir administravimas, No. 13, 2005. p. 28-38.
16. Valikonytė I., Lazutka S., Gudavičius E. Pirmasis Lietuvos Statutas (1529 m.), Vilnius, Vaga, 2001.
17. Justickis V. Kriminologija, Vilnius, 2001. p. 372.
18. Singer M. M. Buying Voters with Dirty Money: The Relationship between Clientelism and Corruption. Annual meeting of the American Political Science Association. Toronto, Canada, Law & Public Policy, 9 (1), 2009.
19. Dawood Y. Classifying corruption. Duke Journal of Constitutional Law & Public Policy, 9 (1), 2014.
20. Gutauskas A., Ragauskas P., Stračinskienė L., Čilinskas K. Skaidrios savivaldos link. Transparency International Lietuvos skyrius, Vilnius, 2005.
21. Ionescu L. Perceptions of corruption in emerging economies. Economics, Management, and Financial Markets, Vol. 8(1), 2013. p. 136-141.
22. Buinickienė N. Korupcijos priežastys ir jų valdymo priemonės Lietuvos sveikatos priežiūros sistemoje. Management Theory and Studies for Rural Business and Infrastructure Development, Vol. 39, No. 2, 2017. p. 148-156.
23. Raudonienė A. Modernėjanti klasikinio korupcijos apibrėžimo Lietuvoje kaita. Jurisprudencija, Vol 32, No 24, 2002. p. 114-121.
24. Hellman D. Defining corruption and constitutionalizing democracy. Michigan Law Review, Vol. 111, No 8, 2013. p. 1385-1422.
25. Ackerman S. R. Korupcija ir valdžia: priežastys, padariniai ir reforma, Vilnius, Vaga, 2001. p. 79.
26. Klitgaard R. Combating Corruption and Promoting Ethics in the Public Service, 2000. The Organisation for Economic Co-operation and Development, http://www.oecd.org [Retrieved on 2019-08-19].
27. Gavelis V. Korupcija – objektyvus valstybės veiklos mechanizmo kliuvinys. Ekonomika ir vadyba: aktualijos ir perspektyvos, No. 2(7), 2006, p. 55-61.
28. Michailovič I. Korupcijos tyrimo problematika. Teisė, No. 60, 2006. p. 68-84.
29. Piliponytė J. Corruption: Theoretical Attempts to Define and Explain. Sociologija. Mintis ir veiksmas, No. 14, 2004. p. 83-95.
30. Sadigov T. Psychological dimension of corruption. International Journal of Sociology and Social Policy, Vol. 38 No. 5-6, 2018. p. 484-508.
31. Radin D. The effect of anticorruption policies on social and political trust: a comparative approach. Social Responsibility Journal, Vol. 15 No. 5, 2019. p. 658-670.
32. Dėl šakinės korupcijos prevencijos sveikatos priežiūros sistemoje 2015–2019 metų programos patvirtinimo. Lietuvos Respublikos sveikatos apsaugos ministro įsakymas, 2015 m. gruodžio 10 d. Nr. V-1433. https://www.e-tar.lt/portal/lt/legalAct/63683d30a27411e58fd1fc0b9bba68a7/asr [Retrieved on 2019-09-18].
33. Cosgrove L., Wheeler Emily E. Drug Firms, the Codification of Diagnostic Categories, and Bias in Clinical Guidelines. Journal of Law, Medicine & Ethics, Vol. 41, Issue 3, 2013. p. 644-653.
34. Sah S., FughBerman A. Physicians under the Influence: Social Psychology and Industry Marketing Strategies. Journal of Law, Medicine & Ethics, Vol. 41, Issue 3, 2013. p. 665-672.
35. Dėl Lietuvos Respublikos specialiųjų tyrimų tarnybos įstatymo patvirtinimo. Lietuvos Respublikos Seimas. 2000 m. gegužės 2 d. No. VIII-1649.

https://e-seimas.lrs.lt/portal/legalAct/lt/TAD/TAIS.100816?jfwid=5sjolfzn1 [Retrieved on 2019-09-12].
36. Lietuvos Respublikos korupcijos prevencijos įstatymas. Valstybės žinios, 2002-06-12, No. 57-2297.
37. Lietuvos Respublikos baudžiamojo kodekso patvirtinimo ir įsigaliojimo įstatymas. Baudžiamasis kodeksas. No. VIII–1968. Valstybės žinios, 2000. No. 89-2741.
38. Jungtinių Tautų Konvencija prieš korupciją. 2003-10-31. Valstybės žinios, 2006-12-14, No. 136-5145.
39. Susitarimas dėl tarptautinės organizacijos – antikorupcijos akademijos – įsteigimo. Valstybės žinios, 2013, No. 19-928.
40. Lietuvos sveikatos apsaugos ministro 2009 m. lapkričio 17 d. įsakymas No. V-942 „Dėl korupcijos prevencijos sveikatos sistemoje programos patvirtinimo“. https://e-tar.lt/acc/legalAct.html?documentId=TAR.FAD63075F32C&lang=lt [Retrieved on 2019-09-21].
41. Lietuvos Respublikos sveikatos apsaugos ministro 2014 m. liepos 7 d. įsakymas No. V-773 „Dėl asmens sveikatos priežiūros įstaigų darbuotojų, susidūrusių su galima korupcinio pobūdžio nusikalstama veika, elgesio taisyklių patvirtinimo”. https://www.e-tar.lt/portal/lt/legalAct/f72f0a1008b711e4adf3c8c5d7681e73 [Retrieved on 2019-09-19].
42. Dėl Lietuvos Respublikos nacionalinė kovos su korupcija 2015–2025 metų programos patvirtinimo: Lietuvos Respublikos Vyriausybės nutarimas. 2015 m. kovo 10 d. No. XII-1537. https://www.e-tar.lt/portal/lt/legalAct/25c529d0cbcd11e4aaa0e90fce879681 [Retrieved on 2019-09-02].
43. Lietuvos Respublikos vyriausybės nutarimas 2015 m. birželio 17 d. įsakymas No. 648 “Dėl Lietuvos Respublikos nacionalinės kovos su korupcija 2015-2025 metų programos įgyvendinimo 2015-2019 metų tarpinstitucinio veiklos plano patvirtinimo suvestinė redakcija nuo 2016-01-01“. TAR, 2015, Nr. 10386. https://www.e-tar.lt/portal/lt/legalAct/13fd20601e6e11e586708c6593c243ce/gCsWGgZdEt [Retrieved on 2019-09-12]

CATALYST HD

# FAST, SAFE AND EASY MONITORING

*C-RAD's unique triple-camera Catalyst HD™ system for stereotactic treatments makes patient monitoring fast, safe and easy.*

Catalyst HD™ ensures optimal and timely positioning. With posture errors projected directly onto the patient, you have the freedom to maintain direct eye contact with your patient at all times. Respiratory gating and 3D intra-fraction motion detection guarantee that you target doses precisely – even with moving tumours – throughout the entire fraction.

Three cameras provide optimal patient coverage for non-coplanar treatments. A 360-degree automated reference rotation ensures continuous motion monitoring.

The Catalyst HD™ patient monitoring system makes it easy to perform treatments. Catalyst HD™ is also readily integrated with immobilisation equipment for optimal accuracy and patient comfort.

Fast, safe and easy: Catalyst HD™ optimizes your workflow.

C-RAD is a leading manufacturer of advanced patient monitoring systems.

**www.c-rad.com**

C-RAD

# THE DOSIMETRY SYSTEM FOR IMPROVED TREATMENT IN HDR BRACHYTHERAPY

BrachyDOSE is a cancer treatment quality control tool for oncologists to reach the best possible treatment results. The solution is suited specially for high dose rate (HDR) brachytherapy treatment.

The quality control system is composed of human tissue equivalent radiation dose measurement tool (dosimeter) and its reader. The dosimeter is placed into one or a few standard implantable tubes near the tumour or at a specific place chosen by oncologist before the brachytherapy procedure.

The dosimeters measure and retrieve dose profile along the whole length of a dosimeter-tube, giving more precise measurements.


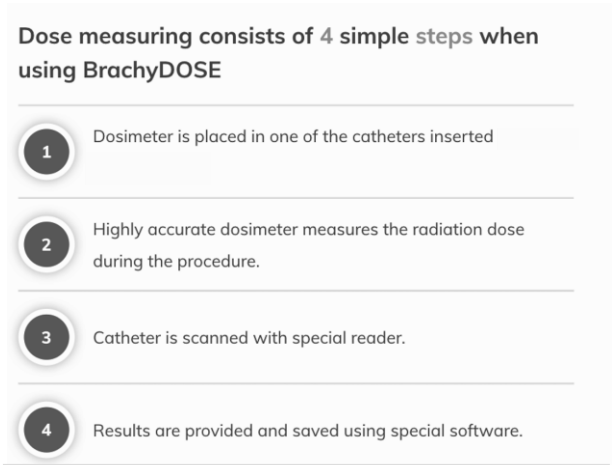


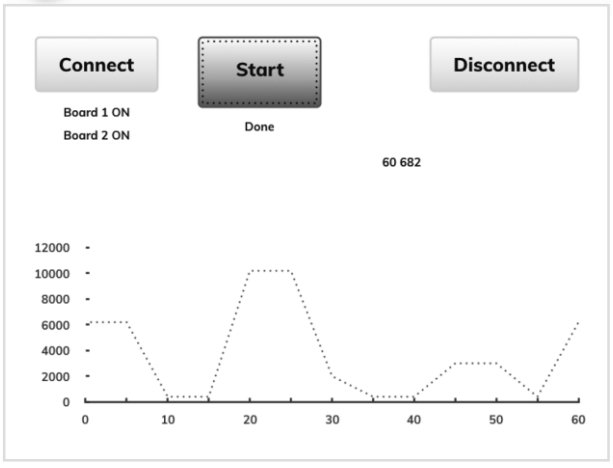


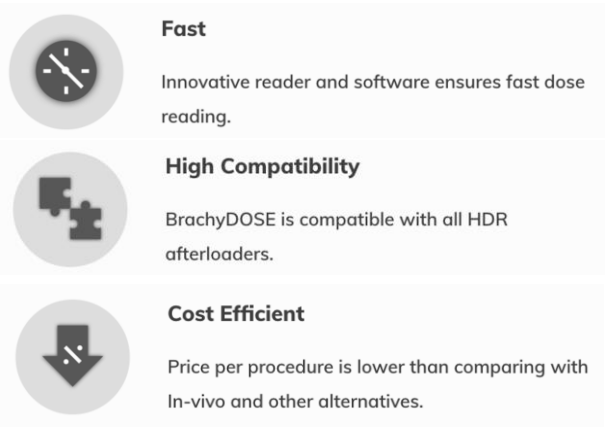


The dosimeter is also highly compatible with standard brachytherapy devices and may be used to measure radiation dose in bladder and other important organs, damage to which would mean severe complications.

The main benefit of our dosimetry system is direct data registering on the radiation dose applied to a patient. Such data allows for treatment plan update, as well as prevention of additional illnesses caused by harmful radiation and unnecessary long-healing radiation wounds. This way, the treatment price is also reduced.


BrachyDOSE development is supported by

**Neringa Šeperienė**
Co-Founder, CEO
Studentų g. 65-301, LT-51369 Kaunas, Lithuania
sesipartneriai@gmail.com
+370 611 34592

## CONTENT

# AUTHOR INDEX

ISSN 1822–5721